An Analysis of Glacial Sediment Dispersion with Applications to Diamond Exploration, Lac de Gras, Northwest Territories

by

Robert Janzen

A thesis

presented to the University of Waterloo

in fulfillment of the

thesis requirement for the degree of

Master of Science

in

Earth Sciences

Waterloo, Ontario, Canada, 2020

Author's Declaration

This thesis consists of material all of which I authored or co-authored: see Statement of Contributions included in the thesis. This is a true copy of the thesis, including any required final revisions, as accepted by my examiners.

I understand that my thesis may be made electronically available to the public.

Statement of Contributions

Barrett Elliott of the Northwest Territories Geological Survey provided the data from the RC drilling program.

Dr. Philippe X. Normandeau of the Northwest Territories Geological Survey provided data in the form of ice flow indicator measurements, locations, and photographs.

Dr. Samuel Kelley of University College Dublin (formerly Post Doctoral Fellow at the University of Waterloo) provided data in the form of pebble counts, ice flow indicator measurements, and photographs.

Robin McKillop and Dave Sacco of Palmer Environmental Consulting Group provided data in the form of striation measurements.

Saskatchewan Research Council conducted kimberlite indicator mineral picking and geochemical analyses of till samples from both the RC drilling program and the surficial till sampling.

Abstract

Diamond exploration is important to the economy of the Northwest Territories and Canada. In recent years, however, there has been a marked decline in the discovery rate of large diamond deposits. Emphasis is being put on improving geological models and developing new approaches of exploration in the hope of finding previously overlooked deposits. A proven approach in diamond exploration in the Northwest Territories and other similarly glaciated terrains has been to characterize the glacial cover to reveal secondary detrital dispersion of indicator minerals and geochemical pathfinders, which can help vector towards a buried kimberlitic source. Typically, only the surficial indicator mineral expression of a kimberlitic signature is known and mapped, which may lead to missed targets, especially in places with shifting ice flows and a complex glacial sedimentary record. This research, in the Lac de Gras area of Northwest Territories, uses a dataset containing both surface and subsurface data, from hand sampling and RC drilling, to bring new knowledge about the glacial geology and to improve our understanding of till production and related detrital dispersion in this prospective region.

Erosional outcrop-scale paleo-ice flow indicators show an evolving history of ice-flow in a clockwise sequence starting in the southeast, then west, and finally to the northwest. The ice-flow indicators in the study area show that the northwest ice-flow phase is prominent accounting for 77% of all observations. The particle size distribution of surficial till samples is relatively homogenous, which lends support to the interpretation that the surface till forms a single till unit. The clast lithological analysis shows that the till contains all the different lithologies present in the study area in variable proportions, which appears to reflect a combination of processes and factors, such as bedrock hardness in the up-ice area versus in the dispersion area. The principal component analysis (PCA) of the major oxides shows the till is a mixture of the local bedrock material, but with end-member categories associated with the different bedrock lithologies mapped in the region. Notably, the till at depth, where till is thicker, appears to show a more distal signature than the overlying till or in areas of thin till.

Kimberlite indicator mineral (KIM) patterns within the envelope of the Monument indicator train (MIT) indicate a shallow dispersal train that is best captured by surficial samples (*i.e.* max. depth of approx. 0.3m). The MIT is an area characterized by thin and highly discontinuous till and results show that the strong surficial dispersal from the Monument kimberlites only weakly extends in the

shallow subsurface (*i.e.* below the first 0.3m). As a result, the MIT is not well-defined in the drill data. In addition, no clear palimpsest dispersal train associated with the older ice flow phases was found close to the Monument kimberlites. The till along the Coppermine indicator train (CIT) in the west-central portion of the study area is, on average, thicker than along the MIT. Results show a subsurface dispersal train that rises to the surface in the NW direction, consistent with the young NW ice flow phase and approximately parallel to the MIT. Also, there is a more subtle dispersal train extending to the SW that seems to start in the same area as the rising dispersal. This SW direction corresponds well with the oldest documented ice flow phase in the study area. The respective head of the two identified dispersal trains thus appear to be in the same area and suggest both dispersal trains emanate from the same local buried source. However, it is not possible to exclude the scenario of a more distal source, but it requires a more complex model involving sustained low effective stress and/or englacial transport during more than one ice flow phase.

Till matrix geochemistry data that was available for this study proved to be of limited use for kimberlite dispersal train mapping and related glacial sediment transport reconstruction. A possible mixed signature from non-kimberlitic sources could not be separated. Therefore, the main available pathfinders for kimberlites also appear to trace dispersal trains from other rock sources such as mafic rocks and perhaps some metasedimentary rocks. Analysis of more elements using a total digestion procedure, along with multivariate analysis of the results, would be useful to further discriminate the more complex overlapping geochemical signatures.

Overall, this study shows that the combined analysis of surface and subsurface till show some contrasting compositional characteristics, which may indicate more complex till stratigraphy or inheritance linked to older ice flow phases than previously considered. It may also have captured the signal of an unknown buried source, although this remains to be confirmed. This study suggests that drift prospecting may be enhanced in the Lac de Gras region by using more subsurface data and this could be critical for future success at the current maturity stage of the diamond district. It may be somewhat surprising given the till is typically relatively thin and discontinuous in this region, but it is clear that despite this situation, the few pockets of thicker till reveal more than what is recorded in the shallow and surficial till. Important corridors may be revealed where till is thicker on average and where surface landforms and bedrock depressions have possibly created till dispersal patterns that are different than the ones associated with previous discoveries.

Acknowledgements

This research was funded by the Northwest Territories Geological Survey (NTGS) through the Slave Province Surficial Materials and Permafrost Study (SPSMPS), as well as through financial support from Dr. Martin Ross with the University of Waterloo. This research would not have been possible without the data provided by the NTGS drilling program or the laboratory analysis of the kimberlite indicator minerals and till geochemistry provided by Saskatchewan Research Council.

I would like to thank Drs. Sam Kelley and Phillipe Normandeau for their mentorship and assistance in the field, as well as Barrett Elliott and the rest of the SPSMPS team for the logistical field support to conduct fieldwork in the remote Canadian tundra. I would like to especially thank Dr. Sam Kelley for his mentorship and patience while guiding me during research, writing, and conferences during my time at the University of Waterloo. The many members of the Quaternary research group at Waterloo made my time enjoyable and you all helped me in one way or another: Shawn, Jessey, Rebecca, Amanda, Andrea, Thomas, Caroline, Grant, Ameerah, and Ying. My committee members, Drs. Chris Yakymchuk, John Johnston, and Martin Ross are all thanked for their valuable comments and direction for this project. My supervisor, Dr. Martin Ross, has been a constant source of information, insight, and guidance. I want to thank him for providing me with this opportunity and sticking with me through 5 years of writing and editing while I dealt with travelling long distances, raising a family, and working.

Finally, I would like to thank my wife, Miranda, for pushing me to complete this thesis. Your enthusiasm and confidence in me are unbelievable, and the sacrifices you made so that I could complete this project are incredible! You made this possible.

Table of Contents

List of Figures

List of Tables

Chapter 1: Introduction

1.1 Research Problem

The Slave Geological Province is the principal diamond district of Canada where mineral exploration for kimberlites has been ongoing since 1981. Currently, there are three operational diamond mines, Ekati, Diavik, and Gahcho Kué, having been in service since 1998, 2003, and 2016, respectively (Dominion Diamond Corp., 2013a, 2013b; De Beers Group of Companies, 2016a). Another mine, Snap Lake, began production in 2008 but was placed on care and maintenance in 2015 (De Beers Group of Companies, 2016b). In recent years there has been a marked decline in the discovery rate of economically viable diamondiferous kimberlites (Hamill, 2014; Heffernan, 2014; Taylor, 2015). Given the lower rate of discovery in well-explored areas (Schodde, 2013; Heffernan, 2014), two different strategies are increasingly considered in an attempt to turn the tide:

1) Increase geosciences knowledge and exploration efforts in regions that were avoided or overlooked in the past due to geological complexities.

2) Improve geological models and develop new approaches of exploration in mature diamond districts in the hope of finding previously overlooked deposits.

The two strategies involve innovation through targeted research and development. Geological surveys' programs tend to be designed to stimulate exploration in greenfield and frontier areas (Strategy #1), but some programs aim at exploration innovation within established mining districts (Strategy #2). The recent collaborative efforts in the Slave Geological Province are mostly related to the second strategy, although the area is large enough with diverse geology to include aspects of strategy #1. Initial exploration occurred rapidly following the discovery of the first kimberlites in the Northwest Territories in 1991. Recently, the discovery rate of kimberlites has slowed. This prompted the territorial government and the Northwest Territories Geological Survey (NTGS) to collect new geological data and publish a wealth of legacy data to stimulate exploration in areas that have previously been examined. Industry highly values large public domain data sets such as geological maps, geophysics data sets, and geochemical data. This also

provides academia with an opportunity to develop and apply new techniques to previously collected large sample/data sets.

Currently, one of the biggest exploration challenges is that new discoveries are deeper, sometimes under thick sediment cover, and in remote areas (logistical and climate-related challenges). This makes discovery risky for mineral exploration companies due to the increased expense, time, and difficulty. In northern Canada, the 'cover' is typically transported regolith related to the Quaternary glaciations (Fulton 1989, 1995). Thus, one important approach is to characterize the glacial cover and use it to reveal possible secondary detrital dispersion of indicator minerals and geochemical pathfinders, which can help vector towards a buried source (Kujansuu and Saarnisto, 1990). The Slave Geological Province is an area of primary till production with a complex entrainment history due to ice flow shifts (*e.g*. Lemmen, 1994; Brown *et al*., 2011) and changing subglacial conditions. The most recent glaciation, the Wisconsinan, deposited a discontinuous till sheet of variable thickness throughout the diamond district (Knight & Kerr, 2007). Glacial erosion, transport, and deposition of material have the potential to mask or hide kimberlite at the bedrock surface. Many subcropping kimberlites have diameters that are notably small or have complex geophysical footprints in the central Slave Province, making them elusive targets if buried under glacial sediments (Smith, 2008; Paulen, 2013). Kimberlite is also relatively soft compared to most other rocks making it more susceptible to erosion than surrounding host rocks. As a result, many kimberlites are located under lakes due to the uppermost kimberlite being eroded and water filling the depression above the remaining kimberlite. Additionally, kimberlite depressions can be partly filled with thick regolith, which contributes to masking their signature. However, because the kimberlite may be eroded by glaciers, glacial sediments containing a kimberlitic signature may extend far beyond the buried kimberlite due to glacial transport.

Typically, only the surficial indicator mineral expression of this kimberlitic signature is known and mapped (Ward *et al.*, 1996; Averill, 2001; McClenaghan *et al*., 2002; Pell *et al*., 2017). Important details about the real shape of kimberlitic dispersal may be missed by representing these trains using surface data only. Till dispersal occurs in three-dimensions and can be quite complex even in areas of relatively thin and discontinuous till which may reveal key aspects about the possible location of their source (McMartin and McClenaghan, 2001; Stea and Finck,

2001; Hooke, *et al*., 2013; Kelley *et al*., 2019). Additionally, till production is a time transgressive event related to glacial dynamics (Stea and Finck, 2001; Hooke *et al*., 2013). A kimberlite deposit could be undergoing intense glacial erosion, directly contributing to the dispersal of kimberlitic material in till, to becoming buried by newly formed till, and thus no longer contributing to dispersal. Yet, the dispersion of kimberlitic material can continue through comminution and entrainment by ongoing ice flow (Paulen, 2017). These factors play a role in the obstruction of traditional exploration techniques. For instance, some kimberlites are discovered mainly using geophysics, but the till does not show a strong indicator mineral signal near the source (GGL Resources, 2004, 2018). In contrast, there are kimberlitic signatures within till that appear not to be linked to a source.

This study was motivated by the occurrence of these two problems in the Slave Province and the recognition of the need to understand, in more detail, the most recent glacial events in Canada's diamond district in an effort to track down potential sources of kimberlite by enhancing exploration methods, understanding processes, and improving the effectiveness of both exploration and mapping (*e.g*., Thorleifson, 2017). This research uses large government datasets to bring new knowledge about the glacial cover to improve our understanding of till production in this prospective region and to enhance exploration techniques. The work is based on a three-dimensional approach combined with detailed ice flow data to gain new insights into the provenance, entrainment, and deposition of till that cannot be captured by traditional surface till sampling surveys. This will increase the likelihood of making new discoveries, or at least optimize exploration strategies and prioritize geophysical targets by deciphering the kimberlite signatures within till. The method, designed to be applicable to mineral exploration, could also be applied in other similar glaciated terrains.

1.1.1 Study Location and Physiographic Setting

The study area is situated ~300 km northeast of Yellowknife, Northwest Territories, within NTS map sheet 76D (**Figure 1-1A**) to the south and west of Lac de Gras, NT. It encompasses an area of approximately 700 km^2 (**Figure 1-1B**). Generally, the study area has low relief defined by topographic variations that are controlled by bedrock ridges.

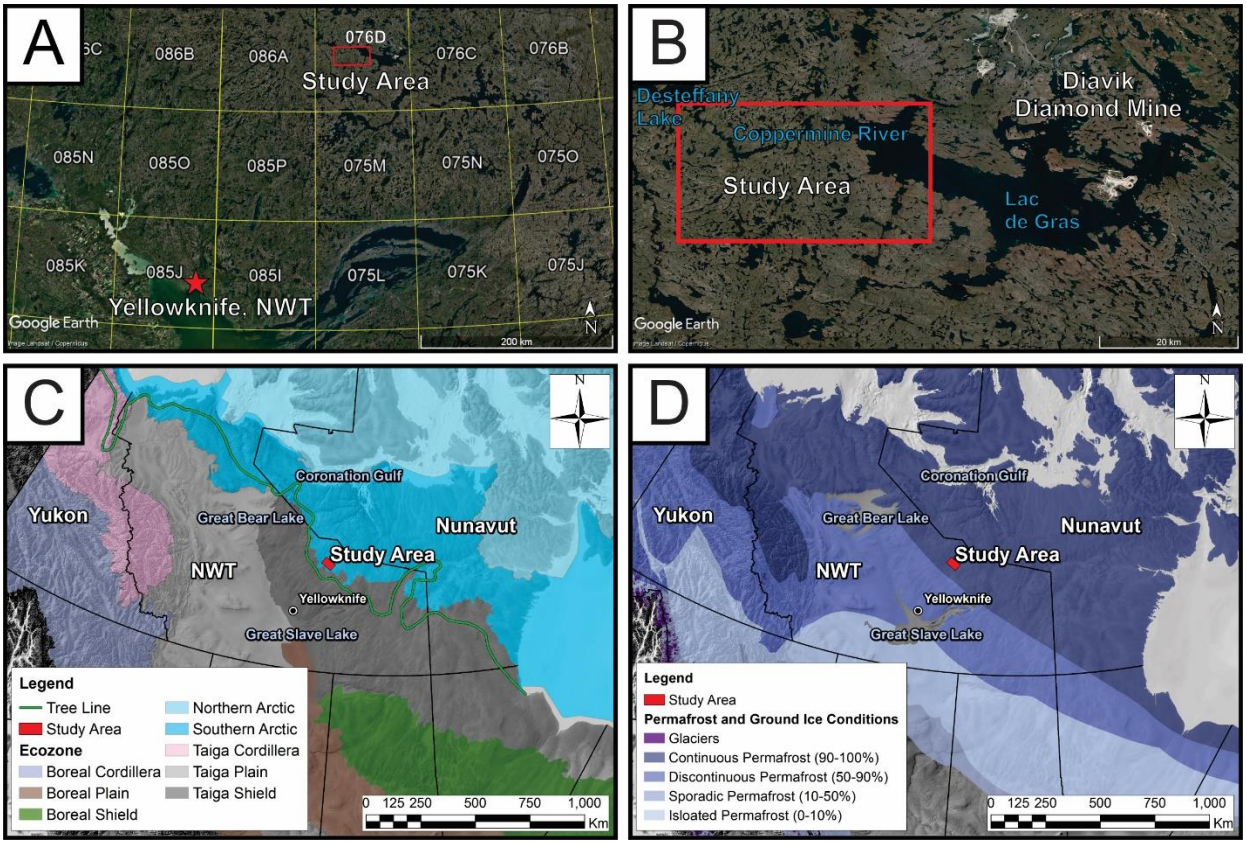

Figure 1-1: The study area is located A: ~300 km NE of Yellowknife within NTS map sheet 76D (NRCAN, 2014); A: west of Diavik Diamond mine and SW of Lac de Gras (Google Earth, 2016); C: within the southern arctic ecozone (bright blue band) and north of the tree line (green line is northernmost tree growth) (modified from Ecological Stratification Working Group, 1996); D: within the zone of continuous permafrost (dark blue area) (modified from Brown et al., 1997).

There are numerous small lakes in the area, but there are also some larger lakes such as Lac de Gras to the northeast of the study area and Desteffany Lake to the northwest. These larger lakes border the study area with the Coppermine River flowing from Lac de Gras to Desteffany Lake. The smaller lakes appear to occupy topographic lows created by glacially scoured bedrock. Wetlands appear to occupy depressions in the till surface. Local drainage consists primarily of small streams occupying depressions or sometimes creating minor incisions into the till surface that trend toward the large lakes at the edge of the study area. The Coppermine River is the modern regional trunk drainage that flows to the NW and ultimately discharges into the Coronation Gulf of the Arctic Ocean. There are many areas of thin till mapped as till veneers (<2 m thick), and till blankets (2-10 m thick) (Ward *et al.*, 1995). The study area is within the Southern Arctic ecozone and classified as Tundra Shield upland in the Point Upland Low Arctic south ecoregion (Ecosystem Classification Group, 2012). The study area is also situated north of

the tree line (**Figure 1-1C**). There are limited strands of stunted white and black spruce, as well as dwarf birch trees located within the lowlands near the Coppermine River (**Figure 1-2A**). Permafrost is continuous (**Figure 1-1D** & **Figure 1-2B**) and frost-shattered bedrock is prevalent, especially in the eastern part of the study area.

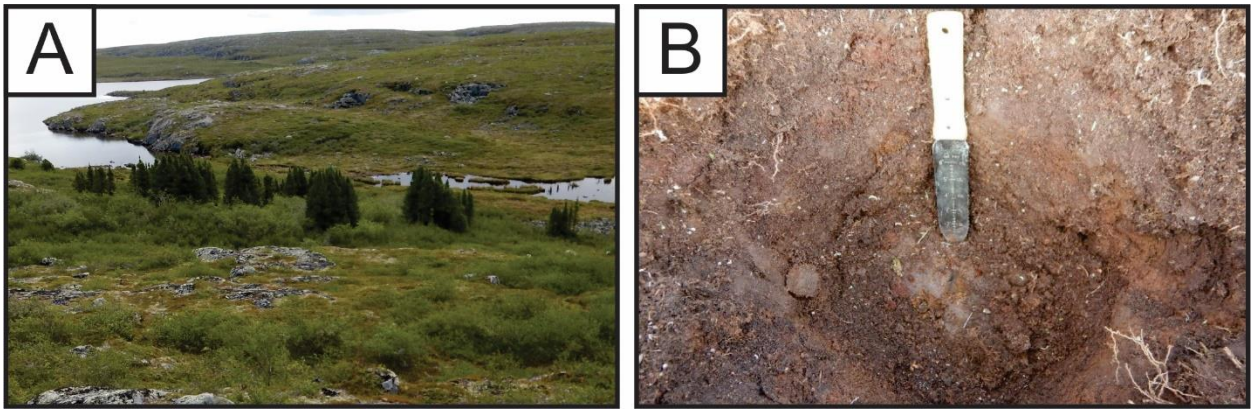

Figure 1-2: A) Landscape photo showing key features. Tributary (right center) leading to the Coppermine River (Left) with stunted white spruce pine trees. B) Shallow hand-dug pit (trowel is ~30 cm) showing soil, oxidized sediment, and permafrost (ice) in the bottom (light brown to grey).

1.2 Background Information

1.2.1 Bedrock Geology

The Slave Geological Province is located in northern Canada, bounded by the Churchill Province to the south and east, the Interior Platform to the west, and the Arctic Platform to the north; the Bear province also forms part of the north and western boundaries (Wheeler *et al*., 1997). The bedrock geology has been mapped extensively by several different researchers since 1949 (Folinsbee, 1949; Lord and Barnes, 1954; Moore, 1956; Bostock, 1980; Dillon-Leitch, 1984; Lambert *et al*., 1992; Kjarsgaard and Wyllie, 1994; Kjarsgaard *et al*., 1994a, 1994b; Kjarsgaard *et al*., 1999; Thompson and Kerswill, 1994; Renaud *et al*., 2001). A compilation map encompassing NTS map sheets 76C (Aylmer Lake), 76D (Lac de Gras), and parts of 76E (Contwoyto Lake, southern half) and 76F (Nose Lake, southwest corner) was constructed by Kjarsgaard *et al.* (2002) to include all of the previous mapping efforts and the Lac de Gras Kimberlite field. The study area is located near the southwest corner of the central Slave Province (**Figure 1-3**). The central Slave Basement Complex, outcropping west of the study area, contains the Jolly Lake Complex layered quartzofeldspathic gneisses, granitoid migmatite,

and foliated meta-granite/tonalite rocks that have an age determination of 3325 to 2681 Ma, making them pre- to syn-Yellowknife Supergroup in age (Bleeker *et al*., 1999; van Breemen *et al*., 1992; Kjarsgaard, *et al*., 2002). The volcanic rocks of the Yellowknife Supergroup contain the North-South trending Courageous Lake greenstone belt to the south of the study area. The main rock types are mafic volcanic and synvolcanic mafic intrusive rocks in the western half and felsic volcanic rocks on the eastern half of the greenstone belt (Thompson and Kerswill, 1994; Kjarsgaard *et al*., 2002). The rocks of the Courageous Lake greenstone belt have been dated from 2729 to 2671 Ma (Villeneuve, 1993). The main Yellowknife Supergroup rocks are the most spatially extensive lithology in the central Slave Province. These are metagreywacke mudstone turbidite sequences that conformably overlie the volcanic rocks (Kjarsgaard *et al*., 2002). The metasedimentary rocks in the eastern half of the study area have been dated from <2664 to 2637 Ma, and do not contain BIF at the interface with the volcanic rocks, making them part of the Itchen formation (Bostock, 1980; King *et al*., 1991; Yamashita *et al*., 2000; Villeneuve *et al*., 2001; Kjarsgaard *et al.*, 2002). The syn-Yellowknife Supergroup granitoid rocks within and near the study area were deposited between 2625 to 2608 Ma (van Breemen *et al*., 1990, 1992; Kjarsgaard *et al*., 2002). The composition of the granitoid plutons within the study area is typically hornblende-biotite tonalite but may be a variable suite of trondhjemite. The plutons appear as rounded units and are located near the southeast corner and in three areas near the center of the study area. The post-Yellowknife Supergroup granites are mainly composed of a biotite monzogranite with a crystallization age of *ca*. 2585 to 2582 (van Breemen *et al*., 1992; Kjarsgaard *et al*., 2002). The monzogranite makes up the western half of the study area. There is also extensive Proterozoic volcanism and faulting that have been dated to *ca*. 2616 Ma and <2679 Ma respectively on the north side of Lac de Gras near the study area (Kjarsgaard & Heaman, 2002; Villeneuve & Kjarsgaard, 2002). The kimberlite volcanism and emplacement took place between the 74 to 45 Ma and will be discussed further in *section 1.2.2*.

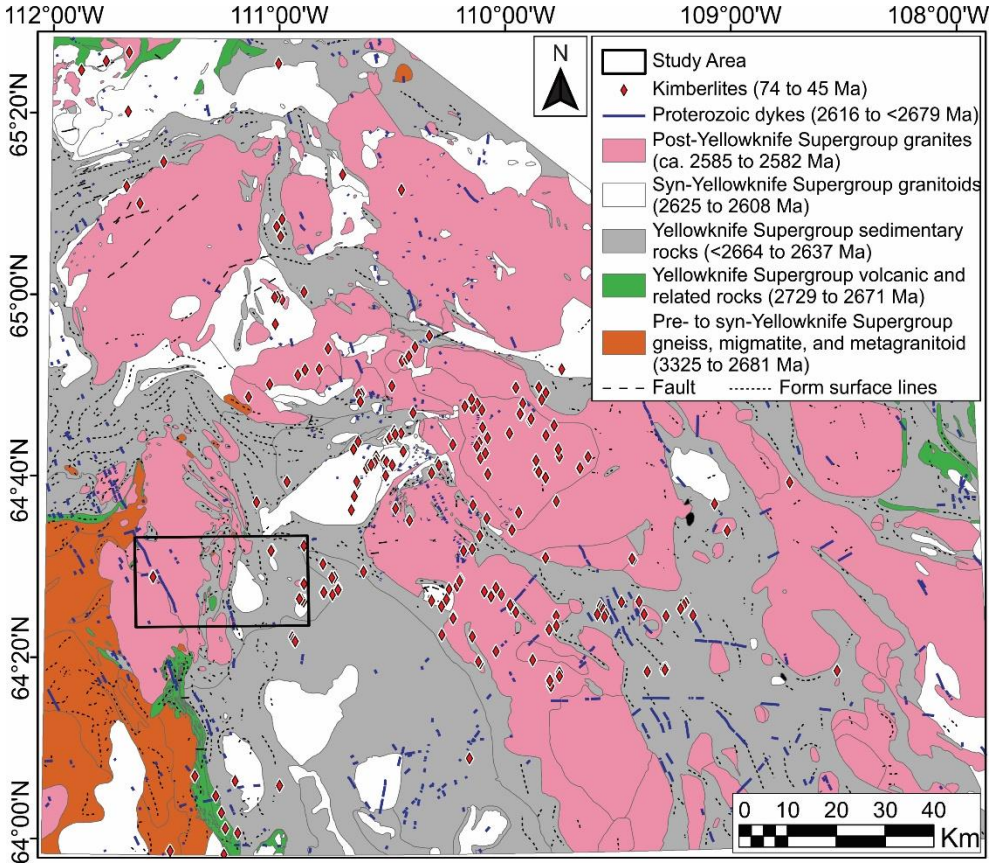

Figure 1-3: Generalized bedrock map of the Central Slave Geological Province. Legend is presented in chronostratigraphic order from youngest (top; kimberlites) to oldest (bottom; pre- to syn-Yellowknife Supergroup). Annotated from Kjarsgaard et al. (2002).

The central Slave Province and the study area bedrock geology consists of 5 main geological elements (**Figure 1-3** and **Figure 1-4**):

1- Pre- to syn-Yellowknife Supergroup gneiss, migmatite, and metagranitoid rocks (3325 to 2681 Ma);

2- Yellowknife Supergroup volcanic and volcaniclastic rocks, and syn-Yellowknife Supergroup felsic porphyritic and mafic intrusive rocks (2729 to 2671 Ma);

3- Yellowknife Supergroup sedimentary rocks (<2664 to 2637 Ma);

4- syn-Yellowknife Supergroup granitoid rocks (2625 to 2608 Ma); and

5- post-Yellowknife Supergroup granites (ca. 2585 to 2582) (Kjarsgaard *et al*., 2002).

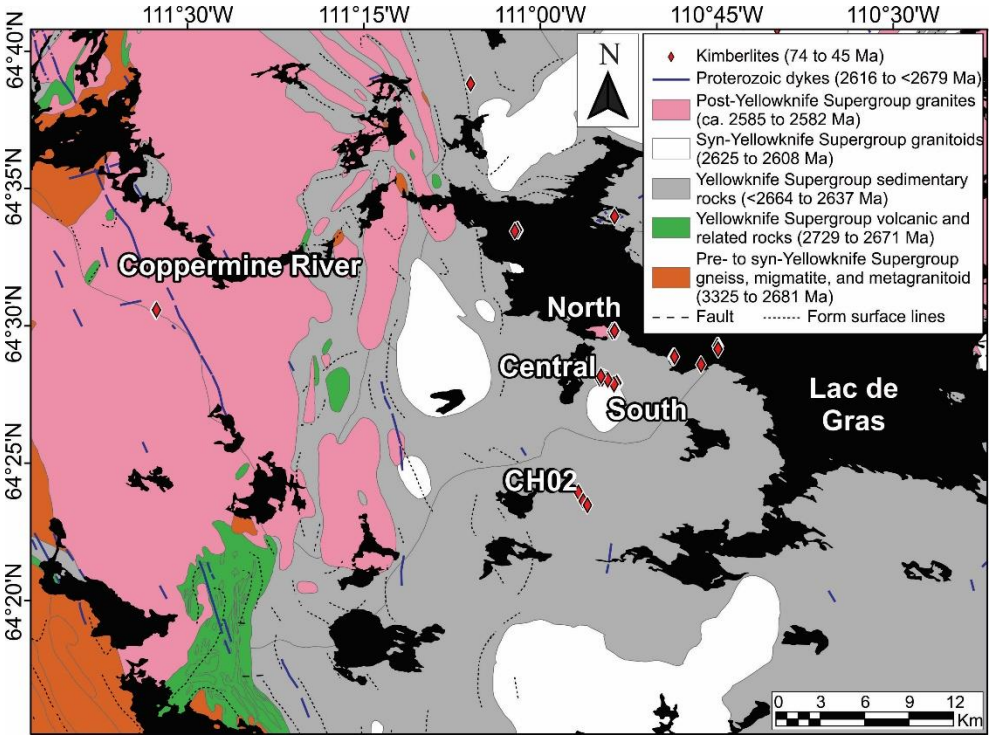

Figure 1-4: Simplified bedrock map of the study area showing known kimberlites. The Monument kimberlites are identified as the North, Central, and South kimberlites. Modified from Kjarsgaard et al. (2002).

The rock lithologies in the area to the south and west of Lac de Gras can be described as follows:

1 - Pre- to syn-Yellowknife Supergroup gneiss, migmatite, and metagranitoid rocks

- Quartzofeldspathic gneiss; Fine- to medium-grained rocks consisting of quartz plus one or two feldspars and minor biotite ± hornblende. They are variably folded with millimetre to decimetre scale gneissic layering and amphibole boudins or inclusions. Anatectic and/or injected leucosomes are typical (Kjarsgaard *et al*., 2002).

- Granitoid migmatite; Granitic to tonalitic rocks of highly irregular grain size. Contain streaky lenticular leucosomes and wispy, biotite-rich melanosomes. Rocks are tightly folded and are commonly sheared (Kjarsgaard *et al*., 2002).

- Foliated meta-granite, tonalite; Rocks are variably foliated, strongly recrystallized, and biotite bearing. Contains metagabbro, granitoid migmatite, and quartzofeldspathic gneiss inclusions. Yellowknife Supergroup metasedimentary inclusions are absent (Kjarsgaard *et al*., 2002).

2 - Yellowknife Supergroup volcanic and volcaniclastic rocks, and syn-Yellowknife Supergroup felsic porphyritic and mafic intrusive rocks

- Felsic volcanic to volcaniclastic rocks; Dacitic to rhyolitic rocks. Weathering is variable from cream, pink, buff, white, pale grey, pale green-grey, to dark grey. There are variable phenocrysts of quartz, plagioclase, and K-feldspar. Phenocrysts of hornblende or biotite are more rare. These rocks occur as massive lava domes, flows, flow breccias, lapilli tuff, and pillow lavas. They are associated with minor proportions of mafic and intermediate volcanic rocks (Kjarsgaard *et al*., 2002).

- Mafic intrusions; Weathering is dark green through light green to chocolate brown. Rocks occur as dykes, sills, and plutons (varied size) of gabbro to diorite composition with well-developed aphanitic chill margins. The texture is massive and rarely well foliated. They are medium-grained with occasional ophitic texture. Phenocrysts are typically hornblende and occasionally plagioclase. The mineralogy is dominated by hornblende and plagioclase, with minor pyroxene and biotite, traces of magnetite, titanite, and pyrite (Kjarsgaard *et al*., 2002).

- Undifferentiated volcanic and volcaniclastic rocks; These rocks are undivided but typically complex interlayered rocks of basaltic, andesitic, dacitic, and rhyolitic compositions. There are wide volcanic textural variations that include pyroclastic and epiclastic rocks, flows and domes (Kjarsgaard *et al*., 2002).

3 - Yellowknife Supergroup sedimentary rocks

- Metamudstone and metagraywacke; Rocks are interlayered with centimetre to metre thick paired units There are thicker massive metagraywacke dominated beds. The metawacke grades into mudstone, characteristic of turbidity current deposits. Thin beds of graphite-rich metasediments and iron-formation are variably present. The metamorphic grade varies from lower greenschist through upper amphibolite (Kjarsgaard *et al*., 2002).

4 - syn-Yellowknife Supergroup granitoid rocks

- Hornblende – biotite tonalite; Weathering is brown-grey. Rocks are equigranular and medium-grained. Contains euhedral to subhedral plagioclase, subhedral quartz, biotite and hornblende, with minor K-feldspar, accessory magnetite, pyrite, epidote, and zircons. Hornblende-rich microdiorite enclaves are common. There are moderate foliation and thin (10 cm to 10 m scale) metasedimentary septae of variable length (10's to 100's of m). Contains minor phases of biotite granodiorite, quartz diorite, and diorite (Kjarsgaard *et al*., 2002).

5 - post-Yellowknife Supergroup granites

- Muscovite-biotite monzogranite; Weathering is white to light grey-green. The texture is massive and equigranular. Contains sub-equal parts quartz, plagioclase, and K-feldspar, and 5-10% of muscovite and biotite. Common accessory minerals are aquamarine apatite, tourmaline, zircon, and monazite. There is garnet, cordierite, and sillimanite present in the granite close to metasedimentary inclusions. Pegmatite dykes are common both within and adjacent to the muscovite biotite granite plutons (Kjarsgaard *et al*., 2002).

- Biotite monzogranite, porphyritic; Rocks are K-feldspar-rich. Weathering is light red to pinkish-white. The texture is medium- to coarse-grained and massive. Typically contains 10% biotite, while muscovite is absent (or <1%). Microcline-rich pegmatite dykes are generally not commonly associated with these granites, when rarely observed, they contain only biotite (Kjarsgaard *et al*., 2002).

- Biotite Monzogranite, equigranular; Rocks are K-feldspar-rich, equigranular equivalent of porphyritic biotite monzogranite. Metasedimentary inclusions are common (Kjarsgaard *et al*., 2002).

1.2.2 Kimberlite Volcanism and Emplacement

The Central Slave Province was modified by episodic volcanism during the Cretaceous (74 Ma) to Eocene (45 Ma) with the emplacement of a spatially extensive kimberlite field, confirmed chiefly through detailed Rb-Sr dating of macrocrystal phlogopite and ^{238}U-^{206}Pb perovskite dating methods (Davis and Kjarsgaard, 1997; Heaman *et al*., 2003; Creaser *et al.*, 2004; Lockhart *et al*., 2004). There are more than 270 intrusive volcaniclastic kimberlite bodies throughout the

central Slave Province (Kjarsgaard, 1996; Creaser *et al*., 2004). Kimberlites are ultrabasic rocks derived from high-pressure partial melting of the mantle and emplaced as magma is extruded under terrestrial, marginal marine, and possibly even marine conditions (Pell, 1997; Kjarsgaard, 1996; McClenaghan & Kjarsgaard, 2001). Kimberlites contain a unique mineralogical composition that provides a signature for identification during exploration. Kimberlite Indicator Minerals (KIMs) include xenocrysts derived from disaggregated peridotite and eclogite mantle xenoliths (Cr-diopside, Cr-pyrope garnet, Cr-spinel, pyrope-almandine garnet, olivine, enstatite, omphacitic pyroxene, and diamond); the associated megacryst suite of minerals (low-Cr Ti-pyrope, Mg-ilmenite, Cr-diopside, phlogopite, zircon and olivine); and kimberlite-derived phenocrystic olivine, spinel, ilmenite, and diamonds (McClenaghan & Kjarsgaard, 2001; McClenaghan, 2005). During the formation of kimberlites, there is a reaction due to decompression by the high-temperature kimberlite magma during ascension (McClenaghan & Kjarsgaard, 2001) which causes some garnets to be partially covered by kelyphite rims. This is a unique feature for garnets associated with kimberlite and thus can be used as a diagnostic feature. There is also geochemical variation between different groups of kimberlite pipes. There may even be a specific mineral (*e.g*. corundum) present in one group of kimberlites that is absent in another group, that can be used to help fingerprint the KIM signature of a specific group of kimberlites.

The study area contains two recognized groups of kimberlites; CH02 and the Monument group. The CH02 kimberlite pipes were drilled by GGL Diamond Corp. in 2002 and are located ~8 km south of the central zone of the Monument kimberlites (**Figure 1-4**). The CH02 kimberlites do not appear to have an associated indicator mineral train. The Monument kimberlites were drilled by Kennecott Canada Exploration Inc. between 1993-1995 and occur on the southern shore of Lac de Gras within three subgroups, the southern zone, central zone, and northern zone (**Figure 1-4** & **Figure 1-5**). The southern zone consists of three kimberlites, DD39, Sparky, and Gemini. The central zone contains six kimberlites, DD17, Sonja, Nic, RIP, Bling, and DD17-11. The northern zone contains two kimberlites, DD42 and Trio (**Figure 1-5**). The Monument group of kimberlites is important to the study because they are the source for the Monument Indicator Train (MIT), which has been documented and publicly reported in the NTGS NT GoData geoscience database collection (2018a).

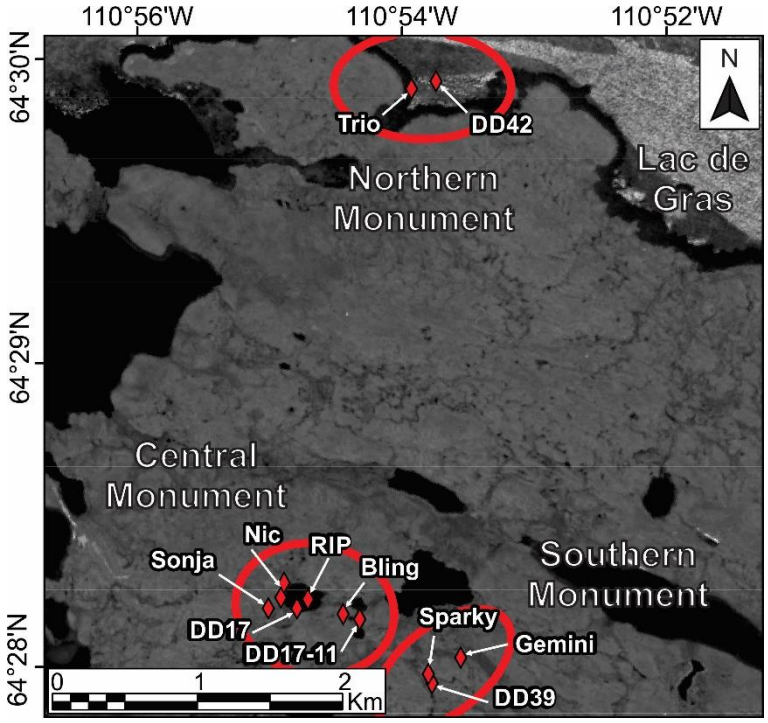

Figure 1-5: Close-up map of Monument kimberlites showing the Northern, Central, and Southern zones with each kimberlite pipe name (Data from NTGS, 2018b).

There is also a second large signal for kimberlites nearby called the Coppermine Indicator Train (CIT) that does not appear to be associated with any known kimberlite deposit (NTGS, 2018b). This unsourced indicator train has been investigated since 2004 using airborne geophysics, till sampling, and drilling (Arctic Star Exploration, 2015; Falck and Gochnauer, 2016). Despite a full suite of KIMs with compositions typical of diamond-bearing kimberlites and displaying signs that the source is nearby (angular KIMs, some with kelyphite rims or attached to kimberlite), no source has been determined (Arctic Star Exploration, 2013a).

Kimberlites often occur in clusters that typically range from 5-10 km across, within fields that can be 30-50 km in diameter (Grégoire *et al*., 2005). The fields make up districts that can be a few hundred kilometres across, and provinces that can be thousands of kilometres across (Grégoire *et al*., 2005). The Monument zones (Northern, Central, and Southern) make up the Monument kimberlite cluster within the larger Lac de Gras kimberlite field, diamond district, and Central Slave geological province. Grégoire *et al*. (2005) proposed a kimberlite production model that identifies the origin of kimberlite melt via dykes that have a lensoidal shape with a typical diameter of ~4 km. These dykes are the source of kimberlite clusters at the surface. These clusters are compositionally similar due to their shared origin and therefore produce a till

signature that can be identified for a specific kimberlite cluster, such as the Monument kimberlite cluster (**Figure 1-5** and **Figure 1-6**).

1.2.3 Regional Glacial History and Surficial Geology

The Geological Survey of Canada started collecting and producing information about the regional glacial geology as early as the late 1800s with expeditions by Tyrrell (1898), mainly along canoe routes such as the Coppermine River, and the Thelon River to the east of the study area. Later in the 1960s, the Glacial Map of Canada was released (Prest *et al*., 1968), which revealed many regional glacial landform features crossing the area in a dominantly southeast-northwest orientation with striations and landforms such as eskers indicating late-stage (deglacial) ice and channelized meltwater flow toward the northwest (**Figure 1-6**). The surficial geology of the Lac de Gras area was later mapped more comprehensively by Ward *et al*. (1995), Ward (1997) and the Geological Survey of Canada (GSC) through helicopter-assisted groundwork including terrain mapping, till sampling, and measuring ice flow indicators. Air photo interpretation (1:60,000 scale) was used in conjunction with field traverses to provide information on the nature and distribution of surface materials (Ward *et al*., 1995; Ward, 1997). The mapping by Ward *et al*. (1995), and Ward (1997) provides a regional framework for geological interpretation, environmental management, and drift prospecting in the central Slave Province. The regional values for KIMs in sediment, as well as regional till geochemical trends were determined in the Lac de Gras area in an attempt to provide background values for future exploration efforts (Dredge *et al*., 1994). The surficial mapping demonstrates that till is the most extensive surficial deposit across the region. Ward *et al*. (1995) recognized one till unit produced by the Laurentide Ice Sheet during late-stage Wisconsinan glaciation, although older tills may exist below the surface in areas where till is thicker. The till was classified into three morpho-sedimentary units based on estimated thickness and surface morphology. The first unit is a till veneer that is <2 metres thick. Areas of till veneer contain bedrock exposures and the landscape conforms to the underlying bedrock morphology. The second unit is a till blanket that is 2 to 10 metres thick, completely covering the underlying bedrock, and is often expressed as gently undulating till plains. The third unit is hummocky till which is 5 to 30 metres thick, completely obscuring the bedrock surface and expressed as hummocks (Dredge *et al*., 1994; Ward *et al*., 1995; Wilkinson *et al*., 2001). While hummocky till occurs on the regional map, it is not present

within my study area. The local till is a silty-sand matrix supported diamicton. The upper meter of the till has been extensively modified by modern permafrost processes, such as cryoturbation and solifluction. Glaciofluvial deposits are found across the study area but are limited in extent, and generally found along narrow corridors associated with eskers and small kame-like mounds. Eskers are found in numerous places throughout the study area and broadly trend from southeast to northwest. The Canadian Geoscience Map (**Figure 1-6**) shows esker locations near the Monument kimberlites and several other locations throughout the study area. There is also a main regional trunk esker ~25 km north of the study area (**Figure 1-7**), suggesting the path of the major drainage system during deglaciation (Brennand, 2000; Menzies, 2002).

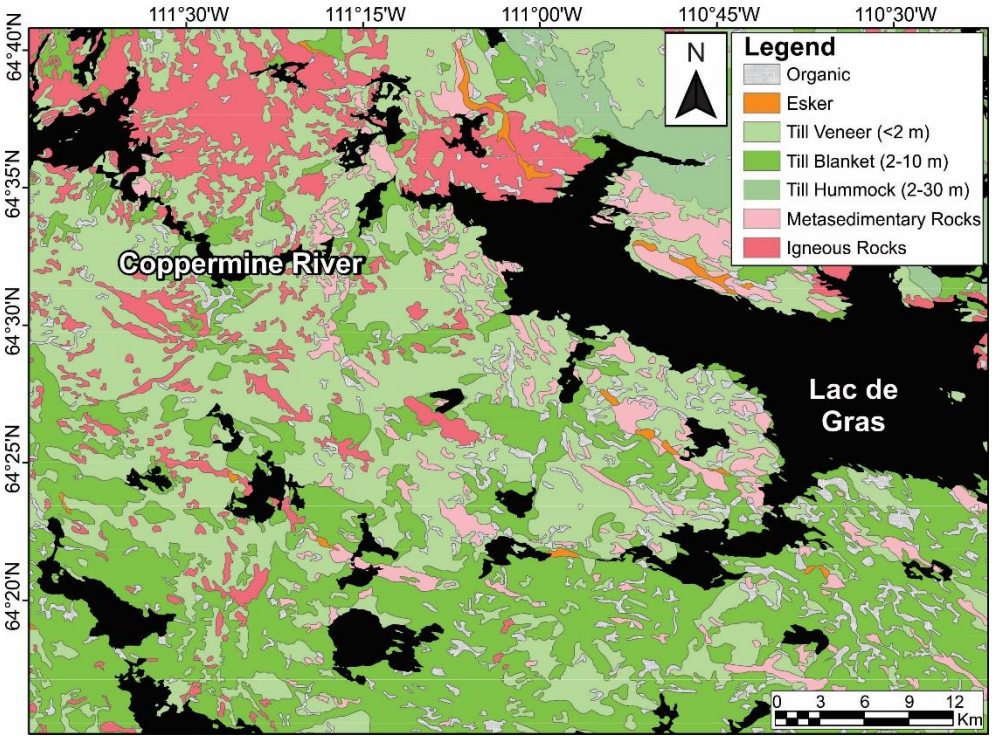

Figure 1-6: Surficial material in the study area. Modified from The Canadian Geoscience Map (Ward *et al*., 1997) and NRCAN (2014).

The study area lies west of the M'Clintock Ice Divide, which was prominent from the late Wisconsinan glacial maximum (19 ka) and remained active until the Younger Dryas (~13 ka) (Dyke & Prest, 1987; Clark *et al*., 2009; Stokes *et al*., 2009). A major shift in ice flow can affect subglacial conditions of an ice sheet, impacting the nature of erosion, down-ice transport, and deposition of sediments (Paulen, 2017). This is important because ice flow indicators measured by Ward *et al*. (1995) document a shift in the direction of regional ice flow in the Lac de Gras

area over time. The relative chronology of the regional ice flow was to the southwest, then west, and finally to the northwest. This relative chronology can also be established in its broader context using the Glacial Map of Canada (Prest *et al*., 1968). Indeed, we can see (**Figure 1-7**) extensive fields of northwest-trending ice flow features of the Lac de Gras area flanked on each side by zones of southwest trending ice flow features. The similarities in the orientation of landforms within these two separated zones suggest they once formed a continuous southwest-trending flowset which was later truncated and erased in their middle portion (the Lac de Gras area) during a younger northwest flow event (**Figure 1-7**).

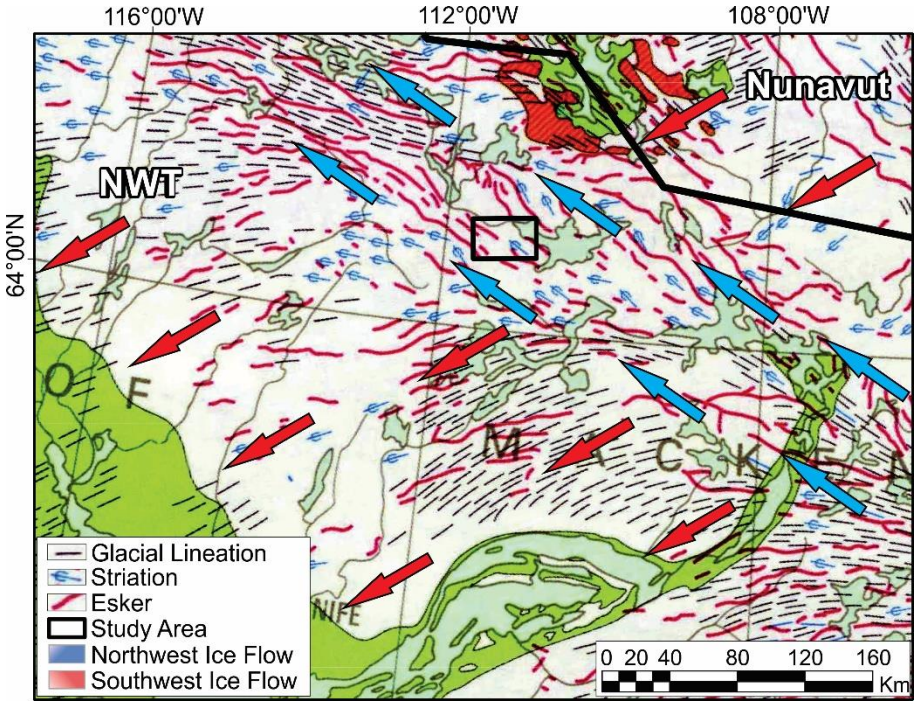

Figure 1-7: The portion of the Glacial Map of Canada by Prest *et al.* (1968) covering the southern and central Northwest Territories. The map has been modified to highlight the features from the southwestern (red) ice flow phase that has been truncated by the northwestern (blue) ice flow phase.

The overall clockwise shift from southwest to northwest is likely due to the southeastern migration of the M'Clintock ice divide, which is an extensive feature in most Laurentide Ice Sheet reconstructions (Dyke *et al*., 1982; Dyke & Dredge, 1989; Ward *et al*., 1995). This interpretation is also supported by more recent modelling experiments (Tarasov & Peltier, 2004; Gowan *et al*., 2016). Fine striations located within the study area were interpreted as late-stage events such as ice creeping towards ice tunnels (eskers) (Ward *et al*., 1995). Based on public datasets, till dispersion appears to be strongly controlled by the northwestern ice flow (Dredge *et*

al., 1994; Ward *et al*., 1995; McClenaghan *et al*., 2002; Arctic Star Exploration, 2013b) (**Figure 1-7**). The Lac de Gras area was deglaciated by 8530 ± 130 ^{14}C years BP based on radiocarbon ages from twigs found in a glaciofluvial deposit in the Aylmer Lake area (southeast of Lac de Gras; Dredge *et al*., 1999; Kjarsgaard *et al*., 2002).

1.2.4 Drift Prospecting

Drift prospecting has become an important method of mineral exploration in glaciated terrains since the pioneering efforts of Grip (1953) and Dreimanis (1956, 1958). Several more recent papers and collections (McClenaghan & Kjarsgaard, 2001; McMartin & Paulen, 2007; Paulen & McClenaghan, 2013; Plouffe *et al*., 2013; McClenaghan & Peter, 2016; McClenaghan & Paulen, 2017) have outlined some of the successes and challenges of the increasing sophistication of drift exploration techniques. Drift prospecting is a common exploration approach used in glaciated terrain which combines knowledge of glacial history (*e.g*. ice flow directions) with information about the spatial extent and concentration of clastic, mineral, and/or geochemical components and to trace them back to their source (Fulton, 1989; Klassen, 2001; Paulen, 2013; Thorleifson, 2017). Geochemical, mineralogical, and lithological methods are employed to identify and outline clastic dispersal trains, which are in turn used to identify and locate mineralized bedrock sources (Parent *et al*., 1996). Dispersal trains are created by glaciers eroding, and entraining clasts from distinctive bedrock source(s) and transporting the debris over distances ranging from a few centimetres to several kilometres (Parent *et al*., 1996). Tracing dispersal trains requires the assessment of indicator mineral character and mapping of concentration gradients. This is supported by the knowledge of past ice flow direction(s) to trace the concentration gradients up-ice. Other variations of glacial dispersal such as glacial sediment thickness, bedrock topography, and bedrock erodibility help to identify complexity that can affect the interpretation of spatial patterns exhibited (McMartin & Paulen, 2007; Paulen, 2013; Thorleifson, 2017). The significance to mineral exploration is the combined knowledge used to determine the up-ice direction and distance of the source mineralization from the much larger, and easier to recognize, down-ice dispersal train (Parent *et al*., 1996; Paulen, 2013).

In Canada, drift prospecting was particularly crucial in the discovery of the first diamondiferous kimberlites in the Northwest Territories (NT) (Fipke *et al*., 1995; Kjarsgaard, 1996) and has

since become a key method in diamond exploration, whether as an initial exploration technique or at more advanced stages to identify and prioritize the most promising geophysical targets under glacial sediment cover (Macnae, 1979; Keating, 1996). As a result, several KIM trains have been identified in the surficial glacial sediments throughout the Lac de Gras area leading to kimberlites. This method of mineral exploration has also played a key role in the discovery of numerous other mineral deposits in Canada and Fennoscandia (Coker *et al*, 1989; Chapman *et al*., 1990; Ashton Mining of Canada Inc., 2000; Harbinger Corp., 2007).

The area near a source of mineralization typically contains the highest concentration of indicator minerals and/or pathfinder elements. This area is described as the "head" of a dispersal train. The area in the down-ice direction that is furthest away from the source, but still contains an anomalous concentration of indicator minerals and/or pathfinder elements, is known as the "tail" of the dispersal train. Indicator minerals and/or pathfinder elements are entrained with the eroded rock/sediment as ice moves over an area of mineralization. Once the indicator minerals/pathfinder elements are entrained, the non-mineralized material in the down ice direction progressively gets mixed with the indicator minerals/pathfinder elements from up-ice. Re-entrainment processes cause the indicator minerals/pathfinder elements to "rise" to the surface as ice continues to migrate in the down-ice direction. The resultant pattern displays a plume of indicators or pathfinders that rises through the till from the source to the till surface (Miller, 1984; Stanley, 2009), with concentration or abundance of indicators/pathfinders diminishing in the down-ice direction in a way that can be sometimes approximated by simple 'decay' functions (Klassen 1997). This conceptual model assumes a single till sheet with one ice flow direction. However, real patterns often deviate from this conceptualization due to complicating factors such as multiple ice flows, sediment re-entrainment, or mixing (dilution) of previous tills with non-mineralized up-ice debris (Parent *et al*., 1996; Paulen, 2017). To help unravel some of these complicating factors, geochemical pathfinder elements can reveal mineralization in till by linking geochemical till associations with rock provenance and mineral assemblages. The major oxide element geochemistry and trace metals are used to relate till composition to bedrock types and mineral assemblages by using the compositional patterns associated with sediment transport direction to vector toward a bedrock source of interest.

The use of glacial sediments for KIM recovery and geochemistry is a mineral exploration approach in Canada and Scandinavia (McClenaghan & Kjarsgaard, 2001; McMartin & Paulen, 2007). Dispersal trains are the net effect of glacial erosion of mineralized bedrock sources, glacial transport, and subglacial deposition as glacial dynamics change over time (Paulen, 2017). In the Lac de Gras area, the trains are often fan-shaped and can extend for tens of kilometres in the direction of the dominant ice flow phase (McClenaghan, 2005). Therefore, the indicator minerals display a dispersed signal that is larger in its aerial footprint than the source (Thorleifson, 2017). The simple one ice-flow event that produces a single till sheet will display a surficial pattern that is linear or ribbon-shaped with sharply defined lateral boundaries that run parallel to the dominant ice flow direction (Miller, 1984; Parent *et al.*, 1996) (**Figure 1-8**: Simple). An exceptional example of a ribbon-shaped dispersal train is ~90 km north of the Lac de Gras area, the Ranch Lake kimberlite, which is 500 metres wide at the head, 2 kilometres wide at the tail, and 20 kilometres long (McClenaghan *et al.*, 2002). Multiple ice-flow events can result in partial re-entrainment in different directions of the material from the first event by the successive event(s). This will result in a composite fan-shaped dispersal pattern (Parent *et al.*, 1996) (**Figure 1-8**: Composite) with multiple and/or composite tail directions controlled by the direction of each successive ice-flow event. These composite trains are created by early ice movement and dispersal of mineral-rich debris, then re-entrained, reworked, and diluted by mineral deficient debris from a later ice flow creating the palimpsest portion of the train.

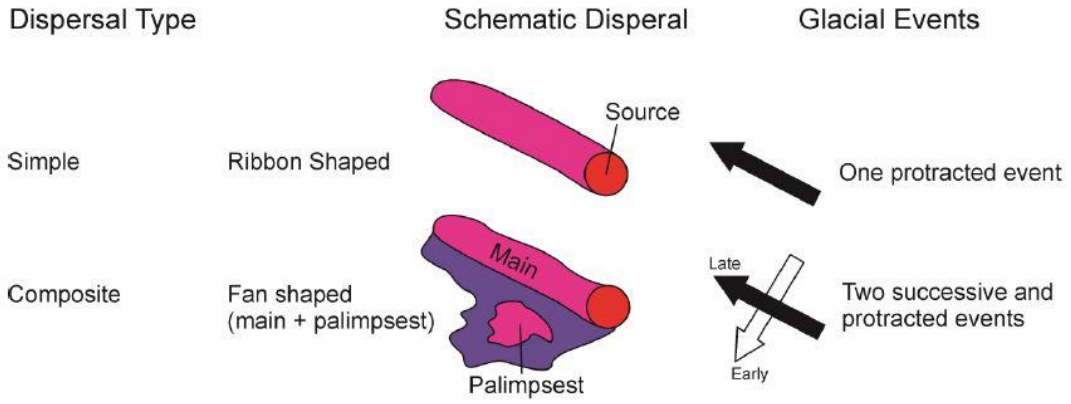

Figure 1-8: Plan view of ribbon-shaped and fan-shaped dispersal patterns that form as a result of different ice flow histories. Modified from Bustard (2016) after Parent et al. (1996).

Geochemical dispersal in areas of thin and/or intermittent drift is also examined to enhance the interpretation of dispersal patterns. Till that has been entrained directly by an ice sheet, then

transported and deposited at or near the base of the ice sheet is termed subglacial till. Subglacial till is the ideal sample media because it is closely related to the underlying bedrock through short-distance transport of material from the most recent ice flow and deposited in areas directly down-ice from its source (Levson, 2001; Benn & Evans, 2014). When it contains anomalous mineralogical or geochemical quantities, it can be closely associated with its bedrock source mineralization (Levson, 2001). In the Lac de Gras area, geochemical element concentrations are variable in areas of till veneer on the surficial geology map (**Figure 1-6**), as till veneers are more sensitive to local variations in the composition of bedrock than till collected from blankets or hummocks (Ward *et al*., 1996). However, complicating factors may exist requiring further investigation to accurately trace mineral indicators back to their source (Parent *et al*., 1996; Stea & Finck, 2001; Klassen, 2001; Trommelen *et al*., 2013). Distal material may cap the locally derived till, preventing it from being exposed at the surface (Hooke *et al.*, 2013). Mixing and overprinting of till from differing sediment sources may result from a change in the ice flow direction (Trommelen *et al*., 2013). Indicator minerals and/or geochemical pathfinders in till may also create a "skip zone" due to the capping or sheltering of the up-ice source material (Stea and Finck, 2001).

Dispersal patterns in till are often expressed in a two-dimensional shape because they are based on data from surficial samples only. In permafrost terrains such as the central Slave Province, well-developed soil horizons are absent due to the formation of mudboils. Mudboils are formed when a poorly sorted sediment is at its liquid limit and driven to the surface in a diapiric fashion by hydrostatic or cryostatic forces (Shilts, 1977). Therefore, this is the best representative surficial sample media for till sampling in glaciated terrain because the surficial material (<2 m) is mixed creating a homogeneous surficial sediment. However, overburden drilling may be necessary for areas of glacial sediments that exceed two metres to characterize till deeper than the active layer (McMartin & McClenaghan, 2001; Thorleifson, 2017). Drilling allows for the identification of separate characteristics throughout the till column by collecting samples that characterize possible till stratigraphy or vertical variations in till geochemistry and/or indicator minerals (McMartin & McClenaghan, 2001). Sampling the drilled material at regular intervals allows any change in composition to be characterized. Palimpsest dispersal patterns may also be recognized using this technique by identifying a shift in till provenance deeper in the till column. Some areas, such as Lac de Gras, may contain till that has been produced as a result of the

recognized changing ice flow conditions, in addition to both thin/intermittent and thicker drift. This complex glacial history requires a combination of surficial sampling and downhole drill data to fully characterize till dispersal patterns.

1.2.5 Slave Province Kimberlite Exploration and Pipe Identification

Charles Fipke and Stewart Blusson discovered the first kimberlites in the Slave Geological Province in September of 1991 following 10 years of systematic heavy mineral sampling (Fipke *et al*., 1995). High concentrations of KIMs were found in a series of sediment samples near Blackwater Lake, NT. The elevated number of KIMs were tracked 300 km east, up paleo-ice flow, following a regional trunk esker (Fipke *et al*., 1995; Kjarsgaard, 1996). An anomalous number of KIMs were found to the north of Lac de Gras, but there was a lack of anomalous KIMs to the east of the area, indicating the kimberlite source for the indicator minerals was somewhere near the head of the train (Fipke *et al*., 1995). A high-density sampling campaign was initiated north of Lac de Gras and identified a target which lead to the discovery of a diamondiferous kimberlite. This triggered one of the most prolific claim staking rushes in Canadian history (Fipke *et al*., 1995; Kjarsgaard, 1996; Pell, 1997).

Bulk sediment sampling of eskers, stream sediments, and till for KIMs has since continued to play an important role for kimberlite exploration in the Slave Province. Regional results lead diamond exploration companies to a region; then aeromagnetic and gravity surveys are used to identify targets, which can be further assessed through denser till sampling and analysis. Results at that scale are used to prioritize drilling of the most promising targets. The targets identified in the Lac de Gras region using airborne electromagnetic surveys did help to locate conspicuous kimberlite targets, which have since been evaluated. Some kimberlites in NT do not have a clear geophysical signature and may be missed by some surveys, whereas others occur in dykes rather than pipes, which may complicate their identification because these often form non-circular features that may be difficult to recognize as important targets in diamond exploration (Keating & Sailhac, 2004). Overall, geophysics often identifies many targets that are not related to kimberlite deposits (Keating & Sailhac, 2004), meaning further analysis is needed to properly identify kimberlitic targets. Drift prospecting can help reduce the number of targets of interest (or help prioritize targets) by examining regional surveys of KIMs and till geochemical

pathfinder elements and comparing the regional background values against anomalous values. Industry has begun to selectively examine previously discovered targets in detail with the hope that advancements in exploration will uncover a missed or misinterpreted deposit. This renewed diamond interest in the Northwest Territories has focused on more complex targets where till sampling suggests the potential for high-grade deposits.

1.2.6 Knowledge Gaps, Important Research Questions, and Opportunities

Knowledge gaps regarding the Quaternary geology of the region include:

- Known changing ice flow conditions through remote and surficial ground observations but limited knowledge of the depositional imprint and till production resulting from each successive ice flow. There is only one recognized till sheet (Ward *et al*., 1995) and no known stratigraphy but the change in ice flow direction suggests there may be either multiple till units and/or a change in the vertical till composition preserved at depth where till is thicker.

- Publicly available data suggests there are two kimberlite indicator mineral trains within a well-explored area to the south and west of Lac de Gras. Of these two trains, only one has a known source. Industry has spent millions of dollars and multiple years conducting airborne surveys, till sampling, ground geophysics, and diamond drilling looking for the origin of the other indicator train with no success. Therefore, the KIMs are either present in the till of the second train because they are from a unique source that has yet to be identified or they are from a known source in a detached location (*e.g*. Monument Field) due to complex ice flow history and till re-entrainment processes.

- Available data is surficial. Therefore, little is known about subsurface composition that may be the key to identifying possible inheritance, overprinting, and/or mixing of sediments that are causing some of the patterns observed at the surface.

Important research questions regarding the Lac de Gras study area are:

- Why is there a second indicator train within the study area but no known source despite extensive exploration effort?

- Are there similarities or differences between the two mineral indicator trains?
- What is the effect of multiple ice-flow directions on the till production and mineral entrainment in the study area?
- What role does the underlying bedrock play in delineating the surficial and subsurface pattern of the indicator mineral trains?

Unique opportunities presented to investigate the complex glacial geology of the Lac de Gras study area includes:

- A new drilling program by the NTGS providing data from 52 reverse circulation (RC) drill holes and 155 samples.
- Access to the remote field area through collaborative work with the NTGS to collect new observations and samples.

1.3 Thesis Objectives

This research is a component of a larger study, the Slave Province Surficial Materials and Permafrost Study (SPSMPS), whose main aspects include an RC drilling campaign, surficial geological mapping, and permafrost monitoring (Elliott, 2015). The research of this thesis focuses on glacial geology. More specifically, it looks at the questions of ice flow shifts, bedrock topography and till thickness variations and the net effect on till dispersion both at the surface and in the subsurface. Based on the knowledge of a clockwise ice flow shift record in the region (Ward *et al*., 1995), two main hypotheses are considered for till entrainment. The **first hypothesis** is that the young northwest ice flow event was sufficiently strong to completely overprint till composition in the Lac de Gras area. In this hypothesis, the influence from the clockwise ice flow shift, as reconstructed by Ward *et al.* (1995) and based on the erosional record, is not preserved in the till at surface and at depth in the form of more complex (*e.g.* fan-shaped) patterns. The **alternate hypothesis** is that the northwest ice flow event did not completely rework till deposited before and/or during the clockwise ice flow shift. In this hypothesis, till at the surface and/or the subsurface, where till is thicker, would contain evidence of a shift in provenance or contrasting composition patterns extending in more than one of the

known ice-flow directions. Based on the current state of knowledge regarding till transport and depositional processes, the second hypothesis is more likely because till is typically deposited in a time-transgressive manner and is more rarely completely re-entrained and homogenized following a shift of ice flow direction. Nonetheless, the known surficial patterns are strongly aligned with the young NW ice flow direction; therefore, the first hypothesis of a single till dispersal direction cannot be ruled out. In the case of the first hypothesis, compositional differences at depth would be explained by a difference in provenance distance, whereas the alternate hypothesis involves a time-transgressive shift in provenance vectors. These things should be testable through careful compositional and spatial analysis of geological information. The specific goals of this study are thus:

1. Add and analyze local ice flow indicators to further constrain the local ice flow history and better understand the main mechanism of subglacial erosion and subglacial flow conditions associated with known clockwise ice flow shift;

2. Analyze the general characteristics and composition of surficial till along selected transects corresponding to well-known KIM dispersal patterns in the study area to better understand surficial till provenance and how the major compositional components (*e,g.* detrital lithologies) vary along the dispersal transects and across bedrock geological contacts;

3. Characterize surface and subsurface till matrix composition with a focus on major oxides and KIM indicators and geochemical pathfinders to determine whether there are clear changes both horizontally across the study area and at depth from one borehole to the next;

4. From the analysis in (3), determine whether the till could have been deposited by a single dominant NW ice flow in the study area or whether there is clear evidence in the available depositional record for palimpsest dispersal patterns inherited from older ice flow phases preserved in the study area;

5. Explore the possible implications of the research findings on the problem of the origin of the CIT.

These objectives will be achieved through mapping and analyzing ice flow and till compositional data and their spatial patterns. Results will be used to test the two hypotheses stated above; *i.e.*, 1- different patterns but single ice flow or 2- different patterns because of a change in the flow direction. As is often the case in geosciences, the available data may allow only partially testing the hypotheses, but insights should be gained to make progress and suggest future directions. The research may also contribute to explaining the CIT with an unknown source (*e.g.* the train is detached from its source due to ice-flow shifts and re-entrainment) (Objective 3).

This research will help extend the regional shape of known dispersal trains into the subsurface and relate it to the ice flow history reconstructed using landforms and striations. This will help improve our understanding of how till was produced and by which ice flow phase through its full thickness by identifying till provenance. This will contribute to understanding the known dispersal trains, identifying new ones, and ultimately giving industry new knowledge to provide additional information about possible associations to older ice flow phases and potential kimberlite source areas for the patterns displayed.

Through identification and visualization of the compositional signature of kimberlite source(s) in both the surface and the subsurface, till dispersal plume(s) can be identified using the third dimension. The data integration will help identify differences between dispersal patterns expressed in the subsurface and those identified at the surface. These patterns could relate to ice flow events delineating the erosional and depositional records. This will enhance our understanding of the complex depositional history and glacial processes that most influence the shape and dispersal of glacial sediments.

1.4 Methodology Overview

To understand the glacial geology of the study area and investigate kimberlite indicator mineral trains through drift prospecting, a combination of remote, field-based and laboratory methods are adopted. Helicopter assisted fieldwork is used to investigate the glacial record through outcrop ice flow indicator mapping, sediment sampling, and pebble lithology identification, while a drilling campaign provides sampling of subsurface till from which data about till thickness, character, KIMs, and geochemistry are obtained. This multi-faceted approach allows for a comprehensive evaluation of the glacial record of the region.

1.4.1 Sampling Procedures

The logistics of drilling in the tundra are complicated but RC drilling is well-suited to glaciated terrain (Averill, 1978; Skinner, 1972; Thorleifson, 2017). A portable RC rig was transported by Snowcat for the SPSMPS drilling program. The RC drilling program was carried out at 52 sites within the study area. Samples were taken at 1.5 m intervals from the surface to the top of bedrock and collected in buckets. This resulted in 155 samples (typically 2-3 samples per hole) with an average weight of ~20 kg per sample. The buckets of sample material were sent directly to Saskatchewan Research Council Geoanalytical Laboratories (SRC) for analyses. In addition, helicopter assisted sampling resulted in the retrieval of 15 hand-dug surficial samples from mud boils following standard procedures for northern terrain as developed by McMartin and McClenaghan (2001) and used for various analysis (*e.g.*, grain size, clast lithology classification). Clast lithology was conducted using 2 methods. The first was in the field, picking pebbles and sorting them according to their lithology (metasedimentary, pink igneous, white igneous, and mafic). The second was by picking the pebbles from the 4-8 mm size fraction of the sieved samples and sorting them according to the same lithology classification.

1.4.2 Kimberlite Indicator Mineral Analysis

KIM analysis was carried out on all RC and hand-dug samples at SRC in Saskatoon, SK, using the kimberlite indicator minerals recovery package. Heavy mineral concentrates were extracted following standard procedures and KIMs were picked from the <1.00 mm and >0.50 mm size fraction being referred to as the "coarse" fraction, and the <0.50 mm and >0.25 mm size fraction being referred to as the "fine" fraction. The KIMs picked for analysis were peridotitic pyrope (Cr-pyrope), eclogitic pyrope (Ti-pyrope), Cr-diopside, olivine, picroilmenite (Mg-ilmenite), and chromite. A full description of analytical techniques can be found in chapter 3.

1.4.3 Geochemical Pathfinder Analysis and matrix characterization

Geochemical pathfinder analysis was conducted on the <63 µm size fraction at SRC in Saskatoon, SK, using the ICPMS2, WR1, and AU1 packages. The ICPMS2 "Basement Exploration Package" analyzed each sample using an 8:1 HNO_3: HCl digestion by Inductively Coupled Plasma-Mass Spectrometry (ICP-MS) for 44 elements. The WR1 "Whole Rock

Analysis Package" analyzed each sample using lithium metaborate fusion by Inductively Coupled Plasma-Optical Emission Spectrometry (ICP-OES) for 16 elements/oxides and loss on ignition (LOI). The AU1 "Gold by Fire Assay Package" analyzed each sample using fire assay fusion by ICP-OES and/or Inductively Coupled Plasma-Atomic Absorption Spectrometry (ICP-AAS) for gold. Grain size analysis was conducted on all samples to compliment the geochemical data. The 15 hand-dug samples were analyzed at the University of Waterloo by laser diffraction using a Fritsch Analysette 22. The grain size and major element data are analyzed and described in chapter 2. The data can be found in the appendices. The full description of geochemical pathfinder analytical techniques can be found in chapter 3, as well as the data in the appendices.

1.4.4 Quality Assurance/Quality Control (QA/QC)

Several procedures were undertaken to ensure proper quality assurance and quality control for the geochemical analyses and KIM identification. All geochemical and KIM analyses were completed at SRC for consistency. The surficial hand samples and the drilled RC samples were sent to SRC and analyzed separately, but SRC delivers the same QA/QC procedures for all analyses. These include data verifying procedures through the preparation and analysis of in-house standards, replicates, and blanks for the whole rock and trace element geochemistry. In addition, the hand samples were sent to SRC with two standards from the CANMET laboratories certified geochemical soil and till reference materials. Once all results were obtained, the duplicates (geochemistry) and repeats (KIMs) were assessed using scatterplots as outlined by Piercey (2014) to validate the results. The details of the QA/QC procedure and results can be found in the appendices of chapters 2 and 3.

1.4.5 Statistical Analysis

Statistical analysis of the KIM and geochemical pathfinder data was completed using exploratory data analysis techniques as outlined by McClenaghan & Kjarsgaard (2001) and Grunsky (2010). These techniques include the construction of histograms, probability plots, quantile-quantile (Q-Q) plots, and scatterplot matrices. A principal component analysis (PCA) was also carried out on the major geochemical oxides in chapter 2, as well as on the geochemical pathfinder elements of kimberlites in chapter 3.

1.4.6 Data Visualization

Visualization of the KIM and geochemical pathfinder data was carried out with several software programs. Plots for basic geochemical data (*e.g.*, scatterplots, histograms, ternary diagrams) were constructed using ioGAS (Reflex) and MS Excel. ArcGIS® (ESRI) was used to produce maps, including KIM distribution and geochemical pathfinder distribution maps.

1.5 Thesis Structure

This thesis contains an abstract, an introduction chapter (Chapter 1), two chapters designed to be released as individual scientific journal articles (Chapters 2 and 3), and a conclusion chapter (Chapter 4). Chapter 1 introduces the overall topic with a relevant review of literature and background information, as well as the research problem, thesis objectives, and research methodology.

Chapter 2 is co-authored with supervisor Dr. Martin Ross (Waterloo) and Dr. Samuel Kelley (now Assistant Professor at University College Dublin), who was a post-doctoral fellow at the University of Waterloo for the main duration of this research. Chapter 2 is the first part paper detailing the provenance of till related to dispersal under multiple, time-transgressive, ice flow movements. A principal component analysis is used to determine major oxide associations of till with the bedrock source areas. Reverse Circulation drilling information is provided by the Northwest Territories Geological Survey from a 2015 winter drilling campaign. Fieldwork was supported by the NTGS and conducted during the summer of 2015 with the help of Dr. Samuel Kelley and Philippe Normandeau. I was jointly responsible for data collection of glacial features, clast lithology classifications, and surficial samples, as well as interpretation, presentation, and writing.

Chapter 3 is also co-authored with supervisor Dr. Martin Ross and Dr. Samuel Kelley. This chapter is the second part paper and describes the association of kimberlite indicator minerals and geochemical pathfinder elements with a known kimberlite source area, as well as an inferred association with an unknown source of kimberlitic material. The spatial patterns associated with the KIMs and geochemical pathfinders have been influenced by regionally shifting ice flow patterns. The NTGS generously provided the RC drilling information from the 2015 winter

drilling campaign. I conducted a summer field season in 2015 with Drs. Samuel Kelley and Philippe Normandeau. Together we collected information on the glacial features and retrieved field samples for further analysis. I was responsible for interpreting and presenting the results, as well as writing. I conducted the lab work of the till sieving and laser grain size analyses, and additional clast lithology classifications at the University of Waterloo.

Chapter 4 summarizes the results of Chapters 2 and 3 while also discussing the implications of this study.

Chapter 2: Till provenance southwest of Lac de Gras, NT; implications for NW Laurentide Ice Sheet history and diamond exploration

2.1 Introduction

The northwest sector of the Laurentide Ice Sheet (LIS) has been extensively studied to understand its maximum extent, ice margin configuration, and processes at different times (Dyke *et al*., 2002; England *et al*., 2009; Kennedy *et al*., 2010; Lakeman and England, 2012, 2013; Lacelle *et al*., 2013), as well as its paleo-ice stream dynamics (Stokes *et al*., 2005, 2006, 2008), and its interaction with glacial lakes and their drainage routing to the Arctic Ocean (Teller *et al*., 2005; Couch and Eyles, 2008; Murton *et al*., 2010). The region also has, in places, rich Quaternary stratigraphic records (Lakeman and England, 2014). The glacial record of the vast interior regions, far away from the margins at the maximum extent and towards the ice divide of the northwestern LIS sector show well-preserved subglacial landscapes (Ward *et al*., 1994; Brown *et al*., 2011) and several glacial sediment dispersal trains (McClenaghan *et al*., 2002; Paulen *et al*., 2013; Sharpe *et al*., 2017). Despite this considerable knowledge, important questions remain about the net effect of the different ice flow phases on the landscape and the glacial sediments of the interior regions. In certain areas, till appears to have been produced by a single dominant ice flow phase (*e.g.* McClenaghan *et al*., 2002, Sharpe *et al*., 2017), whereas in other areas till compositional patterns seem to record sediment re-entrainment from different ice flow phases identified in the erosional record (Stea *et al*., 2009; Paulen *et al*., 2013). This suggests important differences in subglacial conditions at different times and places leading to till production and/or re-entrainment or preservation of previously deposited sediment. Understanding these effects and the regional patterns of till composition and related provenance has important implications for determining the main erosional and till production events and in understanding subglacial conditions at a regional scale.

The Lac de Gras area in the Northwest Territories (NT) is of particular interest because several regional ice flow phases have been recognized in the landscape and striation records (Ward *et al*., 1995); yet few recent studies have looked at till composition and dispersal patterns in this region. This area is also one of the world's major diamond districts where indicator mineral tracing in till has been successfully employed in exploration for over two decades (Fipke *et al*.,

1995; Bryan and Bonner, 2003). The few published indicator mineral dispersal trains in this area mainly show unidirectional transport directions in the form of relatively narrow ribbon-shaped trains in the surficial glacial sediments (*e.g.* Armstrong, 2003), except when subsurface data are considered (Kelley *et al*., 2019). However, some surficial dispersal trains have remained unexplained under this simple scenario of one dominant ice flow phase producing unidirectional till dispersal patterns (McClenaghan and Kjarsgaard, 2007). This problem has raised several questions regarding till production and the possible effects of shifting glacial dynamics. Numerous subglacial processes are involved in producing till (Evans *et al*., 2006) and several factors (*e.g*. ice flow direction, glacial processes, bedrock geology, and topography) can have important effects on till composition (*e.g.* Kelley *et al*., 2019). A better understanding of the local subglacial record with a focus on ice flow and till provenance in the Lac de Gras area could bring important insights into the glacial dynamics and related sediment transport history with implications on indicator mineral studies and, possibly, for the broader LIS dynamics.

This Chapter describes the ice flow record and till composition southwest of Lac de Gras using both surficial and subsurface information, which is then used to better constrain and understand the subglacial conditions that led to till erosion, transport, and deposition in this region.

2.1.1 Study Location and Physiographic Setting

The study area is situated ~300 km northeast of Yellowknife, Northwest Territories, within NTS map sheet 76D (**Figure 2-1A**) to the south and west of Lac de Gras, NT. It encompasses an area of approximately 700 km^2 (**Figure 2-1B**).

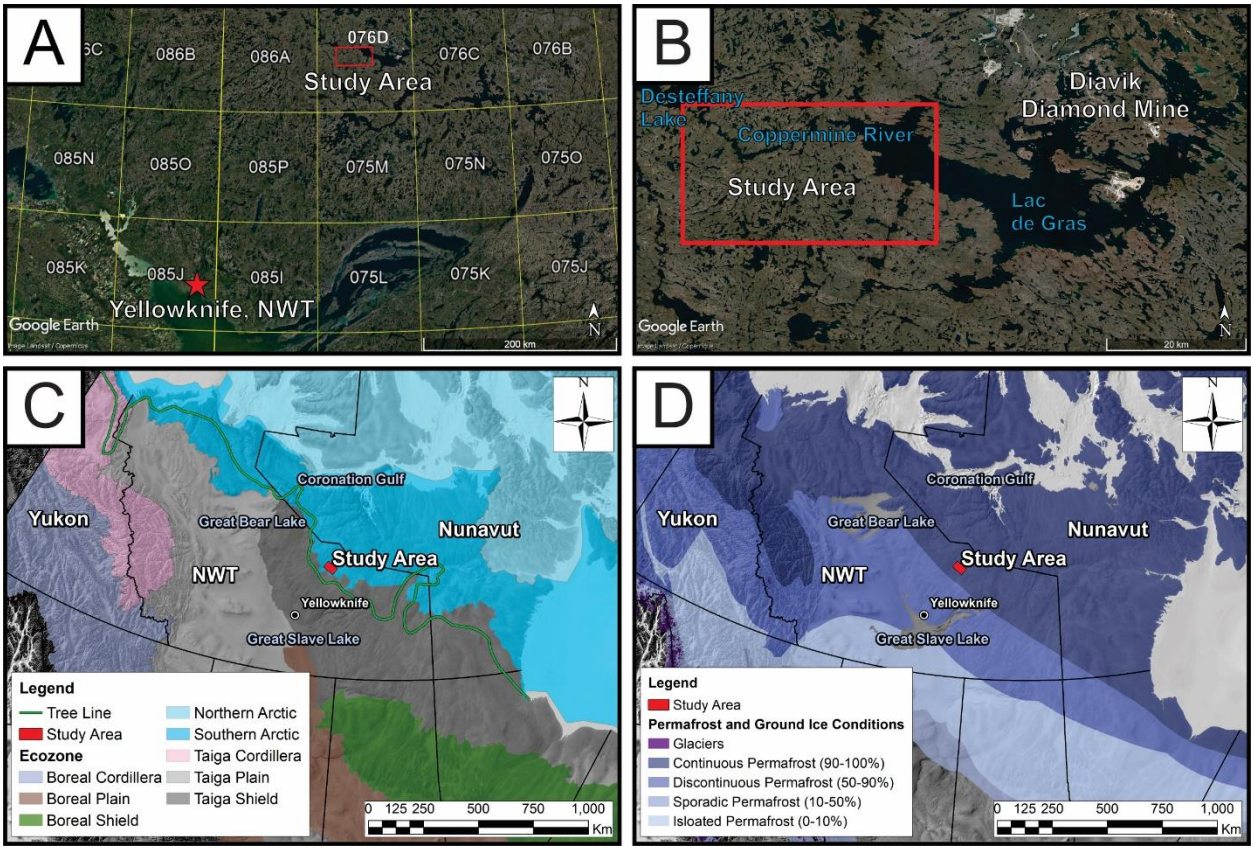

Figure 2-1: The study area is located A) ~300 km NE of Yellowknife within NTS map sheet 76D (NRCAN, 2014); B) west of Diavik Diamond mine and southwest of Lac de Gras (Google Earth, 2016); C) within the southern arctic ecozone (bright blue band) and north of the tree line(green line is northernmost tree growth) (modified from Ecological Stratification Working Group, 1996); D) within the zone of continuous permafrost (dark blue area) (modified from Brown *et al*., 1997).

Generally, the study area has low relief defined by topographic variations that are controlled by bedrock ridges. Elevation ranges from 395 to 511 masl. There are numerous small lakes in the area, but there are also some larger lakes such as Lac de Gras to the northeast and Desteffany Lake to the northwest of the study area. These larger lakes border the study area with the Coppermine River flowing from Lac de Gras to Desteffany Lake. The smaller lakes appear to occupy topographic lows created by glacially scoured bedrock. Wetlands appear to occupy depressions in the till surface. Local drainage consists primarily of small streams occupying depressions or sometimes creating minor incisions into the till surface that trend toward the large lakes at the edge of the study area. The Coppermine River is the modern regional trunk drainage that flows to the northwest and ultimately discharges into the Coronation Gulf of the Arctic Ocean. There are many areas of thin till mapped as till veneers (<2 m thick), and till blankets (2-10 m thick) (Ward *et al*., 1995). The study area is within the Southern Arctic ecozone and

classified as Tundra Shield upland in the Point Upland Low Arctic south ecoregion (Ecosystem Classification Group, 2012). The study area is also situated north of the tree line (**Figure 2-C**). There are limited strands of stunted white and black spruce, as well as dwarf birch trees located within the lowlands near the Coppermine River (**Figure 2-2A**). Permafrost is continuous (**Figure 2-D** and **Figure 2-2B**) and frost-shattered bedrock is prevalent, especially in the eastern part of the field area.

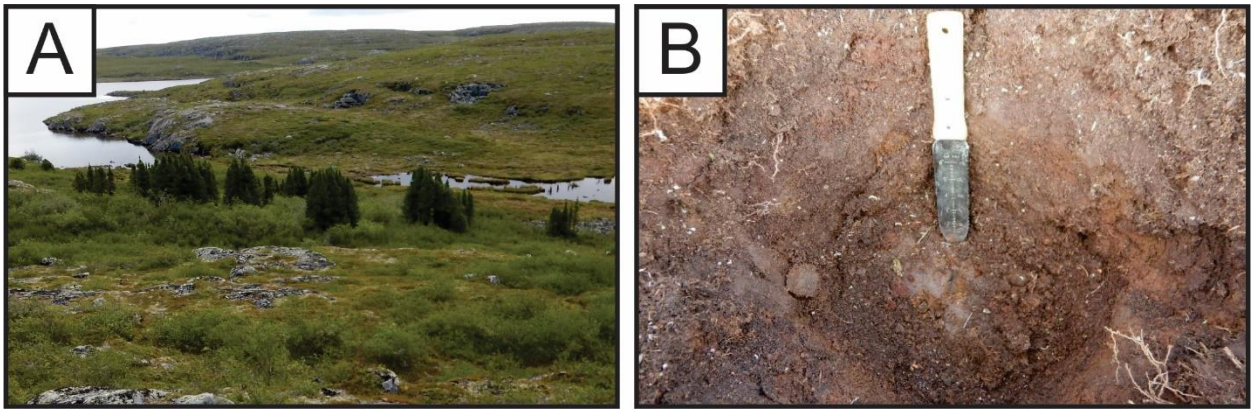

Figure 2-2: A) Landscape photo showing key features. Tributary (right center) leading to the Coppermine River (Left) with stunted white spruce pine trees. B) Shallow hand-dug pit (trowel is ~30 cm) showing soil, oxidized sediment, and permafrost (ice) in the bottom (light brown to grey).

2.2 Geologic Setting

2.2.1 Bedrock Geology

Till is a derivative of bedrock and is the primary cover in glaciated terrain (Klassen, 1997; McMartin and McClenaghan, 2001). Thus, understanding the extent and composition of local bedrock is key to interpreting till deposits. The bedrock geology of the Lac de Gras study area consists of five primary bedrock units (Kjarsgaard *et al*., 2002):

1- pre- to syn-Yellowknife Supergroup gneiss, migmatite, and metagranitoid rocks;
2- Yellowknife Supergroup volcanic and volcaniclastic rocks; and syn-Yellowknife Supergroup mafic intrusive rocks;
3- Yellowknife Supergroup sedimentary rocks;
4- syn-Yellowknife Supergroup granitoid rocks; and
5- post-Yellowknife Supergroup granites.

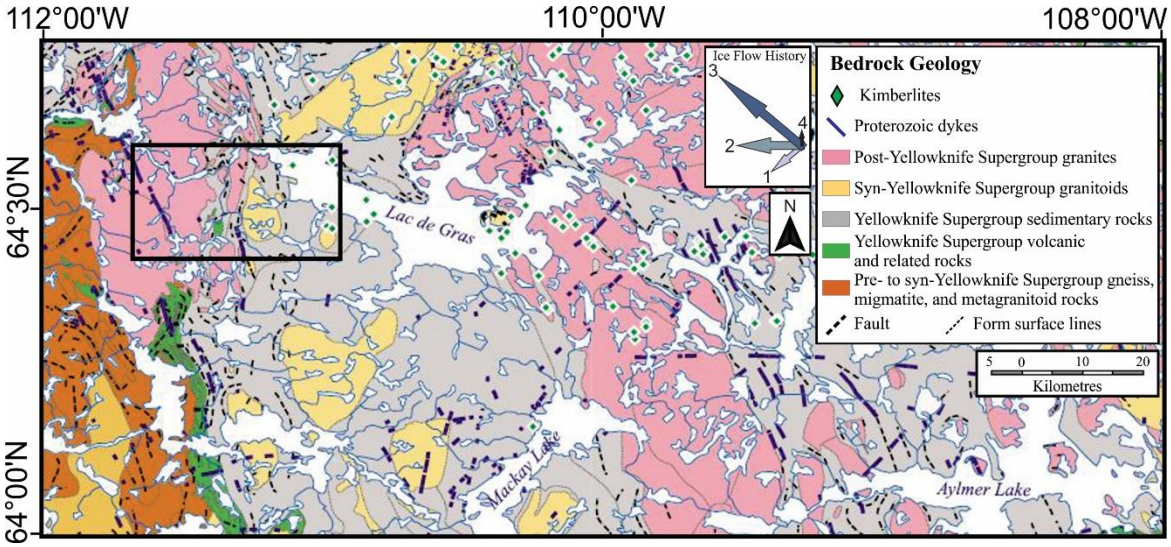

Figure 2-3: Generalized bedrock map of the Central Slave Geological Province. The study area is outlined. Annotated from Kjarsgaard *et al*. (2002).

The Central Slave Province can be characterized as a typical Archean granite-greenstone terrane consisting of sedimentary and volcanic sequences intruded by granitoid rocks (Davis, 1991). The distribution of these rock types is generally defined for the Lac de Gras area. The pre- to syn-Yellowknife Supergroup gneiss, migmatite, and metagranitoid rocks were deposited first, ranging in age from ~2900 to 2681 Ma (Kjarsgaard, *et al*., 2002) but have also been estimated up to 3960 Ma (Davis, 1991). They are located west and southwest of the study area (**Figure 2-3**; Dark Brown). Volcanism then occurred between 2729 to 2701 Ma (Kjarsgaard, *et al*., 2002), emplacing belts such as the Yellowknife supergroup volcanic and related rocks (**Figure 2-3**; Dark Green). These are found trending in a north-south band, as well as a small occurrence in the south-southwest of the study area. The Yellowknife Supergroup sedimentary rocks (**Figure 2-3**; Grey) were deposited before 2637 Ma (Kjarsgaard, *et al*., 2002). These are found throughout the Slave province and are found in the eastern half of the study area. Plutonism occurred across the Slave Province from ~2650 to 2608 Ma forming the syn-depositional Yellowknife Supergroup granitoids (**Figure 2-3**; White) located in the central study area and a smaller area in the southeast of the study area. Plutonic rocks continued to form from ~2599 to 2580 Ma as the post-depositional Yellowknife Supergroup granites (**Figure 2-3**; Pink). These rocks are found across the western half of the study area and into a mixed area with the sedimentary rocks in the central study area. Metamorphism of the sedimentary rocks occurred as a result of the plutonism that occurred. Proterozoic diabase dykes then intruded the Slave Province (Kjarsgaard, *et al*., 2002), with occurrences in the western and south-central study area.

The main bedrock units of the Slave Province were analyzed for major element geochemistry by Davis (1991) using atomic absorption spectrophotometry. The bedrock types described by Davis (1991) are reclassified to be described as either metasedimentary (Yellowknife Supergroup sedimentary rocks), pink igneous (post-Yellowknife Supergroup granites), white igneous (syn-Yellowknife Supergroup granitoid rocks), felsic (Yellowknife Supergroup volcanic and volcaniclastic rocks), or mafic (syn-Yellowknife Supergroup mafic intrusive rocks) (Davis, 1991; Kjarsgaard *et al.*, 2002). This reclassification permits the data to be consistently contrasted and compared. The rock groups chosen in the Davis (1991) dataset are composed of several data points that have been averaged to identify the major geochemistry of each. These rock types are the metasedimentary turbidite sequences (n=9) correlated with the metasedimentary rocks; the Yamba (Wolverine) monzogranite (n=4) associated with the pink igneous rocks; the Concession plutonic suite (n=11) associated with the white igneous rocks; the Wishbone felsic plutonic suite (n=8) associated with the mafic rocks; and the Central Volcanic Belt rocks (n=10) associated with the mafic rocks. The major geochemical data for each rock type in the study area was averaged and summarized below (**Table 2-1**).

Table 2-1: Average geochemical composition for each rock type within the Lac de Gras study area. Major element oxide geochemistry from Davis (1991) was determined by atomic absorption spectrophotometry.

	Metasedimentary Turbidite Sequences (n=9)	Yamba (Wolverine) Monzogranite (Pink Igneous) (n=4)	Concession Plutonic Suite (Hornblende-Biotite/ Diorite) (White Igneous) (n=11)	Wishbone Felsic Plutonic Suite (n=8)	Central Volcanic Belt (CVB) and associated Mafic Rocks (n=10)
SiO_2 (wt. %)	60.30	74.59	62.44	77.25	65.30
TiO_2 (wt. %)	0.92	0.30	0.57	0.15	0.67
Al_2O_3 (wt. %)	18.32	13.71	16.19	12.44	14.65
FeO (wt. %)	9.55	1.59	5.05	1.40	5.60
MnO (wt. %)	0.06	0.01	0.08	0.03	0.10
MgO (wt%)	4.64	0.50	3.55	0.33	3.64
CaO (wt. %)	2.74	1.04	4.90	1.12	5.05
Na_2O (wt. %)	1.09	3.23	4.56	4.03	3.83
K_2O (wt. %)	2.68	4.98	2.36	3.23	1.08
P_2O_5 (wt. %)	0.14	0.05	0.26	0.02	0.19

2.2.2 Glacial History

The Laurentide Ice Sheet (LIS) covered much of Canada and parts of the USA with multiple ice domes during the Last Glacial Maximum (LGM) at ~20 ka (Dyke *et al*., 2002; Dyke, 2004). The Keewatin ice dome covered a large internal region of the LIS during the LGM (Dyke and Prest, 1987). The ice divide extended outward from the thick ice dome, separating the main flow systems creating the M'Clintock Ice Divide. The ice divide was oriented north to south over the study area and is thought to have migrated eastward due to the gradual translocation of the Keewatin ice dome (McMartin and Henderson, 2004) until reaching its final position in eastern Keewatin late in the deglaciation (Dyke and Prest 1987; Ward *et al*., 1995; Dyke *et al*., 2002; McMartin and Henderson 2004; Tarasov and Peltier, 2004; Gowan *et al*., 2016). The ice flow record of the Lac de Gras area shows a clockwise shift due to the movement of the ice dome. The oldest ice flow is southwest trending, the second is westward, and the third is to the northwest. There is also scarce evidence for a fourth weak northern flow (Ward *et al*., 1997).

2.3 Methods

To understand the subglacial conditions that led to till erosion, transport, and deposition in the Lac de Gras region, this research uses a combination of techniques. This includes measurements of ice flow indicators, as well as till texture and compositional analyses of hand-dug surficial till samples, and reverse circulation (RC) drilled subsurface till samples. The sub-sections below provide specific details about each of the methods used.

2.3.1 Ice Flow Indicators

Previous work provided important information about the ice flow history of the region. Ward *et al*. (1995) identified a clockwise shift from the southwest (oldest) to the northwest (youngest) across the region, which is broadly consistent with the regional observations reported on the Glacial Map of Canada (Prest *et al*., 1968). In this study, one of the goals was to augment this knowledge base by collecting additional measurements of ice flow indicators to further constrain the ice flow history within the study area. One specific objective is to determine whether there are differences in the type of ice flow indicators associated with the different ice flow phases to possibly get insights into the dominant mechanisms of glacial erosion in different areas and

through time. Landscape-scale ice flow indicators such as *roches moutonnées*, drumlinoid features, whalebacks, and crag-and-tails were identified throughout the study area during fieldwork and using satellite imagery (Spot 5, 2002). The smaller outcrop-scale ice flow indicators including striations, grooves, chatter marks, and crescentic gouges were measured using a Brunton compass throughout the study area. Crosscutting relationships of these small-scale features were observed and analyzed to establish the relative ice flow chronology following established procedures (Klassen and Bolduc, 1984; Stea, 1994; Rea *et al*., 2000; McMartin and Paulen, 2009). All measurements were plotted on rose diagrams for analysis and GIS software (ArcGIS® (ESRI) 10.5.1) for the spatial distribution of the ice flow data.

2.3.2 Till Sampling Procedures

The RC drilling was carried out using a Northspan Hornet rig transported by snowcat. The RC sampling was conducted at 52 sites within the study area. Samples were collected for each 1.5 m interval in the till column from the surface to the till-bedrock interface. This resulted in 155 samples (typically 2-3 samples per site) with an average weight of ~20 kg per sample. Two holes were drilled side-by-side where sediment cover was less than 1.5 m to ensure sufficient sample material was collected and the results were documented as a single hole. The drilling was monitored to ensure boulders and bedrock were excluded from the sampled material. Samples were sent to the Saskatchewan Research Centre (SRC) laboratory for textural and geochemical analyses.

A total of 13 hand-dug surficial samples were also collected from mudboils in the study area. The sampling of these mudboils was carried out in accordance with standard procedures for northern terrain (McMartin and McClenaghan, 2001). The “silty cap” of the mudboil (Shilts, 1978) is cleared away and any oxidized or biological material is removed. A clean paint-free shovel was used to sample an average of 10.5 kg of unoxidized till. The surficial samples were sent to the University of Waterloo Quaternary laboratory for textural analysis and clast lithology classification. A split of the hand-dug surficial samples was sent to SRC, to maintain consistency with the RC samples. (see sections **2.3.3** and **2.3.4**, respectively).

The spatial coverage of the study area is approximately 700 km^2 and 65 sample sites for a sampling density of 1 site per 10.8 km^2. There was an additional 39 sampling sites for only clast

lithology counts within the study area. **Figure 2-4** displays the sampling sites including the clast lithology counts.

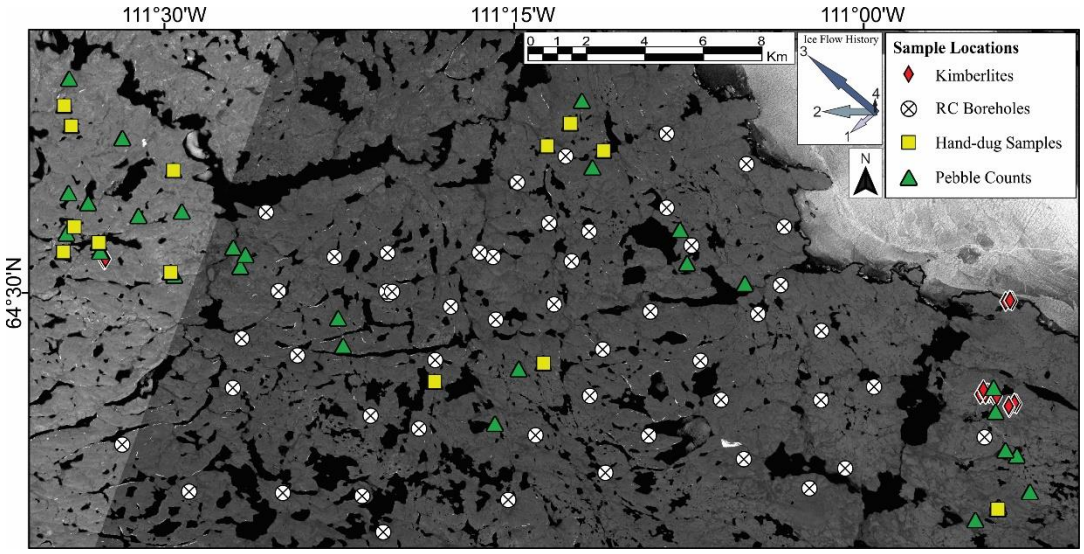

Figure 2-4: Sample locations in the study area for reverse circulation boreholes, hand-dug samples, and pebble counts. The known kimberlite locations (red diamonds) are also displayed.

2.3.3 Textural analysis

The textural analysis may be used to classify sediments based on grain size distribution (*e.g.* sand, silt, clay). This may assist in determining provenance, or at the very least determining if sedimentological differences occur between samples. The textural analysis is conducted by using a sediment sample (*e.g.* till) and characterizing the grain-size as an entire grain size distribution (GSD) that displays the proportion (or percentage) of grains that fall within specified classes (Hoey, 2004). It is necessary to divide the sediment samples into several size fractions that enable the GSD to be constructed from the weight percentage of sediment captured in the pre-defined size fractions. The two types of analyses used are 1) sieve screen GSD for material >63 µm; and 2) laser granulometry GSD of material <63 µm. The results of the two analyses are combined for a full suite of GSD from 0.25 µm to 8000 µm.

The textural analysis was performed on the 13 hand-dug field samples shipped to the University of Waterloo Quaternary laboratory. The sediment from each sample was separated and analyzed following the flowchart in **Figure 2-5**. The material retained in each size fraction was weighed, recorded, and archived. The <63 µm material remaining in the pan after sieving reduces the

accuracy of the statistics being calculated if it accounts for more than 5% of the sediment in the sample (Blott & Pye, 2001). In this study, all samples contained at least 22% of the <63 µm sediment after sieving. The samples need to be analyzed further to account for the large amount of silt and clay. This study uses laser granulometry with a Fritsch Analysette 22 MicroTec Laser Particle Sizer to determine the GSD of the silt and clay size fractions. A portion of the material was slowly poured into the wet dispersion unit of the particle sizer where it was mixed with water. The water/sample mixture circulates through the unit as a laser passes through the mixture. This causes the light to diffract and scatter onto a receiver. The angles of diffraction determine the particle sizes, while the intensity at each angle determines the proportion of particles (Crolly, 2017). Each sample was analyzed using a subsample of the <63 µm split retained after sieving. The size classes produced from the analysis are grouped into the following bins: 32.72 µm, 16.32 µm, 8.14 µm, 4.06 µm, 2.03 µm, 1.01 µm, 0.50 µm, and 0.25 µm. Anything less than 0.25 µm is not used because the laser analysis becomes increasingly inaccurate as the particle size decreases (Crolly, 2017). Data was plotted as a cumulative frequency curve, as well as on a ternary diagram using the software GRADISTAT (Blott and Pye 2001).

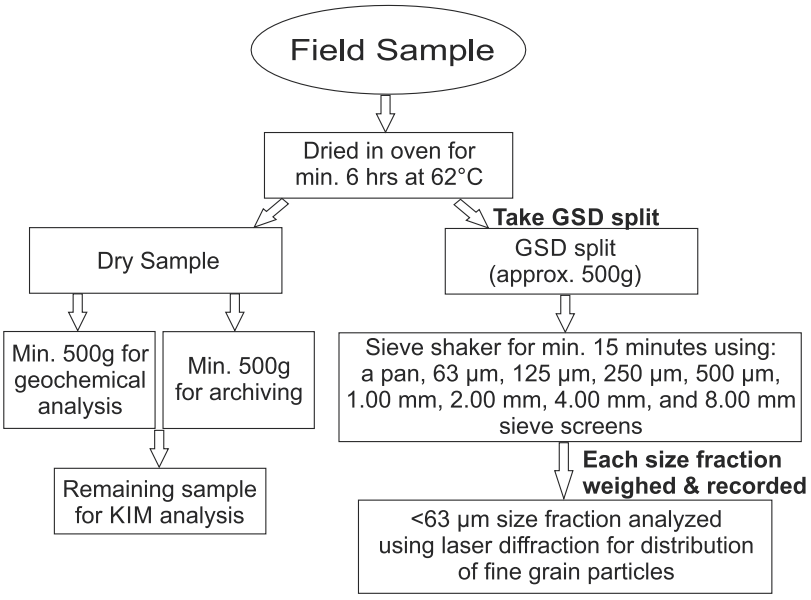

Figure 2-5: Flowchart of the textural analysis process.

2.3.4 Clast Lithology Classification and Shape Analysis

Rock clasts are collected and mapped against existing bedrock maps (Davis, 1991; Ward *et al*., 1995; Kjarsgaard e*t al*., 2002), then analyzed using the main surficial ice-flow direction. This aids in the reconstruction of the direction and distance of glacial transport (Levson, 2001; McMartin and Mclenaghan, 2001). The clasts are sorted into four classes for ease of identification. They are metasedimentary, K-feldspar monzogranite (pink igneous), hornblende-biotite tonalite (white igneous), and mafic rocks. Finally, the clasts are sorted based on shape as described by Benn (2014).

The clast lithological classification was conducted at a total of 37 sites. Clasts were collected and sorted from mudboils at 26 locations during the field study and another 11 till samples during laboratory analysis. A minimum of 100 pebbles were selected for analysis. The size of the field clasts was variable, but an attempt was made to select pebbles between 4-8 mm where possible, as is suggested by Levson (2001). The pebbles were classified by lithology and pictures were taken for future identification and result presentation. The laboratory till samples had the 4-8 mm size fraction sorted and counted for clast lithology classification. The pebbles were cleaned in an ultrasonic bath to aid in identification and the results were recorded and added to the field sample results. The samples are subdivided into the four respective classes (**Figure 2-7**) and the results are summarized in tables as both raw count data and also as percentages (see Appendix A). This table facilitates both a qualitative and quantitative (statistical) comparison between the sample sets (Walden, 2004).

Figure 2-6: Representative grains for clast lithology classification. A) Metasedimentary; B) White Igneous; C) Pink Igneous; and D) Mafic. Clasts have been washed and sorted at the University of Waterloo Quaternary Laboratory.

After the clast lithology classification was completed, they were sorted for shape analysis. The shape is classified by roundness and sphericity. This is useful as it was demonstrated that clasts transported englacially tend to have distinct forms with distinct wear patterns than those

transported subglacially due to differences in transport mechanisms (Benn, 2014). This can give insights into the origin of the till and how it was transported. The spatial distribution of clast counts is concentrated along two mineral indicator trains; the Monument and Coppermine indicator mineral trains. Public indicator mineral data show the surficial expression of the indicator mineral trains trends to the northwest (*c.f.* Chapter 3 – section 3.2.4.). A transect along each of these indicator mineral trains is used to capture clast lithology information pertaining to these trains.

2.3.5 Till Geochemical Pathfinders

The major element geochemistry of both the RC boreholes and hand-dug surficial till samples were analyzed using inductively coupled plasma optical emission spectrometry (ICP-OES) whole rock analysis for 10 major elements (Al_2O_3, CaO, Fe_2O_3, K_2O, MgO, MnO, Na_2O, P_2O_5, TiO_2, and SiO_2) (in Appendix B). All samples were analyzed at SRC geoanalytical laboratories. The flowchart outlining this process is presented in **Figure 2-7**. The RC sampling and analytical procedures are described by Elliott and Normandeau (2016 and 2017).

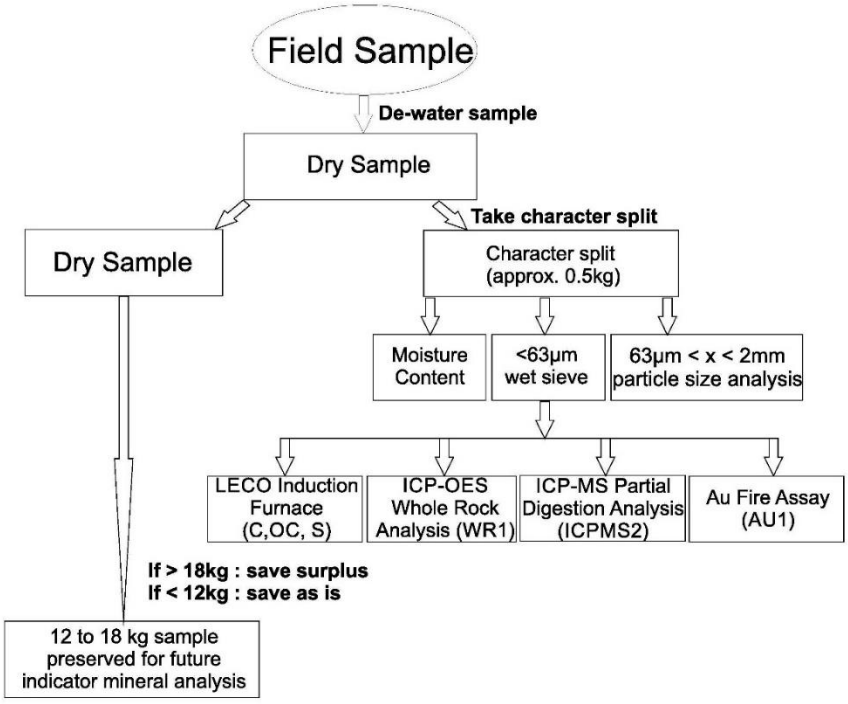

Figure 2-7: Sample preparation flow chart for geochemical pathfinder analyses. Modified from Saskatchewan Research Council Geoanalytical Laboratories.

2.3.6 Principal Component Analysis

The multivariate geochemical pathfinder data from the till samples were used to conduct a principal component analysis (PCA). The PCA identifies patterns in the elemental associations of samples by determining the maximum variance between the geochemical signatures (Gazley *et al*., 2015). These signatures are in turn associated with the primary types of bedrock in the Lac de Gras area. This provides information that is mapped to analyze the spatial distribution of the principal elemental till-bedrock associations throughout the study area.

Multivariate statistics can only be applied to a geochemical dataset if all values have a numeric value (Gazley *et al*., 2015). The major oxide elemental data is measured in weight percent. This presents a constant sum problem as variables are not independent; the distribution of elements will shift but always sum to 100% (Grunsky, 2010). To correct for this, the data is 'opened' using the centre log-ratio method as outlined by Reimann *et al*. (2008). It is not dependent on the results of a single selected variable, rather, it uses the average of all variables which provides a direct relationship between the variables needed (Aitchison, 1986; Reimann *et al*., 2008; Grunsky, 2010). The log-ratio transformation projects the data into the entire (positive and negative) real number space, in which standard statistical methods and procedures may be applied (Grunsky, 2010; Gazley *et al*., 2015).

Multivariate geochemical datasets produce n-dimensional datasets that are difficult to deconstruct. The PCA is a multivariate analysis that reorients the datasets so the greatest variance can be observed in two dimensions (Gazley *et al*., 2015). The PCA explores primary variations or "principal components" in the dataset following the methods of Reimann *et al.* (2008). The first principal component (PC1) is the maximum variance with each successive principal component explaining the maximum variance not including the preceding information. There will be as many principal components as there are elements in the analysis. However, due to the nature of the analysis, the majority of the information is contained within the first few principal components. The individual principal components will represent lithological variations that contribute to the main characteristics of the associated till samples. For example, the first principal component may represent enrichment in one element and depletion in another due to an association with a local bedrock source.

The results of the PCA analysis are interpreted using a bivariate plot (bi-plot). A bi-plot of PC1 vs PC2 summarizes the greatest variance in the dataset for a more comprehensive summary than a plot of any two of the original variables (Gazley *et al*., 2015). The number of significant principal components can be determined by analyzing a scree plot of the variation in the data accounted for by each principal component. The amount of variability accounted for by all components will sum to 100%, and more than 80% of the variability in the data should be explained by the first 4 or 5 components (Reimann *et al*., 2008). The scree plot uses the inflection point as a cut-off that will determine the number of principal components needed to properly analyze the majority of the variation in the dataset (section **2.4.2.3**).

The dimensionality of the data for PCA determines the maximum number of variables that can be examined based on the number of samples within the dataset. This study uses $n > 9p$ (where n is the number of samples and p is the number of variables) to determine the maximum number of variables used for PCA (Le Maitre, 1982; Reimann *et al*., 2008). The Lac de Gras dataset contains 166 samples. Therefore, a maximum of 18 variables can be used [$166 > 18(9)$]. There are 10 major oxides in this study, therefore all the variables may be examined at once.

The major oxide elements are analyzed due to their ability in differentiating the major lithologies represented in the Lac de Gras area. The identification of till associations with source bedrock types was completed by carrying out PCA on till retrieved from the RC drill and surficial hand-dug samples. PCA was carried out using ioGAS (Reflex) geochemical exploratory data analysis software. Each borehole was organized into a column of samples where each sample represents 1.5m of downhole till. The data includes boreholes of less than 1.5 m to a maximum depth of 25 m. This data was then cross-correlated with the average geochemical values of the local types of bedrock analyzed by Davis (1991) (**Table 2-1**). The results were grouped according to their likely bedrock signature and these groups were then plotted spatially using ArcGIS. Each sample is coloured based on the biplot classification of the till-bedrock association. In addition to plotting the borehole data, the surficial sample of each site was examined for PCA along the A-A' (Monument) and B-B' (Coppermine) transects that were also analyzed for pebble lithology, so comparisons could be made. It should be noted that field exploration has shown that the bedrock outcrops are more variable and complex than the 1:250 000 scale bedrock map indicates.

2.3.7 Quality Assurance Quality Control (QA/QC)

The QA/QC procedures ensure accurate data analysis of the major geochemical pathfinder elements used for the PCA. The QA/QC procedures are completed through preparation and analysis of standards and duplicates for the whole rock major oxide element geochemistry. The standards are analyzed using the relative percent difference method and the duplicates are assessed using precision scatterplots and Thompson-Howarth precision plots.

Two standards (CRM Till-1 and CRM Till-3) from the Geological Survey of Canada's certified geochemical soil and till reference materials (Lynch, 1996) were inserted in the sample batch using a project sample ID. The resulting analysis from the standard reference materials are compared against the known values, as published (Lynch, 1996). The relative percent difference uses the analytical results to compare with the published values. This is completed for all major element data and presented in Appendix C. Generally, the relative percent differences are considered to have excellent accuracy between ±0-3%, very good accuracy from ±3-7%, good accuracy from ±7-10%, and values above ±10% are not accurate (Jenner, 1996; Piercey, 2014). The reference materials analyzed are within the excellent to very good accuracy range for all elements except P_2O_5 and MnO. The P_2O_5 is in the good accuracy range for both standards, while the MnO is in the not accurate range for CRM Till-3. The duplicates were assessed further using precision scatterplots to verify these results.

The duplicates were assessed using scatterplots as outlined by Piercey (2014). A confidence interval of 90% was set to ensure the accuracy of the data and the precision of the method used to measure the duplicates. The scatterplot is set so the x-axis is the original weight percent and the y-axis is the duplicate weight percent. The data can be precise (lying within the control lines), moderately precise (data with scatter suggesting no bias), and very imprecise (shotgun scatter). Additionally, the data can have a rotational bias, translational bias, and/or decreasing precision with concentration (Piercey, 2014). Examples of the precision scatterplots are displayed in **Figure 2-8** for Al_2O_3 and P_2O_5 (see Appendix C for full results). The Al_2O_3 scatterplot is precise and representative of the major elements Al_2O_3, CaO, Fe_2O_3, K_2O, MgO, MnO, Na_2O, TiO_2, and SiO_2. The P_2O_5 scatterplot is the only element that contains any duplicate outside the 90% confidence interval, but it is still moderately precise.

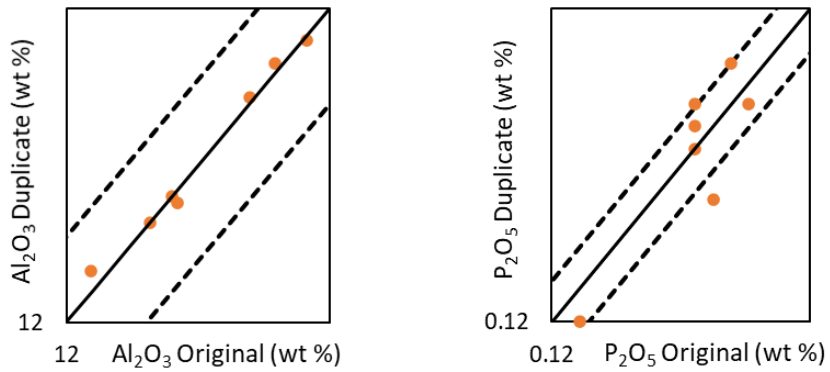

Figure 2-8: Precision scatterplots of sample duplicates. The solid line is the 1:1 sample to duplicate line and the dashed lines are the 90% confidence intervals. The Al_2O_3 scatterplot displays excellent precision for the duplicates. The P_2O_5 scatterplot displays moderate precision for the duplicate samples.

The Thompson-Howarth short method plots are used to confirm the results of the precision scatterplots. The Thompson-Howarth method (1976) tests the precision of a small number of duplicates by assuming error in the duplicate data are random and follow a normal distribution (Piercey, 2014). The median difference of the data is found by examining the relationship between the median of the population and the standard deviation. The precision is set at the 90% confidence interval and a control line is established. If all data fall under the control line then the data is precise to 10%. The Thompson-Howarth plots (see Appendix C for full results) show all the data are precise to 10%.

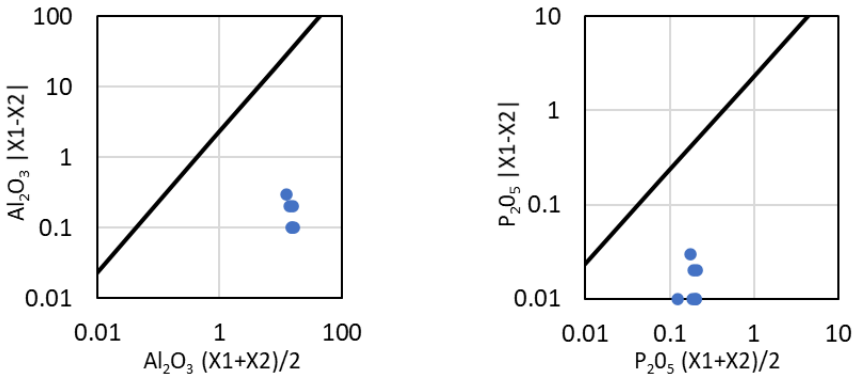

Figure 2-9: Thompson Howarth short method (<50 samples) plots for Al_2O_3 and P_2O_5. The control line is set at the 90% confidence interval and the resultant duplicate analyses plot within 10% precision for all samples in the dataset.

Examining the results from the relative percent difference, precision scatterplots, and Thompson Howarth plots reveal enough evidence to show confidence in the data and analysis of the dataset may proceed.

2.4 Results

2.4.1 Ice Flow Record

Groove and striation measurements were collected during the 2015 field season (**Figure 2-10**). A total of 254 groove and striation measurements were collected and recorded throughout the study area. An additional 18 striation measurements were provided by Palmer Environmental Consulting Group (Sacco and McKillop, 2015). Four separate groups of ice flow indicator directions were recognized in the results (**Figure 2-11**). Based on the well-established criteria for relative age chronology (**Figure 2-10**), it was also possible to assign a relative age to these groups of observations. The earliest ice flow is to the southwest at ~240˚ (*n*=14). The relative age of this group of observations was established at 13 sites (**Figure 2-10A and B**). The second recognized ice flow phase is to the west at ~270˚ (*n*=36), determined through lee side preservations and cross-cutting relationships at 25 sites (**Figure 2-10C**). The indicators of the third ice flow phase reveal ice flow towards the northwest at ~305˚ (*n*=209) and are found on exposed surfaces and cross-cutting the younger ice flows at 29 sites (*e.g.* **Figure 2-10**). The indicators associated with the third ice flow phase are prevalent in the study area accounting for 77% of all observations and is the dominant direction of the known surficial till dispersal. The fourth flow is scarce and weakly developed with only 12 observations. The striations that were found are not well defined, and there is a large variance in the directionality. However, several different researchers observed these striations within this study at ~005˚ north (n=12). Rose diagrams are displayed in **Figure 2-11** to visualize the ice flows within the study area.

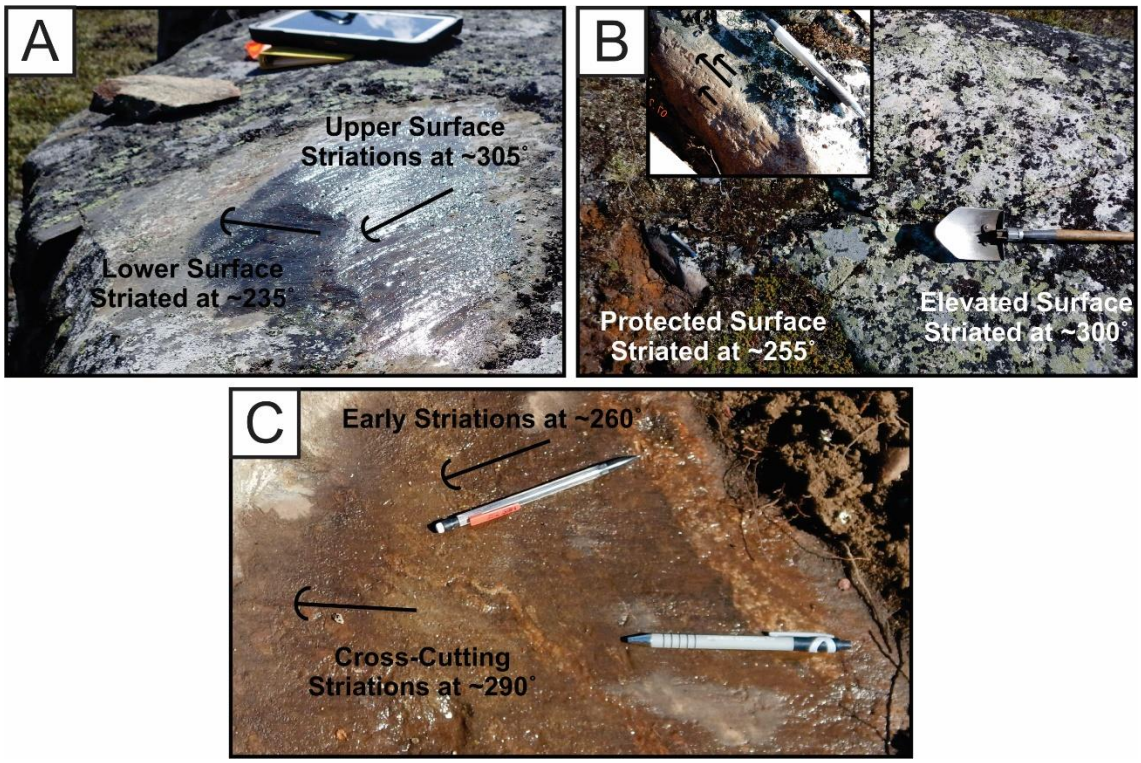

Figure 2-10: A) and B) Striations with lee side preservation of earlier ice flows; C) Cross-cutting relationship between earlier and subsequent ice flows.

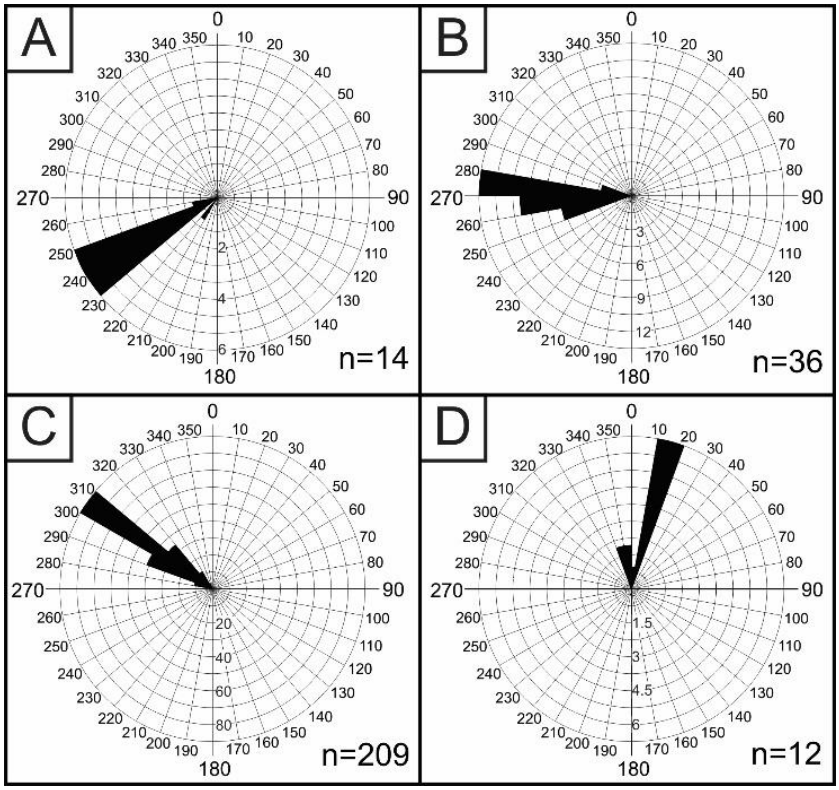

Figure 2-11: The ice flow history of the Lac de Gras, NT study area presented through rose diagrams of the groove and striation measurements. A) Ice flow 1 to the southwest (215° to 254°); B) Ice flow 2 to the west (255° to 284°); C) Ice flow 3 to the northwest (285° to 340°); and D) Ice flow 4 to the north (345° to 020°).

2.4.2 Till Characteristics

2.4.2.1 Textural Analysis

The textural analysis was conducted on all hand-dug samples as described in section **2.3.3**. A GSD is constructed using the cumulative weight percent for each grain size split in phi units and plotted for all samples on a single graph (**Figure 2-12**). Results show all samples are very poorly sorted, which is a texture that is typical of most subglacial traction tills on the Canadian Shield (Haldorsen, 1981). The GSD for the samples in this study are classified as a poorly sorted, gravelly, muddy, sand as defined by the GRADISTAT ternary diagram from Blott and Pye (2001) (**Figure 2-13**). The statistical results are displayed in Appendix D.

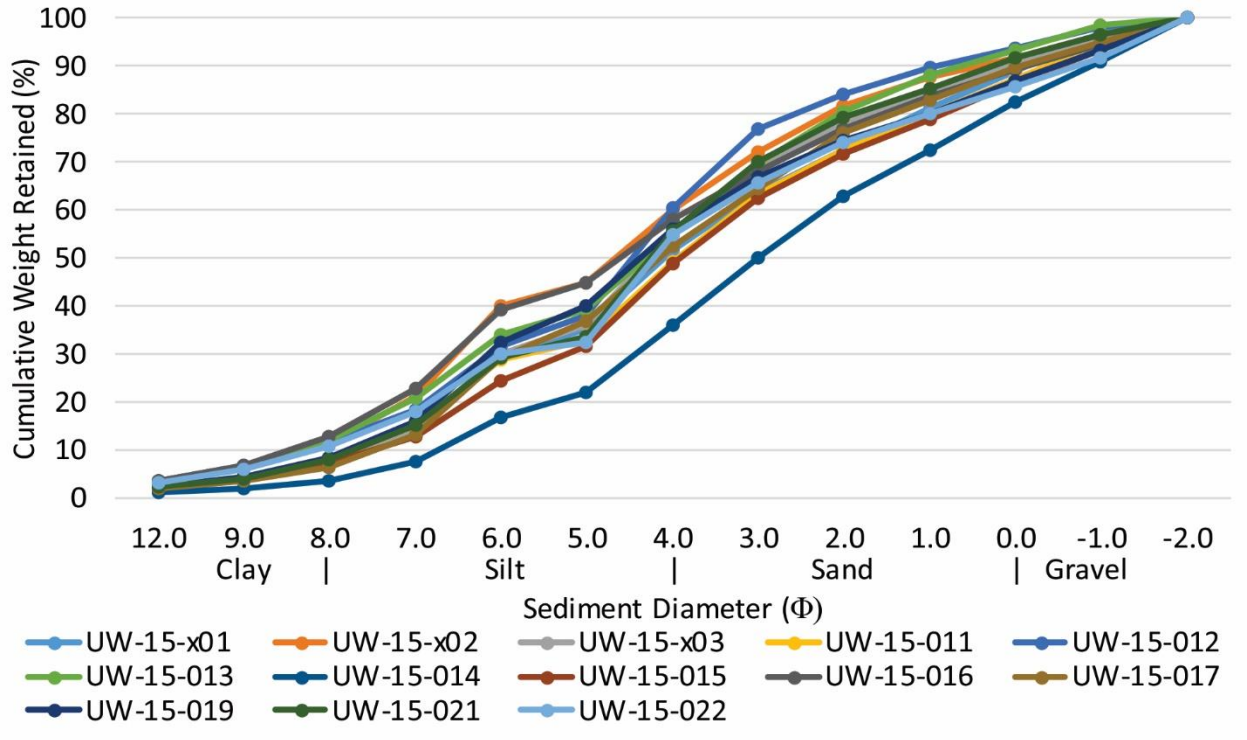

Figure 2-12: Cumulative weight percent of the grain size distribution.

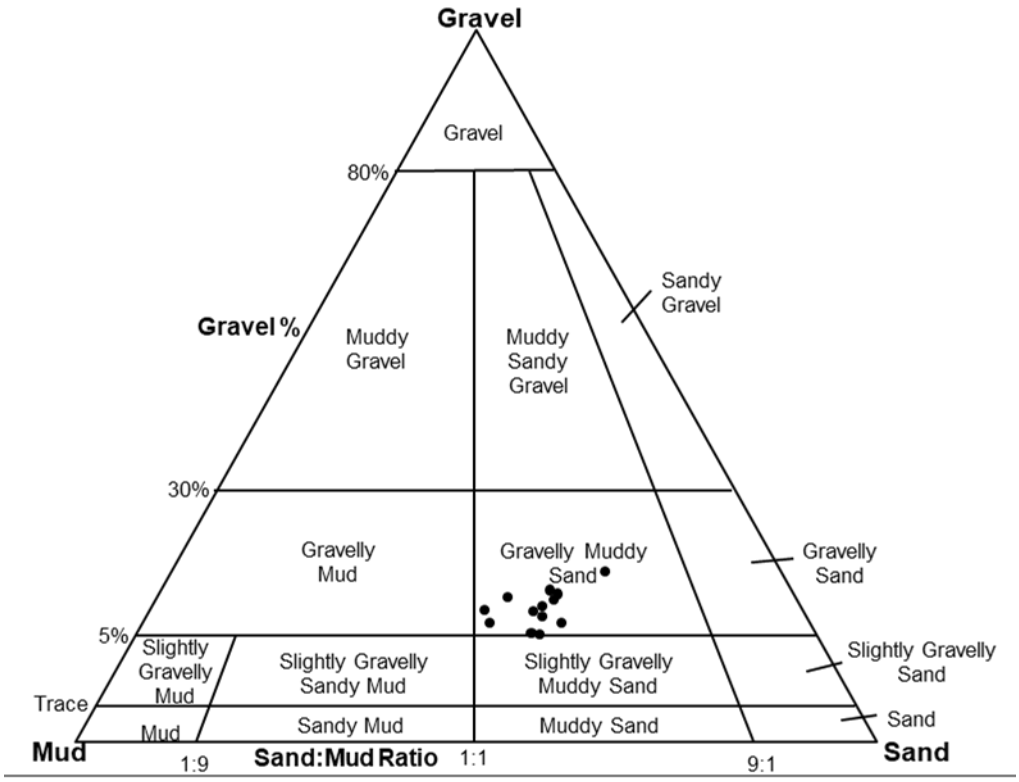

Figure 2-13: Ternary diagram defining the nomenclature of the samples analyzed by grain-size distribution. Mud is the combined proportion of silt and clay. Defined using GRADISTAT (Blott & Pye, 2001).

2.4.2.2 Clast Lithology and Shape Analysis

The clast lithological classification was conducted at a total of 37 sites. The spatial distribution of clast counts is concentrated along two mineral indicator trains; the Monument and Coppermine indicator mineral trains (*c.f.* Chapter 1, section 1.2.2; Chapter 3, section 3.2.4). Results are summarized in tables as both raw count data and as percentages (see Appendix A).

A transect (A to A') along the dominant northwest ice flow direction (**Figure 2-14**) runs along the centre line of the Monument kimberlite indicator train (**Figure 2-15**). The bedrock along the dispersal area is mostly metasedimentary; however, most samples were collected relatively close to areas of white granitoids (**Figure 2-14**) with a large gap that has no samples in-between. Also, the down-ice end of the transect passes the contact with the pink granites (**Figure 2-14**) and the effect on clast composition is apparent with a slight increase in igneous rock content near the end of the transect (**Figure 2-15**). Overall, there is a high proportion of metasedimentary pebbles (>50%) in all samples, even several kilometres down-ice from the igneous contact. Despite the data gap in the middle of the transect, there appears to be little change in clast composition

between the head (A) and the tail (A') of the transect. Another interesting observation is the proportion of pink igneous clasts across the metasedimentary bedrock portion of the transect (**Figure 2-14**). It is not shown as a separate curve in **Figure 2-15**, but a close look at the map (**Figure 2-14**) shows that a certain proportion of pink clasts are maintained across the metasedimentary rocks. Specifically, the samples located at the head of the transect (A), all contain pink igneous clasts (>7%). The closest known sources of pink igneous rocks, given the known ice flow history, for the samples located at the head of the transect (A) are ~40 km southeast (youngest up-ice direction) and 17 km northeast (oldest up-ice direction).

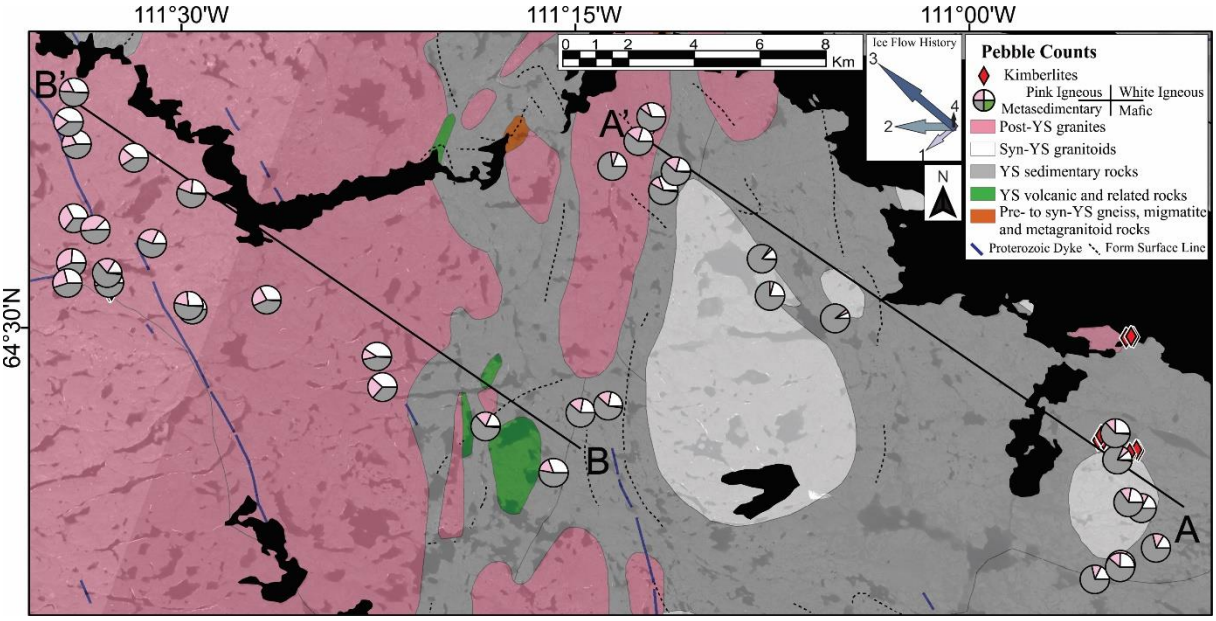

Figure 2-14: Clast lithology distribution in the study area. The A to A' line is the clast lithology counts conducted along the Monument indicator train. The B to B' line is the clast lithology counts conducted along the Coppermine indicator train.

Results of the second transect (B-B') are also shown in **Figure 2-14** and **Figure 2-15**. This one runs parallel to and approximately along the centre line of the Coppermine indicator train (See Chapter 1, section 1.2.2; Chapter 3, section 3.2.4). It is important to note that the bedrock geology of the first 1/3 of the transect consists of metasedimentary and volcanic rocks, whereas the rest of the transect is underlain by igneous rocks. Interestingly, results show that despite igneous rocks being the dominant lithology of 2/3 of the transect, the proportion of

metasedimentary clasts remain high (>40%) (**Figure 2-15**). There is no significant dilution that would fit a 'decay' function, for example, and the proportions remain approximately 50/50.

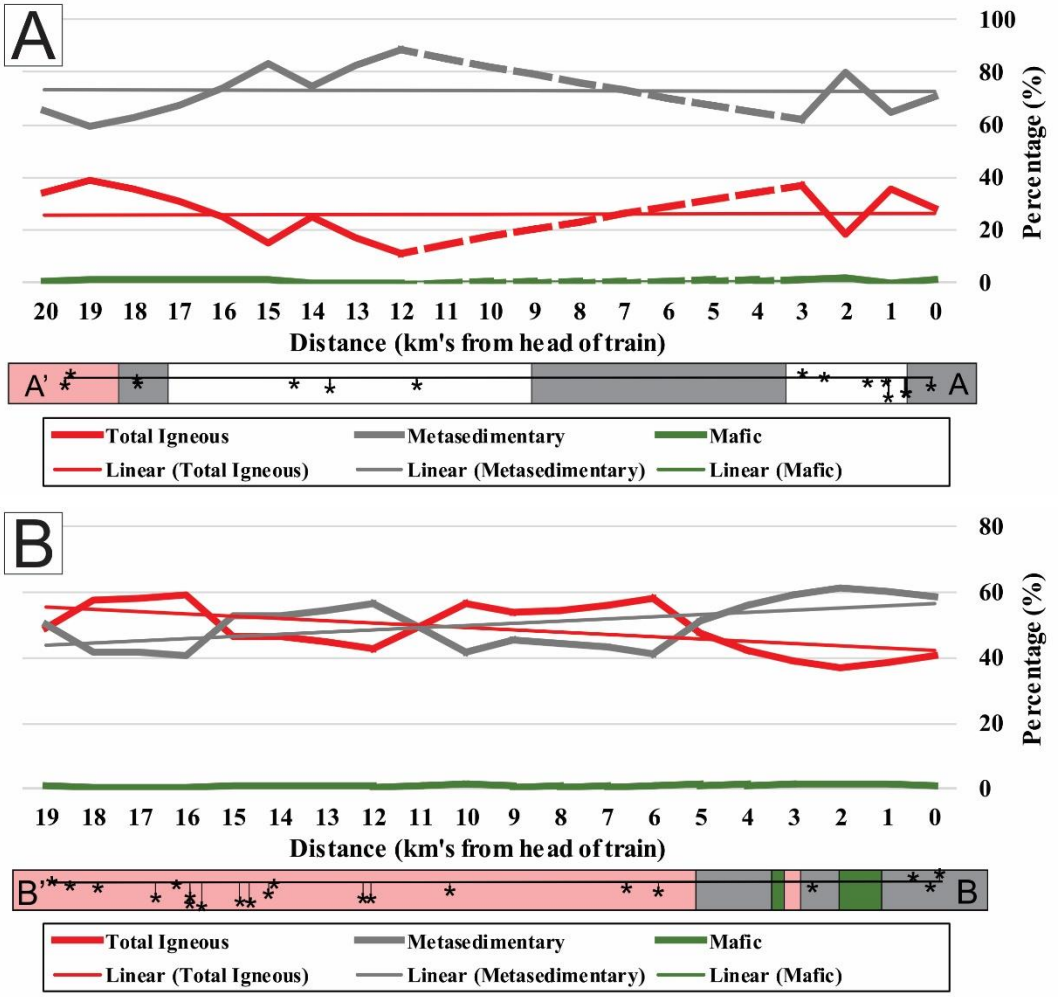

Figure 2-15: Clast lithology distribution curves. Top (A) A to A': Representative of the clast distribution in the down ice direction (to the northwest) from the head to the tail of the Monument train. The dashed portion of the line represents the large data gap; Bottom (B) B to B': Representative of the clast distribution in the down ice direction (to the northwest) along the Coppermine dispersal train. The color strips below the graphs are the corresponding geological maps.

The shape of the clasts observed in the study area are highly variable. One representative sample, UW-15-019, was examined using the Sneed and Folk (1958) classification of the long, intermediate, and short axes of each clast (**Figure 2-16**) to determine if a specific transport method was dominant within the study area. The largest proportion of clasts are bladed (36%),

followed by platy (13%), elongate (13%), and very bladed (13%). The roundness of the clasts is angular to sub-angular.

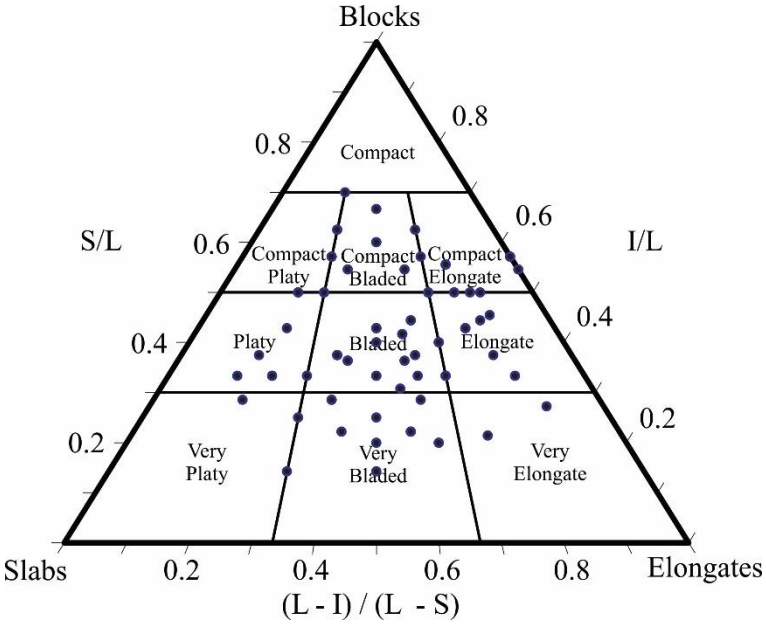

Figure 2-16: Ternary diagram of the Sneed and Folk (1958) clast shape classification for sample UW-15-019. L = long; I = intermediate; S = short.

2.4.2.3 Principal Component Analysis of Till Matrix Geochemistry

The principal component analysis was conducted on 166 samples from a total of 63 sites (52 RC and 11 hand-dug sites). Results are summarized using plots and maps of the samples. **Table 2-2** shows that nearly 70% of the variation in the geochemical data can be explained by the first two principal components. PC1 has an eigenvalue of 4.52 and contains 45.16% of the variance in the dataset, while PC2 has an eigenvalue of 2.27 and contains 22.75% of the variance in the dataset.

Table 2-2: The percent of the variation in the geochemical data that can be explained by each principal component and the cumulative percentage of variation that can be explained by each successive principal component.

Principal Component	Eigenvalue	Percent	Cumulative Percent
1	4.52	45.16%	45.16%
2	2.27	22.75%	67.90%
3	1.08	10.79%	78.69%
4	0.84	8.40%	87.09%
5	0.62	6.23%	93.32%
6	0.35	3.53%	96.85%
7	0.16	1.61%	98.45%
8	0.10	0.97%	99.43%
9	0.06	0.57%	100.00%
10	0.00	0.00%	100.00%

The scree plot in **Figure 2-17** shows the inflection point of the principal components located at PC3. This suggests the most useful factors are PC1 and PC2. The rest of the principal components that are either at or below this threshold are less useful and more difficult to interpret as they do not account for enough variation in the data.

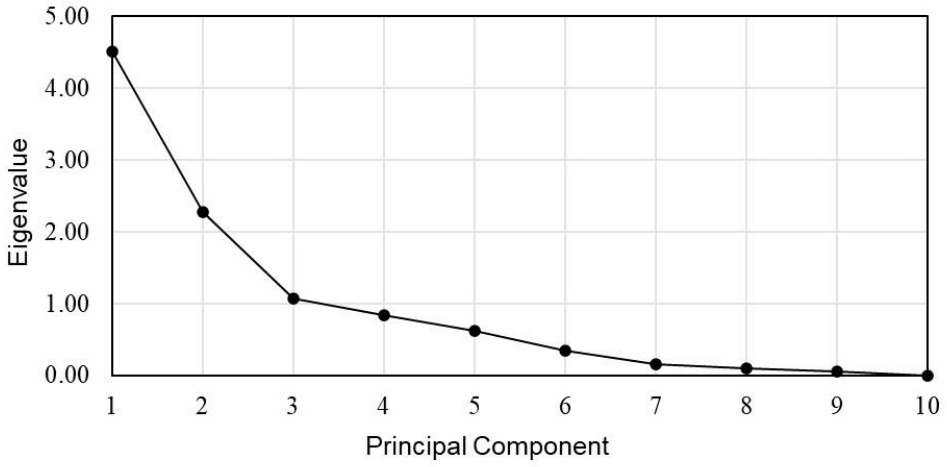

Figure 2-17: Scree plot of the principal component analysis. Note the inflection point at PC3.

The PCA in **Figure 2-18** shows a bi-plot of PC1 v. PC2 of the major oxides (Al_2O_3, CaO, Fe_2O_3, K_2O, MgO, MnO, Na_2O, P_2O_5, TiO_2, and SiO_2). Each dot corresponds to a data instance projected onto the picked eigenvectors.

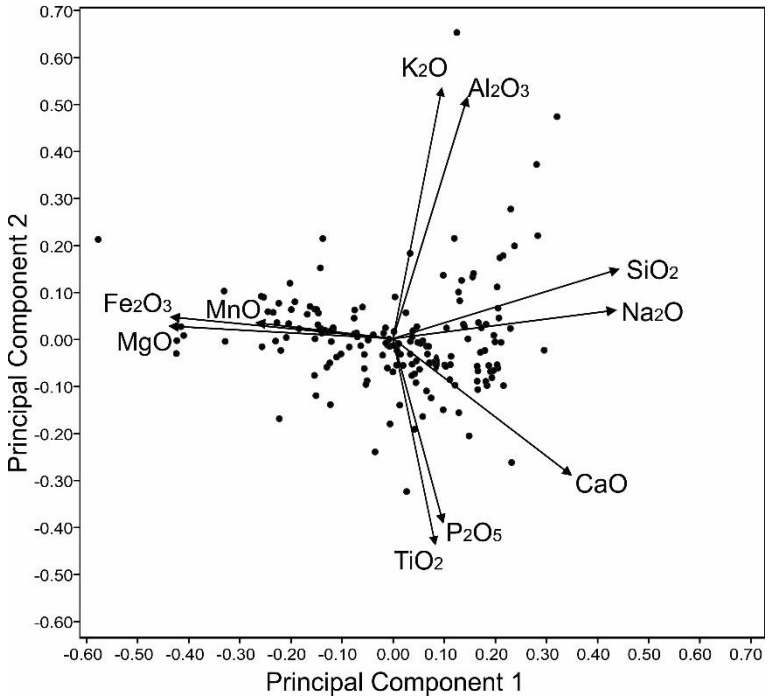

Figure 2-18: Principal component analysis (PCA) bi-plot of the PC1 versus PC2 for major oxides in the till matrix.

After the PCA is classified (in the following section), a map of the classified PCA samples is constructed (**Figure 2-19**) to aid in the interpretation of sediment dispersal and deposition in the study area. The A-A' (Monument) and B-B' (Coppermine) transects are also shown. Generally in glaciated terrain, the surficial material in areas of shallow or intermittent till tends to closely reflect the underlying bedrock (Ward *et al*., 1996; McMartin & McClenaghan, 2001; Wilkinson *et al*., 2001). The data in this study show that only 15 of 62 sample sites contain a surficial sample that has a major oxide signature consistent with the underlying mapped bedrock. Of these samples, 13 are located in shallow till and 2 are located over thick till. Conversely, 6 of 8 samples located over thick till do not have a major oxide signature consistent with the underlying mapped bedrock. The spatial distribution of the classified PCA major oxides (**Figure 2-19**) shows that the eastern half of the study area, defined by metasedimentary and hornblende-biotite tonalite bedrock, is predominantly associated with a mixed till signature. The second most abundant PCA association in the eastern half of the study area is the hornblende-biotite tonalite, and finally, there is a small number of metasedimentary and K-feldspar monzogranite associated till samples. The central study area, which is identified by the intermixing of K-feldspar monzogranite, metasedimentary, and minor amounts of volcanic bedrock, contains till samples that are associated with each bedrock type, as well as that of a mixed till signature with no clear

lithological till association defining this area. The western half of the study area, defined by K-feldspar monzogranite bedrock, contains mainly metasedimentary associated till samples with a smaller amount of mixed till signature and hornblende-biotite tonalite till samples. The till samples furthest to the west are associated with K-feldspar monzogranite. Another important observation is that the deepest boreholes all contain a large number of metasedimentary associated till samples deep in the till column (BHs 15-115, -126, -138, and -144) despite being located in areas overlying igneous rocks and where the surficial till has a major oxides signature trending toward igneous rocks. The two deepest BHs (15-126 and -138) are particularly good examples of this situation.

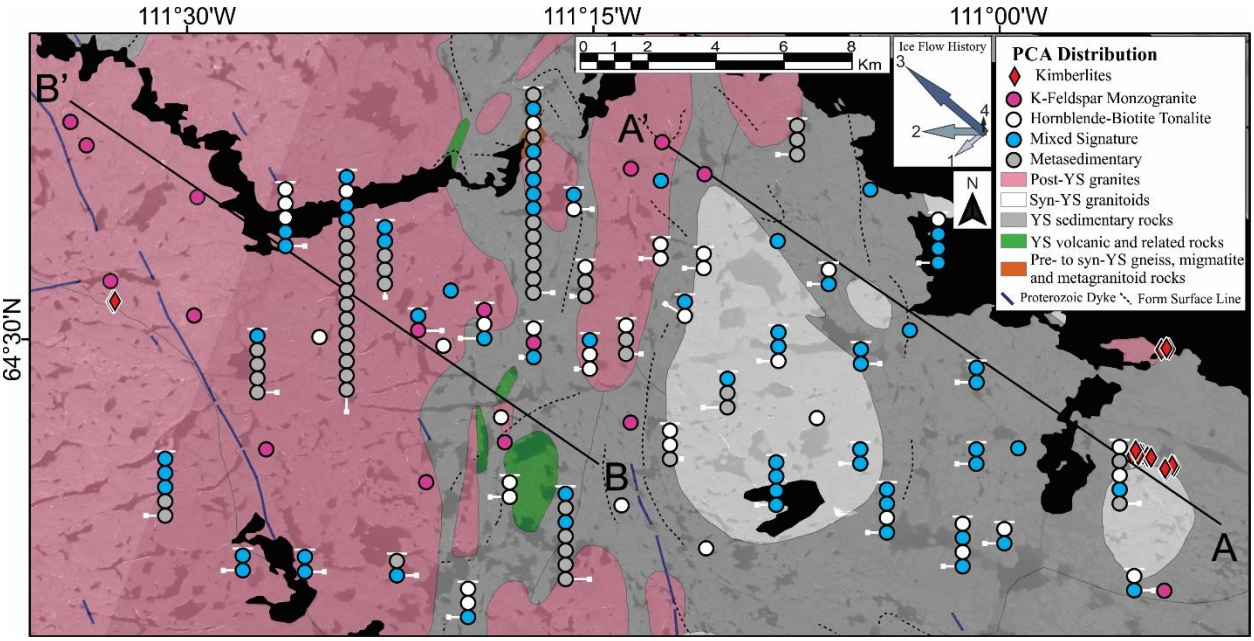

Figure 2-19: Spatial distribution of till matrix compositional groups as interpreted from the PCA analysis of major oxides. Each dot represents 1.5 metres of till. Dots have been stacked vertically for each RC borehole to show changes in till class with depth. A single dot represents a surficial sample.

2.5 Interpretation and Discussion

It has long been assumed that the surficial till in the study area represents a single surficial till sheet produced and deposited during the last glaciation (Ward *et al*., 1995). The chronological events are evident through the ice-flow indicators within the study area. The relative chronology of ice flow events is first to the southwest, second to the west, third to the northwest, and fourth is deglaciation toward the north. The three regional ice flows (SW, W, NW) are interpreted as successive events related to the southeastern migration of the M'Clintock Ice Divide; as these ice

flows have been well documented in the area and attributed to this progressive event (Dyke and Dredge, 1989; Ward, 1995; Tarasov and Peltier, 2004; Gowan *et al.*, 2016). The northern flow appears to be more localized in nature and has been interpreted as trending toward a regional trunk esker north of the study area (Ward *et al*., 1995; 1996). Ice flow can sometimes be linked to esker systems associated with the path of the major drainage during deglaciation (Brennand, 2000; Menzies, 2002). The trunk esker for this system is located ~25 km north, and the dendritic network includes the study area (**Figure 2-20**). The local tributary eskers trend to the north-northwest, north of the study area. This coincides with the north-oriented striations. As a result, the localized ice creep toward the esker during deglaciation may have caused a very light overprinting of the striations in the general direction of the low-pressure channels to the north. The effect of creep toward the low-pressure r-channels is very localized (Alley, 1992) but this effect would explain the scarcity and variability of the observed northern ice flow. Although observed, this ice flow appears to be too weak to have played a role in production, entrainment, and dispersion of till in the study area.

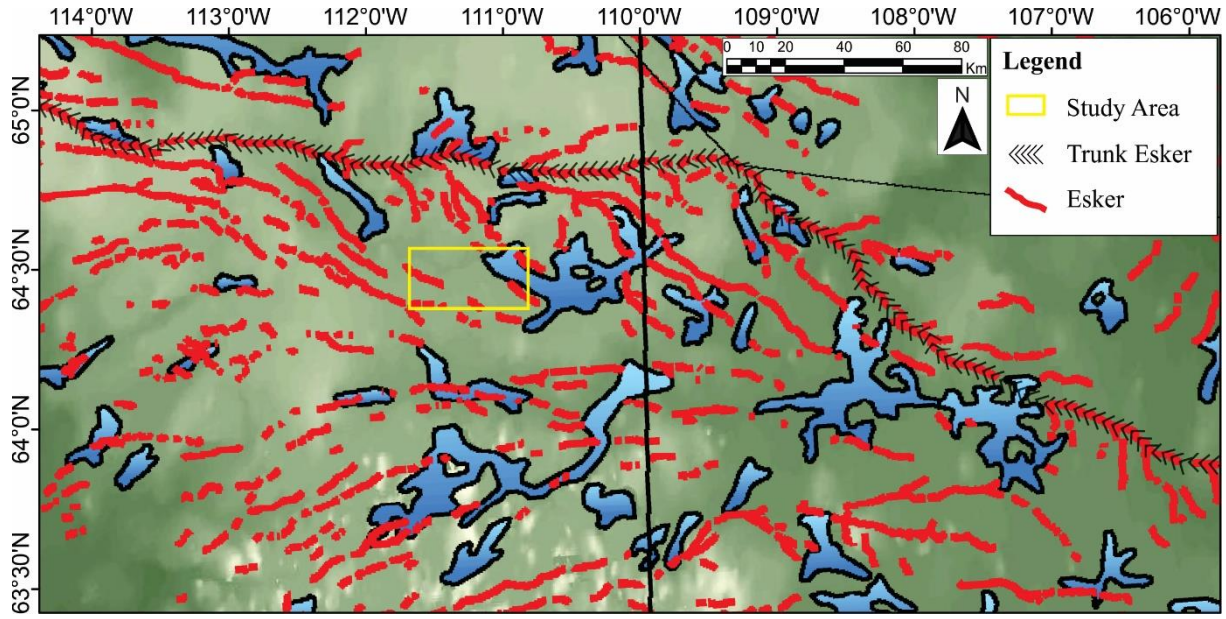

Figure 2-20: Dendritic esker system with the trunk esker north of the study area and the tributary eskers extending throughout the greater study area. Annotated from Storrar *et al*. (2013).

Textural analysis data demonstrates low local variability of the surface till suggesting that, from a textural point of view, it is consistent throughout the study area; the texture should thus not be a factor in surficial till matrix compositional variations. The sediments have been examined

using textural analysis to determine if any major changes in the grain size distribution occur between sample sites. The texture could vary at depth, but this was not possible to assess due to the nature of the RC drilling method. The vectors of the ice flow history indicate the northwestern ice flow is the most prominent and most recent movement. The surficial till is interpreted to reflect this northwestern ice flow phase. Clast lithological analysis of the most recent northwestern ice movement brought large volumes of metasedimentary material over igneous bedrock. The proportion of metasedimentary clasts in till remains above 40% over igneous bedrock several kilometres down-ice of the metasedimentary-igneous rock contact (**Figure 2-14** and **Figure 2-15**). Several researchers have compared dispersal data against general decay functions to interpret provenance, distance and till transport-deposition mechanisms (Shilts, 1982; Clark, 1987; Klassen, 2001; Larson and Mooers, 2004). The two transects investigated in this study show contrasting clast dispersal curves. The one along the Monument train (A-A') is flat, and the transect along the Coppermine train (B-B') shows a slightly 'decaying' clast dispersion which can be approximated by a linear decay function (Klassen, 2001). Linear dispersal trains are often interpreted as evidence of englacial transport and/or fast basal ice flow and associated mobile till (*e.g*. Klassen, 2001), but the interpretation of ice flow processes must also take into account physical bedrock characteristics along the dispersal area, such as bedrock hardness and joint orientation and density (*e.g*. Iverson and Person, 2012; Melanson *et al.,* 2013). The difference in the physical bedrock properties of the metasedimentary rocks is that they are highly jointed (**Figure 2-21**) and more prone to plucking than igneous rocks. Unlike diagenetic sedimentary rocks, metasedimentary rock fragments can resist crushing and survive as coarse fragments during glacial transport. Therefore, when these rocks are dominant at the head of a train there is a rapid uptake of large blocks at the base of the ice and the lithology tends to dominate the coarse fraction of the till. The two transects shown start in jointed metasedimentary rocks and the dispersal of these rocks was sustained over a relatively long distance beyond the contact with the igneous rocks. In contrast, igneous rocks in the area are much less jointed and were perhaps less prone to quarrying/plucking (Iverson and Person, 2012) and thus to generating large debris responsible for producing rock fragments making up the coarse fractions of till (*i.e*. boulders, cobbles, and pebbles). This would have limited the dilution effect down-ice of the metasedimentary contact with the igneous rocks and maintained high proportions of metasedimentary rock fragments. However, if these dispersal

curves were traced further down ice-flow, it is suspected that the tail of the dispersal curves would be better-defined. In summary, the larger clasts in the till were entrained subglacially (in relatively high abundance) for several 10s of kilometres in the direction of the most prominent ice flow vector (to the northwest). This is probably due to a combination of basal ice flow velocity, low effective pressure at the ice-bed interface (reducing stress on particles), the resistance of clasts to comminution, and bedrock characteristics in the dispersion area (hard bedrock with fewer joints that may resist erosion). Thus, the interpretation is that the clast lithological composition is partly controlled by bedrock characteristics.

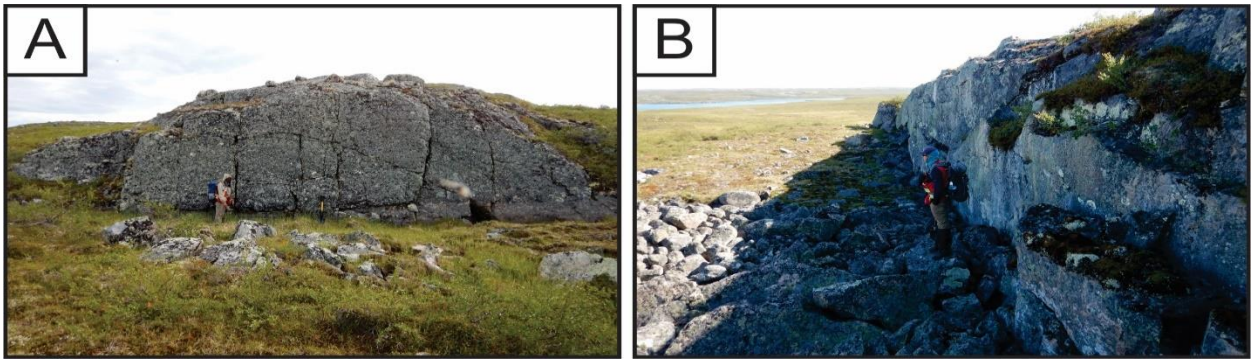

Figure 2-21: Metasedimentary rocks in the study area displaying the typical highly jointed nature (person for scale in each figure). Figure A displays the vertical and horizontal jointing that occurs within the metasedimentary rocks. Figure B displays the plucking of rocks from the lee face of a bedrock ridge with many of the plucked boulders resting within a few metres of the bedrock ridge.

The classified bi-plot (**Figure 2-22**) is used to identify possible till matrix compositional signatures related to the main local bedrock lithologies. Several samples seem to define end-member groups with a characteristic bedrock signature. The metasedimentary, K-feldspar monzogranite (pink igneous), and hornblende-biotite tonalite (white igneous) rocks are widespread rock types in the area and are thus considered important sources of till matrix minerals. Cross-referencing the elemental associations of the rock types (**Table 2-1**; Davis, 1991) with the results of the PCA defines the positive and negative principal components in terms of the rock types that are likely represented. The Fe and Mg are closely correlated in the covariance matrix (0.87). The Slave Province metasedimentary rocks contain a higher weight percentage of Fe and Mg than the other rock types (**Table 2-1**; Davis, 1991). It appears that the Fe and Mg can be correlated with the metasedimentary rocks in the negative direction of the PC1 axis. It is possible that, for some samples, there may be some influence from kimberlitic or mafic sources affecting the PC1 axis because Mg is also a geochemical pathfinder element for

kimberlites and other rock types like mafic rocks (Chapter 3, section 3.3.3). There appears to be a break in the data at -0.10 along the PC1 axis and this is used as a cut-off to classify metasedimentary-rich till (Grey dots in **Figure 2-22**). There are 48 of 166 samples classified as 'metasedimentary' signature. The elements Si and Na correlate (0.88) along the positive PC1 axis. These are indicative of granitic rocks in the Slave Province (**Table 2-1**) but it does not differentiate between the K-feldspar monzogranite and the hornblende-biotite tonalite. There may also be an influence from the volcanic rocks in the area because these contain a greater amount of Si, Na, and Ca. However, the volcanic rocks outcrop in very limited areas and are thus interpreted as having a smaller influence. The PC2 axis is examined for differentiating factors between the igneous rocks. The elements Al and K both vector toward the positive PC2 axis. There is a trend present between K and Si, which is consistent with the K-feldspar monzogranite. The samples that plot along the K-Si trend above the PC2 score of 0.07 and above the PC1 score of 0.09 are interpreted as having a K-feldspar monzogranite signature and are thus grouped (Pink dots on **Figure 2-22**). There are 16 of 166 samples classified as K-felspar monzogranite. Plagioclase rocks have a Na-Ca rich signature, therefore the samples that plot along this Si-Na-Ca trend are consistent with the hornblende-biotite tonalite rocks. These samples plot below the PC2 of 0.07 and above the PC1 score of 0.09. These hornblende-biotite tonalite samples are the white dots in **Figure 2-22**. There are 39 out of 166 samples classified as hornblende-biotite tonalite. All of the remaining dots grouped near the centre of the bi-plot are considered to be a mixture of the bedrock materials and labelled with blue dots in **Figure 2-22**. This shows a large amount of mixing occurring between tills associated with the local bedrock lithologies (63/166 samples mixed till).

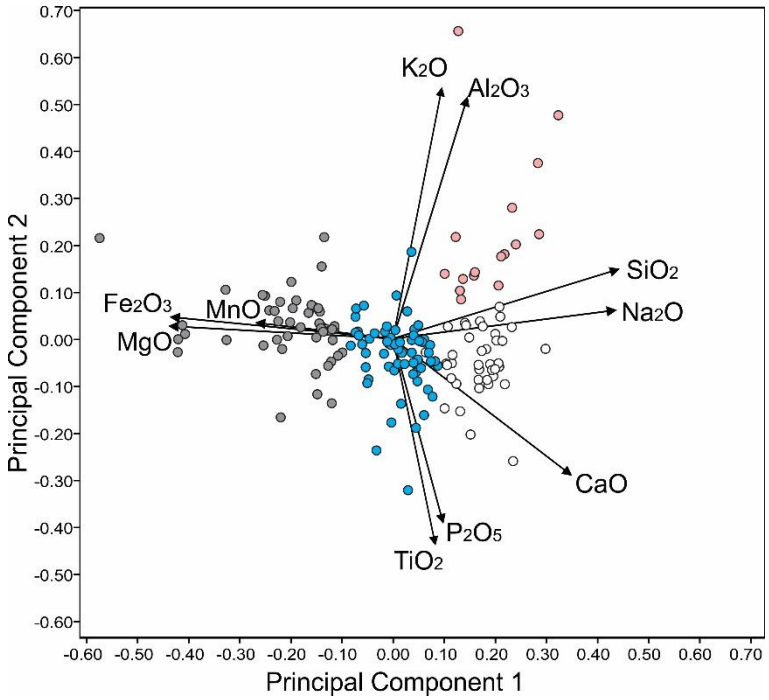

Figure 2-22: Classified principal component analysis (PCA) bi-plot of the PC1 versus PC2 for major oxides in the till matrix. Samples are classified according to their interpreted 'dominant bedrock association' (Grey = metasedimentary; Blue = mixed; Pink = K-feldspar monzogranite; White = Hornblende-biotite tonalite).

2.5.1 Till Dispersal near Lac de Gras, NT

Empirical evidence provided through sedimentological, lithological, and geochemical data helps to define the context for glacial dispersal models. Ice flow indicators are used as a foundation for interpreting ice flow history, with GSD, clast lithology, and PCA as evidence for defining the glacial dispersal in the study area.

Figure 2-23 shows the surficial only PCA transects approximately corresponding to the centre line of the Monument and Coppermine dispersal trains, which are also the same as the ones used for clast lithology analysis (**Figure 2-18**; **Figure 2-19**). These PCA distribution curves use the original weight percent of the geochemical analysis. The Monument distribution curve transect (A-A') shows that, despite a slight variation in proportions of elements, there is no significant change in the abundance of major oxides from the start of the train to the end. This is the same type of distribution curve that has been observed with the pebble clast lithology analysis running along the centre line of the Monument train (*c.f.* section 2.4.2.2). The Coppermine train (B-B') shows an increase in SiO_2 and K_2O, while MgO, FeO, and Al_2O_3 show a slight decrease from the beginning of the train to the end. This is also consistent with the clast lithology distribution curve

for the Coppermine train (*c.f.* section 2.4.2.2). The Coppermine distribution curves show greater variation in the proportion of elements, particularly near 4 km from the head of the transect when the SiO_2 drops by 10% to 64% (this is muted in **Figure 2-23** because of the exponential y-axis scale) and the MgO, FeO, and Al_2O_3 all rise by 2-3%. It should be noted that the transition from metasedimentary to K-feldspar monzogranite occurs at 5 km from the head of the train. However, the overall trend shows SiO_2 and, to a lesser extent K_2O, increase from the beginning to the end of the Coppermine train, while MgO, FeO, and Al_2O_3 all show a slight overall decrease from the beginning to the end of the train. The decreasing abundance of metasedimentary clasts coincides with the decrease in MgO, FeO, and Al_2O_3, while the increase in igneous rocks can be associated with the increase in SiO_2 and K_2O. This shows that there is consistency between the clast lithology and the surficial PCA despite the added contribution of direct bedrock erosion by abrasion for the origin of a portion of the fine particles used for PCA, whereas the larger glacial clasts can only form by the quarrying process and may also be skewed towards more resistant lithologies. The rest of the elements show a negligible change. This is also consistent with the pebble count lithology distribution curve for the Coppermine transect.

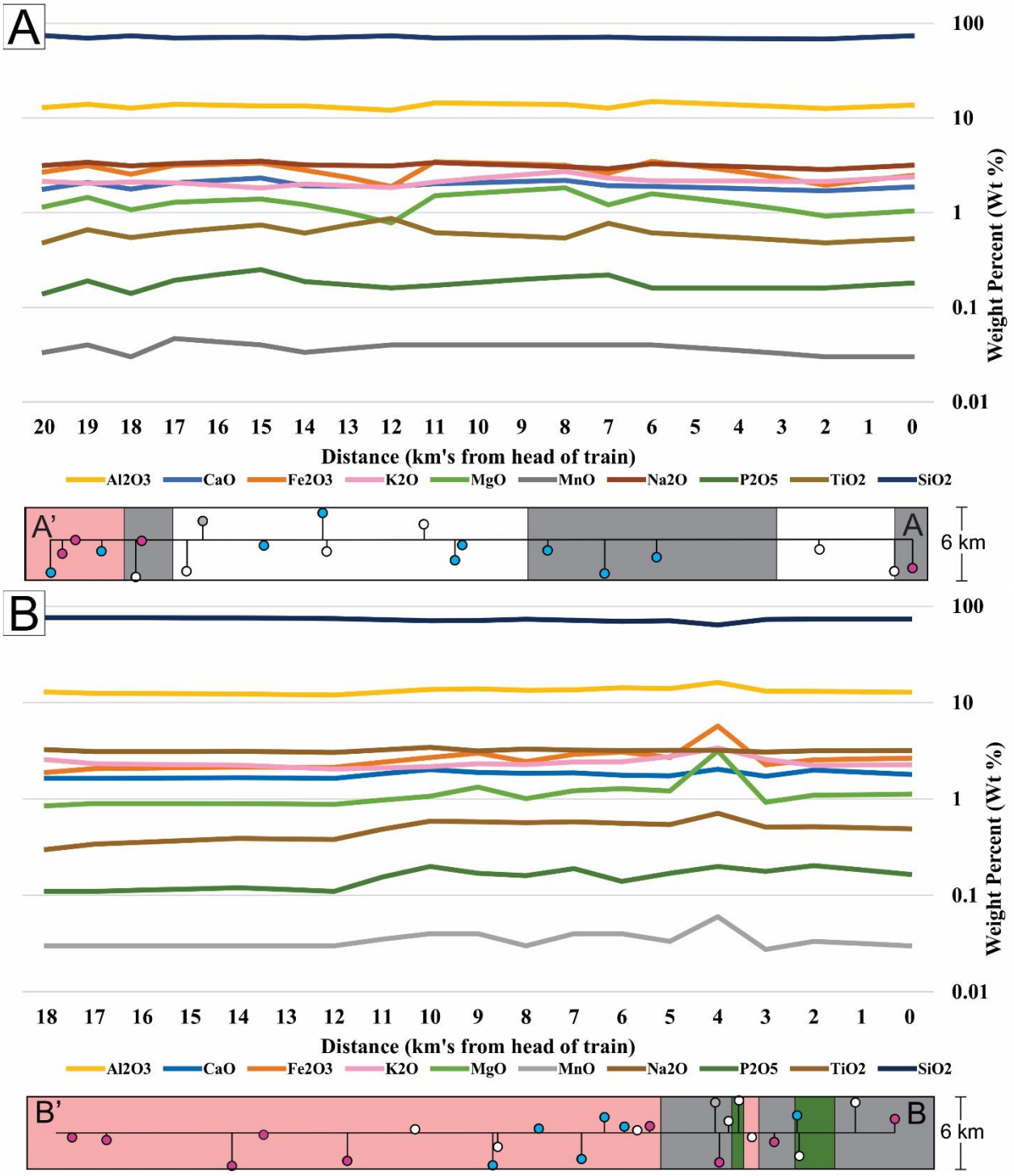

Figure 2-23: PCA distribution curves for the A) Monument (A-A'); and B) Coppermine (B-B') transects from figure 2-19. Only the surficial samples are analysed using the original weight percentage from the geochemical analysis. These are the same transects previously analyzed for clast lithology (Figures 2-14 & 2-15). The y-axis is displayed as a logarithmic scale to better display the data. The color strips below the graphs are the corresponding geological maps.

Combining the information gathered through ice flow indicators, textural analysis, pebble lithology, and principal component analysis, a clearer understanding of the relationship between ice flow history, bedrock, and till composition emerges. Basal glacial movement along with other processes (*e.g.* water pressure fluctuations) can lead to bedrock failure along pre-existing joints as well as abrasion of bedrock surfaces (Benn and Evans, 2010). The newly created particles are then entrained englacially or subglacially as deformation till where they can be further comminuted due to frictional stresses. Pre-existing unconsolidated sediments protect bedrock from direct glacial erosion (Parent *et al*., 1996; Melanson *et al*., 2013), but this material can also be re-entrained and mixed with the freshly produced sediment. Subglacial traction till is thus a blended admixture of sediment of potentially different origins and characterized by a broad range of grain sizes. Despite this complexity and heterogeneity, there is often a strong association with the dominant bedrock types all along the sediment dispersal area. The metasedimentary, K-feldspar monzogranite, and hornblende-biotite tonalite rocks are more abundant in the region and relatively well-distributed spatially and were thus eroded and incorporated into the till draping the study area. The mafic and felsic volcanic rocks are not spatially extensive and so they are not as abundant in the till, with the exception of soft or altered bedrock lithologies (such as kimberlite). The material that does become incorporated in the till can be transported for many kilometres in a down-ice direction (McMartin and McClenaghan, 2001).

This shows that the dominant processes of erosion (plucking and abrasion) produced a mixture with limited compositional fractionation between the coarse and fine fractions. This also suggests that little (if any) pre-existing sediments from other depositional environments (*e.g.* lacustrine, fluvial) were re-entrained and mixed in the till. However, previously deposited tills could have been mixed with the surficial till to some extent. The PCA of the subsurface till, where till is thicker, has a more distal signature from bedrock sources located further up-ice flow direction or from a different, older, ice-flow direction compared to the surface till. Results from this study suggest that till stratigraphy appears to occur locally in the study area. Kelley *et al*. (2019) also reached a similar conclusion in a recent local study further to the southeast.

When considering both surface and subsurface data, a more complex story emerges. There may be areas containing older till units transported and deposited by different ice flow phases flowing in different directions (**Figure 2-24A**). However, it is challenging to confirm stratigraphic layering with either sharp or gradational contacts. The RC drilling method used in this project makes it difficult to detail stratigraphy. The vertical changes may thus reflect increasing inheritance with depth (**Figure 2-24B**), which means a higher proportion of pre-existing till material at depth all within a single till sheet with no clear stratigraphic boundaries, as opposed to true separate stratigraphic units (*e.g.* Trommelen *et al.*, 2013).

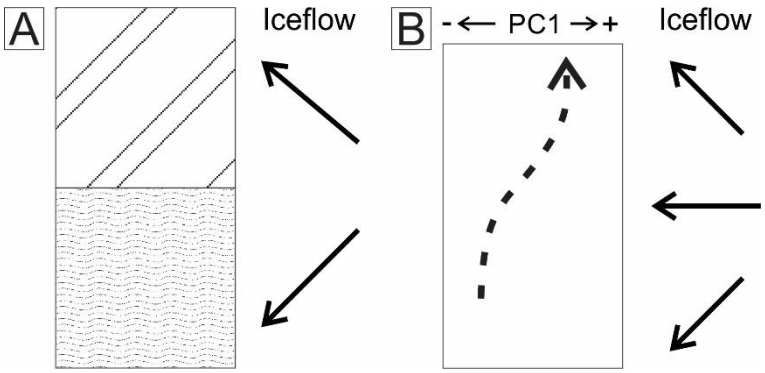

Figure 2-24: Diagrams showing A: till stratigraphy; and B: till inheritance.

One method of defining either stratigraphy or inheritance is to examine a single borehole PCA results to determine if the till-bedrock associations gradationally change from one till type to another, or if the till-bedrock association 'jumps' on the PCA graph between a 'lower till' and an 'upper till'. **Figure 2-25** displays the PCA results for BH 15-144 (A) and BH 15-138 (B). BH 15-144 (A) shows a smooth trend of metasedimentary associated samples at the base of the till column grading into mixed till samples at the top. If this trend were to continue, it is expected that the samples would eventually become associated with the igneous bedrock. In BH 15-138 (B), a large group of metasedimentary associated samples occur in the deep till. The samples then begin to trend toward mixed and igneous associated samples in the shallow till. The transition is not as smooth in this borehole and the shallow samples are associated with both the mixed and igneous till signatures. This displays the high degree of mixing that occurs during till transport, but the shallow samples are nonetheless trending toward an igneous association.

In any case, results show that the deeper till has a clear signature indicating longer transport than the surface till. This is somewhat surprising given the long northwest-trending dispersal trains documented in the surface till (Miller, 1984; McClenaghan *et al*., 2002). It suggests that the deeper till could have been transported even further than the surface till by fast ice flow whereby the ice-bed interface was decoupled (low effective stress) along the hard igneous bedrock (Evans *et al*., 2006; Stokes, 2018), creating a till that has a more 'exotic' bedrock signature relative to the bedrock directly underlying it. The deep till does not have GSD or clast lithology information. This creates an obstacle for defining stratigraphy or inheritance in deeper tills from the previous ice-flow phases. From the PCA classification of major oxides, it appears that some of the BHs are interstratified, or at least show vertical variations in their major oxide composition, while some have a sharp contrast that could reflect stratigraphy. There is a clear vertical trend, however the nature of this trend is unclear. Chapter 3 further explores these possibilities by analyzing additional data (trace elements and kimberlite indicator minerals).

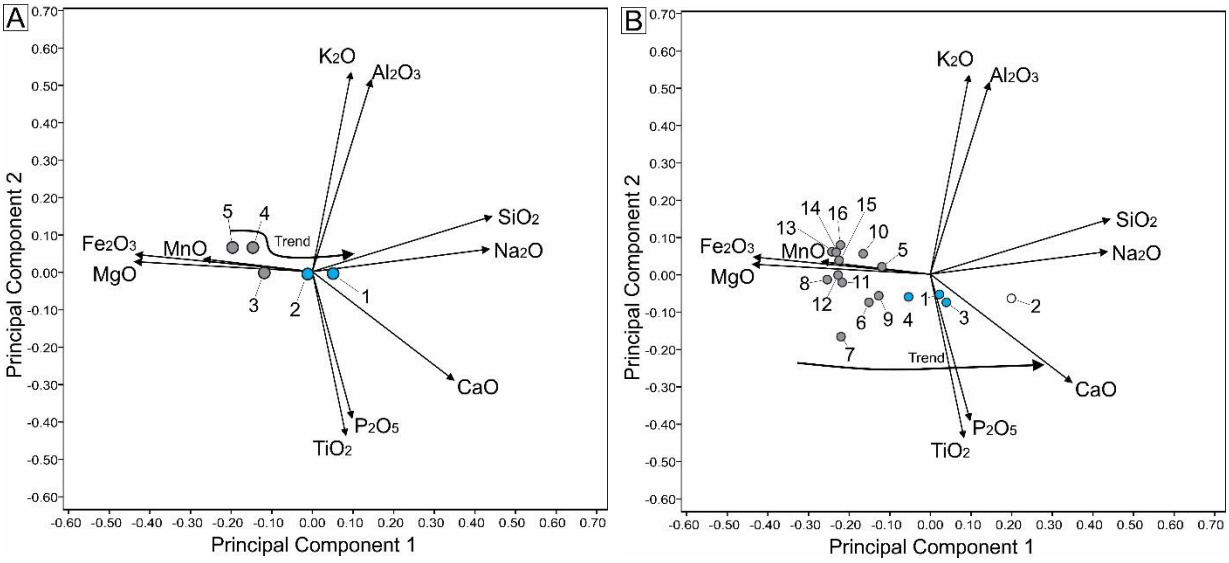

Figure 2-25: Principal Component Analysis (PCA) of A) BH 15-144; and B) BH 15-138 displaying metasedimentary associated till in the deep samples trending toward igneous associated samples in the shallow till samples.

2.5.2 Implications for interpreting till dispersal patterns

The implications for interpreting till dispersal patterns in the study area are:

1) surficial till reflects the most recent glacial movement.

The till at the surface displays compositional patterns associated with the most recent NW-trending ice flow, with a certain degree of inheritance. Inheritance from previous ice flow phases may be limited in the surface till which should simplify provenance analysis when only surficial till is investigated. However, as the results show, a till signature associated with soft rock (metasedimentary) may persist while only slowly integrating new material, which may explain some of the long northwest-trending dispersal trains recognized in the region whereby indicators of interest are found far from their source (*c.f.* Chapter 1, section 1.2.4; McClenaghan *et al*., 2002). It is also worth mentioning that over these hard lithologies with fewer joints, higher inheritance from pre-existing tills may be better preserved in the surface till due to reduced erosion of that local bedrock. This is something that could have affected the Coppermine dispersal train more than the Monument dispersal train, for example.

2) deep till exhibits characteristics of stratigraphy or inheritance that may be linked to an older ice flow phase(s).

In areas of thicker till (≥9 m), there is a noticeable vertical compositional shift in the major oxides of the till matrix, with the deeper till having a signature more characteristic of bedrock located several kilometres up-ice than local underlying bedrock. However, the exact source and sediment transport direction are uncertain; a close look at the regional bedrock map shows that results could be consistent with any of the known ice flow phases (SW, W and NW). This is interesting, because the normal expectation, for a single till unit model, is for till to be increasingly similar to underlying bedrock as it approaches the bedrock surface; the so-called 'basal till' of drift prospectors. Indeed, Boulton (1996) suggests that a vertical compositional change under a single ice flow model shows the sediment at the base of a till sheet should closely reflect the underlying bedrock, progressively shifting to predominantly far travelled lithologies up the till column. Interestingly, the results of this study show the opposite trend. This could indicate that there was a shift in ice flow dynamics, which led far-travelled material to be deposited first, followed by partial erosion of that till sheet and subsequent deposition of more locally derived material. This could happen if there was faster-flowing ice during the early stage of the last northwest ice flow with limited erosion and entrainment of local rock debris, and more basal melt-out, owing to low effective stress and warmer basal ice, respectively, which is commonly associated to warm-based fast-flowing glaciers (Menzies, 2002; Evans *et al*., 2006).

This model does not require a shift in ice flow direction; just a shift in average sediment transport distance as till was being accreted vertically. However, the observed change could also involve a shift in ice flow direction from southwest to northwest and would thus represent the depositional record of the ice flow history as recognized by the erosional ice flow indicators (section 2.4.1). Whatever the case may be, the interpretation of subsurface till data must be done with caution as it appears to have a contrasting composition, at least from the perspective of major oxides in the till matrix, which may have been caused by different ice dynamics. The degree to which this could affect 3D patterns of indicator mineral trains and their interpretation remains unclear. It is possible that the source of some indicator minerals found at depth are different than similar indicators found at the surface because of different transport distance, different transport direction, or a combination of the two. It is also possible that some indicators in the surface till are derived from the re-entrainment of till at depth. It is worth noting that the Coppermine indicator train, for which no source has yet been identified, seems to extend over an area where RC drilling encountered thicker till more frequently than along the Monument indicator train.

3) mineral exploration in areas of complex terrain may be misinterpreted if the glacial history of the area is not fully understood

A common exploration technique is to take surficial till samples and analyze them for indicator minerals. However, indicator minerals generally provide information about an unknown source of economic interest and not necessarily about the main bedrock source. Typically, the source of indicator minerals is determined based on the shape of the dispersal train and geophysical data at the head of the train (McClenaghan *et al*., 2000). This approach is important to the mineral exploration problem; however, indicator minerals alone are not particularly useful to determine the dominant provenance of tills. It is not uncommon to have indicator trains detached from their source making it difficult to use indicator minerals alone to identify a distal source; this is an important limitation of traditional drift prospecting techniques focusing on indicator minerals as opposed to a more holistic ‘till provenance analysis’ approach. A provenance analysis based on clast lithologies and till matrix geochemistry can reveal important information about bedrock sources of the fine till fractions. This can provide important insights for better interpreting indicator mineral trains. The complex interplay between the distance of transport and the ice

flow direction(s) may have major implications on the interpretation of indicator trains and the potential distance and/or up-ice direction to source.

2.6 Conclusions

The evolution of ice-flow direction using erosional outcrop scale paleo-ice flow indicators show an evolving history of ice-flow in a clockwise direction starting in the southeast, then west, and finally to the northwest. There are indications that, during deglaciation, ice flowed toward a regional trunk esker to the north, but it did not play a role in the erosion or dispersal of sediments within the study area.

The till provenance is defined using field-based observations of glacially dispersed detritus. The ice-flow indicators show that the northwest ice-flow phase is prominent in the study area with 77% of all observations in the northwest direction. The particle size distribution of surficial till samples is relatively homogenous, which lends support to the previous interpretation that the surface till forms a single till unit; however, texture alone is rarely sufficient to reach a strong conclusion as to the origin of a till. The clast lithological analysis shows that the till contains all the different lithologies present in the study area in variable proportions, which appears to reflect a combination of processes and factors, such as bedrock hardness in the up-ice area versus in the dispersion area. The PCA of the major oxides shows the till is a mixture of the local bedrock material, but with end-member categories associated with the different bedrock lithologies mapped in the region. Notably, the till at depth, where till is thicker, appears to show a more distal signature than the overlying till or in areas of thin till. This suggests the presence of multi-till stratigraphy or higher compositional inheritance at depth related to older tills. It is unclear whether that apparent stratigraphy reflects a shift in the ice flow direction, a change in subglacial conditions and average sediment transport distance, or a combination of the two.

These findings help improve our understanding of the conditions that led to the deposition of till by ice sheets in the study area. This has the potential to also help link more elusive indicator trains, such as the Coppermine train, to their unknown source. The indicator minerals are typically traced in a single up-ice direction to find their source, but this study shows that the full record is more complex. The material found in deeper tills appears to be compositionally different than the till at the surface. The degree of compositional inheritance from these older

tills into the surface till seems relatively minor. However, it is important to note that all the known lithologies of the study area are present in almost every sample, regardless of their location, and several surface to near-surface till samples have a mixed bedrock signature based on their major oxides. Also, the long clast dispersals suggest long transport distance and limited dilution in some places, possibly due to bedrock hardness in these dispersion areas. The combined effect of inheritance, re-entrainment, and long transport distances in the youngest ice flow direction could have created more complex dispersal trains. If kimberlitic media were to be distributed by the earlier southwest or western ice-flow phases then the indicator minerals would be reoriented to align with the later northwestern ice-flow phase due to the strength and longevity of the movement shown through the strong correlation of the surficial material and the ice flow indicators with the northwestern ice flow phase.

Chapter 3: Surface and Subsurface Glacial Sediment Dispersal Patterns of Kimberlite Indicator Minerals and Geochemical Pathfinders and their Relationship to Regional Ice Flow History, Lac de Gras, NT

3.1 Introduction

Mineral exploration in glaciated terrain often relies on the use of indicator minerals and geochemical pathfinders in the glacial sediments that form spatially recognizable surficial patterns emanating from outcropping or subcropping bedrock sources. These patterns exist due to secondary detrital dispersion by glacial processes (Fipke *et al*, 1995; McClenaghan *et al*., 2002; Pell *et al*., 2017). These surficial patterns are typically more extensive than their bedrock source, making them easier to locate. A classic conceptual model of dispersal patterns in till represents an envelope of anomalous concentrations that extends in a down-ice direction and rises through the till column from a buried source (Miller, 1984). This model assumes a single till sheet from one ice flow phase. Areas with a more complex glacial record may not conform to this classical conceptual model and may thus limit the success of drift prospecting strategies based on this model. Multiple complications may arise in these areas. For example, multiple ice flow phases could result in more complex surficial dispersion patterns (*e.g*. Parent *et al*., 1996; Paulen *et al*., 2013; Oviatt *et al*., 2015), or surficial dispersal patterns may not reflect the full ice flow history with areas where inheritance from older ice flow phases is recognized only in deeper till (*e.g.* Kelley *et al*., 2019). An understanding of the residual till patterns from multiple ice-flow directions is needed to trace mineral signatures back to their source. Additionally, dispersal patterns across areas of discontinuous till cover may be fragmented and difficult to interpret.

Despite these challenges, drift prospecting has been successfully applied in many prospective glaciated areas including in regions of complex glacial history. This is particularly the case in diamond exploration, where drift prospecting is part of the 'standard' exploration toolkit in Canada, whereby well-established suites of kimberlite indicator minerals (KIMs) are used to assess the regional potential for diamondiferous kimberlites or to assess buried targets (Fipke *et al*, 1995; McClenaghan *et al*., 2002; Pell *et al*., 2017; Kelley *et al*., 2019). Many of these buried

targets are first identified through geophysics, but drift prospecting is used to further assess their potential of being buried kimberlites and to assess their potential for being diamondiferous. This is particularly useful because geophysics often identifies too many prospective targets and the cost of drilling all these targets would be prohibitive. Therefore, drift prospecting is used to narrow the number of targets and rank them by their diamondiferous potential based on KIM suites retrieved in the down-ice till.

The Lac de Gras area in the Northwest Territories is Canada's chief diamond district. This area was discovered using drift prospecting. Exploration along the dominant ice flow vector has proven successful (Fipke *et al*., 1995; McClenaghan *et al*., 2002), despite clear evidence for multiple ice flow phases in the region, which was well documented in a series of government mapping projects (Dredge *et al*., 1994; Ward *et al*., 1995; Ward, 1997; Kjarsgaard *et al*., 2002). The early success of drift prospecting using one dominant ice flow vector may have biased subsequent surveys resulting in oversimplified interpretations of some dispersal patterns. It may also have caused areas with atypical or weak surficial patterns to be overlooked. Thus, there is a need to investigate the net effect of regional shifts in ice flow direction on dispersal patterns in the Lac de Gras region and its implications for drift prospecting to identify more elusive buried targets that may have been missed or overlooked.

Chapter 2 came to three main conclusions: 1) Evidence of northwest ice flow is ubiquitous within the study area accounting for 77% of all ice flow erosional indicators; 2) Composition of the surficial till is largely consistent with a southeastern provenance and thus reflects the main northwest ice flow phase; and 3) subsurface till has compositional characteristics and associated spatial patterns that are interpreted to reflect some degree of inheritance or stratigraphy from previous ice-flow phases. Building on this foundation, the spatial patterns of surface and subsurface KIMs and geochemical pathfinder elements are examined in this chapter and compared against surficial-only patterns from publicly available datasets as well as known kimberlite locations and characteristics. The three-dimensional patterns are also compared and contrasted to the spatial dispersal patterns of other constituents of the till (*c.f.* Chapter 2) to provide additional information about the possible association to older ice flow phases. Finally, potential kimberlite source areas for the patterns are discussed.

3.1.1 Study Location and Physiographic Setting

The study area is situated ~300 km northeast of Yellowknife, Northwest Territories, within NTS map sheet 76D (**Figure 3-1 A**) to the south and west of Lac de Gras, NT. It encompasses an area of approximately 700 km^2 (**Figure 3-1 B**). Generally, the study area has low relief defined by topographic variations that are controlled by bedrock ridges. There are many areas of thin till mapped as till veneers (<2 m thick), and till blankets (2 – 10 m thick) (Ward *et al*., 1995). The study area is situated north of the tree line (**Figure 3-1 C**). Permafrost is continuous (**Figure 3-1 D**) and frost-shattered bedrock is prevalent, especially in the eastern part of the field area. A more complete description of the study location and the physiographic setting is presented in Chapter 1 (*c.f.* section 1.1.1).

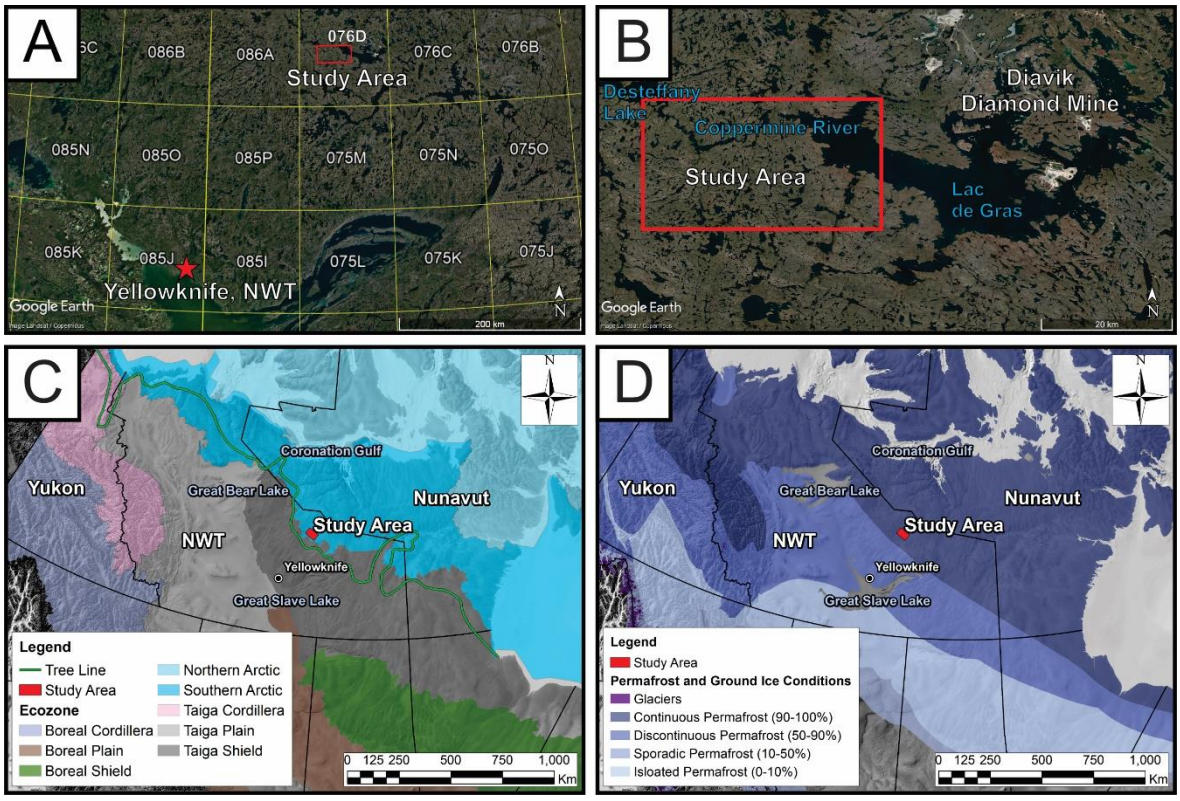

Figure 3-1: The study area is located A) ~300 km NE of Yellowknife within NTS map sheet 76D (NRCAN, 2014; Google Earth, 2020); B) west of Diavik Diamond mine and southwest of Lac de Gras (modified from Google Earth, 2020); C) within the southern arctic ecozone (bright blue) and north of the tree line (green line is northernmost tree growth) (modified from Ecological Stratification Working Group, 1996); and D) within the zone of continuous permafrost (dark blue) (modified from Brown et al., 1997).

3.2 Geologic Setting

3.2.1 Bedrock Geology

The study area is located in the central Slave Geological Province. The central Slave Province can be characterized as a typical Archean granite-greenstone terrane consisting of sedimentary and volcanic sequences intruded by granitoid rocks (Kjarsgaard *et al.*, 2002). The main rock types found within the study area are the Yellowknife Supergroup sedimentary, post-Yellowknife Supergroup K-feldspar rich monzogranite, syn-Yellowknife Supergroup hornblende biotite tonalite, and Yellowknife Supergroup felsic porphyritic and mafic intrusive rocks. The Slave Province was largely emplaced by 2550 Ma (Kjarsgaard *et al.*, 2002), but episodic volcanism associated with the emplacement of a spatially extensive kimberlite field altered the Slave Province from 74 to 45 Ma (Davis and Kjarsgaard, 1997; Heaman *et al*., 2003; Creaser *et al.*, 2004; Lockhart *et al*., 2004). A more complete description of the rock types is presented in Chapter 1 (*c.f.* section 1.2.1).

3.2.2 Kimberlite Emplacement

Kimberlite is an intrusive body of magmatic ultramafic rocks that occurs in Archean cratons around the world (Janse and Sheahan, 1995; Yaxley *et al.*, 2013). These ultramafic rocks are formed through the partial melting of the deep mantle (200 to 250 km depth) at high pressures (6 to 8 GPa) (Wilson and Head, 2007). The rapid ascension of the kimberlitic magma leads to the distinctive inequigranular texture and heterogeneous nature (McClenaghan and Kjarsgaard, 2001; Wilson and Head, 2007). This heterogeneous nature is characterized by numerous sizes and textures of mantle xenoliths, mantle xenocrysts, macrocrysts, crustal xenoliths, and phenocrysts, all set in a groundmass matrix (McClenaghan and Kjarsgaard, 2001). The Lac de Gras kimberlite field contains two forms of kimberlite. The first is the classic kimberlite ‘pipe’ comprised of volcaniclastic and/or diatreme facies kimberlite (McClenaghan and Kjarsgaard, 2001). These may be quite variable in their size and geometry. The kimberlite pipes in the Lac de Gras field form carrot-shaped diatremes that are small (50 – 250 m diameter), steep-sided (75 – 90°) bodies with country-rock contacts, identical to the classical South African style kimberlite bodies (Clement, 1975; Kjarsgaard, 1996; McClenaghan and Kjarsgaard, 2001). An example of the volcaniclastic facies kimberlite is the Misery pipe (Ekati Diamond Mine) and the A154N

pipe (Diavik Diamond Mine). The second type of kimberlite occurrence is thin dykes, blows (enlarged dykes), and sills of hypabyssal facies (McClenaghan and Kjarsgaard, 2001). The kimberlite diatremes grade into root zones at depth, exposing the dykes, blows, and sills. These are typically 1 to 10 m in width and can be laterally extensive. An example of the small hypabyssal facies kimberlite is at Snap Lake, NT. However, these dykes, blows, and sills also occur as larger irregularly shaped, multiple lobed root zone complexes (*e.g*. 5034 kimberlite at Kennady Lake, NT) (McClenaghan and Kjarsgaard, 2001).

The diatreme kimberlites are porous and contain numerous minerals that are unstable at low temperatures and in the presence of oxygenated water. Thus, they are subject to weathering after emplacement (McClenaghan and Kjarsgaard, 2001). Many kimberlites in the Lac de Gras region are found in the low or swampy ground, under small lakes, or covered by thick glacial sediments because weathered kimberlite is more susceptible to glacial erosion than the surrounding bedrock (McClenaghan and Kjarsgaard, 2001). Glacial erosion can remove preglacially weathered soft kimberlite and some of the competent kimberlite below or, due to sheltering effects, the soft pre-weathered kimberlite can remain intact on top of the pipe (McClenaghan and Kjarsgaard, 2001). For example, McClenaghan *et al*. (1996; 1999) studied kimberlite pipes near Kirkland Lake, Ontario. The A4 kimberlite, after exposure to glacial erosion, had all preglacially weathered kimberlite removed. The surface of the kimberlite subcrops beneath 30 m of glacial sediments. In contrast, the B30 kimberlite, 10 km west of the A4 pipe, contains 10 m of soft and highly weathered dark green clay-rich kimberlite at the top of the pipe (McClenaghan *et al*., 1996; 1999). This is important to note because the rapid removal of the weathered kimberlite by glacial processes can generate well-developed indicator mineral trains. In contrast, kimberlites with intact weathered profiles indicate limited glacial erosion, which may have produced a much weaker dispersal train (or lack thereof) in the down-ice till regardless of the kimberlite composition and diamond potential (Kelley *et al*., 2019).

3.2.3 Glacial History

The regional scale surficial geology in the Northwest Territories has been mapped by the Geological Survey of Canada (GSC) to provide a regional framework for the geologic interpretation of surficial deposits and drift prospecting (Dredge *et al.*, 1994; Ward *et al*., 1995; Ward *et al*., 1996). This work produced the basis for surficial geological maps (1:60,000), ice

flow direction, and till composition on a regional scale. The glacial record of the Lac de Gras area indicates a shifting pattern of ice flow to the southwest, then west, and finally to the northwest presumably due to the southeastern migration of the M'Clintock Ice Divide (Dyke and Dredge, 1989; Ward *et al*., 1995; Tarasov and Peltier, 2004; Gowan *et al*., 2016). Several local ice flow indicators have been observed and measured in the study area and the relative age chronology reconstruction of these indicators shows a clockwise shift of ice flow from the southwest to the north that is divided into four phases. The earliest ice flow is 240º southwest; the second is 270˚ west; the third is 305˚ northwest; and the fourth 005˚ north. The northwest ice flow is most prevalent and is the dominant direction of the known surficial KIM dispersal trains in the area, and the northern ice flow has been interpreted as late-stage deglacial. The net effect of the northern ice flow on till dispersal is minimal to null (Chapter 2). A more complete description of the glacial history of the study area is presented in Chapter 1 (*c.f.* section 1.2.3). The complete ice flow history reconstruction derived from this project is presented in Chapter 2 (*c.f.* section 2.4.1).

3.2.4 Kimberlite Indicator Minerals in Till

Diamonds are rare even in productive kimberlites (*e.g.* 4.8 carats per tonne at A154 South pipe, Diavik (Bryan and Bonner, 2003)), thus kimberlite indicator minerals, other than diamonds, are typically used in surficial sediments to trace a buried kimberlitic source and assess its diamond potential. The exploration phase that led to the first discovery of diamondiferous kimberlites in the Lac de Gras region was initiated in 1981 by tracing KIMs from Blackwater Lake, NT, 300 km east, up the paleo-ice flow, following a regional trunk esker (Fipke *et al*., 1995; Kjarsgaard, 1996). A high number of KIMs were then found north of Lac de Gras, with no more KIMs further east of the area suggesting the kimberlitic source for the indicator minerals was nearby (Fipke *et al*., 1995).

A subset of KIMs, found within till from a disaggregated kimberlite, are used to assess the diamondiferous potential of a kimberlite from which the KIMs are derived (McClenaghan, 2005). Each diamondiferous region has a characteristic suite of KIMs. In addition, certain KIMs have a unique chemical composition that provides key insights into the diamond potential of their source (Vasilenko *et al*., 2002). The KIM grains identified as key indicators within the study area are Cr-diopside, chromite, Mg-ilmenite, orthopyroxene, pyrope-almandine garnet,

eclogitic garnet, olivine, and diamond (Ward *et al.*, 1995, 1997; McClenaghan and Kjarsgaard, 2001; McClenaghan, 2005).

Ward *et al.* (1995) conducted regional till sampling across NTS map sheet 76D (Lac de Gras) to provide publicly available regional KIM data. A total of 85 till samples (approx. 10 kg each) were collected for heavy mineral and KIM analysis, as well as 200 smaller samples for textural analysis and trace element geochemistry. The sampling and analysis were conducted to provide baseline data for classifying the background material within the NTS map sheet 76D. Most KIM grains were found in the 0.25 to 0.50 mm size fraction with 49% of samples collected containing at least one KIM grain. In contrast, the 0.50 to 1.00 mm size fraction contained KIM grains in only 11% of samples, suggesting that the 0.25-0.50 mm size fraction is more useful for discovering and evaluating subtle KIM dispersal trains in the region (Ward *et al*., 1995). The KIMs found for the entire Ward *et al.* (1995) dataset is ~73% pyropes, ~24% Cr-diopside, ~2% Mg-Ilmenites, ~1% chromites, and <<1% eclogitic garnets. Ward *et al*. (1995) considered each 10-kg sample containing more than 3 indicator minerals to be anomalous in the area to the south of Lac de Gras. However, the Ward *et al*. (1995) dataset only contains 8 samples within my study area, making it difficult to define this as the appropriate number of anomalous indicator minerals. Nonetheless, it provides baseline information for this study.

Legacy KIM data collected by the exploration industry is also available via the Northwest Territories Geological Survey (NTGS) GoData geoscience database collection of diamond sample information. This includes the Kimberlite Indicator and Diamond Database (KIDD) information compiled by the NTGS from all publicly available assessment reports containing kimberlite indicator mineral data. The dataset includes sample locations, type of KIMs, and the number of grains for each type of KIM (NTGS, 2018b).

The public dataset contains data from surficial samples only. **Figure 3-2** to **Figure 3-7** show levelled and processed data from this database covering the broad study region relevant for this research. The database is heterogeneous because methods used for collecting and analyzing samples differed from one study to the next. Various sampling protocols were used and much of the data lack notes on the type of sediment sampled. The samples were also processed at different labs. Details on the levelling and other processing steps to prepare this dataset for visualization are provided in Appendix E.

Two prominent surficial dispersal trains are outlined in **Figure 3-2** to **Figure 3-7**: the Monument Indicator Train (MIT) and the Coppermine Indicator Train (CIT). The kimberlite source for the MIT has been identified, but the source of the CIT has yet to be identified. Based on the traditional approach of using the dominant northwest ice flow direction to interpret surficial dispersal patterns, exploration efforts to find the source of the CIT has focused on the area at the up-ice end of the CIT. An analysis of the indicator minerals defining the two trains shows similarities between the CIT and MIT in surficial pyrope garnets and chrome diopside (**Figure 3-2** and **Figure 3-3**), but the CIT displays elevated numbers of olivine and orthopyroxene relative to the MIT (**Figure 3-4** and **Figure 3-5**). Furthermore, the MIT has a larger number of surficial eclogitic garnets and total garnets compared to the CIT (**Figure 3-6** and **Figure 3-7**). These differences in KIM patterns suggest the source for the CIT is not the same as that of the MIT. It is thus tempting to assume that these constitute two separate dispersal trains produced by northwest ice flow. However, several exploration companies have searched the region at the southeast (up-ice) end of the CIT with great effort since the early 1990s without discovering a new source for the CIT (Armstrong, 2016). While the available public data shows some evidence indicating the CIT is not a palimpsest train from an old southwest dispersal from the MIT, it is still possible that the CIT has a different, yet known source somewhere else from around the Lac de Gras.

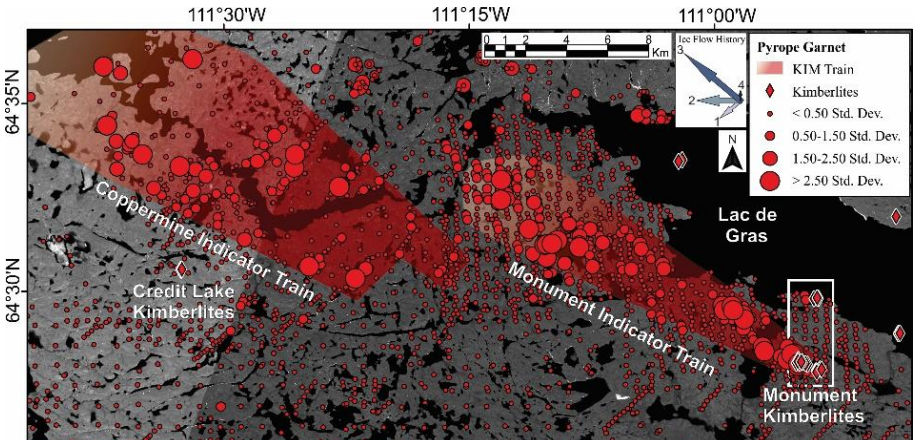

KIM Train	KIM Count
Monument	3218
Coppermine	1316

Figure 3-2: Public KIM data displaying similarities in surficial pyrope garnet grains between the CIT and the MIT. Total KIM counts within the highlighted mineral train. Data from NT GoData (NTGS, 2018).

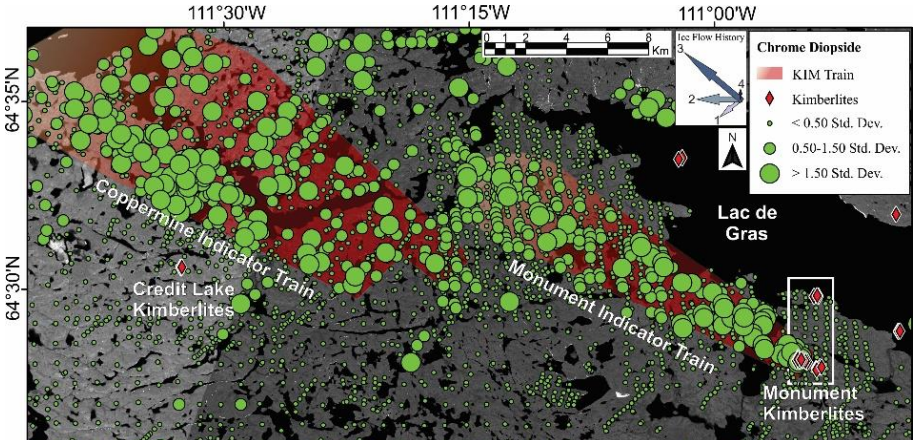

KIM Train	KIM Count
Monument	2803
Coppermine	2923

Figure 3-3: Public KIM data displaying similarities in surficial chrome diopside grains between the CIT and the MIT. Total KIM counts within the highlighted mineral train. Data from NT GoData (NTGS, 2018).

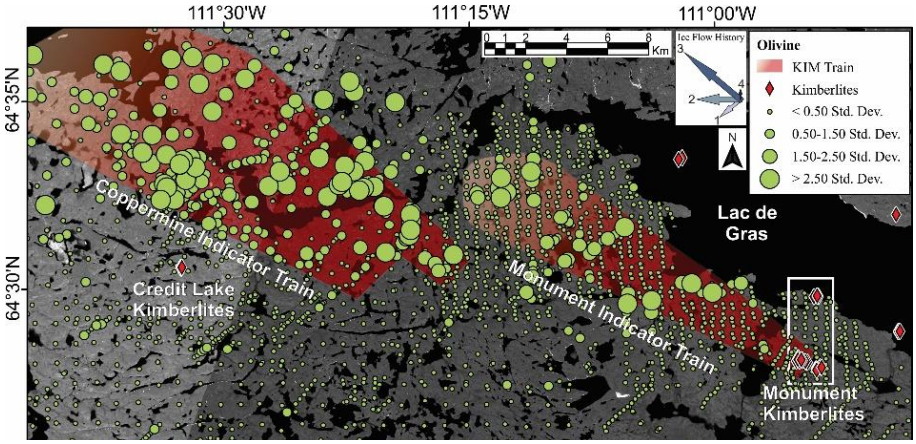

KIM Train	KIM Count
Monument	3140
Coppermine	10380

Figure 3-4: Public KIM data displaying surficial olivine grains within the CIT compared to the MIT. Total KIM counts within the highlighted mineral train. Data from NT GoData (NTGS, 2018).

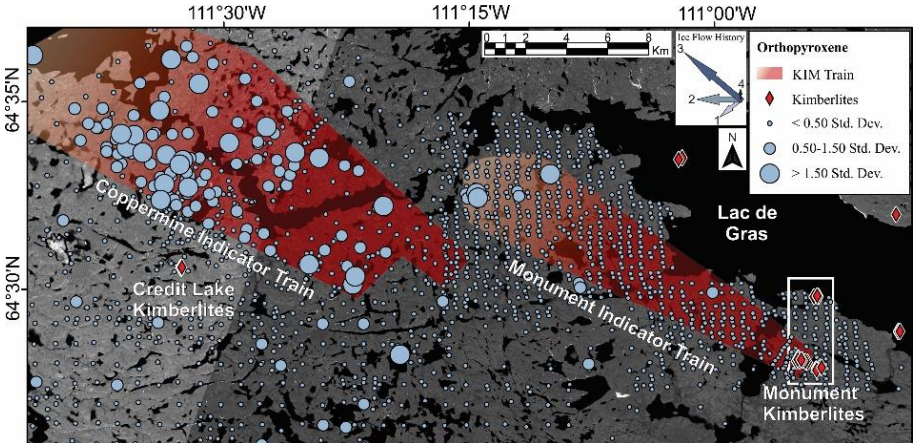

KIM Train	KIM Count
Monument	71
Coppermine	920

Figure 3-5: Public KIM data displaying surficial orthopyroxene grains within the CIT compared to the MIT. Total KIM counts within the highlighted mineral train. Data from NT GoData (NTGS, 2018).

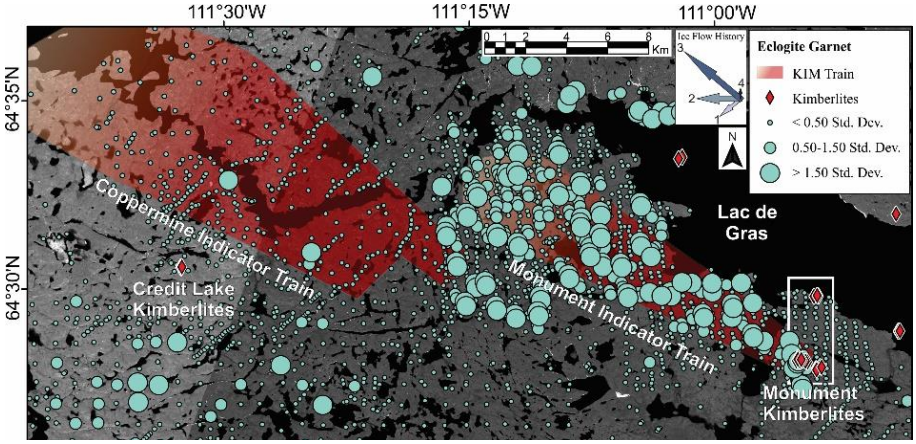

KIM Train	KIM Count
Monument	1279
Coppermine	89

Figure 3-6: Public KIM data displaying surficial eclogitic garnet grains within the MIT compared to the CIT. Total KIM counts within the highlighted mineral train. Data from NT GoData (NTGS, 2018).

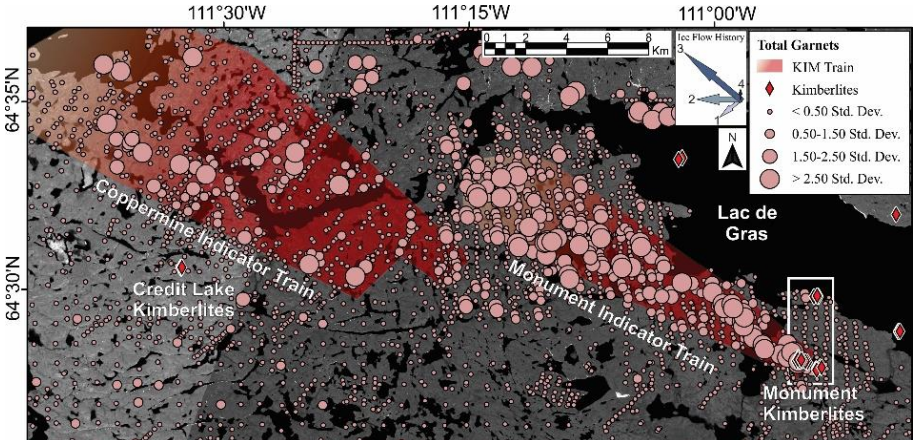

KIM Train	KIM Count
Monument	4497
Coppermine	1405

Figure 3-7: Public KIM data displaying surficial total garnet grains within the MIT compared to the CIT. Total KIM counts within the highlighted mineral train. Data from NT GoData (NTGS, 2018).

There are two locations with known kimberlites close to the study area that do not have an associated KIM train. The first is the CH02 group of kimberlites ~8 km south of the Monument kimberlites (just south of the mapping area). These kimberlites were discovered using geophysical techniques and drilling despite being devoid of an associated indicator mineral train. They were also discovered to be barren of any diamonds and are therefore of no economic interest (Northern Miner, 2002). The second group of kimberlites is the Credit Lake kimberlites located in the western study area, south of the CIT. No information is available on these kimberlites aside from their location detailed in the NTGS GoData. The public data also shows that there is no known indicator mineral train close to this group of kimberlites. These kimberlites are located beneath a cover of sediment as well as being sheltered by surrounding topographic ridges. Together, these observations support the idea that these kimberlites were

sheltered from glacial erosion and dispersal processes. Both groups of kimberlites were likely sheltered from glacial erosion processes, in a similar manner as proposed for the B30 kimberlite pipe at Kirkland Lake, ON (McClenaghan *et al*., 1996). These two groups of kimberlites are thus unlikely to be a source for the CIT. It is possible that the kimberlites in the northwestern part of Lac de Gras deposited indicator minerals in the area at the tail of the Monument train and the head of the Coppermine train from the early southwestern ice flow. However, due to the shape and surficial expression of the surrounding indicator mineral trains, it is unlikely to have deposited a significant number of indicator minerals. There is also an extensive kimberlite field to the east and northeast of the study area as shown in the generalized bedrock map of the Central Slave Geological Province (**Figure 3-8**). Due to the previously identified ice flow phases and evidence of relatively long sediment transport (*c.f.* Chapter 2), it is reasonable to hypothesize that there is some input to both the MIT and CIT but these distal sources are unlikely to cause the surficial expression of these trains (**Figure 3-2** to **Figure 3-7**).

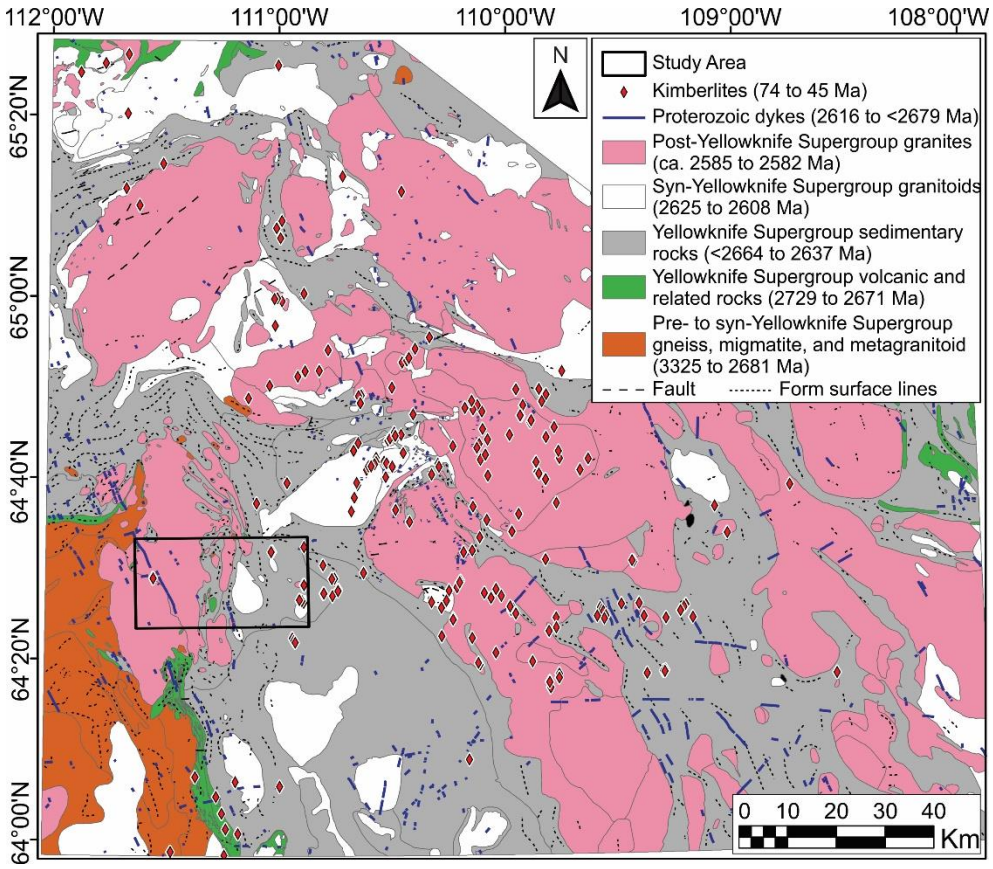

Figure 3-8: Generalized bedrock of the Central Slave Geological Province, including known kimberlites. The study area is outlined. Annotated from Kjarsgaard *et al*. (2002).

3.2.5 Geochemical Pathfinders in Till

Geochemical exploration serves to detect anomalous concentrations of elements in sample media associated with mineralization (Chao, 1984; Kelley *et al*., 2019). Techniques to identify economically important ore bodies and minerals may be used in areas subjected to the physical transportation and deposition of sediment by glaciers to delineate areas of mineralization (Shilts, 1977; Chao, 1984; Kelley *et al*., 2019). These techniques may be used at the reconnaissance scale, down to the property scale for evaluation of geochemical pathfinder elements (McClenaghan and Kjarsgaard, 2007; Kelley *et al*., 2019). Target minerals can be found as small detrital particles in the silt and clay fraction, but they may also become weathered, releasing the cations in solution. The cations can then be fixed by scavengers in the clay-sized fraction of till (Shilts, 1977; McClenaghan and Kjarsgaard, 2007). These cations (*e.g*. cobalt, chromium, nickel, *etc*.) are fixed in the approximate proportion to the minerals originally deposited in the till providing a proxy for the glacial dispersal patterns of target minerals (Shilts, 1977). In some cases, the post-glacial mobility of these cations with groundwater can create secondary dispersal patterns from the initial glacial dispersal trains (Rose *et al*., 1979), but here in the Northwest Territories, permafrost conditions are thought to have minimized these fluxes. Thus, mobile geochemical dispersal with water is assumed to be minimal; they should still largely reflect detrital dispersion by glacial processes. Geochemical pathfinder elements are used to detect elements that are diagnostic of specific mineral grains or their weathering products (Thorleifson, 2017). For example, the presence of olivine in the till will result in an elevated concentration of Ni (McClenaghan and Kjarsgaard, 2007). These associations may be used to identify areas that are most strongly linked with dispersal from areas of mineralization.

3.3 Methods

Several techniques are utilized in this chapter to define the character of the KIM trains within the study area to the southwest of Lac de Gras, NT. Reverse circulation (RC) drilling was conducted, as outlined in Chapter 2, at 52 sites and samples taken at 1.5 m intervals from the surface to the top of bedrock resulting in 155 samples. Hand-dug surficial samples were also collected, as described in Chapter 2, with 13 sites sampled for geochemical pathfinder elements, while 11 of the 13 samples were also analyzed for KIMs. The RC and hand samples were both analyzed at Saskatchewan Research Council (SRC) analytical laboratory to maintain consistency and to

reduce analytical error by comparing samples analyzed within the same laboratory. The samples are used to determine elevated numbers of KIMs and anomalous geochemical pathfinder elements throughout the study area.

3.3.1 Till Analysis

Ice flow indicators, grain size distributions, clast lithology, and till matrix geochemistry were examined in Chapter 2 to define the variation in the composition of till throughout the study area from the ground surface to bedrock. Results from the near-surface till show a stronger matrix geochemical relationship with the underlying bedrock where till is thin (≤ 1.5 m) than where it is thick (≥ 1.5 m) (*c.f.* Chapter 2; Fig. 2-21), although pebble provenance analysis shows long dispersal patterns that are consistent with the dominant northwest ice flow direction (*c.f.* Chapter 2; Fig. 2-15). In areas of thick till, results show a weaker relationship to underlying bedrock, as well as geochemical 'stratigraphy', which suggests changes in provenance (due either to a change in ice flow direction or transport distance). It is not possible to confirm whether these changes correspond to till stratigraphy or more gradual vertical trends, but the observed changes need to be considered in the interpretation of KIM patterns.

3.3.2 Kimberlite Indicator Minerals

KIM analysis was carried out on all hand-dug and RC samples at SRC laboratories using the kimberlite indicator minerals recovery package (SRC, 2017). A flow chart of the KIM separation process is displayed in **Figure 3-9**.

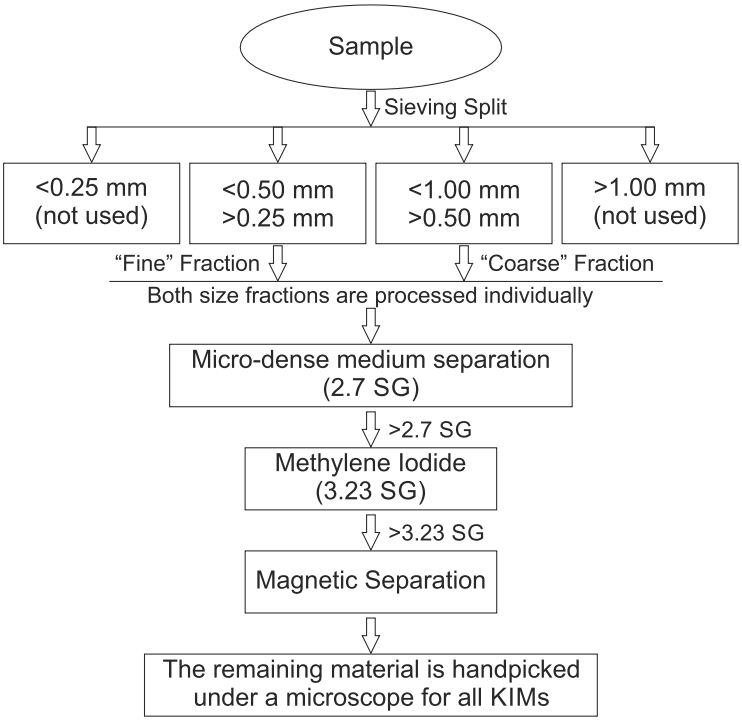

Figure 3-9: Kimberlite indicator mineral recovery flow chart. SG = Specific Gravity.

The KIMs picked for analysis are peridotitic pyrope (Cr-pyrope), eclogitic pyrope (Ti-pyrope), Cr-diopside, olivine, picroilmenite (Mg-ilmenite), and chromite. The picked grains are tallied for each sample and a spreadsheet of the information is provided for further analysis.

The data from the picked KIM grains are processed and levelled for consistency and to validate the results. The average weight of the samples is ~18 Kg. To normalize the data, the number of picked grains is divided by the weight of the dried field sample and multiplied by 20 kg, yielding a normalized value of grains/20 kg. The normalized value of grains/20 kg is used in other case studies in the Lac de Gras region (McClenaghan *et al*., 2002) as well as making the data easier to understand and classify. Quantile-Quantile (Q-Q) plots are then used to determine the thresholds for background, low-count, and high-count data points. The Q-Q plots are used to evaluate the distribution structure of a variable. The predicted normal distribution of the data (x-axis) is plotted against the normalized value of the data (y-axis). Normally distributed data plot along (or close to) a straight line on such a Q-Q plot, whereas data that is not normally distributed shows some departure to a straight line. In mineral exploration, data that plot below the 'normal' line typically correspond to the local background, whereas values that plot above the normal line

typically correspond to anomalies. The Q-Q plot technique works particularly well for geochemical pathfinders that have background values above the detection limit for most samples (Grunsky, 2010); however, it needs to be used differently for indicator minerals where 'background' typically means 'no grain' or zero counts. Kimberlite indicator minerals are not normally distributed across a sampled population because samples with zero KIMs generally dominate a dataset, especially in regional studies. In this case, Q-Q plots are used mainly to identify a threshold between 'low counts' and 'high counts' rather than a threshold between a certain 'background' value and 'anomalies'. This is used to separate samples into a relative 'low count' group and a relative 'high count' group, which can facilitate the spatial and dispersal analysis and interpretation later. The Q-Q plots were completed for the fine and coarse fractions of each KIM. A KIM score is then calculated using the 'low' and 'high' count values determined in the Q-Q plots. The low counts are given a score of one, while the high counts are given a score of two. The low and high count KIM samples are then summed for each sample to calculate the total score (see Appendix F for full results). This approach is used to combine all the KIMs while at the same time avoiding the KIM dispersal maps from being controlled by the most abundant species. It essentially puts the different indicators on the same level. The KIM scores are analyzed spatially, using ArcGIS® (ESRI) 10.5.1, and outlined to define the depositional areas of the KIMs.

Kelyphite rims on pyrope grains are also noted during the counting of indicator minerals in the till; this information is thus part of the dataset. A kelyphite rim refers to the reaction corona that surrounds the pyrope grains (Dredge *et al.*, 1996). It is created during the kimberlite genesis as a reaction between the garnet and the surrounding olivine or orthopyroxene by pressure release during ascension. The significance of the kelyphite rims is that they are easily removed during mechanical abrasion and thus, their presence implies a lack of grain wear, which is typically interpreted to indicate short transport distance from a kimberlite pipe (*e.g.* Dredge *et al*., 1996; Kelley *et al*., 2019). However, Dredge *et al*. (1996) have shown that these grains may be transported distances of up to 30 km from a kimberlite pipe, which show that certain subglacial conditions (*e.g.* high till porewater pressures) can lead to the preservation of these fragile features over relatively long distances. Nonetheless, when carefully analyzed, the overall distribution of grains with kelyphite rims can still bring some insights into relative transport distances (*e.g.* Kelley *et al*., 2019), especially when they show patterns that differ from the rest

of the indicator minerals. The pyrope garnets that contain kelyphite rims are added to the KIM score maps while being analyzed using ArcGIS® (ESRI) 10.5.1 to define the spatial expression of their dispersal.

3.3.3 Till Matrix Geochemistry for Kimberlite

Till geochemistry for diamond exploration focuses on the elements associated with the ultramafic kimberlitic bodies. The key geochemical pathfinder elements for kimberlites in the study area are Ba, Ce, Co, Cr, Hf, La, Mg, Nb, Ni, and Ta (McClenaghan and Kjarsgaard, 2001; Wilkinson *et al*., 2001; Kjarsgaard *et al*., 2002; references therein). The <63-micron size fraction of till is used because it generally provides enough contrast between the anomalous proportion of the cations related to kimberlite and the background material (Shilts, 1977; McClenaghan and Kjarsgaard, 2007). All geochemical pathfinder analyses were performed at SRC laboratories. To measure the elemental pathfinders, partial digestion with Aqua Regia is performed using an aliquot of sample pulp digested in a mixture of concentrated nitric: hydrochloric acid (HNO_3: HCl) in a test tube in a hot water bath, then diluted using de-ionized water. ICP-MS is used for Co, Hf, Nb, Ni, and Ta. Additionally, ICP-OES aliquots fused with lithium metaborate and dilute HNO_3 is used to analyze Ba, Cr, and Mg. This digestion is much more aggressive and is thus considered to be a near-total digest. The elements Ce and La were not included in the analysis.

The elements considered useful kimberlite pathfinders in this study are Co, Cr, and Ni. The measurements indicated Ta was below detection limits and was therefore not used. Some minerals hosting elements of interest are insoluble in weak acid solutions (*e.g*. aqua regia). This is likely the case for Hf and Nb, hosted in minerals like majorite and perovskite. Hf and Nb results, which are only available in the partial digest dataset, are thus not particularly useful for this study and are not included in the analysis. The Mg was used in the analysis of the till-bedrock geochemistry and was found to have a strong association with the metasedimentary rocks in the study area. Therefore, Mg is not used as an indicator of kimberlite in this study. Finally, Ba is associated with the widespread alkaline rocks in the region and is therefore another ambiguous pathfinder not used in this study. This leaves Co, Cr, and Ni as the pathfinder elements used to analyze for kimberlites because of the presence of minerals such as olivine containing elevated concentrations of elements such as Ni; or Cr-spinel, Cr-pyrope, and Cr-diopside reflecting high concentrations of Cr (McClenaghan and Kjarsgaard, 2007).

The geochemistry results are first explored using Q-Q plots to determine the background, elevated, and anomalous data. The data points have been classified according to the bedrock associations of the till matrix (*cf.* Chapter 2; grey = metasedimentary; blue = mixed; pink = K-feldspar monzogranite; and white = hornblende-biotite tonalite). The data is plotted in ArcGIS® (ESRI) for spatial analysis and separated based on the results of the Q-Q plots (see section 3.4.2 for results).

Due to the different digestions used and the relative weights of the pathfinder elements, anomaly scores are calculated for the geochemical pathfinder elements in the same manner as the KIM scores. The anomaly scores are calculated by assigning the elevated samples a score of one and the anomalous samples a score of two. The scores are then tabulated to calculate the total anomaly score for each sample (see Appendix G for full results). The geochemical pathfinder anomaly scores are plotted in ArcGIS® (ESRI) and analyzed spatially (see section 3.4.2 for results).

The aluminum saturation index ($Al2O3/CaO - 1.67 * P2O5 + Na2O + K2O$) (Shand, 1943; Frost, *et al*., 2001) is used to determine the association of sedimentary and granitoid rocks for the top bedrock sample in each RC borehole. Sedimentary rocks and granitoids containing greater proportions of micas (such as those in the study area) have a greater quantity of aluminum. The mafic rocks in the study area are proportionally depleted in aluminum and contain a greater proportion of calcium. Thus, the samples with scores below 0.95 may be mafic bedrock. This is useful for finding links between tills of possible kimberlitic or mafic origins due to the common mineral assemblages for each (Olivine, high proportions of Co, Cr, Ni). If the till sample has a high score but it is overlying bedrock that may be related to mafic rocks, then it is possible that the geochemical pathfinder anomaly score is reflecting a mafic signature rather than a kimberlitic signature.

3.3.4 Quality Assurance Quality Control (QA/QC)

The QA/QC procedures are done to verify the quality of the results to ensure they are suitable for further geological analysis and interpretation. All QA/QC procedures are completed through the preparation and analysis of standards and duplicates. Two standards (CRM Till-1 (1915) and CRM Till-3 (996)) from CANMET certified geochemical soil and till reference materials

(Lynch, 1996) were included within the sample batches. The results from the analysis of the reference materials were evaluated using the relative percent difference method and the duplicates were evaluated using precision scatterplots and Thompson-Howarth precision plots.

There should not be any grains remaining following the picking of the KIM grains. One QA/QC procedure on the KIM samples is to have a second pass observation verification performed on the samples. If more KIMs are identified during the secondary analysis, then the results of the first pass would be considered imprecise. If no more KIMs are found during this verification, then data is considered precise and can be used for further analysis. Other QA/QC techniques are sometimes applied such as adding (spiking) certified blank samples with a known number of KIM grains to verify the quality of the picking process. However, this technique was not performed on the dataset provided for this thesis. The results of the KIM QA/QC are presented in Appendix C.

The relative percent difference uses the analytical results to compare with the published values using the formula $\%RD = 100\left(\frac{x-STD}{STD}\right)$ (Piercey, 2014), where x is the analyte and STD is the certified value of the reference material. This is completed for the relevant geochemical elemental data identified and presented in **Table 3-1**.

Table 3-1: Relative percent difference of Canadian Reference Materials CRM Till-1 and CRM Till-3. The values for Cr are for total digestion, whereas the values for Co and Ni are for partial digestion.

	Analyte	CRM Till-1 (1915)	Relative % difference		Analyte	CRM Till-3 (996)	Relative % difference
Cr (ppm)	61	65	-6.2%		114	123	-7.3%
Co (ppm)	9.85	12	-17.9%		8.47	10	-15.3%
Ni (ppm)	11.9	18	-33.9%		23.6	32	-26.3%

The values for relative percent difference can be positive or negative depending on whether the values are greater or less than the known value. The relative percent differences are considered to have excellent accuracy between ±0-3%, very good accuracy from ±3-7%, good accuracy from

±7-10%, and values above ±10% are not accurate (Jenner, 1996; Piercey, 2014). **Table 3-1** shows the elements for the reference materials till-1 and till-3 are within the very good to good accuracy range for Cr, which was analyzed using a 'total' digestion procedure. However, the reference materials are not accurate for Co and Ni, which were both done using 'Aqua Regia'. This may indicate that the partial digestion method used at SRC differs from the one used by CANMET to determine the certified values. Therefore, and considering the importance of Co and Ni as pathfinders for kimberlites, the duplicates were assessed further using precision scatterplots to verify the internal precision of the results.

The analysis of samples using matching pairs (original vs. duplicate samples) is widely recognized and used on the assumption of a linear relationship between the paired data (Abzalov, 2008; 2011). The precision can then be quantified based on the variance, or scatter, of the data (Abzalov, 2008). This study uses the duplicate assessment as outlined by Piercey (2014). A confidence interval of 90% is set to ensure the accuracy of the data and the precision of the method used to measure the duplicates. The scatterplot is configured with the x-axis as the original weight percent and the y-axis as the duplicate weight percent. The data can be precise (lying within the control lines), moderately precise (data with scatter suggesting no bias), and very imprecise (shotgun scatter) (Fletcher, 2002; Piercey, 2014). Additionally, the data can have a rotational bias, translational bias, and/or decreasing precision with concentration (Fletcher, 2002; Piercey, 2014). The precision scatterplots are displayed in **Figure 3-10** for cobalt, chromium, and nickel. The scatterplots are all precise within the 90% confidence interval.

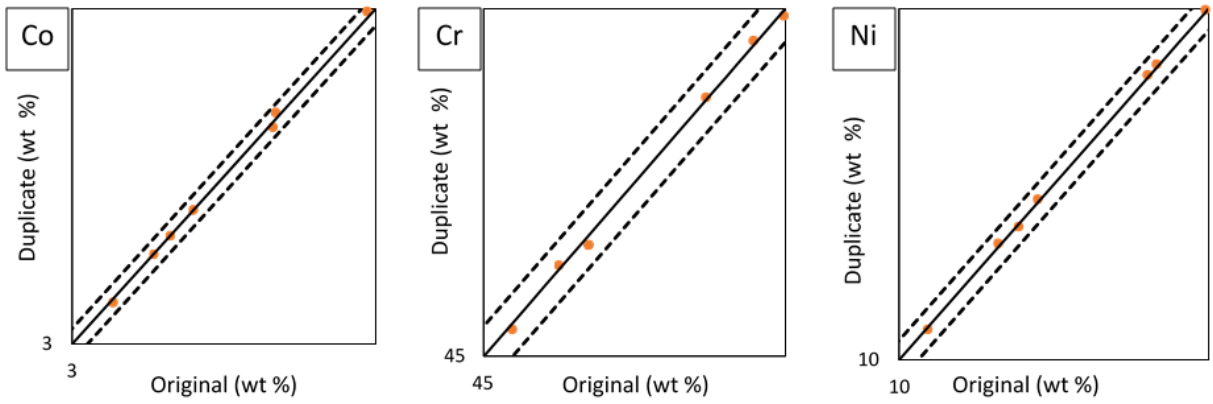

Figure 3-10: Precision scatterplots of sample duplicates. The solid line is the 1:1 sample to duplicate and the dashed lines are the 90% confidence intervals. The scatterplots all display excellent precision for the duplicates.

The Thompson-Howarth short method plots are used to confirm the results of the precision scatterplots. The Thompson-Howarth method (1976) tests the precision of a small number of duplicates by assuming error in the duplicate data are normally distributed and are random (Abzalov, 2008; Piercey, 2014). The median difference of the data is found by examining the relationship between the median of the population and the standard deviation. The precision is set at the 90% confidence interval and a control line is established. If all data fall under the control line then the data is precise to 10%. The Thompson-Howarth plots (**Figure 3-11**) show the data in this dataset are all precise to 10% and therefore, combined with the results from the relative percent difference and precision scatterplots, there is enough evidence to demonstrate confidence in the data and analysis of the dataset may proceed.

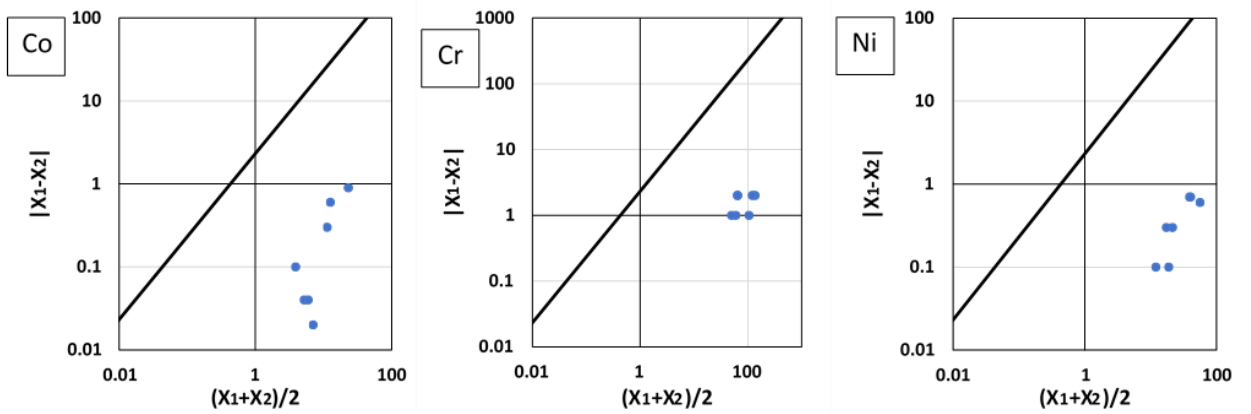

Figure 3-11: Thompson Howarth short method (<50 samples) plots for cobalt, chromium, and nickel. The control line is set at the 90% confidence interval and the resultant duplicate analyses plot with precision to 10% for all the samples in the dataset.

3.4 Results

3.4.1 Kimberlite Indicator Minerals

The Q-Q plots described in section **3.3.2** are displayed in **Figure 3-12** through **Figure 3-17**. The figures display the fine and coarse fractions of till for each of the kimberlite indicator minerals. Each dot corresponds to a sample. The colours are red for relatively 'high' counts and yellow for relatively 'low' counts. Note that the maximum value of each y-axis may be different to help visualize the structure of the data and to better identify the threshold. It is thus important to read these graphs knowing that what is considered 'high' for a mineral in one grain size fraction may be 'low' for a different grain size fraction or another indicator mineral. A table of the normalized

'high' and 'low' grain counts per 20 kg is summarized in **Table 3-2**. The data is plotted in ArcGIS® (ESRI) for spatial analysis based on the results of the Q-Q plots. The results of the individual analysis of each KIM for the fine and coarse fractions are presented in Appendix H.

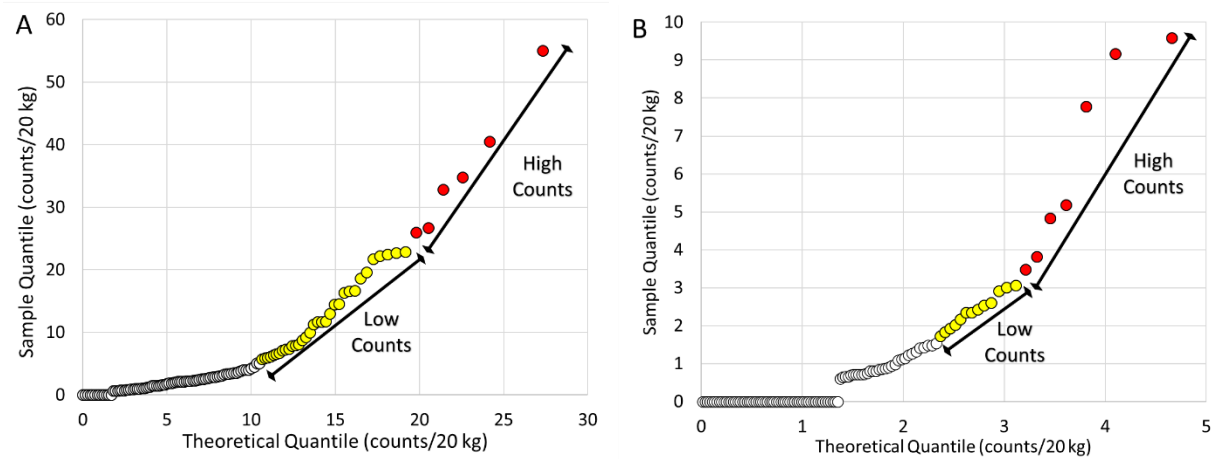

Figure 3-12: Pyrope Garnet Quantile-Quantile (Q-Q) plots for the A) fine size fraction (0.25 – 0.50 mm); and B) coarse size fraction (0.50 – 1.00 mm) displaying the annotated, elevated counts. The elevated grain counts are based on the number of grains in each size fraction and the coarse fraction has lower counts.

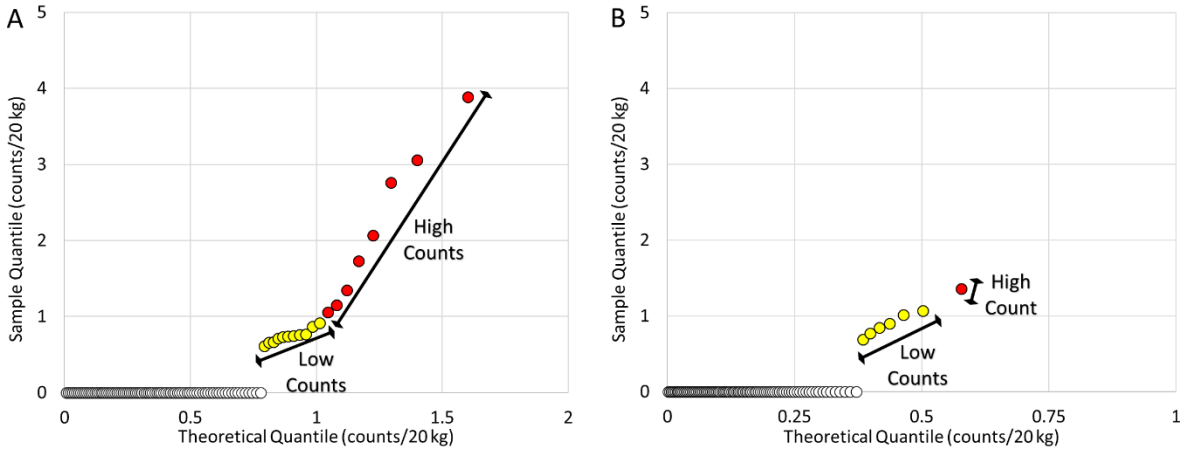

Figure 3-13: Eclogite Garnet Quantile-Quantile (Q-Q) plots for the A) fine size fraction (0.25 – 0.50 mm); and the B) coarse size fraction (0.50 – 1.00 mm) displaying the annotated, elevated counts. Eclogite grains are very low overall.

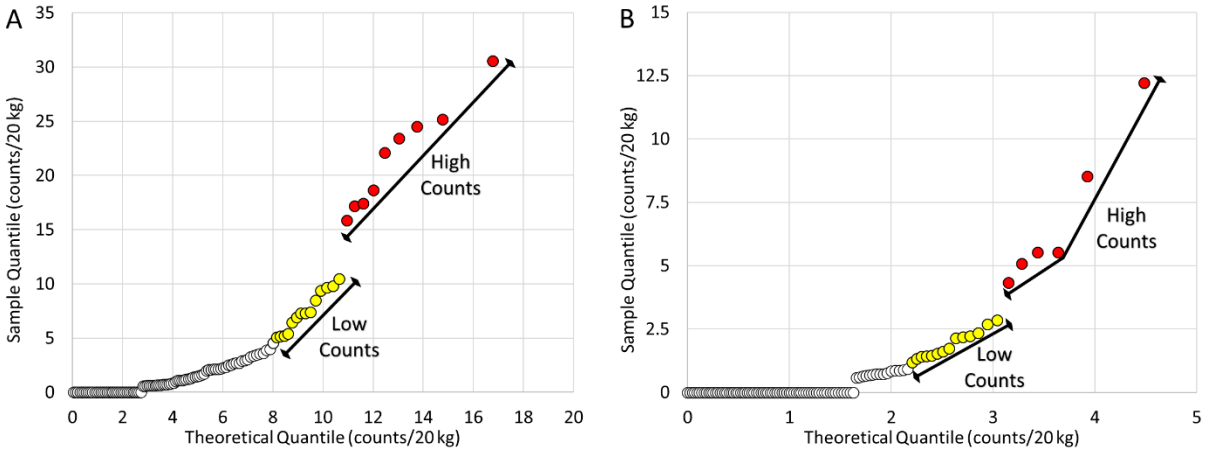

Figure 3-14: Chrome Diopside Quantile-Quantile (Q-Q) plots for the A) fine size fraction (0.25 – 0.50 mm); and the B) coarse size fraction (0.50 – 1.00 mm) displaying the annotated, elevated counts. The elevated grain counts are based on the number of grains in each size fraction and the coarse fraction has lower counts.

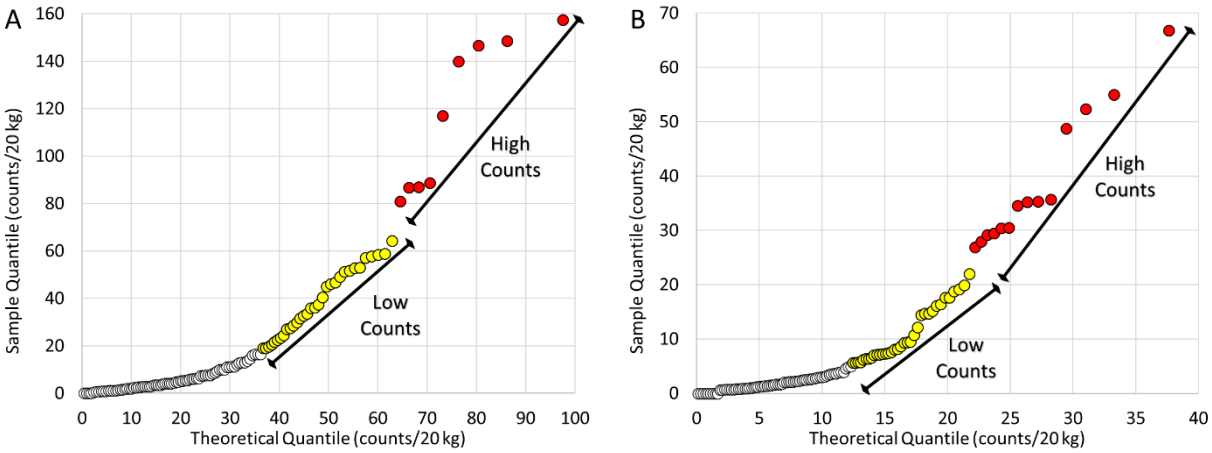

Figure 3-15: Olivine Quantile-Quantile (Q-Q) plots for the A) fine size fraction (0.25 – 0.50 mm); and the B) coarse size fraction (0.50 – 1.00 mm) displaying the annotated, elevated counts. The elevated grain counts are based on the number of grains in each size fraction and the coarse fraction has lower counts.

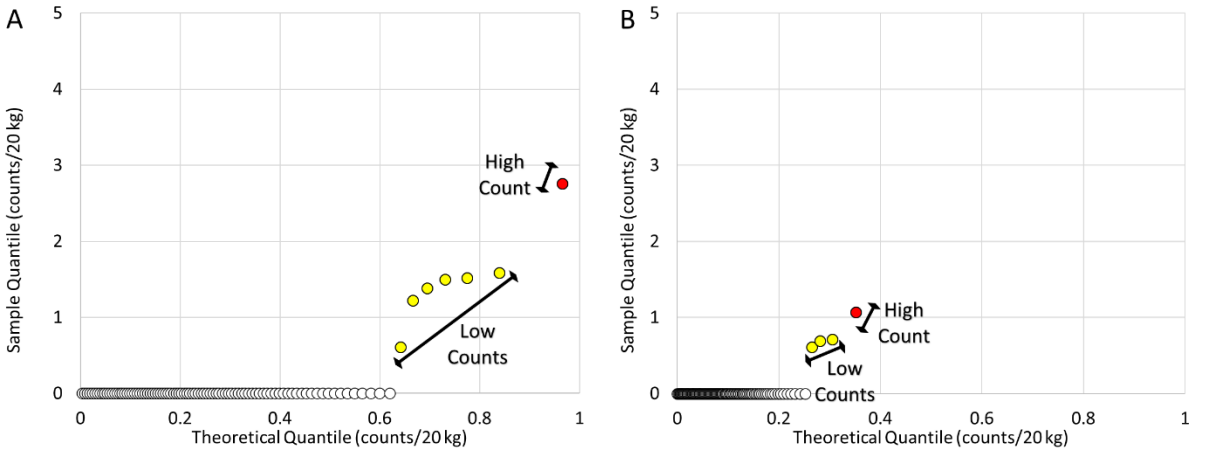

Figure 3-16: Picroilmenite Quantile-Quantile (Q-Q) plots for the A) fine size fraction (0.25 – 0.50 mm); and the B) coarse size fraction (0.50 – 1.00 mm) displaying the annotated, elevated counts.

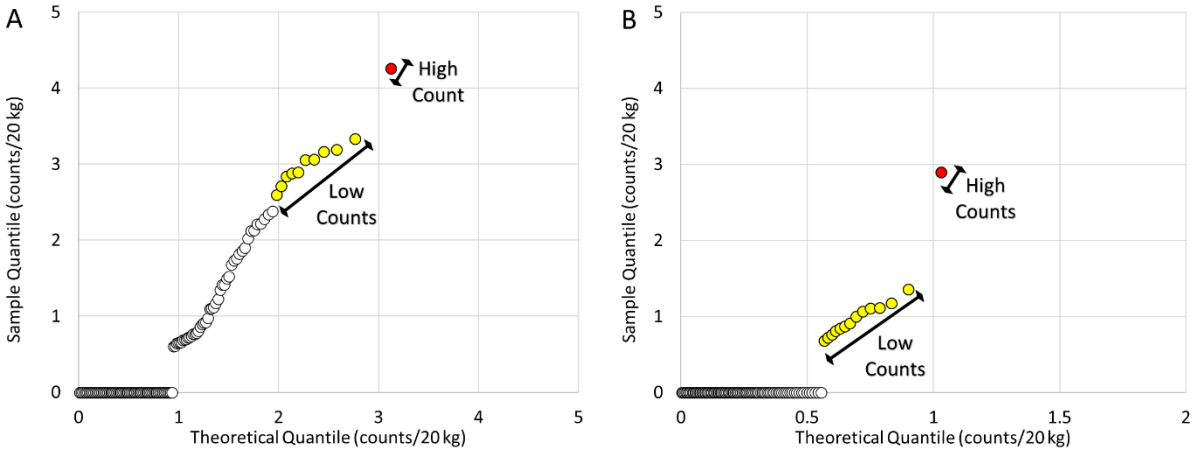

Figure 3-17: Chromite Quantile-Quantile (Q-Q) plots for the A) fine size fraction (0.25 – 0.50 mm); and the B) coarse size fraction (0.50 – 1.00 mm) displaying the annotated, elevated counts.

Table 3-2: Kimberlite indicator mineral grain counts per 20 kg of till sampled for fine (0.25 – 0.50 mm) and the coarse (0.50 – 1.00 mm) size fractions.

	Fine Fraction (0.25-0.50 mm)		Coarse Fraction (0.50-1.00 mm)	
	Low Counts (grains/ 20 kg)	High Counts (grains/ 20 kg)	Low Counts (grains/ 20 kg)	High Counts (grains/ 20 kg)
Pyrope Garnet	5.6 – 24	25 – 55	1.7 – 3.3	3.4 – 10
Eclogitic Garnet	0.7 – 1	1 – 4	0.6 – 1.2	1.3 – 1.5
Cr Diopside	4.5 – 14	15 – 31	1 – 3.9	4 – 13
Olivine	18 – 79	80 – 158	5 – 24.9	25 – 67
Picroilmenite	0.6 – 2.4	2.5 – 3	0.5 – 0.9	1 – 1.1
Chromite	2.5 – 3.9	4 – 4.5	0.5 – 1.9	2 – 3

Fine Fraction of the Kimberlite Indicator Minerals - Score Results

Individual results of the KIM score for the fine fraction (0.25-0.5 mm) of KIMs are in Appendix F, while the individual spatial analyses are in Appendix H. The spatial distribution for the fine fraction of KIM scores is shown in **Figure 3-18**. The highest score achieved for the fine fraction is nine (238.17 grains/ 20kg), in surficial sample 15-014, indicating this sample contains an

elevated number of indicator minerals across multiple species. There are 103 samples that have a score of zero (average of 4.96 grains/ 20kg), 34 samples have a low score of one or two (average of 26.23 grains/ 20kg), 14 samples have a medium-low score of three or four (average of 52.65 grains/ 20kg), 10 samples have a medium-high score of five or six (average of 113.91 grains/ 20kg), and 4 samples have a high score of seven to nine (average of 142.21 grains/ 20kg).

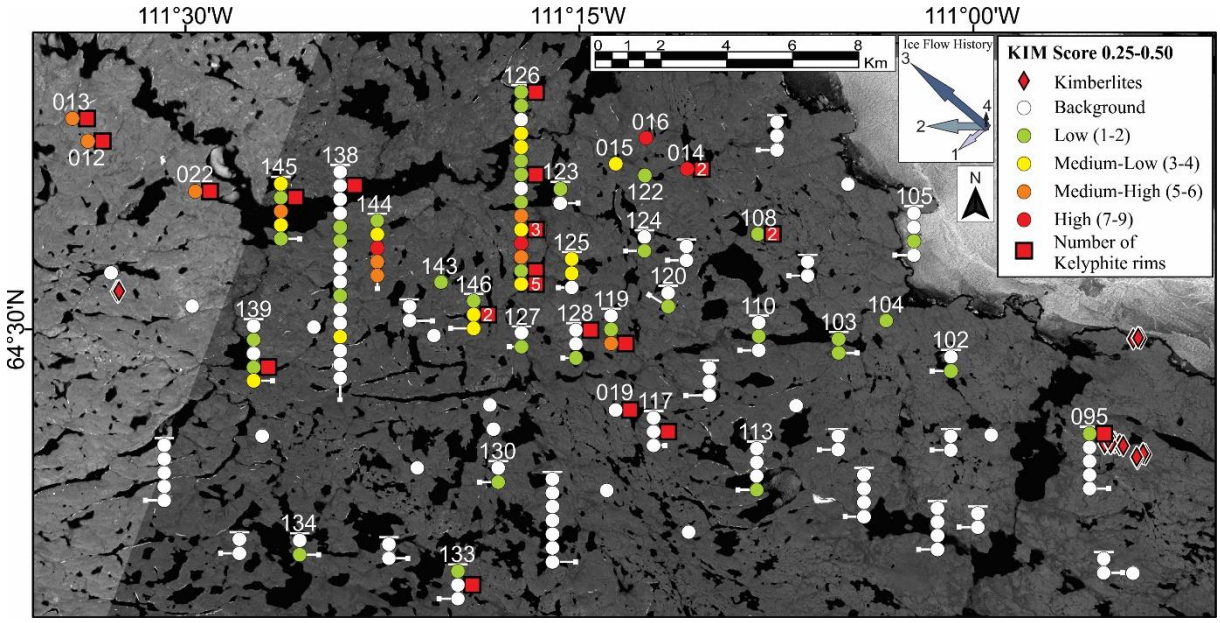

Figure 3-18: KIM score results for the fine fraction (0.25-0.50 mm) of KIMs. The score is plotted according to the number of low score (1 point) and high score (2 points) indicator minerals in each sample for each of the KIMs. The higher scores represent samples with one or more KIM above its anomalous count threshold identified on a Q-Q plot. Each stack of dots is a single borehole and each dot represents 1.5 m of downhole till. Single dots include surface samples. White numbers are the last three digits of boreholes or surface sample station in the database that are discussed in the text. The presence of pyrope grains containing kelyphite rims in the fine fraction (0.25–0.50 mm) of sediments is indicated by a red square (if above 1, the number of grains is also indicated).

The results show that the KIM scores above background level are concentrated in the north-central to the northwest sections of the study area. The low score samples are more widespread than the higher score samples. These low score samples are found from the southern samples (BH-133), to the eastern samples (BH-095), the northern samples (BH-122), and the western samples (BH-139). The low score samples can also be found throughout the areas in-between. The medium-low scores are concentrated in the north-central study area. The medium-low samples can be found in the area generally bordered by samples BH-139 in the southwest, BH-125 to the southeast, surficial sample 015 in the northeast, and BH-145 in the northwest. The medium-high samples are in a southeast to northwest trend between BH-119 and surficial sample

013. The high score samples are in the central to north-central study area. There is a total of 4 sample locations with high score samples. These are surficial samples 014 and 016, as well as BHs 126, and 144.

There are also kelyphite rims on pyrope garnets that are of interest because they are easily eroded by mechanical processes such as transport by glaciers (Dredge *et al*., 1996). The presence of kelyphite rims on indicator mineral grains implies a lack of wear and, most likely, short transport distance. **Figure 3-18** also shows the location of the fine fraction (0.25–0.50 mm) of pyrope grains with kelyphite rims. There are 29 pyropes with kelyphite rims in the fine fraction of till. The pyrope grains with kelyphite rims are widespread throughout the study area. They can be found as far south as BH-133, east to BH-095, north to surficial sample 014, and west to surficial sample 013. However, most of the pyrope grains with kelyphite rims are in the north-central part of the study area, similar to where the medium-high to high KIM score samples are located. The samples in BH-126 contain 11 of the 29 pyropes with kelyphite rims, with a particularly high concentration in the basal sample (5 pyropes with kelyphite rims). There are also 2 pyropes with kelyphite rims in samples that are classified as background in the KIM score (surficial sample 017 and BH-117).

Coarse Fraction of the Kimberlite Indicator Minerals - Score Results

Individual results for the coarse fraction (0.50 – 1.00 mm) of the KIM score are in Appendix F, while the individual spatial analyses are located in Appendix H. **Figure 3-19** shows the spatial distribution for the coarse fraction of KIM scores. The highest score achieved for the coarse fraction is nine (40.43 grains/ 20kg), in BH 15-119 at 4.5 m depth, indicating this sample contains an elevated number of indicator minerals across multiple species. There are 100 samples that have a score of zero (average of 1.19 grains/ 20kg), 45 samples have a low score of one or two (average of 9.92 grains/ 20kg), 14 samples have a medium-low score of three or four (average of 25.19 grains/ 20kg), 4 samples have a medium-high score of five or six (average of 53.03 grains/ 20kg), and 2 samples have a high score of seven to nine (average of 59.46 grains/ 20kg).

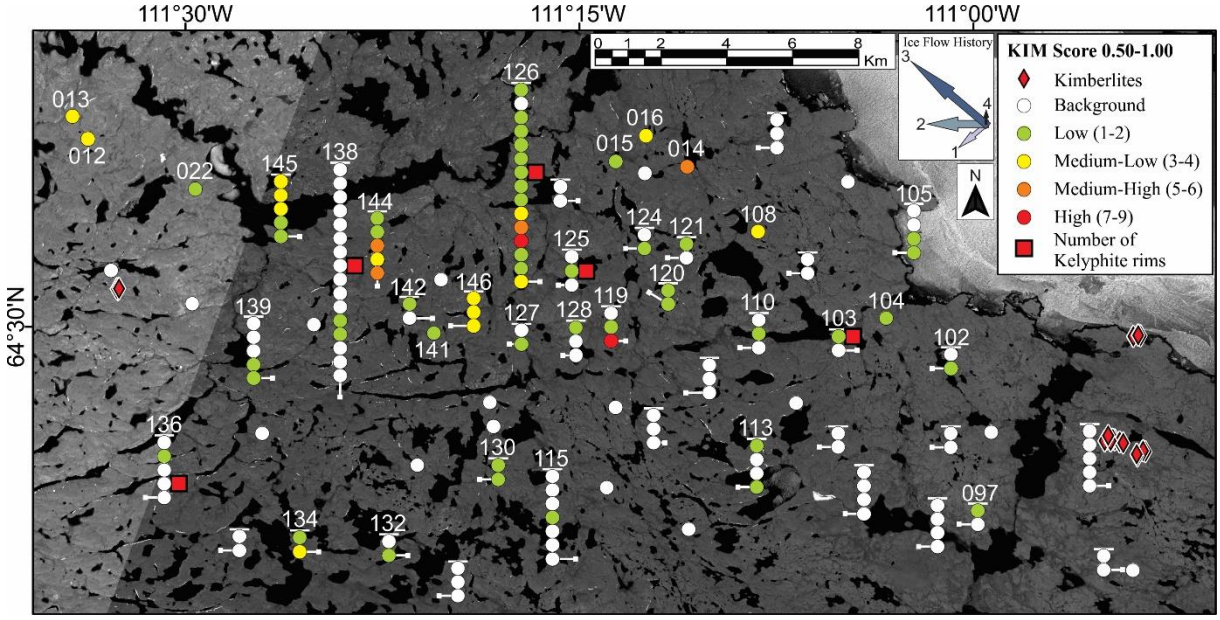

Figure 3-19: KIM score results for the coarse fraction (0.50-1.00 mm) of KIMs. The score is plotted according to the number of low score (1 point) and high score (2 points) indicator minerals in each sample for each of the KIMs. The higher scores represent samples with one or more KIM above its anomalous count threshold identified on a Q-Q plot. Each stack of dots is a single borehole and each dot represents 1.5 m of downhole till. Single dots include surface samples. White numbers are the last three digits of boreholes or surface sample station in the database that are discussed in the text. The presence of pyrope grains containing kelyphite rims in the coarse fraction (0.50–1.00 mm) of sediments is indicated by a red square (no sample has more than 1).

Results show the KIM scores above background level are concentrated in the north-central to the northwest sections of the study area. The low score samples are widespread. They are found from the southwest (BH-136) to the southeast (BH-097), to the northeast (BH-105), to the northwest (surficial sample 022), as well as the areas between. However, the low score samples are sparse in the southern half of the study area. The medium-low scores are concentrated in the north-central study area, with an outlier in the southwest (BH-134). The medium-low samples can be found in the area generally bordered by samples BH-146 to the south, BH-108 to the east, surficial sample 016 in the north, and surficial sample 013 in the northwest. The medium-high samples are in the north-central area. There are 3 locations with a medium-high score (surficial sample 013, BH-126, and -144). The two high score samples are in the central to north-central study area (BH-119 and -126).

Figure 3-19 also shows the location of pyrope grains with kelyphite rims in the coarse fraction (0.50-1.00 mm) of till. There are 5 pyropes with kelyphite rims in the coarse fraction of till. These are found in the southwest (BH-136), west-central (BH-138), north-central (BH-125 and -

126), and east-central (BH-103) parts of the study area. It should also be noted that the pyropes with kelyphite rims in BH-136 and -138 are both located in samples that have been identified as background in the KIM score analysis.

3.4.2 Geochemical Pathfinder Elements

The geochemical pathfinder elements analyzed are cobalt, chromium, and nickel. The concentration of each element is measured in ppm and used to determine the background, elevated, and anomalous samples using the Q-Q plots as outlined in **section 3.3.3**. The Q-Q plots are displayed in **Figure 3-20**. Each dot corresponds to a sample. Each sample is given a colour representing the corresponding bedrock association as determined in Chapter 2. Interestingly, many of the elevated and anomalous samples are associated with metasedimentary and mixed bedrock types, while many of the non-anomalous samples are associated with the hornblende biotite tonalite and K-feldspar monzogranite rock types. The elevated and anomalous concentrations for each element are displayed in Appendix G.

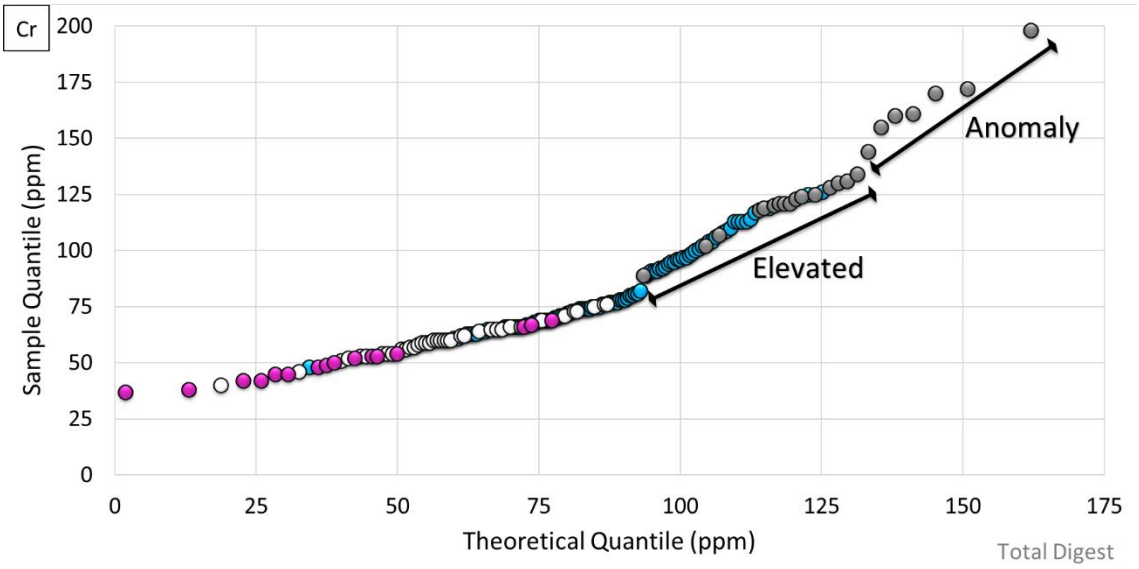

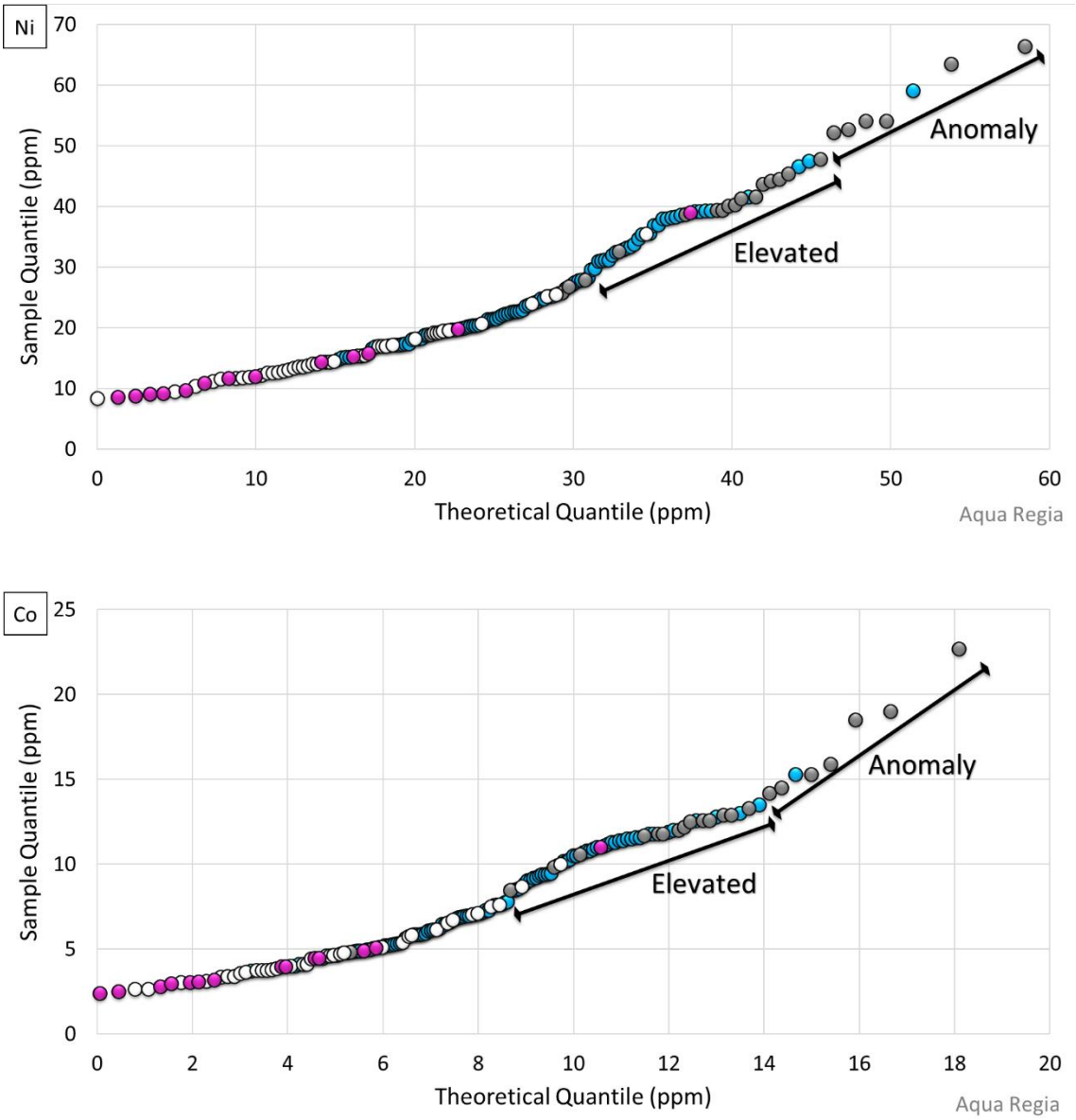

Figure 3-20: Quantile-quantile (Q-Q) plots of the geochemical pathfinder elements Cr, Ni, and Co. The elevated and anomalous data is annotated. The colour scheme is based on the results of the till classification / bedrock association that was delineated in Chapter 2 as follows: grey = metasedimentary; blue = mixed; pink = K-feldspar monzogranite; and white = hornblende-biotite monzogranite.

Till Matrix Geochemistry Results

Individual results for the geochemical pathfinder anomaly score are in Appendix G, while the individual spatial analyses are located in Appendix I. **Figure 3-21** shows the spatial distribution of the geochemistry score. The highest score achieved is six (BH 15-115-06 (9 m depth); -115-07 (10.5 m depth); -125-03 (4.5 m depth); and -126-14 (21 m depth)), indicating these samples contain an anomalous concentration of geochemical pathfinders for multiple elements associated

with kimberlite. A score of zero indicates the sample is within the background concentration of geochemical pathfinders (*i.e*. weak/no association to kimberlite). There are 92 samples that have a score of zero, 27 samples have a low score of one or two, 42 samples have a medium score of three or four, and 5 samples have a high score of five or six. Additionally, 6 bedrock samples scored <0.95 on the aluminum saturation index. These are highlighted blue in **Figure 3-21**.

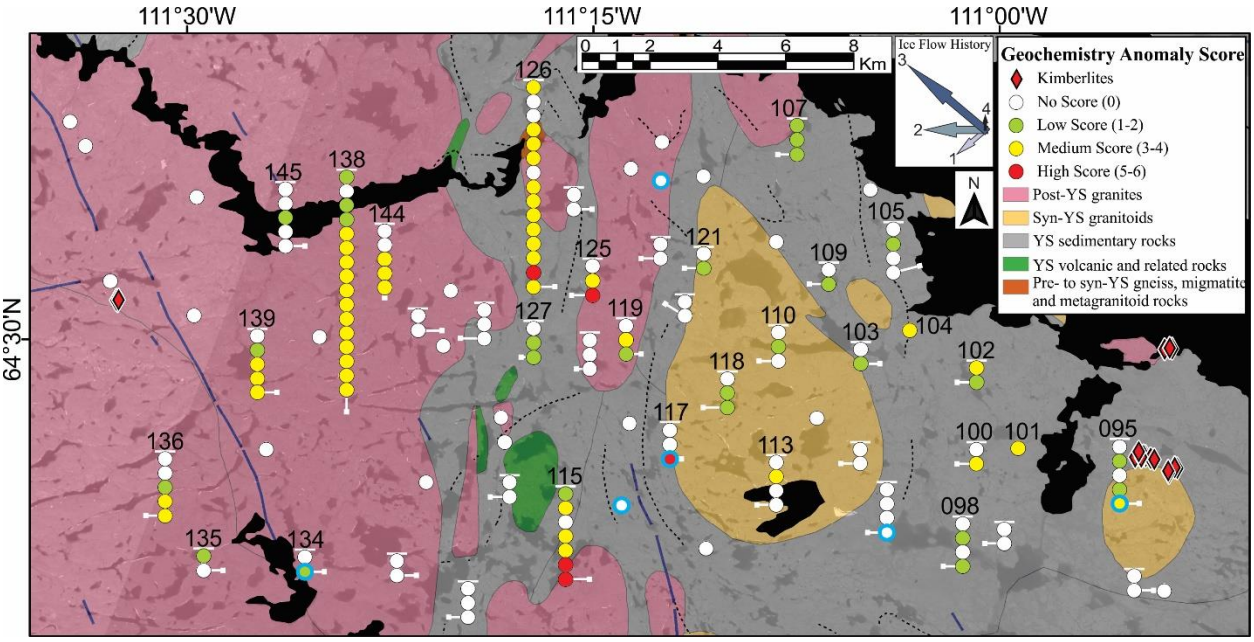

Figure 3-21: Geochemical pathfinder element anomaly score. The score is plotted by the number of elevated (1 point) and anomalous (2 points) concentrations of geochemical pathfinder elements in each sample. Each stack of dots is a single borehole and each dot represents 1.5 m of downhole till. The dots that are highlighted blue have a possible mafic bedrock signature.

The low score dispersal has the widest range covering the area that includes the eastern study area (BH-095 to -107) and extends to the west (BH-135/-136 to -145). The medium score samples are almost as widespread as the low score samples, ranging from the east (BH-095 to -104), to the west of the study area (BH-136 to -139). The high score samples are in the central study area (BH-115 to -126).

3.5 Interpretation

3.5.1 Kimberlite Indicator Minerals

The KIM scores described in section **3.4.1** are interpreted spatially and also within the context of ice flow and general till provenance (*c.f.* Chapter 2).

Fine Fraction of the Kimberlite Indicator Mineral Score

Figure 3-22 is an annotated distribution of the fine fraction of KIMs in the study area. The Monument kimberlites are the closest known potential sources of KIMs in the study area. The high scores (red; **Figure 3-22**) from the near-surface samples are located ~15.5 to 17 km northwest of the Monument kimberlites (surficial samples 014 and 016). This is relatively far from the inferred source, but it is nevertheless the most likely source. The rest of the samples, mostly RC samples, along the known MIT yielded low scores. The other high scores are from deeper samples and found to be spatially associated with the medium-high score samples. The medium-high scores (orange; **Figure 3-22**) are all located in the central to northwest quadrants of the study area (in the subsurface at BH-119, -126, -144, -145, and in surficial samples 022, 012 and 013). Interestingly, these locations are relatively well-aligned in a direction that is consistent with the youngest ice flow phases (WNW-NW). Linking them together forms a narrow ribbon-shaped pattern that appears to rise through the till column and towards the surface in a down-ice direction in a way that resembles Miller's conceptual model (Miller, 1984; **Figure 3-23**). Note, however, that bedrock is also rising in that same direction. That apparent dispersal pattern is within the envelope of the surficial CIT (*c.f.* **Figure 3-2** to **Figure 3-7**). If this pattern were formed by a single ice flow phase, the source would presumably be located somewhere up-ice BH-126 or -119.

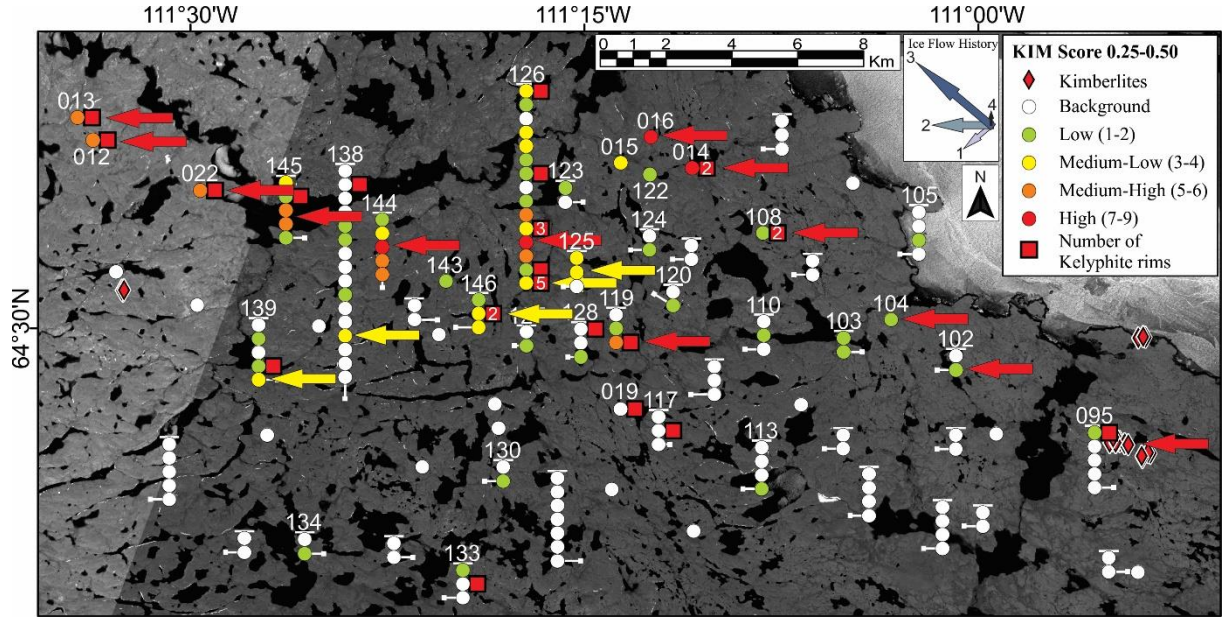

Figure 3-22: The fine size fraction (0.25 – 0.50 mm) of the KIM score. The higher-level scores represent a greater concentration of KIMs. Each stack of dots is a single borehole and each dot represents 1.5 m of downhole till. The red arrows indicate dispersal patterns from the northwestern ice flow phase. The yellow arrows indicate dispersal patterns from earlier southwestern/western ice flow phases.

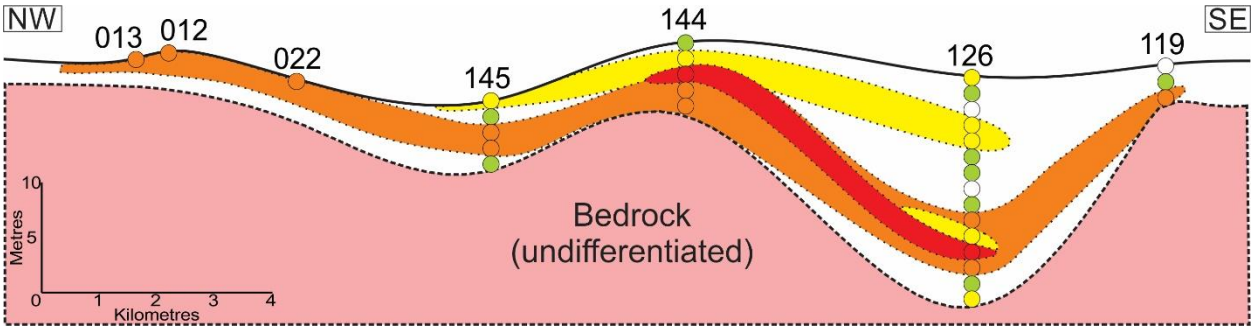

Figure 3-23: Coppermine indicator mineral train till dispersal (0.25-0.50 mm) in the northwest direction. Each dot represents 1.5 m of downhole till.

This does not preclude the Monument kimberlites as a source, but it does support the long-standing hypothesis of an unknown buried source in the area around BH-126, which corresponds to the "head" of the previously documented surficial CIT. The latter is a surficial dispersal train, but here in this study, it seems to have a clear subsurface extension that appears to be stronger/clearer at depth than at the surface in that area. There is also a second, more subtle pattern that emerges when the medium-low scores are considered. The deeply deposited till also displays a ribbon-shaped pattern to the southwest from BH-125 to BH-126, -146, -138, -and -139. It is somewhat weaker (*e.g.* only one sample in BH-138 and in BH-139), but it appears to start in the same area as the other one; specifically, somewhere near BH-126 or BH-125 (**Figure**

3-22). The southwest direction of transport required to form this pattern suggests dispersal from the earlier southwest ice flow phase (*c.f.* Chapter 2). This would suggest till stratigraphy with a lower till preserved in some of the deepest boreholes. This interpretation is also consistent with the interpretation from the analysis of major oxides in Chapter 2, which also considers the possible occurrence of till stratigraphy or higher inheritance from older tills at depth in these boreholes.

Pyrope grains with delicate kelyphite rims are found throughout the map, but there is a clear concentration in the west-central area, particularly in BH-126 (8 grains). This is another line of evidence suggesting a possible local source for the KIMs near the base of BH-126. Few grains are found elsewhere but they are isolated (1 grain), which makes their interpretation difficult and highly uncertain. Nonetheless, a few grains with kelyphite rims are found at the end of the CIT (samples 012-013), as well as up to five grains with kelyphite rims several kilometres down-ice the MIT (BH-108, surface samples 014, 016). These grains are thought to be associated with their respective NW-trending dispersal trains (CIT and MIT), suggesting that some rims may have sustained relatively long glacial transport. The preservation of delicate features in till is possible under low effective stress (high subglacial till pore water pressure). This is further discussed below.

Coarse Fraction of the Kimberlite Indicator Mineral Score

The spatial distribution of the coarse KIM scores shows similar patterns to that of the fine fraction of the KIM scores except with lower scores and concentration overall. Nonetheless, the spatial patterns show a general northwest trend with high and medium scores located to the northwest of the Monument kimberlites, culminating with medium-low and medium-high scores at BH-108 and surficial samples 014 and 015. Considering the dominant northwest ice flow direction, these patterns suggest the Monument cluster is a likely source for these KIMs. Similar to the fine fraction results described in section **3.5.1** , there is a clear pattern that starts at the base of BH-119 and continues to the northwest in what appears to be a rising plume of KIMs through the till column (**Figure 3-24**), or at least along a thinning till with a rising bedrock surface. Similar to the pattern in the fine fraction, this pattern also resembles the classical conceptual model of Miller (1984), with the difference that bedrock is rising in the down-ice direction as opposed to just the dispersal train rising up the till. The relatively narrow ribbon-shaped pattern

is consistent with the dominant northwestern ice flow phase (BH-119, -126, -144, -145, and surficial samples 022, 012 and 013). This pattern is within the envelope of the CIT, but our RC data shows a subsurface extension to it. The reason why the near-surface data is weaker than what is shown in the GoData datasets is unclear. Perhaps it has to do with the discontinuous nature of these patterns and the low horizontal sampling density in our study. There is also a second pattern in the deeply deposited till from BH-126 to BH-146, -138, -and -139. It seems to also start in the same area (near BH-126), but it extends to the southwest along the oldest known ice flow direction (*c.f.* Chapter 2). The source of these patterns is unknown; it could be from an unknown buried kimberlite in the area around BH-125/126 and 119 or it could be from an older till enriched in KIMs and only preserved in that same vicinity. The source of the KIMs from that old till would then have to be in a northeast direction to match the SW-trending pattern and the oldest known ice flow phase. This is not impossible because the area around BH 126 seems to be an area of till blanket and of thicker till in general than most areas around and could thus have preserved older till than elsewhere. Nonetheless, a local kimberlite source is perhaps more likely as it is an easier scenario to produce two dispersal trains (*i.e.* the subtle one to the SW and the rising one to the NW) with their respective head of dispersal located approximately in the same area.

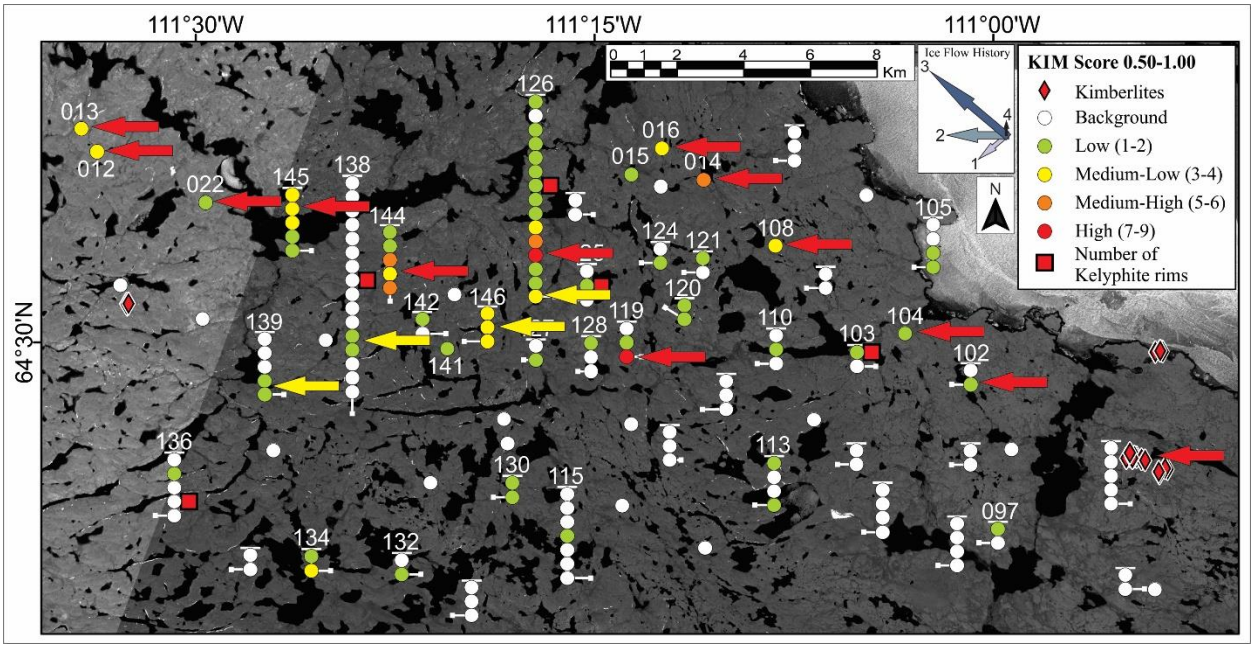

Figure 3-24: The coarse size fraction (0.50 – 1.00 mm) of the KIM score. The higher-level scores represent a greater concentration of KIMs. Each stack of dots is a single borehole and each dot represents 1.5 m of downhole till. The red arrows indicate dispersal patterns from the northwestern ice flow phase. The yellow arrows indicate dispersal patterns from earlier southwestern/western ice flow phases.

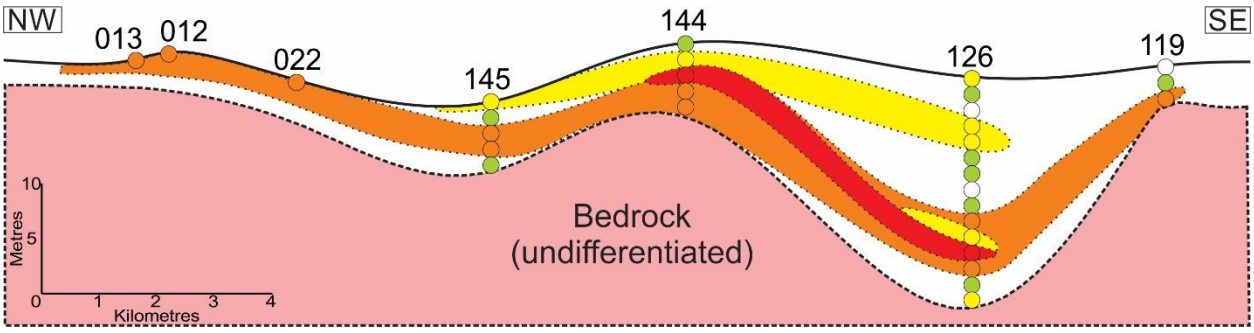

Figure 3-25: Coppermine indicator mineral train till dispersal (0.50-1.00 mm) in the northwest direction. Each dot represents 1.5 m of downhole till.

The pyrope grains with kelyphite rims in the coarse fraction occur in very low numbers. It is thus difficult to extract any meaningful spatial patterns from just a few grains scattered throughout the study area. Nonetheless, most of these grains are located within the west-central portion of the study area; therefore, relatively close to the head of the CIT as defined by the other data.

3.5.2 Till Matrix Geochemistry

The Monument kimberlites are the closest known potential sources of geochemical pathfinder elements in the study area. There is a trend of pathfinders down-ice (northwest) of the Monument

kimberlites extending from about 6 to 15 km to the northwest (**Figure 3-26**). The greatest concentration of geochemical pathfinders is found at BH-104, 8.5 km northwest of the Monument kimberlites. The geochemical pathfinders down-ice from the Monument kimberlites are found closer to their inferred source than the KIMs (*c.f.* **Figure 3-22**, **Figure 3-24**). There also appears to be a trend from the Monument kimberlites in the southwest direction (yellow arrows; **Figure 3-26**; BH-095 and -098) and to the west (green arrows; **Figure 3-26**; BH-101 and 100), which correspond to older ice flow phases. The southwest trend appears to occur at the base of the till column and is thus consistent with the relative age of the SW ice flow phase. This suggests till stratigraphy or compositional inheritance related to till deposition during older ice flow phases. The western dispersal occurs up to 6 km west of the Monument kimberlites in shallower boreholes. The overall pattern of dispersal from the Monument kimberlites appears to be consistent with the Parent *et al*. (1996) model of dispersal of palimpsest trains to the southwest and west, which are overprinted by the surficial materials deposited during a younger northwestern ice flow phase.

Similar to the KIM trains, there appears to be a dispersal pattern from BH-125 and extending in a northwest direction to BH-126, -144, and 145. It also gently rises towards the surface like the Miller (1984) model; however, as previously mentioned, the bedrock surface is also rising. There also appears to be a southwestern trend from BH-126 to BH-138 and -139, although it is not well defined. In BH-138, there are several samples from 7.5m to 24m depth that are all medium score samples. Few KIMs were recovered from these samples in BH-138, so there is a discrepancy between KIM data and geochemical pathfinders. It is important to note that these 'anomalous' samples in BH-138 were classified as 'metasedimentary and/or mafic' based on their major oxides signature (mainly Fe_2O_3, MgO and MnO). However, these samples are also enriched or anomalous in Co, Cr and Ni, which together with Fe, Mg, and Mn oxides could form a mafic assemblage instead of a metasedimentary or kimberlite signature.

There are a few other samples that have high score geochemical pathfinders but may or may not be linked to a kimberlitic source. For example, BH-117 contains a high score sample at 4.5m depth. However, the bedrock sample immediately below this scored a 0.9101 on the aluminum saturation index. This may be an indication that the bedrock in this location is of a mafic origin contributing Co, Cr, and/or Ni from a non-kimberlitic source. The basal medium-low score till

sample in BH-134 at 3m depth also has an aluminum saturation index of 0.9134. The association with mafic bedrock does not explain the elevated till geochemical pathfinder scores in BH-115 or -136. However, a cross-reference with the kimberlite indicator mineral data shows that both of these boreholes are entirely composed of samples with a score of zero in the fine fraction of till and contain one sample each with a low score in the coarse fraction of till. This suggests that the geochemical pathfinder elements in this area are derived from a non-kimberlitic source, possibly due to a nearby mafic source. There is thus a certain degree of confusion between the geochemical pathfinders used in this study and their potential sources (*i.e*. metasediments, mafic rocks, kimberlites), which limits the use of till matrix geochemistry in the study area. More elements analyzed from total digestion, and perhaps isotope data would help further discriminate these possible sources.

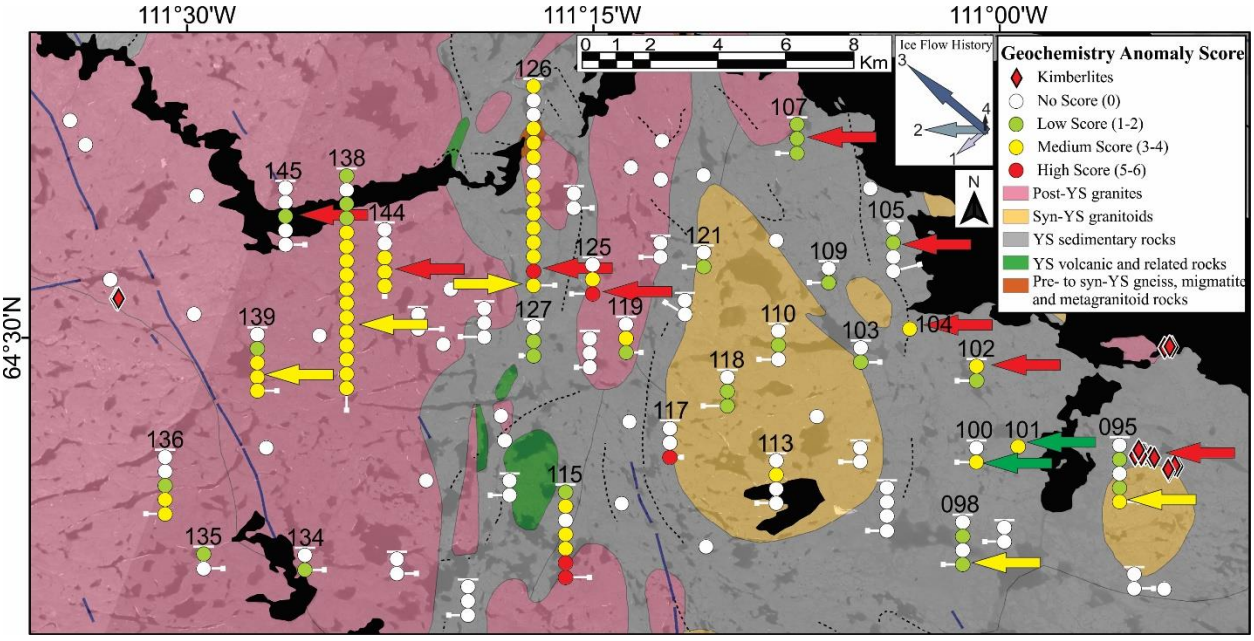

Figure 3-26: Geochemical pathfinder element anomaly score. The score is plotted by the number of elevated (1 point) and anomalous (2 points) concentrations of geochemical pathfinder elements in each sample. Each stack of dots is a single borehole and each dot represents 1.5 m of downhole till. The red arrows indicate dispersal patterns from the northwestern ice flow phase. The yellow arrows indicate dispersal patterns from the southwestern ice flow phase. The green arrows indicate dispersal patterns from the western ice flow phase.

3.6 Synthesis of Till Compositional Data

The patterns displayed by the indicator minerals and geochemical pathfinders are analyzed comprehensively to fully understand the implications of the spatial distribution. The analysis of KIMs and geochemical pathfinder elements has demonstrated some very clear patterns.

Examining these patterns provides insight into possible relationships that may exist between the dispersal of the indicators and their source.

3.6.1 Characteristics of Till Dispersal

The Monument kimberlites are a source of mineralization that, within the publicly available GoData dataset (**section 3.2.4**), display a very clear pattern of surficial dispersal to the northwest as a result of the dominant northwestern ice flow phase. The data used in this study show a weaker near-surface (first 1.5 m) dispersal train within the envelope of the MIT, except the few surficial samples (*i.e*. 014-016; **Figure 3-22**) which show a clear KIM signal despite being located further down-ice than the RC borehole locations within the MIT area. There is no deep BHs (>6 m) within the northwest MIT. The GoData, and results from this study, suggest the MIT is a thin surficial train with material that gets diluted quickly due to glacial processes. There is weak evidence to suggest that dispersal from the earlier southwest and/or western ice flow phase(s) from the Monument kimberlites may have been partially preserved as delineated by the presence of palimpsest geochemical pathfinders from the Monument kimberlites 1 to 5 km to the southwest and west. However, the absence of a relationship with KIM results and the possible confusion due to mixed signature with other possible sources (*e.g*. mafic rocks) make this interpretation highly uncertain.

Data from within the envelope of the CIT are quite interesting. There is a clear NW-trending KIM dispersal pattern that rises towards the surface, as till is thinning, from the vicinity of BH-125/126) and extending to the last available surficial samples (012-013) in the NW (down-ice) direction. There is also a more subtle SW-trending pattern that seems to start at about the same location (*i.e*. BH125/126), Patterns extending to the southwest and west could represent palimpsest trains from the older SW and W ice flow phases (*c.f.* Parent *et al*., 1996). The source of this material thus appears to be located somewhere within the area surrounding BH-126 in the central study area. Whether the source is a kimberlite pipe(s) or an old till enriched in KIMs remains uncertain.

Pyrope grains with kelyphite rims have been found throughout the study area and may bring additional useful insights for the interpretation of the dispersal patterns and their possible source(s), as well as on the subglacial conditions as these features are expected to be easily

eroded during transport under high effective stresses. Several of these grains are found in BH-126 and surrounding boreholes, which may be additional supporting evidence for a local unknown kimberlite source in that vicinity. However, delicate features such as kelyphite rims may survive glacial transport under certain glaciological conditions. Low effective pressures can develop at the ice-bed interface and in the shallow till below (Tulaczyk *et al*., 2001). Delicate grain features, such as kelyphite rims, could thus be preserved in a weak dilated and water-saturated till characterized by low internal friction owing to high porewater pressures. This may even explain the long NW-dispersal trains, as such conditions are known to be associated with fast basal ice velocity and associated deformation and advection of till in the down-ice direction. These conditions could thus explain the few occurrences of pyrope with kelyphite rims further down-ice near the end of the MIT and CIT (**Figure 3-22**). In summary, a single or a few kelyphite rims may be found far from their source, but relatively higher counts (*e.g.* BH-126) could indicate proximity to a source.

The interpretation of a local buried source at the head of the CIT is thus supported by KIM counts, dispersal patterns, and abundance of pyrope with kelyphite rims. A distal source cannot be ruled out, but it requires a more complex model of dispersion. It would indeed require special conditions for kelyphite rims within the CIT to have been transported from the Monument kimberlites first by the SW ice flow phase and then re-entrained by the younger NW ice flow phase without being eroded out. This would require transport and preservation under stable and widespread subglacial conditions of low effective stress during more than 1 ice flow phase or it would require englacial transport. None of this is impossible, but it is more complicated than the local source scenario. Based on this, it seems reasonable to infer these grains are sourced from a kimberlite other than the Monument kimberlites. It could be a relatively local kimberlite in the vicinity of BH-125/126 or kimberlites from more distal sources to the SE (single ice flow phase). However, a distal source for the CIT is perhaps less likely given the apparent palimpsest SW train from the same local area surrounding BH-125/126. This would indeed be difficult to form if the source of both trains (the SW palimpsest and younger NW trains) is not located in that vicinity. So, why have the multi-year exploration efforts not led to a discovery in that area?

There is a difference between the surficial geology along the MIT and the one along the CIT. The regional drift thickness map of Knight and Kerr (2007) shows a few NW-SE strips of thicker

till approximately aligned with the CIT, whereas the MIT largely occurs over thin and discontinuous till. The RC data presented in this thesis are generally consistent with this as most deep RC boreholes are located within the CIT and none are located along the MIT. The combination of thicker till blanket and metasedimentary rocks could have presented several challenges to the geophysical exploration of that area making it difficult to find the source of the CIT. Indeed, the geophysical signature of metasedimentary rocks is perhaps more complex and noisier than igneous rocks, and laterally extensive patches of thick till could have also created low gravity anomalies due to the much lower density of till relative to bedrock. These low gravity anomalies could have masked gravity lows sometimes associated with smaller buried kimberlites (depending on their physical properties). This situation could have complicated geophysical exploration in that area. Whatever the case may be, the findings from this research cannot exclude the possibility of a local source for the CIT. In fact, the data and interpretation presented in this chapter suggest a local source near the head of the CIT may be the most likely scenario.

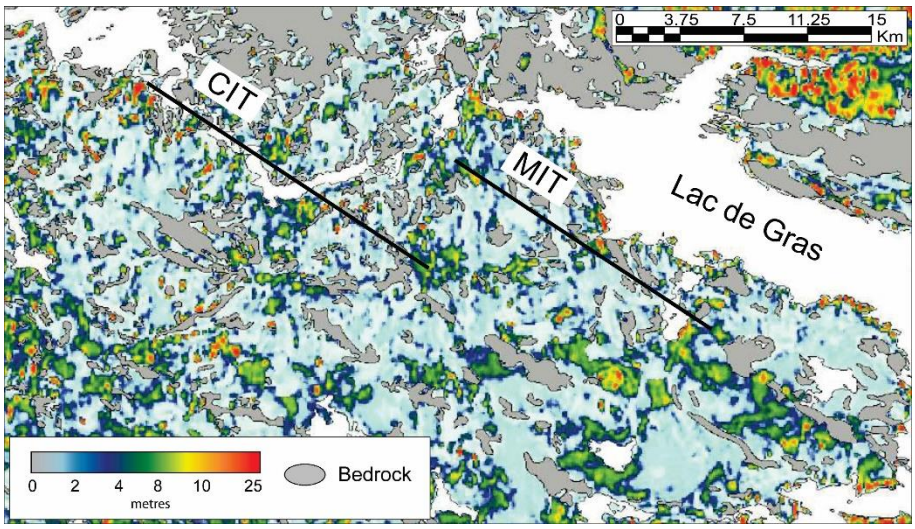

Figure 3-27: Till thickness in the study area. Modified from Knight and Kerr (2007).

3.7 Conclusions

Indicator minerals and geochemical pathfinders in glacial sediments typically form spatially recognizable patterns with a relationship to the regional ice flow history. In areas of thick till, an indicator mineral train may rise through the till column from a buried source (Miller, 1984; Stanley, 2009), but in places where multiple ice flow phases are documented, and where till is

discontinuous and of variable thickness, care must be taken to interpret dispersal patterns as till may have been transported in different directions resulting in more complex dispersal patterns (*e.g*. Parent *et al*., 1996). Sampling the full till column, using knowledge of previous ice flow phases, and using spatial analysis of patterns provides insight into the deposition of sediments associated with kimberlitic material.

Results from this chapter show clear NW-trending patterns associated with the dominant young NW ice flow phase (*c.f*. Chapter 2). Patterns within the envelope of the previously recognized MIT indicate a shallow dispersal train that is best captured by surficial samples, *i.e*. samples collected at the surface (max. of approx. 0.3m). As soon as near-surface till is integrated (1.5 m or greater), the signal becomes weak. The MIT is an area characterized by thin and highly discontinuous till and results from this study show that the strong surficial dispersal train from the Monument kimberlites only weakly extends in the shallow subsurface. As a result, the MIT is not well-defined in the RC data, at least not as much as with the surficial database. In addition, no clear palimpsest dispersal train associated with the older ice flow phases was found close to the Monument kimberlites.

The till along the previously documented CIT in the west-central portion of the study area is, on average, thicker than along the MIT. This is based on the RC data presented in this thesis, as well as from Knight and Kerr (2007) regional drift thickness map. Results from this study show a subsurface dispersal train that rises to the surface in the NW direction, consistent with the young NW ice flow phase and approximately parallel to the MIT described above. In addition, there is a more subtle dispersal train extending to the SW that seems to start in the same area as the rising dispersal. This SW direction corresponds well with the oldest documented ice flow phase in the study area (Ward, 1997; and this study). The respective head of the two identified dispersal trains thus appear to be located in the same area and this suggests both dispersal trains emanate from the same local buried source. However, it is not possible to exclude that they both originated from an old buried till enriched in KIMs; but this is a less likely scenario. In summary, the analysis presented in this chapter suggests a buried source possibly occurs near BH-119/BH-125/126. The combination of metasedimentary rocks and thicker (low density) till may have presented several challenges to kimberlite exploration in that area, which could explain why the source has not yet been found. However, it is not possible to exclude the scenario of a more

distal source, but it requires a more complex model involving sustained low effective stress and/or englacial transport during more than one ice flow phase, to re-entrain and preserve kelyphite rims on pyrope grains recovered from the CIT.

Till matrix geochemistry data that was available for this study proved to be of limited use for kimberlite dispersal train mapping and related glacial sediment transport reconstruction. A possible mixed signature from non-kimberlitic sources could not be separated. Therefore, the main available pathfinders for kimberlites also appear to trace dispersal trains from other rock sources such as mafic rocks and also perhaps some metasedimentary rocks. Analysis of more elements using a total digestion procedure, along with multivariate analysis of the results, would be useful to further discriminate the more complex overlapping geochemical signatures. An isotopic analysis would also be useful along with a detailed investigation of kimberlite geochemistry from the district. Finally, another study using KIM probe data would be useful to further analyze the KIM dispersal trains and associated interpretation presented herein.

Chapter 4: Conclusions

4.1 Identifying Kimberlitic Signatures in Till

The research presented herein used information from a targeted field investigation and a large RC drilling dataset to improve knowledge of the ice flow history and related subglacial sediment (mainly till) distribution, thickness, and composition across a large study area (700 km^2) southwest of Lac de Gras, Northwest Territories. The research was conducted in the context of addressing some of the challenges related to drift prospecting for kimberlite. One important challenge is related to mainly using surficial data and the dominant ice flow direction without a good understanding of the effect of variable till thickness and ice flow shifts on those surficial patterns. To address this problem, the research was designed with three main components. The first component (1) was to further constrain bedrock provenance of till and its transport in relation to the ice flow history in the study area. The ice flow history was further constrained with new observations and provenance was analyzed based on pebble lithology counts in the surficial till and major oxides in till matrix from RC samples. The latter provided insights about the provenance signature of till in the near-surface and at greater depth in areas of thicker till. The second component (2) involved analyzing the distribution and abundance of kimberlite indicator minerals at the surface and in the subsurface, using both surficial data and the RC data to determine whether the KIM abundance and patterns at depth differ from those at the surface. The third component (3) was to repeat the analysis in (2), this time using geochemical pathfinder elements. This strategy provided valuable information about the relationship between shifting ice flow directions and till composition in the context of discontinuous till deposits of variable thickness. This was used to improve understanding of how till was produced and transported over time in a way that was not captured in previous studies that focused on surficial till only. This could help enhance drift prospecting strategies and interpretation of related data and help resolve some important problems such as surficial patterns with unknown sources or, in some other cases, known buried sources lacking a surficial expression in glacial sediments. The sub-section below describes the main contributions of the thesis, in order of appearance in the main chapters, in more detail.

4.1.1 Thesis Contributions

The most significant contributions of this thesis are:

1) The ice flow history was further constrained with the addition of 254 groove and striation measurements, including 67 sites where relative age chronology could be established. While the new data generally agree with the previously reconstructed ice flow history (Ward *et al*., 1995), it added much needed field-based data constraints to an area that had previously only been mapped at the NTS map sheet scale.
2) Till characteristics including textural analysis, clast lithology classification, and analysis of major oxides show that the surficial till in the study area can be interpreted as being strongly overprinted by the dominant NW-trending ice flow phase.
3) A principal component analysis (PCA) of the major oxides from till matrix geochemistry data showed contrasting signatures and mixed signatures that have been interpreted in terms of possible bedrock sources. The spatial distribution of results also revealed important new insights:
    a. The spatial distribution of till matrix groups based on the PCA analysis shows that areas of thin till have a greater local bedrock signature, whereas deeper till often has a more contrasting signature relative to the surficial till of surrounding shallower areas. In most cases, the till at depth is interpreted as having a more dominantly 'distal' signature. This finding suggests the presence, in isolated pockets of thicker till, of multi-till stratigraphy (older tills) or higher compositional inheritance at depth and, possibly, different ice flow regime. However, in just a few cases, the contrasting major oxides signature at depth could be indicative of unmapped local bedrock sources including unknown buried mafic rocks or even kimberlites.
4) Indicator minerals and geochemical pathfinders used in diamond exploration form spatially recognizable patterns in glacial sediment, including notable differences between surficial patterns and subsurface ones.
    a. At the surface, patterns show clear NW-trending patterns associated with the dominant young NW ice flow phase.
    b. Combining surficial and near-surface data with deeper data has revealed interesting patterns, such as a subsurface dispersal train that rises to the surface in

the NW direction consistent with the young NW ice flow phase. There is also a subtle dispersal train that extends to the SW in the same area as the rising NW dispersal. This SW direction corresponds well with the oldest documented ice flow phase in the study area. This indicates a possible source for these two dispersal trains may be the same but dispersed under different ice flow conditions.

c. One possibly important implication of this finding is that it may indicate the presence of an unknown buried source for the KIMs forming the surficial Coppermine train somewhere within the area bounded by BH-119/BH-125/126. The exact location cannot be determined with the available low-density dataset.

5) When adding the analysis of dispersion patterns of kimberlite indicators to the one based on till matrix major oxides (point 3 above), it becomes clearer that the youngest northwest ice flow did not completely rework the till and a signature of the older ice flows has been preserved in the deeper till.

4.1.2 Research Questions

The introduction chapter posed several questions (**section 1.2.6**) for this thesis to which an answer has been attempted.

- Why is there a second indicator train within the study area but no known source despite extensive exploration effort?

Results show differences between the thin and discontinuous till of the MIT and the pockets of thicker till deposited in the envelope of the CIT. The complex ice flow history and higher compositional inheritance at depth are contributing factors to the complicated depositional history of the CIT. The surficial patterns may be misinterpreted if subsurface information is not considered during exploration efforts for the source of the CIT. There also may be unmapped sources of mafic rocks complicating the geochemical signature in till up-ice of the CIT.

- Are there similarities or differences between the two mineral indicator trains?

The similarities between the MIT and CIT appear to be limited to the NW-trending surficial indicator mineral trains. There are differences between the concentration of indicator minerals and geochemical pathfinders. The CIT displays a greater number/concentration of each.

Additionally, the till in the envelope of the MIT is thin, discontinuous, and only displays a weak palimpsest dispersal signal. The CIT contains pockets of thicker till that have a compositional inheritance at depth and there is a clear palimpsest signature to the southwest of the 'head' of the CIT.

- What is the effect of multiple ice-flow directions on the till production and mineral entrainment in the study area?

In areas of thin and discontinuous till (the MIT) the effects of multiple ice-flow directions are negligible as the till that is deposited reflects the most recent ice flow direction. In areas where there are pockets of thicker till there is evidence of till stratigraphy and/or inheritance from the previous ice flow phases. Till production and mineral entrainment may be increased or decreased in an area depending on the ice flow direction and the availability of material (if materials were sheltered under certain flow conditions or not).

- What role does the underlying bedrock play in delineating the surficial and subsurface pattern of the indicator mineral trains?

The lithology of bedrock is important for till production. A 'soft' bedrock, such as metasedimentary, is highly jointed and more prone to plucking than igneous rocks. This may lead to a rapid uptake of large metasedimentary blocks at the base of the ice and the lithology will dominate the coarse fraction of till. In contrast, igneous rocks are much less jointed and less prone to quarrying/plucking and thus to generating large debris making up the coarse fraction of till. This can also lead to greater dilution of indicator minerals in till over areas of metasedimentary bedrock as opposed to igneous bedrock.

4.2 Implications for Mineral Exploration

4.2.1 Drift Prospecting in Areas of Discontinuous Till

Drift prospecting has been successful in the Lac de Gras region (Fipke *et al.*, 1995), but now that exploration is shifting to more elusive sources under glacial cover, it is becoming increasingly important to better understand the net effect of ice flow shifts and discontinuous till of variable thickness on the full dispersal patterns. In these kinds of settings, well-defined patterns of kimberlite-associated material can occur at the surface, but the exact transport pathways and distance from its source may be difficult to determine. The Miller model (1984) and the Parent *et al.* (1996) model provide useful conceptual insights into dispersal patterns, but the net effect of ice flow shifts, changing subglacial conditions, variable bedrock topography, and discontinuous and variable till thickness remains poorly understood. In the Lac de Gras area, the surficial till dispersal patterns are strongly aligned with a late-glacial NW ice flow phase; yet, the source of certain dispersal trains, such as the Coppermine dispersal train, has remained elusive while other known subcropping kimberlites have not produced discernible surficial patterns. Clearly, the surface data and the dominant ice flow direction do not capture the full complexity of till dispersion.

In this study, the combined analysis of surface and subsurface data has provided new insights into this problem. From this work, it has become clear that surface and subsurface till show some contrasting compositional characteristics, which may indicate more complex till stratigraphy or inheritance linked to older ice flow phases than previously considered. It may also have captured the signal of an unknown buried source, although this remains to be confirmed. In summary, this study suggests that drift prospecting may be enhanced in the Lac de Gras region by using more subsurface data and this could be critical for future success at the current maturity stage of the diamond district. It may be somewhat surprising given the till is typically relatively thin and discontinuous in this region, but it is clear now that despite this situation, the few pockets of thicker till reveal more than what is recorded in the shallow and surficial till. The next generation of drift thickness maps (*i.e.* building on Knight and Kerr, 2007) produced using different techniques may further guide future RC drilling programs and geophysical exploration. They may reveal important corridors where till is thicker on average and where surface landforms and

bedrock depressions have possibly created till dispersal patterns that are different than the ones associated with previous discoveries.

4.2.2 Future Work

During the investigation into till composition and distribution, complications arose in part due to both the sampling strategy and the type of analyses carried out on the samples.

The RC drilling technique reworks material, which leads to some limitations as to what can be done. RC drilling uses air pressure to suck the sediments from the borehole and blows it into buckets for sampling. The technique is cost-effective, but it comes at the expense of losing some fine material and, more importantly, valuable stratigraphic and sedimentological information. Future drilling surveys in the region could use drilling techniques (*e.g.* sonic drilling) that provide continuous and mostly intact till cores. This could help address the question of till stratigraphy raised in this thesis and provide more intact samples of till matrix instead of a mixture over 1.5 m intervals. These future drilling programs should also take advantage of drift thickness maps to help create better drilling grids; furthermore, sonic drilling could be focused on areas with a higher probability of thick till whereas more economical sampling techniques could be used in areas where till is thin and highly discontinuous. It remains important to sample as randomly as possible (not just where till is thickest) to minimize sampling biases.

The coarse fraction (clast) of RC samples were not made available for this research. Clast lithology analysis of subsurface till would greatly assist the interpretation of subsurface till provenance, which is currently based on the major oxides from till matrix geochemistry. The coarsest fraction of the till (>8 mm) sometimes differs in provenance compared to the till matrix due to rock properties (*i.e.* the most resistant rocks tend to be overrepresented in the coarse fraction). Nonetheless, there tends to be a relatively strong relationship with certain fractions like the 2-4 mm and 4-8 mm and till matrix geochemistry. Therefore, comparing till matrix geochemistry with certain clast fractions would be useful for all samples, not just the surficial ones.

The till geochemistry analysis could use more elements analyzed by a total digestion procedure, along with multivariate analysis of the results, to further discriminate the more complex overlapping geochemical signatures. An isotopic analysis would also be useful along with a

detailed investigation of kimberlite geochemistry from the district. Finally, another study using KIM probe data would be useful to further analyze the KIM dispersal trains and associated interpretation presented herein.

In terms of mineral exploration, it would be useful to follow-up with a higher density of sampling in the area near BH-119/BH-125/126 to better delineate the head of the elevated KIM counts and anomalous geochemical pathfinders in the subsurface. Additionally, extending the study area to the east would provide more detail for the composition of till in the up-ice direction of the Monument kimberlites to compare with the patterns exhibited by the Coppermine indicator train.

References

Abzalov, M. (2008). Quality control of assay data: A review of procedures for measuring and monitoring precision and accuracy. *Exploration and Mining Geology, 17*(3-4), 131-144.

Abzalov, M. (2011). Sampling errors and control of assay data quality in exploration and mining geology. *Applications and experiences of quality control*. InTech.

Aitchison, J. (1986). The statistical analysis of compositional data.

Alley, R. B. (1992). How can low-pressure channels and deforming tills coexist subglacially? *Journal of Glaciology, 38*(128), 200-207.

Arctic Star Exploration. (2013a). *Numerous kimberlite targets identified on redemption project; Lac de Gras, NWT.* Arctic Star Exploration.

Arctic Star Exploration. (2013b). *The Northwest Territories diamond redemption project.* Arctic Star Exploration.

Arctic Star Exploration. (2015). *Management discussion and analysis for the year ended December 31, 2014.* Arctic Star Exploration.

Armstrong, J. P. (2003). Diamond discovery in the Slave Craton: Compilations of exploration data as tools for future discovery. Paper presented at the *International Kimberlite Conference: Extended Abstracts. 8.*

Armstrong, K. (2016). *The Redemption Project video presentation update*. North Arrow Minerals Inc.

Ashton Mining of Canada Inc. (2000). Ashton finds kimberlite sill on Ric property. *The Northern Miner,* pp. 18.

Averill, S. (1978). Overburden exploration and glacial history of northern Canada. *Canadian Mining Journal, 99*(4), 58.

Averill, S. A. (2001). The application of heavy indicator mineralogy in mineral exploration with emphasis on base metal indicators in glaciated metamorphic and plutonic terrains. *Geological Society, London, Special Publications, 185*(1), 69-81.

Benn, D.I., & Evans, D. J. (2014). *Glaciers and glaciation.* Routledge.

Benn, D. I. (2014). Clast morphology. *A practical guide to the study of glacial sediments* (pp. 92-106) Routledge.

Bleeker, W., Ketchum, J. W., Jackson, V. A., & Villeneuve, M. E. (1999). The Central Slave basement complex, part I: Its structural topology and autochthonous cover. *Canadian Journal of Earth Sciences, 36*(7), 1083-1109.

Blott, S. J., & Pye, K. (2001). GRADISTAT: A grain size distribution and statistics package for the analysis of unconsolidated sediments. *Earth Surface Processes and Landforms, 26*(11), 1237-1248.

Bostock, H. H. (1980). *Geology of the Itchen Lake area, District of Mackenzie* Geological Survey of Canada.

Boulton, G. (1996). The origin of till sequences by subglacial sediment deformation beneath mid-latitude ice sheets. *Annals of Glaciology, 22*, 75-84.

Brennand, T. A. (2000). Deglacial meltwater drainage and glaciodynamics: Inferences from Laurentide eskers, Canada. *Geomorphology, 32*(3), 263-293.

Brown, J., Ferrians Jr, O., Heginbottom, J., & Melnikov, E. (1997). *Circum-arctic map of permafrost and ground-ice conditions.*

Brown, V. H., C. R. Stokes, and C. O'Cofaigh. 2011. "The Glacial Geomorphology of the North-West Sector of the Laurentide Ice Sheet." *Journal of Maps* 7(1):409–28

Bryan, D., & Bonner, R. (2003). The Diavik diamond mine, Lac de Gras, Northwest Territories, Canada. Paper presented at the *8th International Kimberlite Conference, Slave Province and Northern Alberta Field Trip*, 61-65.

Bustard, A. (2016). *Fingerprinting and tracing the signature of basement-hosted unconformity-type uranium alteration through thick Quaternary tills: an example from the Thelon Basin, Nunavut* (Master's thesis, University of Waterloo).

Chao, T. (1984). Use of partial dissolution techniques in geochemical exploration. *Journal of Geochemical Exploration, 20*(2), 101-135.

Chapman, R., Curry, G. T., & Sopuck, V. (1990). The Bakos deposit discovery-a case history.

Clark, P. U. (1987). Subglacial sediment dispersal and till composition. *The Journal of Geology, 95*(4), 527-541.

Clark, P. U., Dyke, A. S., Shakun, J. D., Carlson, A. E., Clark, J., Wohlfarth, B., . . . McCabe, A. M. (2009). The last glacial maximum. *Science (New York, N.Y.), 325*(5941), 710-714. DOI:10.1126/science.1172873 [doi]

Clement, C. (1975). The emplacement of some diatreme-facies kimberlites. *Physics and Chemistry of the Earth, 9*, 51-59.

Coker, W. B., Robertson, D. J., & Snow, R. J. (1989). Till geochemistry at the Great Gull scheelite prospects, Newfoundland, Canada: A case history in orientation and discovery. *Journal of Geochemical Exploration, 32*(1), 291-293.

Couch, A. G., & Eyles, N. (2008). Sedimentary record of glacial Lake Mackenzie, Northwest Territories, Canada: Implications for arctic freshwater forcing. *Palaeogeography, Palaeoclimatology, Palaeoecology, 268*(1-2), 26-38.

Creaser, R. A., Grütter, H., Carlson, J., & Crawford, B. (2004). Macrocrystal phlogopite Rb–Sr dates for the Ekati property kimberlites, Slave Province, Canada: Evidence for multiple intrusive episodes in the Paleocene and Eocene. *Lithos, 76*(1), 399-414.

Crolly, G. (2017). *Laser-scattering - basics* Fritsch Gmbh.

Davis, W. J. (1991). *Granitoid Geochemistry and Late Archean Crustal Evolution in the Central Slave Province.*

Davis, W., & Kjarsgaard, B. (1997). A Rb-Sr isochron age for a kimberlite from the recently discovered Lac de Gras field, Slave Province, northwest Canada. *The Journal of Geology, 105*(4), 503-510.

De Beers Group of Companies. (2016). Gahcho kué mine. Retrieved from http://www.debeersgroup.com/Canada/en/operations/mining/gahcho-kue-project.html

De Beers Group of Companies. (2016). Snap lake mine. Retrieved from http://www.debeersgroup.com/Canada/en/operations/mining/snap-lake.html

Dillon-Leitch, H. (1984). Geology of Courageous Lake-Mackay Lake greenstone belt, NWT, parts of NTS 75M/14, 15, 76D/2, 3, 4, 5. *Department of Indian Affairs and Northern Development, Northwest Territories Geology Division, EGS Open File, 4*

Dominion Diamond Corp. (2013a). Diavik diamond mine. Retrieved from http://www.ddcorp.ca/operations/diavik-mine

Dominion Diamond Corp. (2013b). Ekati diamond mine. Retrieved from http://www.ddcorp.ca/operations/Ekati-mine

Dredge, L., Ward, B., & Kerr, D. (1994). Glacial geology and implications for drift prospecting in the Lac de Gras, Winter Lake and Aylmer Lake map areas, Central Slave Province, Northwest Territories. *Current Research,* 33-38.

Dredge, L., Ward, B., & Kerr, D. (1996). Morphology and kelyphite preservation on glacially transported pyrope grains. *Searching for Diamonds in Canada. Open File, 3228,* 197-204.

Dredge, L. A., Kerr, D. E., & Wolfe, S. A. (1999). Surficial materials and related ground ice conditions, Slave Province, NWT, Canada. *Canadian Journal of Earth Sciences, 36*(7), 1227-1238.

Dreimanis, A. (1956). Steep rock iron ore boulder train, part 1. *Geological Association of Canada, Ottawa, Ont.* 17-70.

Dreimanis, A. (1958). Tracing ore boulders as a prospecting method in Canada. *The Canadian Mining and Metallurgical Bulletin, 51*, 73-79.

Dyke, A. S. (2004). An outline of North American deglaciation with emphasis on central and northern Canada. *Developments in Quaternary Sciences, 2*, 373-424.

Dyke, A., Andrews, J., Clark, P., England, J., Miller, G., Shaw, J., & Veillette, J. (2002). The Laurentide and Innuitian Ice Sheets during the last glacial maximum. *Quaternary Science Reviews, 21*(1-3), 9-31.

Dyke, A. S., & Dredge, L. A. (1989). Quaternary geology of the Canadian shield. In R. J. Fulton (Ed.), *Quaternary geology of Canada and Greenland* (1st ed., pp. 175-214). Ottawa, Canada: Canadian Government Publishing Centre.

Dyke, A.S., Dredge, L.A., & Vincent, J. (1982). Configuration and dynamics of the Laurentide ice sheet during the late Wisconsin maximum. *Géographie Physique Et Quaternaire, 36*(1-2), 5-14.

Dyke, A. S., & Prest, V. K. (1987). Late Wisconsinan and Holocene history of the Laurentide ice sheet. *Géographie Physique Et Quaternaire, 41*(2), 237-263.

Ecological Stratification Working Group. (1996). *A national ecological framework for Canada*. State of the Environment Directorate Centre for Land and Biological Resources Research; Hull, Quebec: State of the Environment Directorate.

Ecosystem Classification Group. (2012). *Ecological Regions of the Northwest Territories - southern arctic.* Yellowknife, NT, Canada: Department of Environment and Natural Resources, Government of the Northwest Territories.

Elliott, B. (2015). Slave Province surficial materials and permafrost study overview - revitalizing multi-commodity mineral exploration and facilitating sustainable development in a key economic region. Paper presented at the *43rd Yellowknife Geoscience Forum Abstracts*, Yellowknife, NT., *2015*-35.

Elliott, B. and Normandeau, P.X. (2016). Slave Province Surficial Materials and Permafrost Study – Kimberlite indicator mineral counts and grain morphology from the 2015 Reverse Circulation Drilling Program; Northwest Territories Geological Survey, NWT Open Report 2016-018, 6 pages, and appendix.

Elliott, B., and Normandeau, P.X. (2017). Slave Province Surficial Materials and Permafrost Study — Kimberlite indicator mineral chemistry from the 2015 Reverse Circulation Drilling Program, Northwest Territories; Northwest Territories Geological Survey, NWT Open Report 2017-011, 7 pages and appendix.

England, J. H., Furze, M. F., & Doupé, J. P. (2009). Revision of the NW Laurentide Ice Sheet: Implications for paleoclimate, the northeast extremity of Beringia, and arctic ocean sedimentation. *Quaternary Science Reviews, 28*(17-18), 1573-1596.

Evans, D., Phillips, E., Hiemstra, J., & Auton, C. (2006). Subglacial till: Formation, sedimentary characteristics and classification. *Earth-Science Reviews, 78*(1-2), 115-176.

Falck, H., & Gochnauer, K. (2016). 2015 Northwest Territories mineral exploration overview: Updated February 2016.

Fipke, C., Dummett, H., Moore, R., Carlson, J., Ashley, R., Gurney, J., & Kirkley, M. (1995). History of the discovery of diamondiferous kimberlites in the Northwest Territories, Canada. Paper presented at the *Sixth International Kimberlite Conference,* 158-160.

Fletcher, W. (2002). Quality control in exploration geochemistry. *Mineral Exploration Research Centre, Unpublished Short Course Notes: Laurentian University, Sudbury, ON*. 67.

Folinsbee, R. E. (1949). *Lac de Gras, District of Mackenzie, Northwest Territories* Geological Survey of Canada.

Folk, R. L., & Ward, W. C. (1957). Brazos River bar: A study in the significance of grain size parameters. *Journal of Sedimentary Research, 27*(1)

Fulton, R. J. (1989). *Quaternary geology of Canada and Greenland: Supplement* International Specialized Book Service Incorporated.

Fulton, R. J. (1995). *Surficial materials of Canada: Map 1880A* Geological Survey of Canada.

Gazley, M., Collins, K., Roberston, J., Hines, B., Fisher, L., & McFarlane, A. (2015). Application of principal component analysis and cluster analysis to mineral exploration and mine geology.

Geological Survey of Canada, Thompson, P., & Kerswill, J. (1994). *Preliminary geology of the Winter Lake-Lac de Gras area, District of Mackenzie, Northwest Territories*

GGL Resources. (2004). *Management discussion and analysis.*

GGL Resources. (2018). CH project area - project status.

Google Earth. (2016). *Northern Canada. Google Earth (version 7.1.5.1557) [software]*

Gowan, E. J., Tregoning, P., Purcell, A., Montillet, J., & McClusky, S. (2016). A model of the western Laurentide Ice Sheet, using observations of glacial isostatic adjustment. *Quaternary Science Reviews, 139*, 1-16.

Grégoire, M., Rabinowicz, M., & Janse, A. (2005). Mantle mush compaction: A key to understand the mechanisms of concentration of kimberlite melts and initiation of swarms of kimberlite dykes. *Journal of Petrology, 47*(3), 631-646.

Grip, E. (1953). Tracing of glacial boulders as an aid to ore prospecting in Sweden. *Economic Geology, 48*(8), 715-725.

Grunsky, E. C. (2010). The interpretation of geochemical survey data. *Geochemistry: Exploration, Environment, Analysis, 10*(1), 27-74.

Haldorsen, S. (1981). Grain-size distribution of subglacial till and its relation to glacial crushing and abrasion. *Boreas, 10*(1), 91-105.

Hamill, D. (2014). Diamond exploration in Canada: Opportunity knocking or a fool's errand? *Mining.Com* Retrieved from http://www.mining.com/web/diamond-exploration-in-Canada-opportunity-knocking-or-a-fools-errand/

Harbinger Corp. (2007). Mega uranium announces discovery of nine uranium mineralized zones on its Aillik east property and the completion of drilling at Mustang Lake, central mineral belt, Labrador. Retrieved from http://search.proquest.com.proxy.lib.uwaterloo.ca/docview/447913273/abstract/AB87DE0CE3004F6BPQ/1?accountid=14906

Heaman, L., Kjarsgaard, B., & Creaser, R. (2003). The timing of kimberlite magmatism in North America: Implications for global kimberlite genesis and diamond exploration. *Lithos, 71*(2), 153-184.

Heffernan, V. (2014). Rediscovering its swagger. *Core Magazine,* 4. Retrieved from http://www.pdac.ca/docs/default-source/core2/pdac-core-(fall-2014).pdf?sfvrsn=4

Hoey, T. (2004). The size of sedimentary particles. *A Practical Guide to the Study of Glacial Sediments: London, UK, Arnold Publishers.* 52-77.

Hooke, R. L., Cummings, D. I., Lesemann, J., & Sharpe, D. R. (2013). Genesis of dispersal plumes in till. *Canadian Journal of Earth Sciences, 50*(8), 847-855.

Iverson, N., & Person, M. (2012). Glacier-bed geomorphic processes and hydrologic conditions relevant to nuclear waste disposal. *Geofluids, 12*(1), 38-57.

Janse, A. B., & Sheahan, P. A. (1995). Catalogue of worldwide diamond and kimberlite occurrences: A selective and annotative approach. *Journal of Geochemical Exploration, 53*(1-3), 73-111.

Jenner, G. A. (1996). Trace element geochemistry of igneous rocks: Geochemical nomenclature and analytical geochemistry. *Trace Element Geochemistry of Volcanic Rocks: Applications for Massive Sulfide Exploration.* 51-77.

Keating, P. (1996). Kimberlites and aeromagnetics. *Searching for Diamonds in Canada: Geological Survey of Canada, Open File, 3228,* 233-236.

Keating, P., & Sailhac, P. (2004). Use of the analytic signal to identify magnetic anomalies due to kimberlite pipes. *Geophysics, 69*(1), 180-190.

Kelley, S., Ross, M., Elliott, B., & Normandeau, P. (2019). Effect of shifting ice flow and basal topography in shaping three-dimensional dispersal patterns, Lac de Gras region, Northwest Territories, Canada. *Journal of Geochemical Exploration.*

Kennedy, K., Froese, D., Zazula, G., & Lauriol, B. (2010). Last glacial maximum age for the northwest Laurentide maximum from the eagle river spillway and delta complex, northern Yukon. *Quaternary Science Reviews, 29*(9-10), 1288-1300.

King, J., Van Nostrand, T., Bethune, K., Wingate, M., & Relf, C. (1991). Final field report on the Contwoyto-Nose Lakes map area, Central Slave Province, District of Mackenzie, NWT. *Current Research, Part C, Pap., 91*, 99-108.

Kjarsgaard, B. (1996). Slave Province kimberlites, NWT. *Searching for Diamonds in Canada. Geological Survey of Canada Open File, 3228,* 55-60.

Kjarsgaard, B., & Heaman, L. (2002). *[Zircon age dating, Lac de Gras, NT].* Unpublished manuscript.

Kjarsgaard, B. A., Jakob, Z. J., & Spark, R. N. (1999). *Preliminary geology, Exeter Lake, NTS 76 D/15, District of Mackenzie, Northwest Territories* (Open File 3702 ed.) Geological Survey of Canada.

Kjarsgaard, B., Spark, R., & Jakop, Z. (1994a). Preliminary geology, Koala, 76D/10, Northwest Territories. *Geological Survey of Canada, Open File Map, 2966*

Kjarsgaard, B., Spark, R., & Jakop, Z. (1994b). Preliminary geology, Ursula Lake, 76D/16, Northwest Territories. *Geological Survey of Canada, Open File Map, 2967*

Kjarsgaard, B., Wilkinson, L., & Armstrong, J. (2002). Geology, Lac de Gras kimberlite field, Central Slave Province, Northwest Territories-Nunavut. *Open File, 3228*

Kjarsgaard, B., & Wyllie, R. (1994). Geology of the Paul Lake area, Lac de Gras du Sauvage region of the Central Slave Province, District of Mackenzie, Northwest Territories. *Geological Society of Canada Current Research,* 23-32.

Klassen, R., & Bolduc, A. (1984). Ice flow directions and drift composition, Churchill Falls, Labrador. *Current Research.Geological Survey of Canada, Part A, Paper.* 255-258.

Klassen, R.A. (1997). Glacial history and ice flow dynamics applied to drift prospecting and geochemical exploration. Paper presented at the *Proceedings of Exploration, 97,* 221-232.

Klassen, R. A. (2001). *A Quaternary Geological Perspective on Geochemical Exploration in Glaciated Terrain, Geological Society, London, Special Publications 2001; v. 185; p. 1-17*

Knight, R. D., & Kerr, D. E. (2007). An overburden thickness model for Lac de Gras and Aylmer Lake, Northwest Territories, Canada. *Journal of Maps, 3*(1), 296-310.

Kujansuu, R., & Saarnisto, M. (1990). Glacial indicator tracing: AA balkema.

Lacelle, D., Lauriol, B., Zazula, G., Ghaleb, B., Utting, N., & Clark, I. D. (2013). Timing of advance and basal condition of the Laurentide Ice Sheet during the last glacial maximum in the Richardson Mountains, NWT. *Quaternary Research, 80*(2), 274-283.

Lakeman, T. R., & England, J. H. (2012). Paleoglaciological insights from the age and morphology of the Jesse moraine belt, western Canadian arctic. *Quaternary Science Reviews, 47*, 82-100.

Lakeman, T. R., & England, J. H. (2013). Late Wisconsinan dynamics of the northwest Laurentide Ice Sheet on Banks Island, Northwest Territories.

Lakeman, T. R., & England, J. H. (2014). Facies and stratigraphical analyses of glacial and interglacial sediments at Morgan Bluffs, Banks Island, Canadian Arctic Archipelago. *Boreas, 43*(4), 895-913.

Lambert, M., Beaumont-Smith, C., & Paul, D. (1992). Structure and stratigraphic succession of an Archean stratovolcano, Slave Province, Northwest Territories. *Geological Survey of Canada Paper*, 189-200.

Larson, P. C., & Mooers, H. D. (2004). Glacial indicator dispersal processes: A conceptual model. *Boreas, 33*(3), 238-249.

Le Maitre, R. (1982). Numerical petrology, statistical interpretation of geochemical data, developments in petrology 8.

Lemmen, D. S., A. Duk-Rodkin, and J. M. Bednarski. 1994. "Late Glacial Drainage Systems along the Northwestern Margin of the Laurentide Ice Sheet." *Quaternary Science Reviews* 13(9–10):805–28.

Levson, V. M. (2001). Regional till geochemical surveys in the Canadian cordillera: Sample media, methods and anomaly evaluation. *Geological Society, London, Special Publications, 185*(1), 45-68.

Lockhart, G., Grutter, H., & Carlson, J. (2004). Temporal and geomagnetic relationship of Ekati economic kimberlites. Paper presented at the *8th International Kimberlite Conference, Victoria, C.-B*

Lord, C., & Barnes, F. (1954). Aylmer lake. *District of Mackenzie, Northwest Territories, Geological Survey of Canada, Map A, 1031*

Lynch, J. (1996). Provisional elemental values for four new geochemical soil and till reference materials, till-1, till-2, till-3 and till-4. *Geostandards and Geoanalytical Research, 20*(2), 277-287.

Macnae, J. C. (1979). Kimberlites and exploration geophysics. *Geophysics, 44*(8), 1395-1416.

McClenaghan, M. B. (2005). Indicator mineral methods in mineral exploration. *Geochemistry: Exploration, Environment, Analysis, 5*(3), 233-245.

McClenaghan, M., & Kjarsgaard, B. (2001). Indicator mineral and geochemical methods for diamond exploration in glaciated terrain in Canada. *Geological Society, London, Special Publications, 185*(1), 83-123.

McClenaghan, M., & Kjarsgaard, B. (2007). Indicator mineral and surficial geochemical exploration methods for kimberlite in glaciated terrain, examples from Canada. *Mineral Resources of Canada: A Synthesis of Major Deposit-Types, District Metallogeny, the Evolution of Geological Provinces and Exploration Methods. Geological Association of Canada, Special Publication,* (5), 983-1006.

McClenaghan, M., Kjarsgaard, I., Schulze, D., Stirling, J., Pringle, G., & Berger, B. (1996). Mineralogy and geochemistry of the B30 kimberlite and overlying glacial sediments, Kirkland Lake, Ontario. *Open File, 3295*

McClenaghan, M., McClenaghan, M., Kjarsgaard, I., & Stirling, J. (1999). *Mineralogy and geochemistry of the A4 kimberlite and associated glacial sediments, Kirkland Lake, Ontario*

McClenaghan, M., & Paulen, R. (2017). Application of till mineralogy and geochemistry to mineral exploration. *Past glacial environments (second edition)* (pp. 689-751) Elsevier.

McClenaghan, M., & Peter, J. (2016). Till geochemical signatures of volcanogenic massive sulphide deposits: An overview of Canadian examples. *Geochemistry: Exploration, Environment, Analysis, 16*(1), 27-47.

McClenaghan, M., Thorleifson, L., & DiLabio, R. (2000). Till geochemical and indicator mineral methods in mineral exploration. *Ore Geology Reviews, 16*(3-4), 145-166.

McClenaghan, M., Ward, B., Kjarsgaard, I., Kjarsgaard, B., Kerr, D., & Dredge, L. (2002). Indicator mineral and till geochemical dispersal patterns associated with the Ranch Lake kimberlite, Lac de Gras region, NWT, Canada. *Geochemistry: Exploration, Environment, Analysis, 2*(4), 299-319.

McMartin, I., & Henderson, P. J. (2004). Evidence from Keewatin (central Nunavut) for paleo-ice divide migration. *Géographie Physique Et Quaternaire, 58*(2-3), 163-186.

McMartin, I., & McClenaghan, M. B. (2001). Till geochemistry and sampling techniques in glaciated shield terrain: A review. *Geological Society, London, Special Publications, 185*(1), 19-43.

McMartin, I., & Paulen, R. C. (2007). Application of till and stream sediment heavy mineral and geochemical methods to mineral exploration in western and northern Canada. Geological Association of Canada

McMartin, I., & Paulen, R.C. (2009). Ice-flow indicators and the importance of ice-flow mapping for drift prospecting. *Application of Till and Stream Sediment Heavy Mineral and Geochemical Methods to Mineral Exploration in Western and Northern Canada. Edited by RC Paulen and I.McMartin. Geological Association of Canada, Short Course Notes, 18,* 15-34.

Melanson, A., Bell, T., & Tarasov, L. (2013). Numerical modelling of subglacial erosion and sediment transport and its application to the North American ice sheets over the last glacial cycle. *Quaternary Science Reviews, 68,* 154-174.

Menzies, J. (2002). *Modern and past glacial environments: Revised student edition.* Butterworth-Heinemann.

Miller, J. (1984). Model for clastic indicator trains in till. *Prospecting in Areas of Glaciated Terrain,* 69-77.

Mitchell, R. H. (1986). *Kimberlites: Mineralogy, geochemistry, and petrology.* Springer Science & Business Media.

Moore, J. C. G. (1956). *Courageous-Matthews Lakes area, District of Mackenzie, Northwest Territories.* Department of Mines and Technical Surveys, Canada.

Murton, J. B., Bateman, M. D., Dallimore, S. R., Teller, J. T., & Yang, Z. (2010). Identification of Younger Dryas outburst flood path from Lake Agassiz to the arctic ocean. *Nature, 464*(7289), 740.

Northern Miner. (2002). Seahorse douses GGL's hopes. *The Northern Miner*. Retrieved from http://www.northernminer.com/news/seahorse-douses-ggl-s-hopes/1000148404/

NRCAN. (2014). In Earth Sciences Sector, Canada Centre for Mapping and Earth Observation (Ed.), *CanVec+ data product specifications* (GeoGratis Client Services Trans.). (1.0th ed.) Natural Resources Canada.

NTGS. (2018a). *Detailed showing report for DD-17 kimberlite.* (No. 076DSE0022). Northwest Territories Geological Survey.

NTGS. (2018b). *Northern mineral showings database.* Northwest Territories Geological Survey. Retrieved from http://ntgodata.nwtgeoscience.ca/

Oviatt, N., Gleeson, S., Paulen, R., McClenaghan, M., & Paradis, S. (2015). Characterization and dispersal of indicator minerals associated with the Pine Point Mississippi Valley-Type (MVT) district, Northwest Territories, Canada. *Canadian Journal of Earth Sciences, 52*(9), 776-794.

Parent, M., Paradis, S. J., & Doiron, A. (1996). Palimpsest glacial dispersal trains and their significance for drift prospecting. *Journal of Geochemical Exploration, 56*(2), 123-140.

Paulen, R. C. (2017). A revised look at Canada's landscape: Glacial process and dynamics, *in* New frontiers for exploration in glaciated terrain, (ed) R.C. Paulen and M.B. McClenaghan; Geological Survey of Canada, open file 7374., p. 5-12.

Paulen, R. (2013). A revised look at Canada's landscape: Glacial processes and dynamics. *New frontiers for exploration in glaciated terrain* (pp. 21-26)

Paulen, R., & McClenaghan, M. (2013). *New frontiers for exploration in glaciated terrain* Natural Resources Canada.

Paulen, R. C., McClenaghan, M. B., & Hicken, A. K. (2013). Regional and local ice-flow history in the vicinity of the Izok Lake Zn–Cu–Pb–Ag deposit, Nunavut 1. *Canadian Journal of Earth Sciences, 50*(12), 1209-1222.

Pell, J., Clements, B., Grütter, H., Neilson, S., & Grenon, H. (2017). Following kimberlite indicator minerals to source in the Chidliak kimberlite province, Nunavut, *in* New frontiers for exploration in glaciated terrain, (ed) R.C. Paulen and M.B. McClenaghan; Geological Survey of Canada, open file 7374., p. 47-52.

Pell, J. (1997). Kimberlites in the Slave Craton, Northwest Territories, Canada. *Geoscience Canada, 24*(2)

Piercey, S. J. (2014). Modern analytical facilities 2. A review of quality assurance and quality control (QA/QC) procedures for lithogeochemical data. *Geoscience Canada, 41*(1), 75-88.

Plouffe, A., McClenaghan, M., Paulen, R., McMartin, I., Campbell, J., & Spirito, W. (2013). Processing of glacial sediments for the recovery of indicator minerals: Protocols used at the geological survey of Canada. *Geochemistry: Exploration, Environment, Analysis, 13*(4), 303-316.

Prest, V., Grant, D., & Rampton, V. (1968). Glacial map of Canada., *Geological Survey of Canada Map 1253 A,*

Rea, B. R., Evans, D. J., Dixon, T. S., & Whalley, W. B. (2000). Contemporaneous, localized, basal ice-flow variations: Implications for bedrock erosion and the origin of p-forms. *Journal of Glaciology, 46*(154), 470-476.

Reimann, C., Filzmoser, P., Garrett, R. G., & Dutter, R. (2008). *Statistical data analysis explained: applied environmental statistics with R* Wiley Online Library.

Renaud, J., MacLachlan, K., Relf, C., & Duke, N. (2001). *Volcanic stratigraphy and mineral potential of the Aylmer Dome, southeastern Slave Province, Northwest Territories.* Citeseer.

Rose, A.W., Hawkes, H.E., Webb, J.S. (1979). Geochemistry in Mineral Exploration. Second Edition, Academic Press, New York, 657 pages.

Sacco, D., & McKillop, R. (2015). Strategies for resolving misleading surface sediment dispersal patterns based on local surficial geology. Paper presented at the *Yellowknife Geoscience Forum,* Yellowknife, Northwest Territories. PowerPoint Presentation.

Saskatchewan Research Council (SRC). (2017). *Geoanalytical laboratories 2017 services schedule.* (Services Schedule). Saskatoon, SK: Retrieved from https://www.src.sk.ca/sites/default/files/files/resource/Geoanalytical%20Services%20Schedule.pdf#page=37

Schodde, R. (2013). Long term outlook for the global exploration industry - gloom or boom? Paper presented at the *Strategic Advice on Mineral Economics & Exploration,* Johannesburg, South Africa. PowerPoint Presentation. Retrieved from http://www.minexconsulting.com/publications/Long%20Term%20Outlook%20for%20Exploration%20-%20Schodde%20-%20GSSA%20Conf%20July%202013%20FINAL.pdf

Sharpe, D., Kjarsgaard, B., Knight, R., Russell, H., & Kerr, D. (2017). Glacial dispersal and flow history, east arm area of Great Slave Lake, NWT, Canada. *Quaternary Science Reviews, 165,* 49-72.

Shilts, W. W. (1977). Geochemistry of till in perennially frozen terrain of the Canadian Shield—Application to prospecting. *Boreas, 6*(2), 203-212.

Shilts, W. W. (1978). Nature and genesis of mudboils, central Keewatin, Canada. *Canadian Journal of Earth Sciences, 15*(7), 1053-1068.

Shilts, W.W. (1982). Glacial dispersal-principles and practical applications. *Geoscience Canada, 9*(1)

Skinner, R. G. (1972). *Drift prospecting in the Abitibi clay belt overburden: Drilling program, methods and costs.* Geological Survey of Canada.

Smith, B. H. S. (2008). Canadian kimberlites: Geological characteristics relevant to emplacement. *Journal of Volcanology and Geothermal Research, 174*(1-3), 9-19.

Sneed, E. D., & Folk, R. L. (1958). Pebbles in the lower Colorado River, Texas a study in particle morphogenesis. *The Journal of Geology, 66*(2), 114-150.

Spot 5. (2002). *Spot 5 scenes s4_11203_6428_20070628_p10_1_lcc00 and S5_11050_6428_20060613_p10_1_lcc00.* (Lac de Gras, NWT ed.) Geogratis.

Stanley, C. (2009). Geochemical, mineralogical, and lithological dispersal models in glacial till: Physical process constraints and application in mineral exploration. *Application of Till and Stream Sediment Heavy Mineral and Geochemical Methods to Mineral Exploration in Western and Northern Canada. Edited by RC. Paulen and I. McMartin. Geological Association of Canada, Short Course Notes, 18,* 35-48.

Stea, R.R. (1994). Relict and palimpsest glacial landforms in Nova Scotia, Canada. *Formation and Deformation of Glacial Deposits. Edited by WP Warren and DG Croot.AA Balkema, Rotterdam.* 141-158.

Stea, R. R., & Finck, P. W. (2001). An evolutionary model of glacial dispersal and till genesis in maritime Canada. *Geological Society, London, Special Publications, 185*(1), 237-265.

Stea, R., Johnson, M., Hanchar, D., Paulen, R., & McMartin, I. (2009). The geometry of kimberlite indicator mineral dispersal fans in Nunavut, Canada. *Application of Till and Stream Sediment Heavy Mineral and Geochemical Methods to Mineral Exploration in Western and Northern Canada. Edited by RC Paulen and I.McMartin. Geological Association of Canada, Short Course Notes, 18*, 1-13.

Stokes, C. R. (2018). Geomorphology under ice streams: Moving from form to process. *Earth Surface Processes and Landforms, 43*(1), 85-123.

Stokes, C. R., Clark, C. D., Darby, D. A., & Hodgson, D. A. (2005). Late Pleistocene ice export events into the Arctic Ocean from the M'clure Strait ice stream, Canadian Arctic Archipelago. *Global and Planetary Change, 49*(3-4), 139-162.

Stokes, C. R., Clark, C. D., & Storrar, R. (2009). Major changes in ice stream dynamics during deglaciation of the north-western margin of the Laurentide ice sheet. *Quaternary Science Reviews, 28*(7), 721-738.

Stokes, C., Clark, C., & Winsborrow, M. (2006). Subglacial bedform evidence for a major palaeo-ice stream and its retreat phases in Amundsen Gulf, Canadian Arctic Archipelago. *Journal of Quaternary Science: Published for the Quaternary Research Association, 21*(4), 399-412.

Stokes, C. R., Lian, O. B., Tulaczyk, S., & Clark, C. D. (2008). Superimposition of ribbed moraines on a palaeo-ice-stream bed: Implications for ice stream dynamics and shutdown. *Earth Surface Processes and Landforms: The Journal of the British Geomorphological Research Group, 33*(4), 593-609.

Storrar, R. D., Stokes, C. R., & Evans, D. J. (2013). A map of large Canadian eskers from Landsat satellite imagery. *Journal of Maps, 9*(3), 456-473.

Tarasov, L., & Peltier, W. R. (2004). A geophysically constrained large ensemble analysis of the deglacial history of the North American ice-sheet complex. *Quaternary Science Reviews, 23*(3), 359-388.

Taylor, S. (2015). Canada's once-booming arctic diamond sector loses lustre. *CBC News* Retrieved from http://www.cbc.ca/news/Canada/north/Canada-s-once-booming-arctic-diamond-sector-loses-lustre-1.3290437

Teller, J. T., Boyd, M., Yang, Z., Kor, P. S., & Fard, A. M. (2005). Alternative routing of Lake Agassiz overflow during the Younger Dryas: New dates, paleotopography, and a re-evaluation. *Quaternary Science Reviews, 24*(16-17), 1890-1905.

Thompson, M., & Howarth, R. J. (1976). Duplicate analysis in geochemical practice. part I. theoretical approach and estimation of analytical reproducibility. *Analyst, 101*(1206), 690-698.

Thorleifson, L. H. (2017). History and status of till geochemical and indicator mineral methods in mineral exploration, *in* New frontiers for exploration in glaciated terrain, (ed) R.C. Paulen and M.B. McClenaghan; geological survey of Canada, open file 7374., p. 1-4.

Trommelen, M. S., Ross, M., & Campbell, J. E. (2013). Inherited clast dispersal patterns: Implications for palaeoglaciology of the SE Keewatin Sector of the Laurentide ice sheet. *Boreas, 42*(3), 693-713.

Tulaczyk, S., Kamb, B. & Engelhardt, H. F. (2001). Estimates of effective stress beneath a modern West Antarctic ice stream from till preconsolidation and void ratio. Boreas, Vol. 30: 101–114.

Tyrrell, J. B. (1898). The glaciation of north-central Canada. *The Journal of Geology, 6*(2), 147-160.

van Breemen, O., Davis, W. J., & King, J. E. (1992). Temporal distribution of granitoid plutonic rocks in the Archean Slave Province, northwest Canadian shield. *Canadian Journal of Earth Sciences, 29*(10), 2186-2199.

van Breemen, O., King, J., & Davis, W. (1990). U-Pb zircon and monazite ages from plutonic rocks in the Contwoyto-Nose Lakes map area, Central Slave Province, District of Mackenzie, Northwest Territories. *Radiogenic Age and Isotopic Studies: Report 3, 13*(14.84), 29.

Vasilenko, V., Zinchuk, N., Krasavchikov, V., Kuznetsova, L., Khlestov, V., & Volkova, N. (2002). Diamond potential estimation based on kimberlite major element chemistry. *Journal of Geochemical Exploration, 76*(2), 93-112.

Villeneuve, M., & Kjarsgaard, B. (2002). *[Zircon age dating, Lac de Gras, NT].* Unpublished manuscript.

Villeneuve, M. (1993). Preliminary geochronological results from the winter lake-Lac de Gras Slave Province NATMAP project, Northwest Territories. *Papers-Geological Survey of Canada,* 29-29.

Villeneuve, M., Lambert, L., van Breemen, O., & Mortensen, J. (2001). *Geochronology of the Back River Volcanic Complex, Nunavut-Northwest Territories* Natural Resources Canada, Geological Survey of Canada.

Walden, J. (2004). Particle lithology (or mineral and geochemical analysis). *A Practical Guide to the Study of Glacial Sediments. Arnold, London.* 145-180.

Ward, B. C. (1997). In Dredge L. A., Kerr D. E. (Eds.), *Surficial geology, Lac de Gras, District of Mackenzie, Northwest Territories*. Ottawa: Geological Survey of Canada. DOI:10.4095/209260

Ward, B. C., Dredge, L., & Kerr, D. E. (1996). *Trace element geochemistry and gold grain results from till samples, Lac de Gras area, Northwest Territories (NTS 76D)* Terrain Sciences Division, Geological Survey of Canada.

Ward, B. C., Dredge, L., Kerr, D. E., & Kurfurst, D. (1997). *Surficial geology, Lac de Gras, District of Mackenzie, Northwest Territories* Geological Survey of Canada.

Ward, B. C., Kjarsgaard, I. M., Dredge, L. A., & Kerr, D. E. (1995). *Distribution and chemistry of kimberlite indicator minerals, Lac de Gras map area (76D), Northwest Territories* Geological Survey of Canada.

Wheeler, J., Hoffman, P., Card, K., Davidson, A., Sanford, B., Okulitch, A., & Roest, W. (1997). Geological map of Canada, geological survey of Canada, map D1860A.

Wilkinson, L., Harris, J., Kjarsgaard, B., McClenaghan, B., & Kerr, D. (2001). *Influence of till thickness and texture on till geochemistry in the Lac de Gras area, Northwest Territories, with applications for regional kimberlite exploration.* Natural Resources Canada, Geological Survey of Canada.

Wilson, L., & Head Iii, J. W. (2007). An integrated model of kimberlite ascent and eruption. *Nature, 447*(7140), 53-57.

Yamashita, K., Creaser, R. A., & Villeneuve, M. E. (2000). Integrated Nd isotopic and U–Pb detrital zircon systematics of clastic sedimentary rocks from the Slave Province, Canada: Evidence for extensive crustal reworking in the early-to mid-Archean. *Earth and Planetary Science Letters*, *174*(3-4), 283-299.

Yaxley, G. M., Kamenetsky, V. S., Nichols, G. T., Maas, R., Belousova, E., Rosenthal, A., & Norman, M. (2013). The discovery of kimberlites in Antarctica extends the vast Gondwanan Cretaceous Province. *Nature Communications, 4*, 2921.

Appendix A: Clast lithology counts

Field Counted Samples

Sample ID	Easting	Northing	White Igneous (Counts)	White Igneous (%)	Pink Igneous (Counts)	Pink Igneous (%)	Metasedimentary (Counts)	Metasedimentary (%)	Mafic (Counts)	Mafic (%)
15-RJ-004	-111.52718	64.54747	51	39%	27	20%	53	40%	1	1%
15-RJ-011	-111.56553	64.56553	29	32%	15	17%	45	50%	1	1%
15-RJ-021	-111.19177	64.53922	31	30%	12	12%	58	56%	2	2%
15-RJ-026	-111.22415	64.54588	34	19%	14	8%	129	73%	1	1%
15-RJ-029	-111.19953	64.55962	42	30%	13	9%	85	60%	1	1%
15-RJ-039	-111.48936	64.50541	21	20%	16	16%	66	64%	0	0%
15-RJ-044	-111.44241	64.50825	47	33%	34	24%	60	42%	2	1%
15-RJ-060	-111.24368	64.47737	26	22%	20	17%	73	61%	0	0%
15-RJ-063	-111.26054	64.46065	32	31%	17	16%	55	53%	0	0%
15-RJ-071	-111.56504	64.53052	51	33%	50	32%	55	35%	0	0%
15-RJ-076	-111.55119	64.52745	11	13%	33	39%	41	48%	0	0%
15-RJ-082	-111.56619	64.51809	30	24%	42	33%	54	43%	0	0%
15-RJ-084	-111.56854	64.51247	52	29%	47	26%	81	45%	0	0%
15-RJ-086	-111.54220	64.51264	31	19%	54	34%	74	47%	0	0%
15-RJ-089	-111.51523	64.52369	24	18%	35	26%	75	56%	0	0%
15SK052	-111.37248	64.49270	29	41%	9	13%	32	45%	1	1%
15SK053	-111.36886	64.48422	21	38%	14	25%	20	36%	0	0%
15SK182	-110.91900	64.43126	20	18%	12	11%	80	71%	0	0%
15SK187	-110.90254	64.43530	26	17%	24	16%	100	67%	0	0%
15SK190	-110.88029	64.43992	18	17%	13	12%	77	71%	1	1%

Laboratory Counted Samples

Sample ID	Easting	Northing	White Igneous (Counts)	White Igneous (%)	Pink Igneous (Counts)	Pink Igneous (%)	Metasedimentary (Counts)	Metasedimentary (%)	Mafic (Counts)	Mafic (%)
15SK191	-110.88945	64.45103	28	17%	28	17%	106	65%	0	0%
15SK192	-110.89767	64.45265	27	22%	15	12%	79	65%	0	0%
15SK195	-110.90453	64.46445	13	11%	9	8%	95	80%	2	2%
15SK197	-110.90588	64.47183	40	25%	19	12%	100	62%	2	1%
15SK224	-111.12924	64.52027	11	12%	3	3%	76	84%	1	1%
15SK226	-111.12414	64.50997	22	21%	5	5%	80	75%	0	0%
15SK230	-111.08293	64.50373	10	7%	6	4%	126	89%	0	0%
UW-15-011	-110.90304	64.43459	93	25%	53	14%	230	61%	1	0%
UW-15-012	-111.56361	64.55110	68	33%	43	21%	96	46%	1	0%
UW-15-013	-111.56879	64.55728	132	41%	64	20%	127	39%	0	0%
UW-15-014	-111.18386	64.54451	52	21%	43	17%	151	61%	3	1%
UW-15-016	-111.20768	64.55286	28	20%	26	19%	83	61%	0	0%
UW-15-017	-111.49187	64.50650	48	27%	36	20%	94	52%	2	1%
UW-15-019	-111.22625	64.47932	43	22%	32	16%	117	60%	5	2%
UW-15-021	-111.30357	64.47346	33	18%	33	18%	109	62%	3	2%
UW-15-022	-111.49046	64.53767	62	24%	51	20%	141	55%	4	2%
UW-15-x03	-111.54343	64.51541	25	16%	31	20%	95	62%	3	2%

Appendix B: Whole Rock Geochemistry Data

Sample ID	Easting	Northing	Al_2O_3 (wt %)	CaO (wt %)	Fe_2O_3 (wt %)	K_2O (wt %)	MgO (wt %)	MnO (wt %)	Na_2O (wt %)	P_2O_5 (wt %)	TiO_2 (wt %)	SiO_2 (wt %)
15-095-01	504222	7147912	12.6	1.7	1.95	2.14	0.92	0.03	2.85	0.16	0.48	68.5
15-095-02	504222	7147912	11.9	1.14	3.11	2.19	1.39	0.03	1.79	0.17	0.46	49.9
15-095-03	504222	7147912	13.1	1.92	2.34	2.21	0.99	0.03	3.15	0.2	0.56	74.3
15-095-04	504222	7147912	15.3	1.92	3.54	2.38	1.71	0.04	3.16	0.17	0.57	69
15-095-05	504222	7147912	16.8	1.79	4.03	2.44	1.98	0.04	3.23	0.16	0.54	67.1
15-096-01	504668	7145443	13.7	1.87	2.47	2.38	1.04	0.03	3.16	0.18	0.53	73.8
15-096-02	504668	7145443	13.8	1.82	2.79	2.33	1.14	0.04	3.08	0.23	0.56	72.8
15-097-01	499444	7146849	13.6	1.83	2.51	2.32	1.05	0.03	3.14	0.19	0.5	73.5
15-097-02	499444	7146849	13.8	1.89	2.78	2.28	1.13	0.04	3.17	0.19	0.55	72.5
15-098-01	498220	7146166	13.7	1.84	2.64	2.52	1.1	0.03	3.08	0.2	0.52	72.4
15-098-02	498220	7146166	14	1.85	3.35	2.54	1.45	0.04	3	0.21	0.59	71.4
15-098-03	498220	7146166	13.3	2.05	2.61	2.43	1.09	0.03	3.31	0.2	0.52	73.5
15-098-04	498220	7146166	13.6	1.92	2.72	2.44	1.22	0.04	3.2	0.2	0.52	72.8
15-099-01	495990	7147159	13	1.97	2.56	2.58	1.23	0.04	3.16	0.19	0.58	73.5
15-099-02	495990	7147159	13	1.95	2.58	2.41	1.21	0.04	3.14	0.18	0.52	73.1
15-099-03	495990	7147159	12.9	1.97	2.4	2.45	1.04	0.03	3.17	0.23	0.52	73.3
15-099-04	495990	7147159	13.5	2.38	2.86	2.47	1.51	0.04	3.51	0.23	0.62	71.5
15-100-01	498624	7149185	12.7	1.93	2.62	2.32	1.21	0.04	2.91	0.22	0.77	71.7
15-100-02	498624	7149185	18.6	1.79	3.49	2.87	1.63	0.04	3.1	0.16	0.59	65.6
15-101-01	500436	7149639	14.9	1.9	3.48	2.17	1.58	0.04	3.28	0.16	0.61	69.8
15-102-01	498627	7151539	13.9	2.19	3.17	2.72	1.83	0.04	3.06	0.21	0.54	70.8
15-102-02	498627	7151539	13.8	2.02	3.02	2.11	1.28	0.04	3.33	0.18	0.62	72.3
15-103-01	496477	7152124	13.6	1.84	3.04	2.22	1.22	0.04	3.13	0.17	0.59	71.2
15-103-02	496477	7152124	14.1	2.35	3.35	2.06	1.33	0.04	3.47	0.23	0.64	71
15-104-01	497233	7153113	15.2	2.19	3.84	1.98	1.8	0.04	3.63	0.17	0.64	69.1
15-105-01	497365	7155104	12.1	1.89	1.89	1.84	0.78	0.04	3.11	0.16	0.87	73.7
15-105-02	497365	7155104	14.1	1.87	3.46	2.83	1.57	0.04	3.07	0.17	0.63	70.6
15-105-03	497365	7155104	13.6	1.86	2.59	2.43	1.16	0.04	3.38	0.23	0.56	72.5
15-105-04	497365	7155104	13.9	1.98	2.76	2.37	1.27	0.04	3.36	0.18	0.59	72.4
15-106-01	496076	7157249	13.8	1.8	3.06	1.82	1.21	0.03	3.18	0.15	0.61	68.5
15-107-01	493338	7158286	14.7	2.07	3.8	2.01	1.52	0.06	3.32	0.21	0.61	67.8
15-107-02	493338	7158286	15.1	1.83	4.17	2.64	1.76	0.04	3.14	0.18	0.63	68.8
15-107-03	493338	7158286	15	1.82	3.95	2.73	1.76	0.04	3.08	0.19	0.63	69

15-108-01	493338	7155761	13.4	2.32	3.34	1.82	1.39	0.04	3.49	0.25	0.74	71.7
15-109-01	494185	7154467	13.1	2.06	2.55	1.83	1.23	0.03	3.28	0.21	0.65	69.6
15-109-02	494185	7154467	12.8	2.08	3.03	2.3	1.87	0.03	2.92	0.28	0.64	63.1
15-110-01	492790	7152206	13.2	1.89	2.84	2.37	1.2	0.04	3.13	0.2	0.56	72.4
15-110-02	492790	7152206	13.7	2.02	2.97	2.08	1.26	0.04	3.27	0.19	0.59	72.4
15-110-03	492790	7152206	13.9	1.91	2.58	2.16	1.15	0.03	3.36	0.14	0.58	73.1
15-111-01	494499	7150529	13	1.7	2.61	2.15	1.03	0.03	3.13	0.15	0.54	71.8
15-112-01	495199	7149195	13.6	1.89	2.96	2.4	1.24	0.04	3.25	0.18	0.55	72.6
15-112-02	495199	7149195	13.3	2.03	2.77	2.33	1.21	0.04	3.26	0.17	0.58	73
15-113-01	492730	7147972	13.5	1.87	3.08	2.66	1.35	0.04	3.11	0.2	0.56	72.1
15-113-02	492730	7147972	14.6	2.02	3.77	2.7	1.67	0.04	3.28	0.19	0.57	70
15-113-03	492730	7147972	13.5	2.71	3.36	2.69	1.75	0.04	3.33	0.26	0.57	70.9
15-113-04	492730	7147972	13.7	1.87	3.03	2.46	1.38	0.04	3.18	0.16	0.57	72.7
15-114-01	491240	7146693	12.9	1.86	2.58	1.99	1.03	0.03	3.24	0.15	0.55	72.9
15-115-01	487922	7145775	14.6	1.78	3.44	2.54	1.59	0.04	3.11	0.16	0.58	70
15-115-02	487922	7145775	14.9	1.82	3.83	2.59	1.84	0.04	2.91	0.19	0.58	69.3
15-115-03	487922	7145775	13.7	1.91	2.92	2.52	1.38	0.04	3.12	0.18	0.58	72.2
15-115-04	487922	7145775	14.2	1.79	3.6	2.67	1.75	0.04	2.9	0.18	0.6	70.6
15-115-05	487922	7145775	15.4	1.74	4.11	2.89	2	0.04	2.88	0.18	0.61	68.4
15-115-06	487922	7145775	16.8	1.8	5.3	2.74	2.76	0.06	2.89	0.19	0.69	64.2
15-115-07	487922	7145775	18.6	1.49	6.21	3.8	3.38	0.06	2.47	0.23	0.62	59.8
15-116-01	488855	7147978	12.9	1.8	2.33	2.33	0.98	0.04	3.28	0.31	0.5	72
15-117-01	490712	7149336	13.2	1.75	2.16	2.07	1.04	0.03	3.23	0.13	0.52	71.4
15-117-02	490712	7149336	13.1	2.02	2.44	2.22	1.08	0.03	3.29	0.21	0.55	73.7
15-117-03	490712	7149336	15.8	1.99	5.34	3.19	2.72	0.06	2.78	0.18	0.7	64.4
15-118-01	491161	7150913	13.4	1.99	2.82	2.28	1.19	0.04	3.31	0.2	0.63	72.1
15-118-02	491161	7150913	14.4	1.83	3.8	2.35	1.63	0.04	3.13	0.17	0.65	70.2
15-118-03	491161	7150913	15.2	1.85	4.09	2.67	1.87	0.04	3.23	0.2	0.6	67.8
15-119-01	489492	7152457	13.6	1.92	2.91	2.32	1.24	0.03	3.32	0.19	0.6	72.2
15-119-02	489492	7152457	15.1	2.1	4.14	2.48	1.98	0.04	3.36	0.2	0.62	68.2
15-119-03	489492	7152457	16.2	1.92	5.28	2.64	2.54	0.05	3.08	0.19	0.67	65.2
15-120-01	490087	7153921	13.7	1.93	3.04	2.22	1.17	0.04	3.25	0.19	0.61	71.9
15-120-02	490087	7153921	13.6	1.99	2.59	2.08	1.06	0.03	3.39	0.2	0.56	73.6
15-121-01	490700	7154946	13.4	2.17	2.68	2	1.18	0.04	3.34	0.18	0.64	70.2
15-121-02	490700	7154946	12.9	1.77	2.5	1.75	1.03	0.03	3.23	0.17	0.54	72.5
15-122-01	489889	7157515	14	2.08	3.13	2.04	1.45	0.04	3.41	0.19	0.66	69.6
15-123-01	488228	7156621	13.6	1.92	2.89	2.13	1.2	0.04	3.29	0.18	0.59	71.8
15-123-02	488228	7156621	13.7	2.01	2.72	2.06	1.17	0.03	3.5	0.19	0.55	72

15-124-01	489319	7155224	13	1.85	2.5	2.15	1.07	0.03	3.18	0.17	0.65	72.8
15-124-02	489319	7155224	13	1.97	2.58	2.07	1.05	0.03	3.35	0.18	0.6	73
15-125-01	487406	7154072	13	1.86	2.4	2.02	1.08	0.03	3.33	0.21	0.55	72.9
15-125-02	487406	7154072	15.8	1.97	4.09	2.38	1.93	0.04	3.39	0.17	0.62	68.1
15-125-03	487406	7154072	16.2	2.03	5.7	3.38	3.13	0.06	3.2	0.23	0.71	63.7
15-126-01	486934	7154220	16.2	2.04	5.72	3.38	3.16	0.06	3.2	0.2	0.71	63.8
15-126-02	486934	7154220	13.5	1.88	2.93	2.49	1.24	0.04	3.32	0.19	0.51	72.9
15-126-03	486934	7154220	12.8	2.05	2.51	2.13	1.05	0.04	3.32	0.2	0.63	74.2
15-126-04	486934	7154220	15	1.88	3.74	2.53	1.87	0.04	3.16	0.18	0.59	69.2
15-126-05	486934	7154220	15.3	1.99	3.74	2.35	1.75	0.04	3.24	0.2	0.59	69.1
15-126-06	486934	7154220	15.1	1.89	3.97	2.58	2.02	0.04	3.14	0.19	0.61	68.6
15-126-07	486934	7154220	13.9	1.89	3.11	2.44	1.46	0.04	3.22	0.17	0.54	71.2
15-126-08	486934	7154220	15	2.07	3.56	2.26	1.63	0.04	3.2	0.21	0.66	70.1
15-126-09	486934	7154220	15.2	1.91	3.5	2.39	1.65	0.04	3.14	0.2	0.58	69.9
15-126-10	486934	7154220	17	1.85	4.47	2.52	2.26	0.04	3.11	0.17	0.57	66.1
15-126-11	486934	7154220	17.2	1.95	4.37	2.16	2.17	0.05	3.39	0.19	0.64	66.2
15-126-12	486934	7154220	16.4	2.17	4	2.3	2.03	0.04	3.3	0.23	0.59	67.4
15-126-13	486934	7154220	16.5	2.01	4.22	2.63	2.04	0.05	3.16	0.21	0.59	66.4
15-126-14	486934	7154220	18	1.9	5.02	3	2.67	0.05	2.95	0.2	0.64	63.1
15-126-15	486934	7154220	16.7	2.12	4.13	2.68	2.16	0.04	3.26	0.22	0.61	66.4
15-127-01	485954	7152366	13.5	1.84	2.83	2.36	1.1	0.03	3.05	0.2	0.58	71.6
15-127-03	485954	7152366	14.6	1.9	2.8	2.8	1.19	0.03	3.22	0.2	0.5	71.6
15-127-04	485954	7152366	14.5	2.04	3.17	2.43	1.48	0.04	3.17	0.18	0.59	71.1
15-128-01	487499	7151934	14.2	2.28	2.93	2.37	1.26	0.04	3.34	0.25	0.59	71.5
15-128-02	487499	7151934	13.4	2.07	2.41	2.15	1.01	0.03	3.24	0.21	0.58	74
15-128-03	487499	7151934	13.5	2.04	2.44	2.22	1.05	0.03	3.26	0.2	0.55	73.5
15-129-01	485422	7150553	12.8	1.89	1.96	2.25	0.78	0.03	3.12	0.19	0.53	74.7
15-130-01	484873	7148205	13	1.95	2.51	2.1	1.04	0.03	3.04	0.22	0.56	73.1
15-130-02	484873	7148205	13.2	1.85	2.2	2.32	0.94	0.03	3.17	0.17	0.53	74.1
15-131-01	483209	7148649	13.3	1.29	1.86	3.65	0.75	0.02	2.8	0.11	0.38	73.3
15-132-01	482932	7145900	9.07	1.05	3.16	1.43	0.64	0.02	1.62	0.38	0.29	41.2
15-132-02	482932	7145900	13.7	1.82	2.8	2.39	1.17	0.04	3	0.17	0.58	72.6
15-133-01	483645	7144672	13.4	1.85	2.5	2.41	1.12	0.03	3.02	0.18	0.56	73.1
15-133-02	483645	7144672	13.4	1.97	2.51	2.39	1.08	0.04	3.07	0.21	0.56	73.9
15-133-03	483645	7144672	13.8	1.96	2.96	2.52	1.31	0.04	2.94	0.19	0.58	72.4
15-134-01	480216	7146008	13.9	2.06	3.05	2.43	1.34	0.04	2.99	0.2	0.58	71.5
15-134-02	480216	7146008	14	1.9	3.46	2.77	1.53	0.04	3.12	0.21	0.58	71
15-135-01	477013	7146052	14.1	1.43	3.54	2.46	1.53	0.03	3.4	0.21	0.53	62.8

15-135-02	477013	7146052	13.4	1.82	3.07	2.62	1.34	0.04	3.02	0.19	0.61	72.1
15-136-01	474722	7147659	13.4	1.79	2.91	2.58	1.29	0.04	3.03	0.18	0.6	72.2
15-136-02	474722	7147659	13.4	1.9	2.73	2.65	1.21	0.04	3.19	0.2	0.55	72.8
15-136-03	474722	7147659	13.9	1.84	3.18	2.73	1.48	0.04	3.09	0.18	0.6	71.6
15-136-04	474722	7147659	15.2	1.79	3.93	2.73	1.95	0.04	3.05	0.16	0.63	69.3
15-136-05	474722	7147659	15.3	1.82	3.92	2.71	1.92	0.04	3.06	0.17	0.62	69.1
15-137-01	478502	7149600	12.1	1.47	2.67	2.23	0.84	0.03	2.7	0.06	0.56	71.4
15-138-01	480711	7150705	13.2	1.86	2.97	2.44	1.22	0.04	3.15	0.2	0.58	72.3
15-138-02	480711	7150705	12.9	1.88	2.41	2.3	0.99	0.03	3.26	0.21	0.56	74
15-138-03	480711	7150705	13.5	2.07	3.05	2.34	1.3	0.04	3.32	0.2	0.57	72.7
15-138-04	480711	7150705	14	1.97	3.42	2.48	1.6	0.04	3.15	0.19	0.63	71.5
15-138-05	480711	7150705	15.6	1.98	4.02	2.46	1.97	0.04	3.33	0.17	0.62	68
15-138-06	480711	7150705	15	2.23	3.99	2.31	2.01	0.05	3.36	0.18	0.63	69
15-138-07	480711	7150705	14.7	2.45	4.07	2.45	2.63	0.05	3.08	0.21	0.68	68.5
15-138-08	480711	7150705	15.6	2.02	4.27	2.56	2.55	0.05	3.14	0.18	0.64	67.2
15-138-09	480711	7150705	15.4	2.72	3.82	2.35	1.84	0.06	3.27	0.17	0.57	68.4
15-138-10	480711	7150705	15.7	1.95	4.2	2.41	2.14	0.04	3.17	0.16	0.58	66.1
15-138-11	480711	7150705	16.3	2.12	4.29	2.53	2.34	0.05	3.27	0.2	0.64	66.2
15-138-12	480711	7150705	16.4	1.99	4.38	2.52	2.26	0.05	3.25	0.19	0.66	66.4
15-138-13	480711	7150705	16.3	1.89	4.31	2.76	2.24	0.05	3.1	0.18	0.63	66.4
15-138-14	480711	7150705	16.5	1.96	4.36	2.65	2.27	0.05	3.19	0.18	0.61	66.7
15-138-15	480711	7150705	16.4	2.06	4.29	2.67	2.32	0.05	3.19	0.18	0.62	66
15-138-16	480711	7150705	16.6	2.04	4.28	2.87	2.31	0.05	3.23	0.18	0.6	66
15-139-01	478809	7151294	13.9	1.89	2.99	2.33	1.33	0.04	3.16	0.17	0.58	71.1
15-139-02	478809	7151294	15.6	1.88	4.13	2.46	1.85	0.05	3.27	0.17	0.63	67.7
15-139-03	478809	7151294	16.7	1.97	4.81	2.66	2.3	0.05	3.26	0.17	0.58	65.6
15-139-04	478809	7151294	16.8	2.14	4.09	2.77	2.08	0.05	3.51	0.2	0.56	65.7
15-139-05	478809	7151294	16.6	1.89	3.95	3.06	2.08	0.04	3.26	0.15	0.52	66.4
15-140-01	480071	7152906	13.4	1.85	2.44	2.28	1.01	0.03	3.3	0.16	0.57	73.3
15-141-01	483821	7152800	14.2	1.84	2.9	2.42	1.26	0.03	3.33	0.18	0.57	70.6
15-142-01	483758	7152902	14	1.66	2.78	3.01	1.17	0.04	3.13	0.15	0.5	72.2
15-142-02	483758	7152902	13.7	1.14	1.97	4.76	0.72	0.04	2.76	0.11	0.31	72.9
15-143-01	483795	7154213	14.3	1.77	3.07	2.43	1.28	0.04	3.18	0.14	0.56	69.8
15-144-01	481983	7154069	13.9	1.87	2.83	2.4	1.22	0.04	3.28	0.18	0.58	71
15-144-03	481983	7154069	14.7	2.03	3.42	2.54	1.5	0.04	3.43	0.19	0.59	70.4
15-144-04	481983	7154069	15.3	2.11	3.98	2.52	1.74	0.05	3.53	0.17	0.62	68.6
15-144-05	481983	7154069	15.6	2.05	3.95	2.79	1.9	0.05	3.41	0.16	0.6	68
15-144-06	481983	7154069	15.8	1.95	4.16	2.88	2.07	0.05	3.34	0.18	0.6	66.9

15-145-01	479638	7155611	13.7	2.02	2.69	2.16	1.07	0.04	3.43	0.2	0.59	70.8
15-145-02	479638	7155611	13.9	1.98	2.55	2.51	1.08	0.03	3.58	0.22	0.53	72.3
15-145-03	479638	7155611	13.8	2.14	2.69	2.29	1.24	0.04	3.5	0.18	0.58	72.4
15-145-04	479638	7155611	14.2	1.94	2.85	2.66	1.34	0.04	3.4	0.18	0.57	71.7
15-145-05	479638	7155611	14.8	1.93	2.96	2.93	1.42	0.04	3.45	0.21	0.55	70.2
15-146-01	483951	7152884	13.8	1.71	2.39	2.87	1.21	0.03	3.14	0.18	0.56	69.8
15-146-02	483951	7152884	13.8	1.99	2.31	2.35	1.14	0.03	3.4	0.17	0.58	73.5
15-146-03	483951	7152884	14.1	1.96	2.86	2.46	1.38	0.04	3.3	0.19	0.6	71.9
15-X03	473911	7154562	12.2	1.66	2.07	2.22	0.86	0.03	3.07	0.11	0.39	76.2
15-X011	504669	7145447	11.9	1.54	1.82	2.2	0.74	0.03	3.02	0.12	0.36	77.7
15-X012	472977	7158547	12.5	1.64	2.07	2.32	0.90	0.03	3.1	0.11	0.34	76
15-X013	472735	7159238	12.9	1.64	1.89	2.56	0.85	0.03	3.25	0.11	0.3	76
15-X014	491182	7157706	12.4	1.7	2.59	2.06	1.08	0.03	3.06	0.11	0.44	75.1
15-X015	489251	7157864	12.3	1.68	2.43	2.12	1.05	0.03	3.08	0.12	0.42	76.1
15-X016	490043	7158640	12.9	1.72	2.77	2.17	1.22	0.03	3.1	0.12	0.44	74.6
15-X017	476378	7153548	12	1.64	2.13	2.05	0.88	0.03	3.05	0.11	0.38	74.4
15-X019	489124	7150447	12.1	1.68	2.39	2.22	1.01	0.03	3.04	0.14	0.38	75
15-X021	485404	7149810	12	1.75	2.19	2.24	0.98	0.03	3.11	0.14	0.4	76.8
15-X022	476473	7157021	12.4	1.67	2.21	2.27	0.93	0.03	3.17	0.13	0.39	75.2

Appendix C: QAQC

Relative percent difference of Canadian Reference Materials CRM Till-1 and CRM Till-3

	Analyte	CRM Till-1	Relative % difference		Analyte	CRM Till-3	Relative % difference
Al2O3 (wt %)	13.4	13.7	-2.2%		11.7	12.2	-4.1%
CaO (wt %)	2.78	2.72	2.2%		2.66	2.63	1.1%
Fe2O3 (wt %)	6.89	6.82	1.0%		3.94	3.92	0.5%
K2O (wt %)	2.11	2.22	-5.0%		2.33	2.42	-3.7%
MgO (wt %)	2.12	2.15	-1.4%		1.69	1.71	-1.2%
MnO (wt %)	0.19	0.18	5.6%		0.07	0.06	16.7%
Na2O (wt %)	2.86	2.71	5.5%		2.74	2.64	3.8%
P2O5 (wt %)	0.2	0.22	-9.1%		0.1	0.11	-9.1%
TiO2 (wt %)	0.96	0.98	-2.0%		0.49	0.49	0.0%
SiO2 (wt %)	62.3	60.9	2.3%		69.7	69.1	0.9%

Precision scatterplots

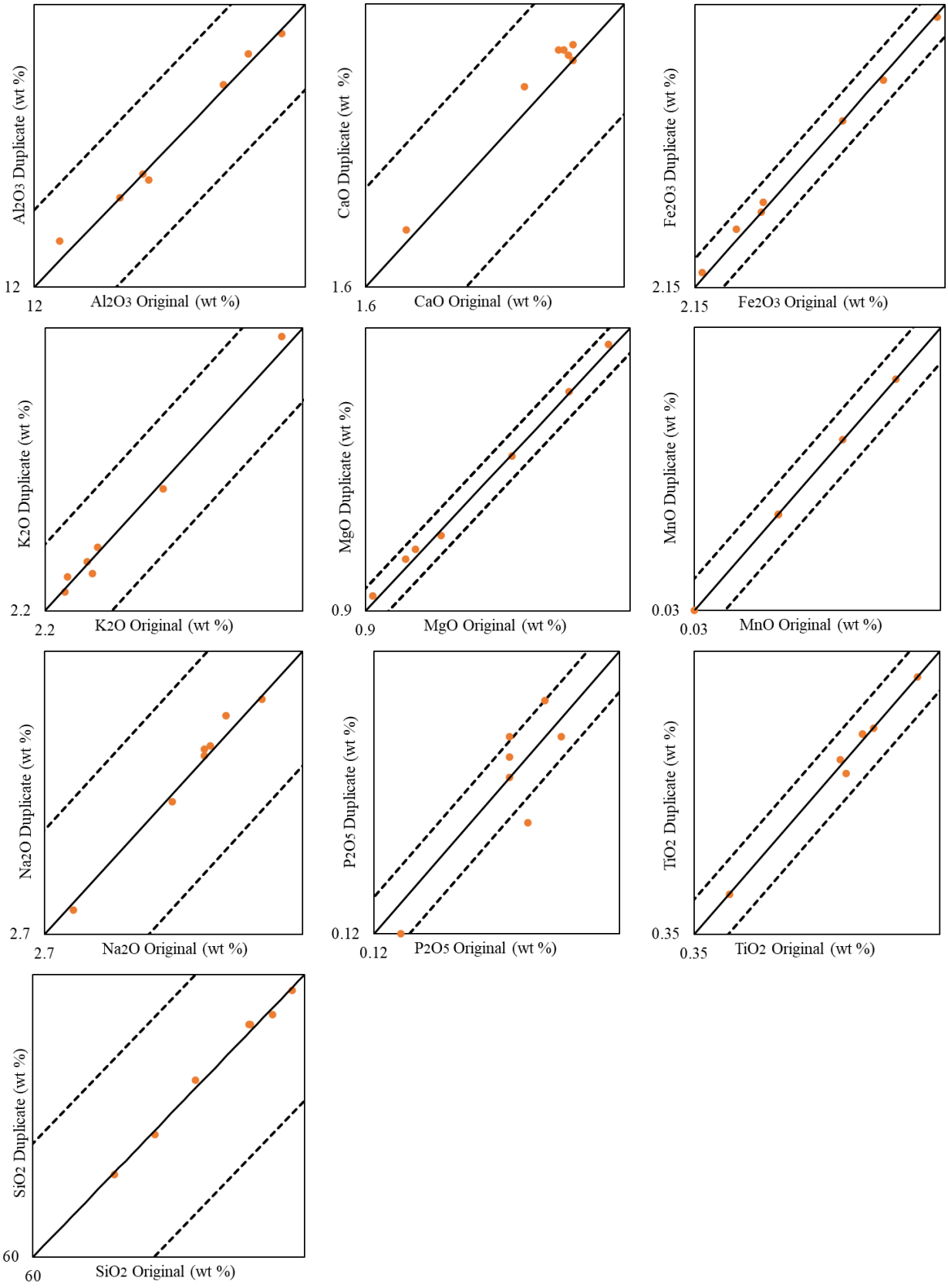

Thompson-Howarth Plots

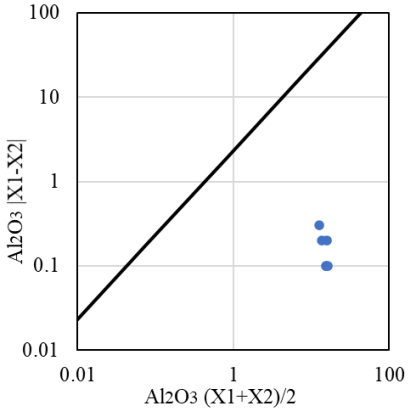

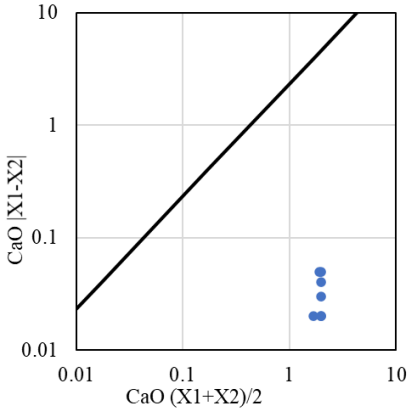

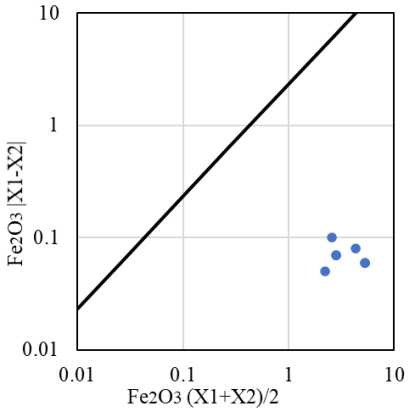

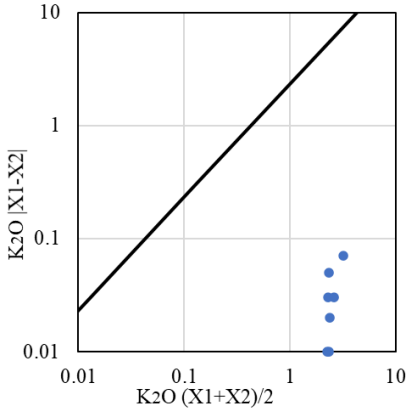

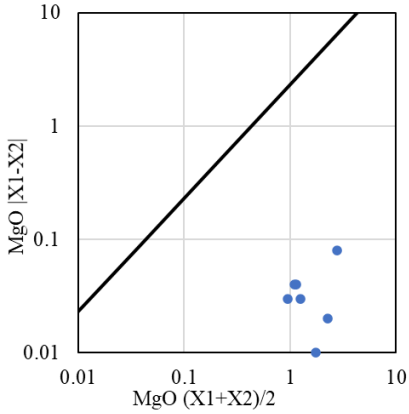

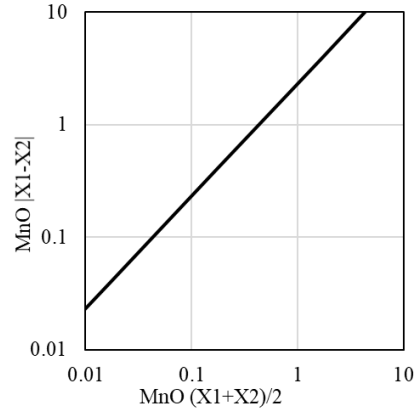

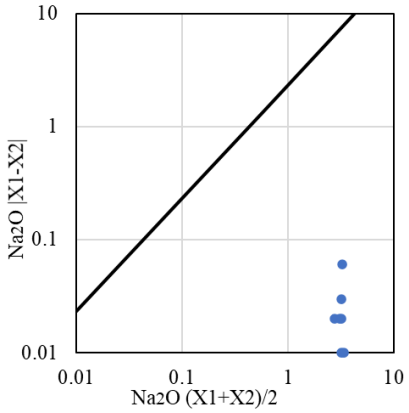

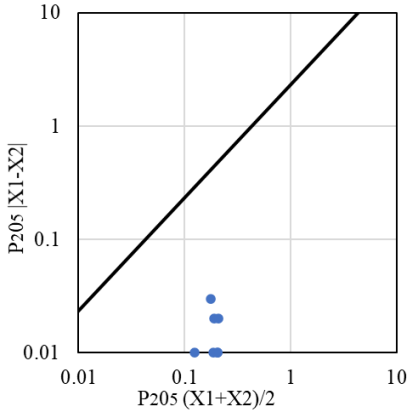

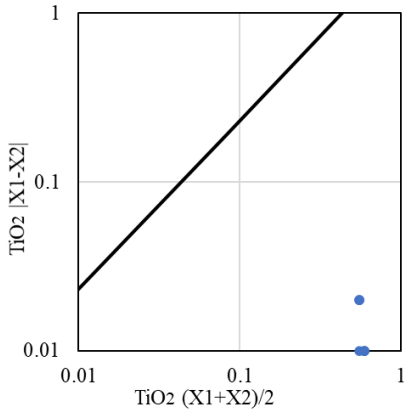

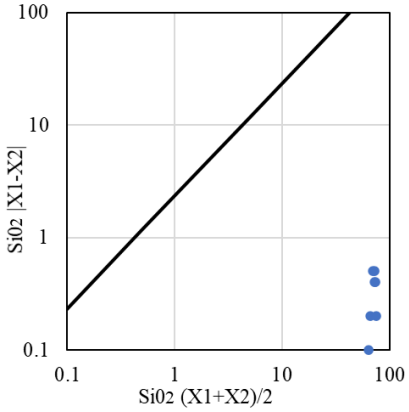

Kimberlite Indicator Mineral Duplicates

The QA/QC for duplicate analysis of KIM picked grains. All the duplicate data contain zero additional picked grains, which indicates all of the KIMs were identified in the initial picking.

Sample	Type	Pyrope (count)	Eclogite (count)	Cr-Diopside (count)	Olivine (count)	Picroilmentite (count)	Chrome (count)
RC15-095-04	Kimberlite	0	0	0	0	0	0
RC15-095-04 R	Duplicate	0	0	0	0	0	0
RC15-097-01	Kimberlite	0	0	0	0	0	0
RC15-097-01 R	Duplicate	0	0	0	0	0	0
RC15-098-05	Kimberlite	0	0	0	0	0	0
RC15-098-05 R	Duplicate	0	0	0	0	0	0
RC15-105-02	Kimberlite	0	0	0	0	0	0
RC15-105-02 R	Duplicate	0	0	0	0	0	0
RC15-106-01	Kimberlite	0	0	0	2	0	0
RC15-106-01 R	Duplicate	0	0	0	0	0	0
RC15-110-01	Kimberlite	1	0	0	1	0	0
RC15-110-01 R	Duplicate	0	0	0	0	0	0
RC15-113-01	Kimberlite	0	1	0	0	0	0
RC15-113-01 R	Duplicate	0	0	0	0	0	0
RC15-117-01	Kimberlite	0	0	0	0	0	0
RC15-117-01 R	Duplicate	0	0	0	0	0	0

RC15-120-02	Kimberlite	0	0	0	5	0	0
RC15-120-02 R	Duplicate	0	0	0	0	0	0
RC15-123-01	Kimberlite	1	0	0	4	0	0
RC15-123-01 R	Duplicate	0	0	0	0	0	0
RC15-126-04	Kimberlite	0	0	0	6	0	0
RC15-126-04 R	Duplicate	0	0	0	0	0	0
RC15-126-11	Kimberlite	0	1	1	15	0	0
RC15-126-11 R	Duplicate	0	0	0	0	0	0
RC15-131-01	Kimberlite	0	0	0	0	0	0
RC15-131-01 R	Duplicate	0	0	0	0	0	0
RC15-133-03	Kimberlite	0	0	0	0	0	0
RC15-133-03 R	Duplicate	0	0	0	0	0	0
RC15-136-05	Kimberlite	0	0	0	0	0	0
RC15-136-05 R	Duplicate	0	0	0	0	0	0
RC15-138-09	Kimberlite	0	0	0	3	0	0
RC15-138-09 R	Duplicate	0	0	0	0	0	0
RC15-138-11	Kimberlite	0	0	0	2	0	0
RC15-138-11 R	Duplicate	0	0	0	0	0	0
RC15-139-05	Kimberlite	2	0	0	1	0	0
RC15-139-05 R	Duplicate	0	0	0	0	0	0

RC15-142-02	Kimberlite	0	0	0	0	0	0
RC15-142-02 R	Duplicate	0	0	0	0	0	0
RC15-144-06	Kimberlite	2	0	0	37	0	3
RC15-144-06 R	Duplicate	0	0	0	0	0	0
UW-15-012	Kimberlite	1	0	1	8	0	0
UW-15-012 R	Duplicate	0	0	0	0	0	0
UW-15-016	Kimberlite	0	0	2	11	0	0
UW-15-016 R	Duplicate	0	0	0	0	0	0
39160	Kimberlite	0	0	0	0	0	0
39160 R	Duplicate	0	0	0	0	0	0
39172	Kimberlite	0	0	0	0	0	0
39172 R	Duplicate	0	0	0	0	0	0

Appendix D: Textural analysis sample statistics

	UW-15-x03	**UW-15-x02**	**UW-15-x01**	**UW-15-22**	**UW-15-021**	**UW-15-019**	**UW-15-17**
DATE:	2017-06-07	2017-06-07	2017-06-08	2017-06-09	2017-06-10	2017-06-11	2017-06-12
SAMPLE TYPE:	Trimodal, Very Poorly Sorted	Trimodal, Very Poorly Sorted	Trimodal, Very Poorly Sorted	Bimodal, Very Poorly Sorted	Bimodal, Very Poorly Sorted	Trimodal, Very Poorly Sorted	Bimodal, Very Poorly Sorted
TEXTURAL GROUP:	Gravelly Muddy Sand	Gravelly Muddy Sand	Gravelly Muddy Sand	Gravelly Muddy Sand	Gravelly Muddy Sand	Gravelly Muddy Sand	Gravelly Muddy Sand
SEDIMENT NAME:	Very Fine Gravelly Coarse Silty Very Fine Sand	Very Fine Gravelly Coarse Silty Very Fine Sand	Very Fine Gravelly Coarse Silty Very Fine Sand	Very Fine Gravelly Coarse Silty Very Fine Sand	Very Fine Gravelly Coarse Silty Very Fine Sand	Very Fine Gravelly Coarse Silty Very Fine Sand	Very Fine Gravelly Coarse Silty Very Fine Sand
Φ MEAN (M_z):	3.044	3.574	2.854	2.911	3.116	2.912	2.913
Φ SORTING (σ_I):	2.886	2.996	2.973	3.156	2.835	3.027	2.895
Φ SKEWNESS (Sk_I):	-0.103	-0.054	-0.076	-0.032	-0.063	-0.129	-0.107
Φ KURTOSIS (K_G):	0.990	1.025	0.854	0.854	1.027	0.851	0.934
MEAN Description:	Very Fine Sand	Very Fine Sand	Fine Sand	Fine Sand	Very Fine Sand	Fine Sand	Fine Sand
SORTING Description:	Very Poorly Sorted	Very Poorly Sorted	Very Poorly Sorted	Very Poorly Sorted	Very Poorly Sorted	Very Poorly Sorted	Very Poorly Sorted
SKEWNESS Description:	Coarse Skewed	Symmetrical	Symmetrical	Symmetrical	Symmetrical	Coarse Skewed	Coarse Skewed
KURTOSIS Description:	Mesokurtic	Mesokurtic	Platykurtic	Platykurtic	Mesokurtic	Platykurtic	Mesokurtic
% GRAVEL:	9.6%	8.4%	11.3%	14.2%	8.4%	13.0%	10.5%
% SAND:	54.6%	46.8%	53.7%	53.5%	58.2%	47.2%	52.6%
% SILT & CLAY:	35.9%	44.8%	35.0%	32.3%	33.4%	39.8%	36.9%

	UW-15-16	**UW-15-15**	**UW-15-14**	**UW-15-13**	**UW-15-12**	**UW-15-11**
DATE:	2017-06-13	2017-06-14	2017-06-15	2017-06-16	2017-06-17	2017-06-18
SAMPLE TYPE:	Bimodal, Very Poorly Sorted	Trimodal, Very Poorly Sorted	Trimodal, Very Poorly Sorted	Bimodal, Very Poorly Sorted	Trimodal, Very Poorly Sorted	Bimodal, Very Poorly Sorted
TEXTURAL GROUP:	Gravelly Muddy Sand	Gravelly Muddy Sand	Gravelly Muddy Sand	Gravelly Muddy Sand	Gravelly Muddy Sand	Gravelly Muddy Sand
SEDIMENT NAME:	Very Fine Gravelly Coarse Silty Very Fine Sand	Very Fine Gravelly Coarse Silty Very Fine Sand	Very Fine Gravelly Coarse Silty Fine Sand	Very Fine Gravelly Coarse Silty Very Fine Sand	Very Fine Gravelly Coarse Silty Very Fine Sand	Very Fine Gravelly Coarse Silty Very Fine Sand
Φ MEAN (M_z):	3.376	2.634	1.939	3.439	3.589	2.762
Φ SORTING (σ_I):	3.224	2.950	2.709	2.955	2.805	3.037
Φ SKEWNESS (Sk_I):	-0.075	-0.050	0.081	0.056	0.052	-0.041
Φ KURTOSIS (K_G):	0.918	0.859	0.777	0.964	1.210	0.860
MEAN Description:	Very Fine Sand	Fine Sand	Medium Sand	Very Fine Sand	Very Fine Sand	Fine Sand
SORTING Description:	Very Poorly Sorted	Very Poorly Sorted	Very Poorly Sorted	Very Poorly Sorted	Very Poorly Sorted	Very Poorly Sorted
SKEWNESS Description:	Symmetrical	Symmetrical	Symmetrical	Symmetrical	Symmetrical	Symmetrical
KURTOSIS Description:	Mesokurtic	Platykurtic	Platykurtic	Mesokurtic	Leptokurtic	Platykurtic
% GRAVEL:	10.6%	13.5%	17.6%	6.6%	6.3%	12.5%
% SAND:	44.7%	55.0%	60.3%	54.3%	55.9%	54.8%
% SILT & CLAY:	44.7%	31.5%	22.1%	39.1%	37.8%	32.7%

Appendix E: Levelling Public Datasets

Data from the KIDD needs to be normalized to make use of it in a meaningful way due to multiple researchers and methods for collecting the field samples, as well as the inconsistent weight of the samples, all of which result in skewed data. To make use of large KIM datasets, such as the KIDD, filtering and levelling the dataset is necessary. The methods used for collecting samples differ from study to study, leaving a large degree of variability. The samples are processed at different labs, the protocols for collecting samples can be different, and much of the data lacks notes on the type of sediment sampled. To help mitigate these problems, a subject area is defined, and all non-significant data is removed. This includes only considering the samples that analyze for the same KIM grains, and the analysis of a consistent size fraction (e.g. 0.25 to 0.50 mm), as is suggested by Ward *et al*. (1995) in the Lac de Gras area. Samples with poor results due to the type of analysis (*e.g*. Shaker table only) are also removed to avoid skewing the data. Once the filtering is complete, the data is levelled by converting the number of KIM grains in each sample to a z-score within each indicator mineral group. These z-scores are plotted to visually demonstrate the anomalous KIM data within the study area.

Appendix F: KIM Scores

KIM Score – Fine Fraction (0.25 – 0.50 mm)

Kimberlite indicator mineral score for the fine fraction (0.25 – 0.50 mm) of KIMs. A low score sample equals 1 point. A high score sample equals 2 points. The total score is tabulated on the right. The borehole number is listed as NGO-RC15-###-## with the first three numbers being the borehole number and the last 2 numbers are the depth of the sample (*e.g.* sample 03 is the 3rd 1.5 m depth sample for a total depth of 3x1.5=4.5 m). The surficial samples are listed as UW-15-###.

Sample ID (0.25-0.50 mm)	Pyrope (grains/20kg)	Pyrope Score	Eclogite (grains/20kg)	Eclogite Score	Chrome Diopside (grains/20kg)	Chrome Diopside Score	Olivine (grains/20kg)	Olivine Score	Picroilmenite (grains/20kg)	Picroilmenite Score	Chromite (grains/20kg)	Chromite Score	Total (grains/20kg)	Total Score
15-095-01	11.6883	1	0		1.2987		0		0		0		12.987	1
15-095-02	0		0		0		0		0		0		0	0
15-095-03	0		0		0		0		0		0		0	0
15-095-04	0		0		1.1019		0		0		0		1.1019	0
15-095-05	0.9238		0		0		0		0		0.9238		1.8476	0
15-096-01	0		0		0		0		0		2.381		2.381	0
15-096-02	0		0		0		0		0		0		0	0
15-097-01	0.6745		0		0		0		0		2.0236		2.6981	0
15-097-02	0		0		2.1164		0		0		0		2.1164	0
15-098-01	3.3003		0		0.6601		16.5017		0		0.6601		21.1222	0
15-098-02	0.6525		0		0.6525		0		0		0		1.305	0
15-098-03	0.907		0		0		0		0		0		0.907	0
15-098-04	0.6525		0		0		0.6525		0		0.6525		1.9575	0

15-099-01	1.173		0		0		1.173		0		0		2.346	0
15-099-02	0		0		0		2.6608		0		0		2.6608	0
15-099-03	0		0		0.6462		0		0		0.6462		1.2924	0
15-099-04	0		0		0		0		0		0		0	0
15-100-01	2.1858		0		0		1.0929		0		0		3.2787	0
15-100-02	0		0		0		0		0		0		0	0
15-101-01	0		0		0		0.8811		0		1.7621		2.6432	0
15-102-01	0.7767		0		0		10.0971		0		0		10.8738	0
15-102-02	16.6667	1	0		0		0		0		0		16.6667	1
15-103-01	4.4944		0		1.4981		2.9963		1.4981	1	1.4981		11.985	1
15-103-02	2.5237		0		1.2618		18.9274	1	0		0		22.7129	1
15-104-01	5.0179		0		2.1505		35.8423	1	0		0		43.0107	1
15-105-01	0		0		0		0		0		0		0	0
15-105-02	1.1561		0		0		1.1561		0		0		2.3122	0
15-105-03	2.1779		0		0.726		33.3938	1	0		0		36.2977	1
15-105-04	0.8403		0		0		4.2017		0		1.6807		6.7227	0
15-106-01	0		0		0		5.2632		0		0		5.2632	0
15-107-01	3.1128		0		0		1.5564		0		0.7782		5.4474	0
15-107-02	2.0906		0		0.6969		7.6655		0		0		10.453	0
15-107-03	0		0		0		0		0		0		0	0
15-108-01	11.7302	1	0		9.3842	1	9.3842		0		1.173		31.6716	2

15-109-01	2.5478		0		2.5478		0		0		0		5.0956	0
15-109-02	3.5088		0		0		0		0		0		3.5088	0
15-110-01	2.2409		0		1.1204		0		0		1.1204		4.4817	0
15-110-02	2.277		0.759	1	0		0		0		2.277		5.313	1
15-110-03	2.5918		0		0		0		0		0		2.5918	0
15-111-01	0		0		0		0		0		0		0	0
15-112-01	0		0		0		0		0		1.7316		1.7316	0
15-112-02	0.9302		0		0		0		0		1.8605		2.7907	0
15-113-01	0		0		0		0		0		0		0	0
15-113-02	1.6461		0		0		0		0		0		1.6461	0
15-113-03	1.581		0		0		0		0		0		1.581	0
15-113-04	0		0		0		0		0		2.8369	1	2.8369	1
15-114-01	0		0		1.0363		0		0		0		1.0363	0
15-115-01	1.81		0		0		0		0		0		1.81	0
15-115-02	1.8265		0		0		0.6088		0		0		2.4353	0
15-115-03	0		0		0.8421		0		0		0		0.8421	0
15-115-04	0		0		0		2.3669		0		0		2.3669	0
15-115-05	0		0		0		0		0		0		0	0
15-115-06	0		0		0		0		0		0		0	0
15-115-07	0		0		0		0		0		0		0	0
15-116-01	0		0		0		0		0		1.5209		1.5209	0

15-117-01	0		0		0		0		0		0		0	0
15-117-02	1.061		0		0		0		0		2.122		3.183	0
15-117-03	0		0		0		0		0		0		0	0
15-118-01	0		0		0		0		0		0		0	0
15-118-02	1.9608		0		0		0		0		0		1.9608	0
15-118-03	0		0		0		0		0		0		0	0
15-119-01	0		0		0		2.1277		0		0		2.1277	0
15-119-02	5.6838	1	0		2.1314		3.5524		0		2.1314		13.499	1
15-119-03	40.4255	2	0		24.4681	2	36.1702	1	0		3.1915	1	104.2553	6
15-120-01	0.8065		0		0		11.2903		0		0		12.0968	0
15-120-02	5.8824	1	0		0		52.9412	1	0		0		58.8236	2
15-121-01	3.9867		0		3.9867		0		0		0		7.9734	0
15-121-02	0		0		0		0		0		0		0	0
15-122-01	8.6957	1	0		0		13.0435		0		0		21.7392	1
15-123-01	7.2848	1	0.6623		2.649		11.2583		0		0		21.8544	1
15-123-02	4.0201		0		2.0101		6.0302		0		0		12.0604	0
15-124-01	3.0303		0		2.2727		12.1212		0		0		17.4242	0
15-124-02	0		0		0		80.7339	2	0		0		80.7339	2
15-125-01	7.7922	1	0		5.1948	1	19.0476	1	0		0		32.0346	3
15-125-02	6.5455	1	0.7273	1	2.9091		23.2727	1	0		0.7273		34.1819	3
15-125-03	0		0		0		16		0		0		16	0

15-126-01	7.3059	1	0.9132	1	2.7397		16.4384		0		0.9132		28.3104	2
15-126-02	6.3269	1	0		2.109		19.6837	1	0		0		28.1196	2
15-126-03	2.8419		0		2.1314		9.9467		0		0		14.92	0
15-126-04	8.0717	1	0		5.3812	1	51.1211	1	0		0.8969		65.4709	3
15-126-05	5.9369	1	0.7421	1	2.9685		46.7532	1	0		0		56.4007	3
15-126-06	3.4483		0		1.7241		28.4483	1	0		0		33.6207	1
15-126-07	6.1303	1	0		1.5326		45.977	1	0		0.7663		54.4062	2
15-126-08	0.7168		0		0		16.4875		0		0.7168		17.9211	0
15-126-09	1.318		0.659		3.2949		31.631	1	0		0.659		37.5619	1
15-126-10	6.6667	1	0		7.2727	1	86.6667	2	0.6061	1	1.8182		103.0304	5
15-126-11	18.5654	1	0		8.4388	1	88.6076	2	0		0		115.6118	4
15-126-12	14.4578	1	2.0654	2	15.8348	2	2.0654		2.7539	2	0.6885		37.8658	7
15-126-13	7.0922	1	0.7092	1	3.5461		48.9362	1	0		4.2553	2	64.539	5
15-126-14	1.8209		0		0.607		22.4583	1	0		0		24.8862	1
15-126-15	9.9548	1	0		4.5249	1	51.5837	1	0		0		66.0634	3
15-127-01	1.4159		0		0		4.2478		0		1.4159		7.0796	0
15-127-02	0		0		2.1978		37.3626	1	0		1.0989		40.6593	1
15-128-01	1.0076		0		0		0		0		0		1.0076	0
15-128-02	0.7042		0		0		6.338		0		0		7.0422	0
15-128-03	16.3265	1	0		0		24.4898	1	0		0		40.8163	2
15-129-01	0		0		0		12.9555		0		0		12.9555	0

15-130-01	1.4159		0		0		6.3717		0		1.4159		9.2035	0
15-130-02	0		0		0		32.6531	1	0		0		32.6531	1
15-131-01	0		0		0		0		0		0		0	0
15-132-01	2.7972		0		0		0		0		0		2.7972	0
15-132-02	0		0		1.108		11.0803		0		2.2161		14.4044	0
15-133-01	1.9967		0		0.6656		1.9967		0		3.3278	1	7.9868	1
15-133-02	2.454		0		0.6135		2.454		0		1.227		6.7485	0
15-133-03	0		0		2.5263		5.8947		0		0		8.421	0
15-134-01	2.2099		0		0		5.5249		0		2.2099		9.9447	0
15-134-02	2.7119		0		2.7119		4.0678		0		2.7119	1	12.2035	1
15-135-01	0		0		0.7678		1.5355		0		0.7678		3.0711	0
15-135-02	0.978		0		0		2.934		0		0.978		4.89	0
15-136-01	2.1016		0		0.7005		4.9037		0		0.7005		8.4063	0
15-136-02	3.9801		0		0		2.9851		0		0		6.9652	0
15-136-03	2.7682		0		0		8.3045		0		0.692		11.7647	0
15-136-04	0		0		0		11.0906		0		0.7394		11.83	0
15-136-05	0		0		0		0		0		0		0	0
15-137-01	0		0		0		0		0		0		0	0
15-138-01	0		0		0		4.2424		0		0.6061		4.8485	0
15-138-02	1.4363		0		0		3.5907		0		0		5.027	0
15-138-03	0		0		0		0.7407		0		0		0.7407	0

15-138-04	0		0		0.8621		0.8621		0		0		1.7242	0
15-138-05	0		0.6098		0.6098		4.878		1.2195	1	0.6098		7.9269	1
15-138-06	0.7561		0		0		7.5614		1.5123	1	0		9.8298	1
15-138-07	0		0		0		4.3478		0		0		4.3478	0
15-138-08	0		0		0.6452		5.1613		0		0		5.8065	0
15-138-09	0		0		0		2.8674		0		0		2.8674	0
15-138-10	0		1.0554	2	0		0		0		0		1.0554	2
15-138-11	2.1277		0		1.4184		3.5461		0		0		7.0922	0
15-138-12	0		0		0		1.4388		0		0		1.4388	0
15-138-13	0		0		0		20.5534	1	1.581	1	3.1621	1	25.2965	3
15-138-14	1.5152		0		0		6.0606		0		0		7.5758	0
15-138-15	0		0		0		5.5249		0		1.105		6.6299	0
15-138-16	2.3576		0		2.3576		8.6444		0		0		13.3596	0
15-139-01	1.421		0		0.7105		3.5524		0		0		5.6839	0
15-139-02	2.0725		0		0		2.7634		1.3817	1	0		6.2176	1
15-139-03	0		0		1.1494		1.1494		0		0		2.2988	0
15-139-04	2.952		0.738	1	0.738		7.3801		0		0		11.8081	1
15-139-05	11.6505	1	3.8835	2	3.8835		58.2524	1	0		0		77.6699	4
15-140-01	0		0		0		0		0		0		0	0
15-141-01	4.2105		0		1.4035		4.2105		0		0		9.8245	0
15-142-01	3.2193		0		1.6097		12.8773		0		0.8048		18.5111	0

15-142-02	0		0		0		13.7931		0		0		13.7931	0
15-143-01	0		0		0		21.5054	1	0		0		21.5054	1
15-144-01	3.4934		0		3.4934		27.0742	1	0		0		34.061	1
15-144-02	11.245	1	0		6.4257	1	64.257	1	0		0		81.9277	3
15-144-03	25.9179	2	1.7279	2	6.9114	1	57.0194	1	0		2.5918	1	94.1684	7
15-144-04	22.8571	1	1.3445	2	7.395	1	40.3361	1	0		1.3445		73.2772	5
15-144-05	22.1687	1	0		9.6386	1	139.759	2	0		2.8916	1	174.4579	5
15-145-01	9.1778	1	0.7648	1	3.0593		29.8279	1	0		3.0593	1	45.8891	4
15-145-02	5.036		0		3.5971		27.3381	1	0		2.8777	1	38.8489	2
15-145-03	22.4138	1	1.1494	2	9.7701	1	44.8276	1	0		0		78.1609	5
15-145-04	12.931	1	0.8621	1	5.1724	1	57.7586	1	0		0		76.7241	4
15-145-05	14.5455	1	0		7.2727	1	14.5455		0		0		36.3637	2
15-146-01	7.9137	1	0		5.036	1	0		0		0		12.9497	2
15-146-02	26.6667	2	0		17.1429	2	1.9048		0		1.9048		47.6192	4
15-146-03	19.5652	1	0		17.3913	2	58.6957	1	0		0		95.6522	4
15-011	0		0		0		2.9851		0		0		2.9851	0
15-012	32.7485	2	0		23.3918	2	116.9591	2	0		2.3392		175.4386	6
15-013	34.7826	2	0		10.4348	1	86.9565	2	0		0		132.1739	5
15-014	54.9618	2	3.0534	2	30.5344	2	146.5649	2	0		3.0534	1	238.1679	9
15-015	21.7054	1	0		18.6047	2	52.7132	1	0		0		93.0233	4
15-016	16.5517	1	2.7586	2	22.069	2	157.2414	2	0		0		198.6207	7

15-017	3.3613		0		3.3613		10.084		0		0		16.8066	0
15-019	3.7915		0		0		7.5829		0		0		11.3744	0
15-021	0		0		0		0.8602		0		0.8602		1.7204	0
15-022	22.6415	1	0		25.1572	2	148.4277	2	0		0		196.2264	5
15-x03	3.6697		0		1.2232		7.3394		0		0		12.2323	0

KIM Score – Coarse Fraction (0.50 – 1.00 mm)

Kimberlite indicator mineral score for the coarse fraction (0.50 – 1.00 mm) of KIMs. A low score sample equals 1 point. A high score sample equals 2 points. The total score is tabulated on the right. The borehole number is listed as NGO-RC15-###-## with the first three numbers being the borehole number and the last 2 numbers are the depth of the sample (*e.g.* sample 03 is the 3rd 1.5 m depth sample for a total depth of 3x1.5=4.5 m). The surficial samples are listed as UW-15-###.

Sample ID (0.50–1.00 mm)	Pyrope (grains/20kg)	Pyrope Score	Eclogite (grains/20kg)	Eclogite Score	Chrome Diopside (grains/20kg)	Chrome Diopside Score	Olivine (grains/20kg)	Olivine Score	Picroilmenite (grains/20kg)	Picroilmenite Score	Chromite (grains/20kg)	Chromite Score	Total (grains/20kg)	Total Score
15-095-01	0.00		0.00		0.00		1.30		0.00		0.00		1.30	0
15-095-02	0.00		0.00		0.00		1.66		0.00		0.00		1.66	0
15-095-03	0.95		0.00		0.00		0.00		0.00		0.00		0.95	0
15-095-04	0.00		0.00		0.00		0.00		0.00		0.00		0.00	0
15-095-05	0.00		0.00		0.00		0.00		0.00		0.00		0.00	0
15-096-01	0.00		0.00		0.00		1.59		0.00		0.00		1.59	0
15-096-02	0.00		0.00		0.00		0.00		0.00		0.00		0.00	0
15-097-01	0.00		0.00		0.67		0.67		0.00		0.67	1	2.02	1
15-097-02	0.00		0.00		0.00		2.12		0.00		0.00		2.12	0
15-098-01	0.00		0.00		0.00		4.62		0.00		0.00		4.62	0
15-098-02	0.00		0.00		0.00		1.31		0.00		0.00		1.31	0
15-098-03	0.00		0.00		0.00		0.91		0.00		0.00		0.91	0
15-098-04	0.65		0.00		0.65		0.65		0.00		0.00		1.96	0
15-099-01	0.00		0.00		0.00		1.17		0.00		0.00		1.17	0

15-099-02	0.00		0.00		0.00		1.77		0.00		0.00		1.77	0
15-099-03	0.00		0.00		0.00		0.65		0.00		0.00		0.65	0
15-099-04	0.00		0.00		0.00		0.00		0.00		0.00		0.00	0
15-100-01	0.00		0.00		0.00		0.00		0.00		0.00		0.00	0
15-100-02	0.00		0.00		0.00		0.00		0.00		0.00		0.00	0
15-101-01	0.00		0.00		0.00		0.88		0.00		0.00		0.88	0
15-102-01	0.00		0.00		0.00		0.78		0.00		0.00		0.78	0
15-102-02	0.00		0.00		0.00		5.56	1	0.00		0.00		5.56	1
15-103-01	3.00	1	0.00		0.00		3.00		0.00		0.00		5.99	1
15-103-02	1.26		0.00		0.00		2.52		0.00		0.00		3.79	0
15-104-01	0.72		0.00		0.72		9.32	1	0.00		0.00		10.75	1
15-105-01	0.00		0.00		0.00		0.00		0.00		0.00		0.00	0
15-105-02	0.00		0.00		0.00		0.00		0.00		0.00		0.00	0
15-105-03	0.00		0.00		0.00		9.44	1	0.00		0.00		9.44	1
15-105-04	0.00		0.00		0.00		7.56	1	0.00		0.84	1	8.40	2
15-106-01	0.00		0.00		0.00		3.51		0.00		0.00		3.51	0
15-107-01	0.00		0.00		0.00		3.11		0.00		0.00		3.11	0
15-107-02	0.00		0.00		0.00		4.88		0.00		0.00		4.88	0
15-107-03	0.00		0.00		0.00		0.00		0.00		0.00		0.00	0
15-108-01	2.35	1	0.00		0.00		17.60	1	0.00		1.17	1	21.11	3
15-109-01	0.00		0.00		0.00		0.00		0.00		0.00		0.00	0

15-109-02	0.00		0.00		0.00		0.00		0.00		0.00		0.00	0
15-110-01	1.12		0.00		0.00		1.12		0.00		0.00		2.24	0
15-110-02	0.00		0.00		0.00		0.00		0.00		0.76	1	0.76	1
15-110-03	0.00		0.00		0.00		0.00		0.00		0.00		0.00	0
15-111-01	0.00		0.00		0.00		0.00		0.00		0.00		0.00	0
15-112-01	0.00		0.00		0.00		0.00		0.00		0.00		0.00	0
15-112-02	0.00		0.00		0.93		0.00		0.00		0.00		0.93	0
15-113-01	0.00		0.90	1	0.00		0.00		0.00		0.00		0.90	1
15-113-02	0.00		0.00		0.00		1.65		0.00		0.00		1.65	0
15-113-03	0.00		0.00		0.00		0.00		0.00		0.00		0.00	0
15-113-04	0.00		0.00		2.84	1	0.00		0.00		0.00		2.84	1
15-114-01	0.00		0.00		0.00		0.00		0.00		0.00		0.00	0
15-115-01	0.00		0.00		0.00		0.00		0.00		0.00		0.00	0
15-115-02	0.61		0.00		0.00		0.00		0.00		0.00		0.61	0
15-115-03	0.00		0.00		0.00		0.84		0.00		0.00		0.84	0
15-115-04	0.00		0.00		1.18	1	7.10	1	0.00		0.00		8.28	2
15-115-05	0.00		0.00		0.00		0.00		0.00		0.00		0.00	0
15-115-06	0.00		0.00		0.00		0.00		0.00		0.00		0.00	0
15-115-07	0.00		0.00		0.00		0.00		0.00		0.00		0.00	0
15-116-01	0.00		0.00		0.00		0.00		0.00		0.00		0.00	0
15-117-01	1.15		0.00		0.00		0.00		0.00		0.00		1.15	0

15-117-02	0.00		0.00		0.00		0.00		0.00		0.00		0.00	0
15-117-03	0.00		0.00		0.00		0.00		0.00		0.00		0.00	0
15-118-01	0.00		0.00		0.00		0.00		0.00		0.00		0.00	0
15-118-02	0.00		0.00		0.00		0.00		0.00		0.00		0.00	0
15-118-03	0.00		0.00		0.00		0.00		0.00		0.00		0.00	0
15-119-01	0.00		0.00		0.00		0.00		0.00		0.00		0.00	0
15-119-02	0.71		0.00		2.13	1	0.71		0.71	1	0.00		4.26	2
15-119-03	9.57	2	1.06	1	8.51	2	19.15	1	1.06	2	1.06	1	40.43	9
15-120-01	0.81		0.00		0.00		0.81		0.00		0.81	1	2.42	1
15-120-02	0.00		0.00		0.00		14.71	1	0.00		0.00		14.71	1
15-121-01	0.00		0.00		1.33	1	0.00		0.00		0.00		1.33	1
15-121-02	0.00		0.00		0.00		0.00		0.00		0.00		0.00	0
15-122-01	0.00		0.00		0.00		0.00		0.00		0.00		0.00	0
15-123-01	1.32		0.00		0.00		2.65		0.00		0.00		3.97	0
15-123-02	0.00		0.00		0.00		0.00		0.00		0.00		0.00	0
15-124-01	0.00		0.00		0.76		0.00		0.00		0.00		0.76	0
15-124-02	0.00		0.00		0.00		7.34	1	0.00		0.00		7.34	1
15-125-01	0.87		0.00		0.87		2.60		0.00		0.00		4.33	0
15-125-02	2.91	1	0.00		0.73		6.55	1	0.00		0.00		10.18	2
15-125-03	0.00		0.00		0.00		2.29		0.00		0.00		2.29	0
15-126-01	1.83	1	0.00		0.00		2.74		0.00		0.00		4.57	1

15-126-02	0.00		0.00		0.00		4.92		0.00		0.00		4.92	0
15-126-03	0.71		0.00		0.00		7.10	1	0.00		0.00		7.82	1
15-126-04	0.00		0.00		0.90		8.07	1	0.00		0.00		8.97	1
15-126-05	1.48		0.00		0.00		16.33	1	0.00		0.00		17.81	1
15-126-06	0.00		0.00		0.00		19.83	1	0.00		0.00		19.83	1
15-126-07	1.53		0.00		1.53	1	17.62	1	0.00		0.00		20.69	2
15-126-08	1.43		0.00		0.00		7.17	1	0.00		0.00		8.60	1
15-126-09	0.66		0.00		0.00		9.23	1	0.00		0.00		9.88	1
15-126-10	2.42	1	0.00		0.61		34.55	2	0.61	1	0.00		38.18	4
15-126-11	2.53	1	0.84	1	5.06	2	52.32	2	0.00		0.00		60.76	6
15-126-12	4.82	2	0.69	1	5.51	2	66.78	2	0.69	1	0.00		78.49	8
15-126-13	1.42		0.00		1.42	1	21.99	1	0.00		0.00		24.82	2
15-126-14	0.00		0.00		0.00		7.28	1	0.00		0.00		7.28	1
15-126-15	0.90		0.00		0.00		35.29	2	0.00		0.90	1	37.10	3
15-127-01	0.00		0.00		0.00		0.71		0.00		0.00		0.71	0
15-127-02	0.00		0.00		0.00		12.09	1	0.00		0.00		12.09	1
15-128-01	0.00		1.01	1	0.00		1.01		0.00		0.00		2.02	1
15-128-02	0.00		0.00		0.00		1.41		0.00		0.00		1.41	0
15-128-03	0.00		0.00		0.00		0.00		0.00		0.00		0.00	0
15-129-01	0.00		0.00		0.00		1.62		0.00		0.00		1.62	0
15-130-01	0.71		0.00		0.71		6.37	1	0.00		0.00		7.79	1

15-130-02	0.00		0.00		0.00		8.16	1	0.00		0.00		8.16	1
15-131-01	0.00		0.00		0.00		0.00		0.00		0.00		0.00	0
15-132-01	0.00		0.00		0.00		0.00		0.00		0.00		0.00	0
15-132-02	0.00		0.00		0.00		5.54	1	0.00		1.11	1	6.65	2
15-133-01	0.00		0.00		0.67		0.00		0.00		0.00		0.67	0
15-133-02	0.00		0.00		0.00		1.23		0.00		0.00		1.23	0
15-133-03	0.84		0.00		0.84		2.53		0.00		0.00		4.21	0
15-134-01	0.00		0.00		0.00		2.21		0.00		1.10	1	3.31	1
15-134-02	0.00		1.36	2	0.00		1.36		0.00		1.36	1	4.07	3
15-135-01	0.00		0.00		0.00		0.00		0.00		0.00		0.00	0
15-135-02	0.98		0.00		0.00		0.98		0.00		0.00		1.96	0
15-136-01	0.00		0.00		0.00		0.70		0.00		0.00		0.70	0
15-136-02	0.00		0.00		0.00		1.99		0.00		1.00	1	2.99	1
15-136-03	0.69		0.00		0.00		2.08		0.00		0.00		2.77	0
15-136-04	1.48		0.00		0.00		1.48		0.00		0.00		2.96	0
15-136-05	0.00		0.00		0.00		0.00		0.00		0.00		0.00	0
15-137-01	0.00		0.00		0.00		0.00		0.00		0.00		0.00	0
15-138-01	0.00		0.00		0.00		2.42		0.00		0.00		2.42	0
15-138-02	0.00		0.00		0.00		0.72		0.00		0.00		0.72	0
15-138-03	0.00		0.00		0.00		0.00		0.00		0.00		0.00	0
15-138-04	0.00		0.00		0.00		0.00		0.00		0.00		0.00	0

15-138-05	0.00		0.00		0.00		0.00		0.00		0.00		0.00	0
15-138-06	0.76		0.00		0.00		1.51		0.00		0.00		2.27	0
15-138-07	1.09		0.00		0.00		2.17		0.00		0.00		3.26	0
15-138-08	0.65		0.00		0.00		3.23		0.00		0.00		3.87	0
15-138-09	0.00		0.00		0.00		2.15		0.00		0.00		2.15	0
15-138-10	0.00		0.00		0.00		0.00		0.00		0.00		0.00	0
15-138-11	0.00		0.00		0.00		2.84		0.00		0.00		2.84	0
15-138-12	0.00		0.00		1.44	1	2.88		0.00		0.00		4.32	1
15-138-13	0.00		0.00		0.00		6.32	1	0.00		0.00		6.32	1
15-138-14	0.00		0.00		0.00		0.00		0.00		0.00		0.00	0
15-138-15	0.00		0.00		0.00		2.21		0.00		0.00		2.21	0
15-138-16	0.00		0.00		0.00		3.93		0.00		0.00		3.93	0
15-139-01	0.00		0.00		0.00		0.00		0.00		0.00		0.00	0
15-139-02	0.00		0.00		0.00		3.45		0.00		0.00		3.45	0
15-139-03	0.00		0.00		0.00		0.00		0.00		0.00		0.00	0
15-139-04	0.00		0.00		2.21	1	3.69		0.00		0.00		5.90	1
15-139-05	7.77	2	0.00		0.00		3.88		0.00		0.00		11.65	2
15-140-01	0.00		0.00		0.00		0.00		0.00		0.00		0.00	0
15-141-01	0.00		0.00		1.40	1	7.02	1	0.00		0.00		8.42	2
15-142-01	0.80		0.00		1.61	1	5.63	1	0.00		0.00		8.05	2
15-142-02	0.00		0.00		0.00		0.00		0.00		0.00		0.00	0

15-143-01	0.00		0.00		0.00		0.00		0.00		0.00		0.00	0
15-144-01	0.87		0.00		0.00		6.11	1	0.00		0.00		6.99	1
15-144-02	0.80		0.00		0.00		16.06	1	0.00		0.00		16.87	1
15-144-03	2.59	1	0.00		1.73	1	29.37	2	0.00		0.86	1	34.56	5
15-144-04	2.02	1	0.00		2.69	1	26.89	2	0.00		0.00		31.60	4
15-144-05	1.93	1	0.00		0.00		35.66	2	0.00		2.89	2	40.48	5
15-145-01	3.06	1	0.76	1	0.00		10.71	1	0.00		0.00		14.53	3
15-145-02	2.16	1	0.00		0.72		8.63	1	0.00		0.72	1	12.23	3
15-145-03	5.17	2	0.00		0.57		14.37	1	0.00		0.00		20.11	3
15-145-04	1.72	1	0.00		0.86		14.66	1	0.00		0.00		17.24	2
15-145-05	0.00		0.00		0.00		29.09	2	0.00		0.00		29.09	2
15-146-01	0.72		0.00		4.32	2	15.11	1	0.00		0.00		20.14	3
15-146-02	3.81	2	0.00		0.00		5.71	1	0.00		0.00		9.52	3
15-146-03	0.00		0.00		2.17	1	30.43	2	0.00		0.00		32.61	3
15-011	0.00		0.00		0.00		2.99		0.00		0.00		2.99	0
15-012	2.34	1	0.00		2.34	1	18.71	1	0.00		0.00		23.39	3
15-013	3.48	2	0.00		0.00		48.70	2	0.00		0.00		52.17	4
15-014	9.16	2	0.00		12.21	2	54.96	2	0.00		0.00		76.34	6
15-015	0.00		0.00		0.00		27.91	2	0.00		0.00		27.91	2
15-016	0.00		0.00		5.52	2	30.34	2	0.00		0.00		35.86	4
15-017	0.00		0.00		0.00		0.00		0.00		0.00		0.00	0

15-019	0.00		0.00		0.00		3.79		0.00		0.00		3.79	0
15-021	0.00		0.00		0.00		0.86		0.00		0.00		0.86	0
15-022	0.00		0.00		0.00		35.22	2	0.00		0.00		35.22	2
15-x03	1.22		0.00		0.00		3.67		0.00		0.00		4.89	0

Appendix G: Geochemical Pathfinder Scores

Anomaly score for the geochemical pathfinder elements. A low anomaly equals 1 point. A High anomaly equals 2 points. The total score is tabulated on the right. The borehole number is listed as NGO-RC15-###-##(-63µm) with the first three numbers being the borehole number and the last 2 numbers are the depth of the sample (*e.g*. sample 03 is the 3rd 1.5 m depth sample for a total depth of 3x1.5=4.5 m). The -63µm portion identifies the sediment size sampled. The surficial samples are listed as UW-15-### (-63µm).

Sample ID (<63µm)	Cobalt (ppm)	Cobalt Score	Nickel (ppm)	Nickel Score	Chromium (ppm)	Chromium Score	Average (ppm)	Total Score
RC15-095-01	3.04		11.90		56		23.65	0
RC15-095-02	6.62		27.90		89	1	41.17	1
RC15-095-03	4.00		12.60		57		24.53	0
RC15-095-04	7.60		25.30		93	1	41.97	1
RC15-095-05	11.20	1	38.20	1	113	1	54.13	3
RC15-096-01	4.63		14.10		56		24.91	0
RC15-096-02	6.08		18.80		63		29.29	0
RC15-097-01	5.11		15.40		60		26.84	0
RC15-097-02	5.27		17.30		66		29.52	0
RC15-098-01	5.42		17.00		58		26.81	0
RC15-098-02	10.80	1	27.90		76		38.23	1
RC15-098-03	7.50		25.20		60		30.90	0
RC15-098-04	8.50	1	24.80		68		33.77	1
RC15-099-01	4.01		14.40		67		28.47	0
RC15-099-02	6.14		22.10		63		30.41	0
RC15-099-03	5.75		17.00		53		25.25	0
RC15-099-04	6.47		20.40		65		30.62	0
RC15-100-01	3.71		17.20		61		27.30	0
RC15-100-02	13.50	1	59.10	2	125	1	65.87	4
RC15-101-01	10.20	1	31.20	1	92	1	44.47	3
RC15-102-01	10.50	1	39.20	1	96	1	48.57	3
RC15-102-02	9.20	1	31.00	1	75		38.40	2
RC15-103-01	5.91		20.90		72		32.94	0

RC15-103-02	8.46	1	26.50		68		34.32	1
RC15-104-01	11.90	1	39.30	1	100	1	50.40	3
RC15-105-01	2.24		9.48		40		17.24	0
RC15-105-02	8.57	1	22.30		77		35.96	1
RC15-105-03	7.28		21.50		63		30.59	0
RC15-105-04	6.91		21.50		66		31.47	0
RC15-106-01	4.90		19.70		72		32.20	0
RC15-107-01	12.80	1	24.20		81		39.33	1
RC15-107-02	8.85	1	27.80		97	1	44.55	2
RC15-107-03	9.09	1	28.30		96	1	44.46	2
RC15-108-01	5.65		20.30		82		35.98	0
RC15-109-01	4.10		18.20		75		32.43	0
RC15-109-02	5.38		22.80		89	1	39.06	1
RC15-110-01	4.47		17.10		69		30.19	0
RC15-110-02	9.21	1	27.50		74		36.90	1
RC15-110-03	7.04		24.00		76		35.68	0
RC15-111-01	3.35		11.80		67		27.38	0
RC15-112-01	6.47		18.30		70		31.59	0
RC15-112-02	6.81		22.70		63		30.84	0
RC15-113-01	7.12		18.20		75		33.44	0
RC15-113-02	10.50	1	33.20	1	91	1	44.90	3
RC15-113-03	6.86		18.10		80		34.99	0
RC15-113-04	6.96		20.00		77		34.65	0
RC15-114-01	3.59		11.20		66		26.93	0
RC15-115-01	9.32	1	27.10		95	1	43.81	2
RC15-115-02	9.44	1	29.80	1	99	1	46.08	3
RC15-115-03	6.24		19.90		78		34.71	0
RC15-115-04	11.10	1	32.90	1	97	1	47.00	3
RC15-115-05	10.60	1	32.60	1	119	1	54.07	3

RC15-115-06	15.30	2	52.20	2	160	2	75.83	6
RC15-115-07	18.50	2	63.50	2	198	2	93.33	6
RC15-116-01	2.65		10.40		60		24.35	0
RC15-117-01	4.74		17.00		76		32.58	0
RC15-117-02	3.86		13.10		62		26.32	0
RC15-117-03	22.70	2	54.10	2	134	1	70.27	5
RC15-118-01	5.24		15.40		73		31.21	0
RC15-118-02	6.12		20.40		91	1	39.17	1
RC15-118-03	7.28		24.40		102	1	44.56	1
RC15-119-01	5.10		14.40		69		29.50	0
RC15-119-02	11.50	1	41.60	1	109	1	54.03	3
RC15-119-03	4.83		18.90		155	2	59.58	2
RC15-120-01	5.24		21.40		74		33.55	0
RC15-120-02	4.64		15.50		64		28.05	0
RC15-121-01	3.77		12.90		73		29.89	0
RC15-121-02	10.00	1	35.50	1	73		39.50	2
RC15-122-01	4.80		17.40		80		34.07	0
RC15-123-01	4.99		15.20		74		31.40	0
RC15-123-02	4.11		13.40		65		27.50	0
RC15-124-01	3.76		13.80		60		25.85	0
RC15-124-02	3.75		13.60		59		25.45	0
RC15-125-01	3.41		12.20		59		24.87	0
RC15-125-02	11.30	1	38.00	1	113	1	54.10	3
RC15-125-03	19.00	2	66.40	2	170	2	85.13	6
RC15-126-01	8.46	1	25.80		172	2	68.75	3
RC15-126-02	5.93		17.20		66		29.71	0
RC15-126-03	6.53		19.60		54		26.71	0
RC15-126-04	9.49	1	29.60	1	104	1	47.70	3
RC15-126-05	11.80	1	39.20	1	101	1	50.67	3

RC15-126-06	10.20	1	38.00	1	113	1	53.73	3
RC15-126-07	6.94		21.40		77		35.11	0
RC15-126-08	10.30	1	31.20	1	90	1	43.83	3
RC15-126-09	10.80	1	34.70	1	91	1	45.50	3
RC15-126-10	11.80	1	41.60	1	131	1	61.47	3
RC15-126-11	12.50	1	45.40	1	125	1	60.97	3
RC15-126-12	11.40	1	35.60	1	119	1	55.33	3
RC15-126-13	12.20	1	40.30	1	118	1	56.83	3
RC15-126-14	15.90	2	54.10	2	161	2	77.00	6
RC15-126-15	13.00	1	47.50	1	126	1	62.17	3
RC15-127-01	3.78		12.70		60		25.49	0
RC15-127-02	11.00	1	39.00	1	67		39.00	2
RC15-127-03	9.39	1	32.00	1	78		39.80	2
RC15-128-01	4.89		17.40		65		29.10	0
RC15-128-02	3.66		13.60		54		23.75	0
RC15-128-03	4.60		14.10		54		24.23	0
RC15-129-01	2.66		8.39		46		19.02	0
RC15-130-01	3.11		11.60		65		26.57	0
RC15-130-02	3.40		11.70		51		22.03	0
RC15-131-01	3.05		9.17		45		19.07	0
RC15-132-01	4.10		16.90		48		23.00	0
RC15-132-02	4.66		14.80		65		28.15	0
RC15-133-01	4.79		17.20		60		27.33	0
RC15-133-02	5.83		19.20		59		28.01	0
RC15-133-03	7.05		22.70		69		32.92	0
RC15-134-01	5.30		19.50		71		31.93	0
RC15-134-02	10.90	1	24.80		77		37.57	1
RC15-135-01	7.81		23.60		98	1	43.14	1
RC15-135-02	4.85		15.20		70		30.02	0

RC15-136-01	5.34		15.10		69		29.81	0
RC15-136-02	7.19		19.70		61		29.30	0
RC15-136-03	9.06	1	25.70		75		36.59	1
RC15-136-04	11.50	1	33.80	1	104	1	49.77	3
RC15-136-05	10.70	1	32.50	1	108	1	50.40	3
RC15-137-01	2.17		6.39		49		19.19	0
RC15-138-01	11.00	1	20.50		66		32.50	1
RC15-138-02	6.71		14.50		52		24.40	0
RC15-138-03	9.94	1	25.20		71		35.38	1
RC15-138-04	11.60	1	31.10	1	81		41.23	2
RC15-138-05	15.30	2	46.60	1	113	1	58.30	4
RC15-138-06	11.80	1	36.90	1	106	1	51.57	3
RC15-138-07	12.90	1	52.70	2	130	1	65.20	4
RC15-138-08	13.30	1	47.80	1	144	2	68.37	4
RC15-138-09	11.60	1	39.30	1	94	1	48.30	3
RC15-138-10	11.40	1	38.30	1	117	1	55.57	3
RC15-138-11	11.80	1	39.40	1	124	1	58.40	3
RC15-138-12	14.50	2	44.50	1	123	1	60.67	4
RC15-138-13	12.60	1	38.70	1	121	1	57.43	3
RC15-138-14	12.00	1	41.30	1	120	1	57.77	3
RC15-138-15	12.60	1	40.10	1	121	1	57.90	3
RC15-138-16	11.70	1	39.40	1	121	1	57.37	3
RC15-139-01	5.88		21.80		74		33.89	0
RC15-139-02	9.82	1	26.80		102	1	46.21	2
RC15-139-03	14.20	2	44.20	1	128	1	62.13	4
RC15-139-04	11.30	1	38.60	1	110	1	53.30	3
RC15-139-05	9.40	1	33.40	1	114	1	52.27	3
RC15-140-01	4.44		12.60		53		23.35	0
RC15-141-01	7.10		20.70		71		32.93	0

RC15-142-01	5.86		20.20		66		30.69	0
RC15-142-02	4.46		14.40		38		18.95	0
RC15-143-01	5.88		18.90		74		32.93	0
RC15-144-01	4.98		16.60		64		28.53	0
RC15-144-02	6.96		22.40		78		35.79	0
RC15-144-03	12.60	1	37.00	1	92	1	47.20	3
RC15-144-04	12.00	1	35.40	1	95	1	47.47	3
RC15-144-05	12.90	1	43.70	1	107	1	54.53	3
RC15-145-01	7.61		19.30		62		29.64	0
RC15-145-02	6.16		19.50		57		27.55	0
RC15-145-03	8.70	1	25.50		66		33.40	1
RC15-145-04	7.59		23.00		64		31.53	0
RC15-145-05	7.76		22.60		69		33.12	0
RC15-146-01	5.07		19.80		66		30.29	0
RC15-146-02	5.04		19.20		65		29.75	0
RC15-146-03	7.67		23.80		79		36.82	0
UW-15-011	2.40		8.11		37		15.84	0
UW-15-012	3.08		9.67		45		19.25	0
UW-15-013	2.97		8.57		42		17.85	0
UW-15-014	3.17		10.90		54		22.69	0
UW-15-015	3.97		12.00		53		22.99	0
UW-15-016	4.92		15.80		69		29.91	0
UW-15-017	2.51		8.75		48		19.75	0
UW-15-019	4.47		15.30		52		23.92	0
UW-15-021	2.78		9.07		53		21.62	0
UW-15-022	3.98		11.70		50		21.89	0
UW-15-X03	2.41		7.60		42		17.34	0

Appendix H: KIM Analysis for Each Indicator Mineral

Fine Fraction of Pyrope Garnet

The fine fraction (0.25 – 0.50 mm) of the KIM pyrope garnet contains 6 high count and 33 low count samples. Four depositional areas have been identified for the pyrope garnets.

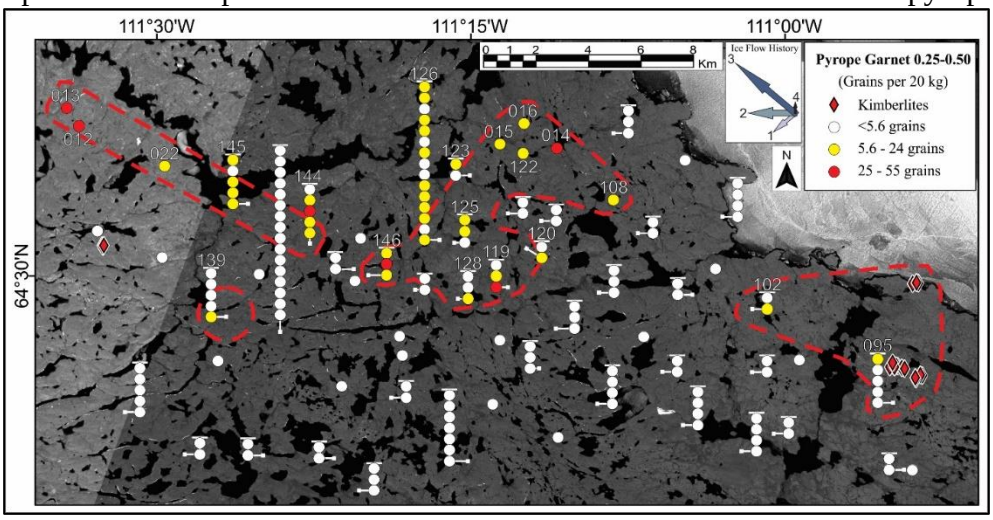

The fine size fraction (0.25 – 0.50 mm) of pyrope garnets plotted according to the background (<5.5), low counts (5.6 – 24), and high counts (25 – 55) in grains per 20 kg of till. The red lines are the expressions of the pyrope grain dispersal. Each stack of dots is a single borehole and each dot represents 1.5 m of downhole till.

Coarse Fraction of Pyrope Garnets

The coarse fraction (0.50 – 1.00 mm) of the KIM pyrope contains 7 high scores and 13 low scores.

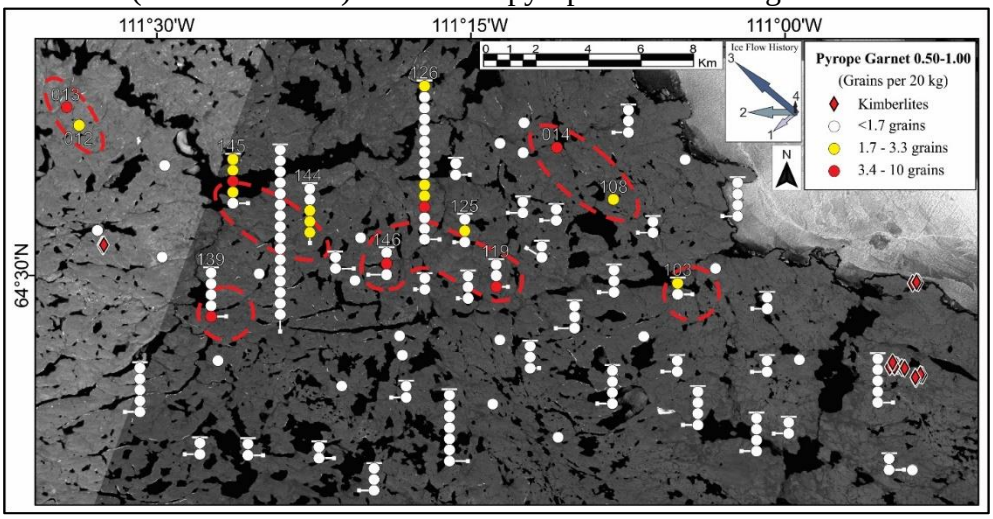

The coarse size fraction (0.50 – 1.00 mm) of pyrope garnet plotted according to the background (<1.7), low score (1.7 – 3.3), and high score (3.4 – 10) in number of grains per 20 kg of till. The red lines are the expression of the pyrope grain dispersal. Each stack of dots is a single borehole and each dot represents 1.5 m of downhole till.

Fine Fraction of Eclogite

The fine fraction (0.25 – 0.50 mm) of the KIM eclogite contains 8 high scores and 11 low scores. Five depositional areas have been identified for eclogite.

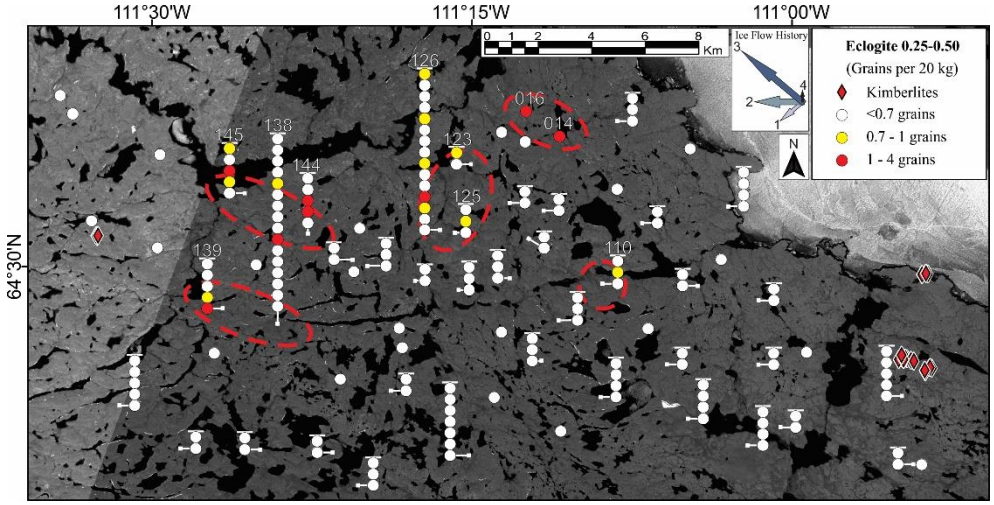

The fine size fraction (0.25 – 0.50 mm) of eclogite plotted according to the background (<0.7), low counts (0.7 – 0.79), and high counts (0.8 – 4) in grains per 20 kg of till. The red lines are the expressions of the eclogite grain dispersal. Each stack of dots is a single borehole and each dot represents 1.5 m of downhole till.

Coarse Fraction of Eclogite Garnets

The coarse fraction (0.50 – 1.00 mm) of the KIM eclogite contains 6 low counts and 1 high count.

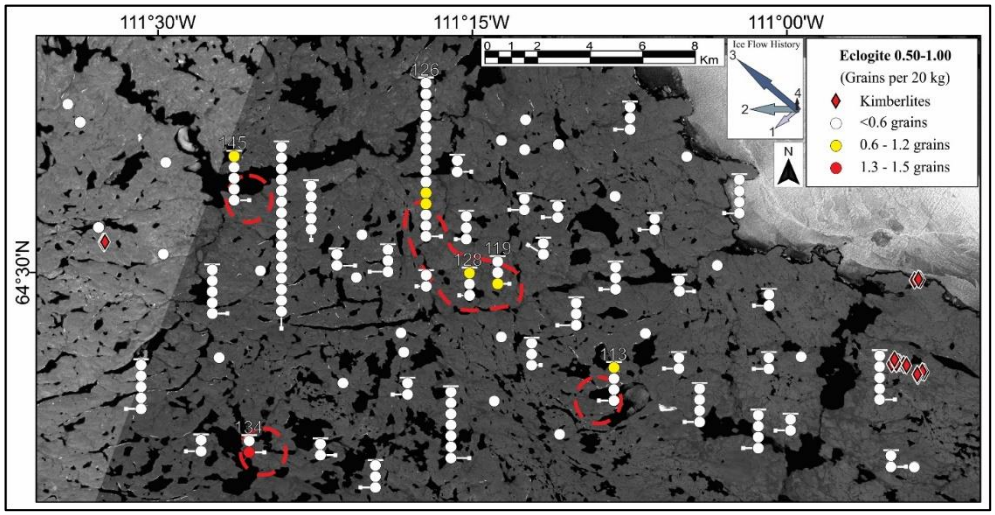

The coarse size fraction (0.50 – 1.00 mm) of eclogite plotted according to the background (<0.6), low score (0.6 – 1.2), and high score (1.3 – 1.5) in number of grains per 20 kg of till. The red lines are the expression of the eclogite grain dispersal. Each stack of dots is a single borehole and each dot represents 1.5 m of downhole till.

Fine Fraction of Chrome Diopside

The fine fraction (0.25 – 0.50 mm) of the KIM chrome diopside contains 9 high scores and 15 low scores. Three depositional areas have been identified for chrome diopside.

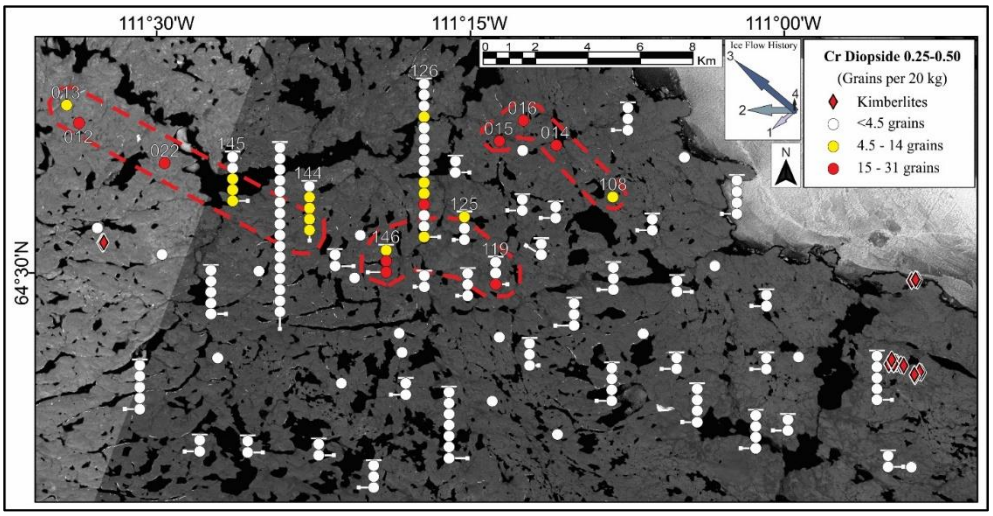

The fine size fraction (0.25 – 0.50 mm) of chrome diopside plotted according to the background (<4.5), low counts (4.5 – 14), and high counts (15 – 31) in grains per 20 kg of till. The red lines are the expression of the chrome diopside grain dispersal. Each stack of dots is a single borehole and each dot represents 1.5 m of downhole till.

Coarse Fraction of Chrome Diopside

The coarse fraction (0.50 – 1.00 mm) of the KIM chrome diopside contains 6 high scores and 14 low scores.

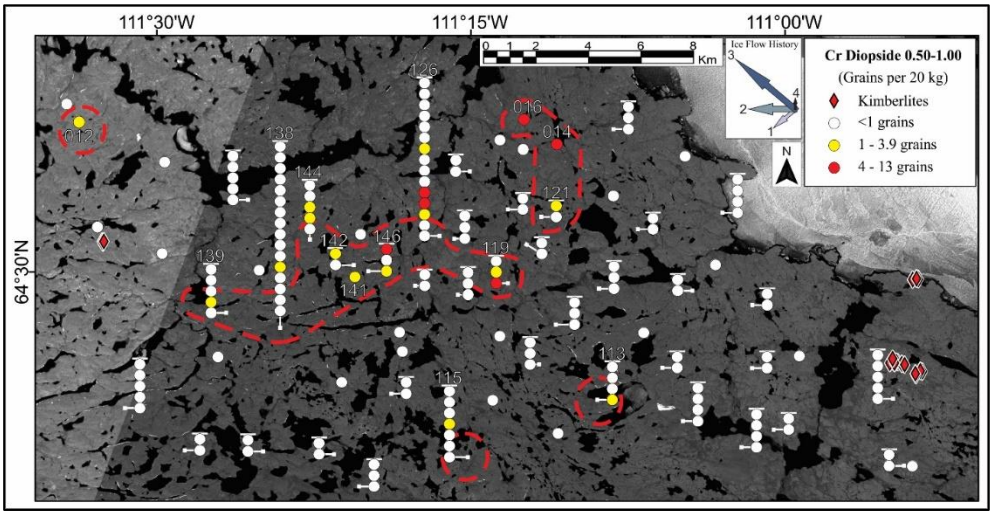

The coarse size fraction (0.50 – 1.00 mm) of chrome diopside plotted according to the background (<1), low score (1 – 3.9), and high score (4.0 – 13) in number of grains per 20 kg of till. The red lines are the expression of the chrome diopside grain dispersal. Each stack of dots is a single borehole and each dot represents 1.5 m of downhole till.

Fine Fraction of Olivine

The fine fraction (0.25 – 0.50 mm) of the KIM olivine contains 9 high scores and 32 low scores. Three depositional areas have been identified for olivine.

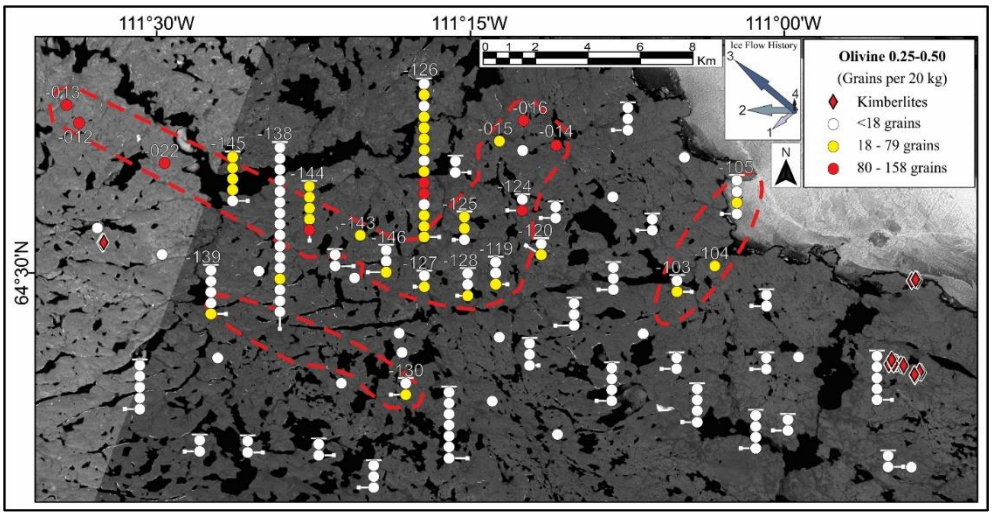

The fine size fraction (0.25 – 0.50 mm) of olivine plotted according to the background (<18), low counts (18 – 79), and highly counts (80 – 158) in grains per 20 kg of till. The red lines are the expression of the olivine grain dispersal. Each stack of dots is a single borehole and each dot represents 1.5 m of downhole till.

Coarse Fraction of Olivine

The coarse fraction (0.50 – 1.00 mm) of the KIM olivine contains 14 high scores and 35 low scores.

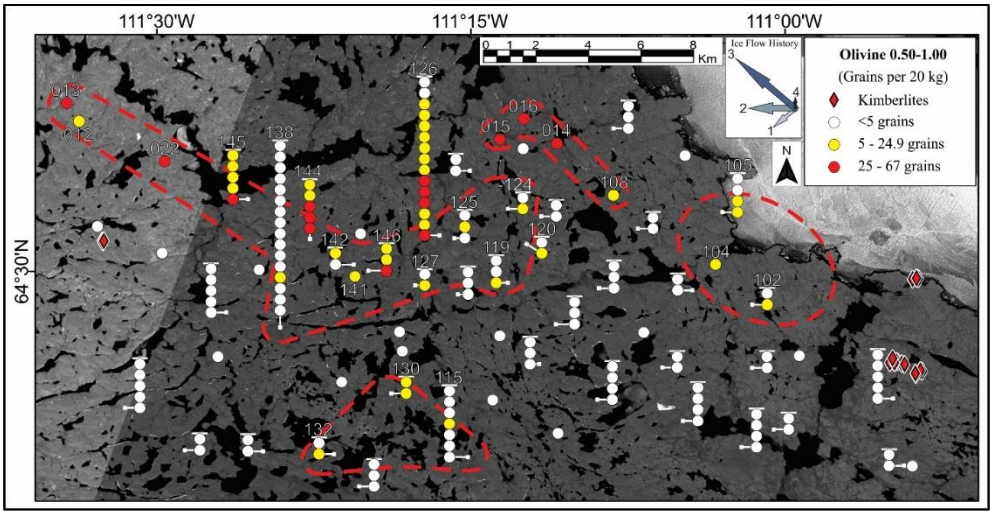

The coarse size fraction (0.50 – 1.00 mm) of olivine plotted according to the background (<5), low score (5 – 24.9), and high score (25 – 67) in number of grains per 20 kg of till. The red lines are the expression of the olivine grain dispersal. Each stack of dots is a single borehole and each dot represents 1.5 m of downhole till.

Fine Fraction of Picroilmenite

The fine fraction (0.25 – 0.50 mm) of the KIM picroilmenite contains 1 high score and 6 low scores. Five depositional areas have been identified for picroilmenite.

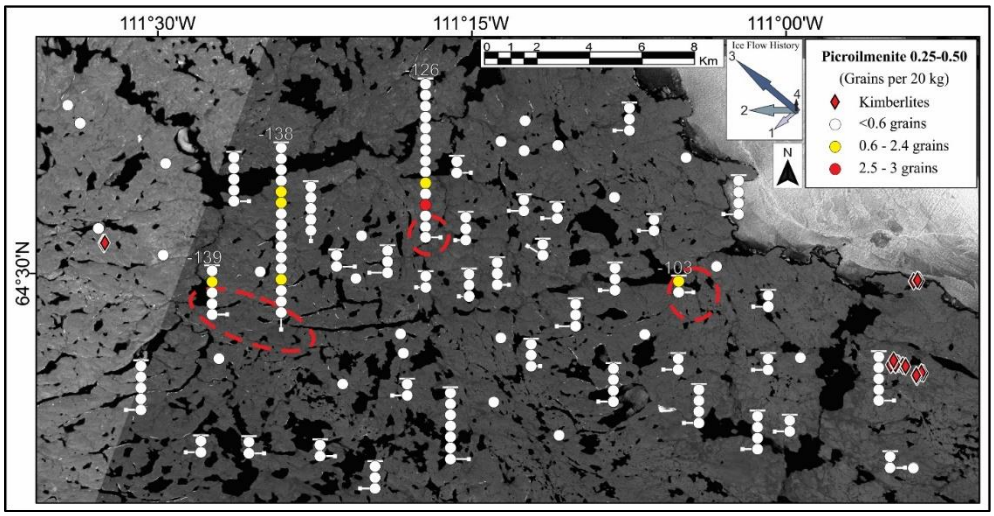

The fine size fraction (0.25 – 0.50 mm) of picroilmenite plotted according to the background (<0.6), low counts (0.6 – 2.4), and high counts (2.5 – 3) in grains per 20 kg of till. The red lines are the expression of the picroilmenite grain dispersal. Each stack is a single borehole and each dot represents 1.5 m of downhole till.

Coarse Fraction of Picroilmenite

The coarse fraction (0.50 – 1.00mm) of the KIM picroilmenite contains 1 high score and 3 low scores.

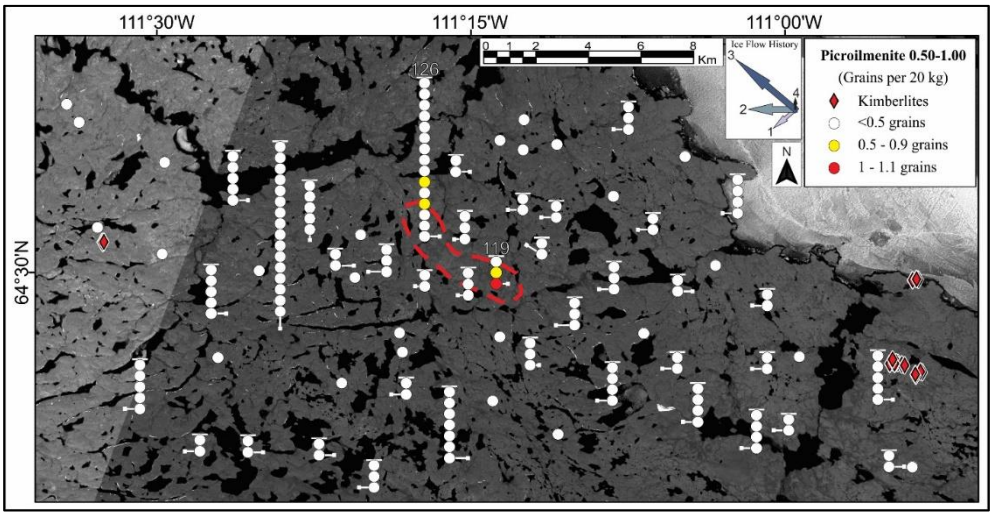

The coarse size fraction (0.50 – 1.00 mm) of picroilmenite plotted according to the background (<0.5), low score (0.5 – 0.9) and high score (1 – 1.1) in number of grains per 20 kg of till. The red lines are the expression of the picroilmenite grain dispersal. Each stack of dots is a single borehole and each dot represents 1.5 m of downhole till.

Fine Fraction of Chromite

The fine fraction (0.25 – 0.50 mm) of the KIM chromite contains 1 high score and 10 low scores. Five depositional areas have been identified for chromite.

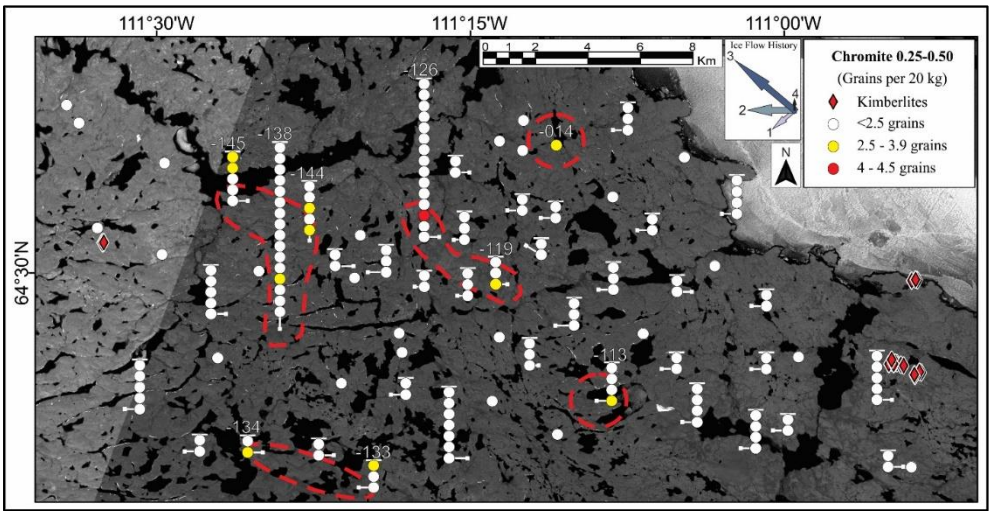

The fine size fraction (0.25 – 0.50 mm) of chromite plotted according to the background (<2.5), low score (2.5 – 3.9), and high score (4 – 4.5) in grains per 20 kg of till. The red lines are the expression of the chromite grain dispersal. Each stack of dots is a single borehole and each dot represents 1.5 m of downhole till.

Coarse Fraction of Chromite

The coarse fraction (0.50 – 1.00 mm) of the KIM chromite contains 1 high score and 13 low scores.

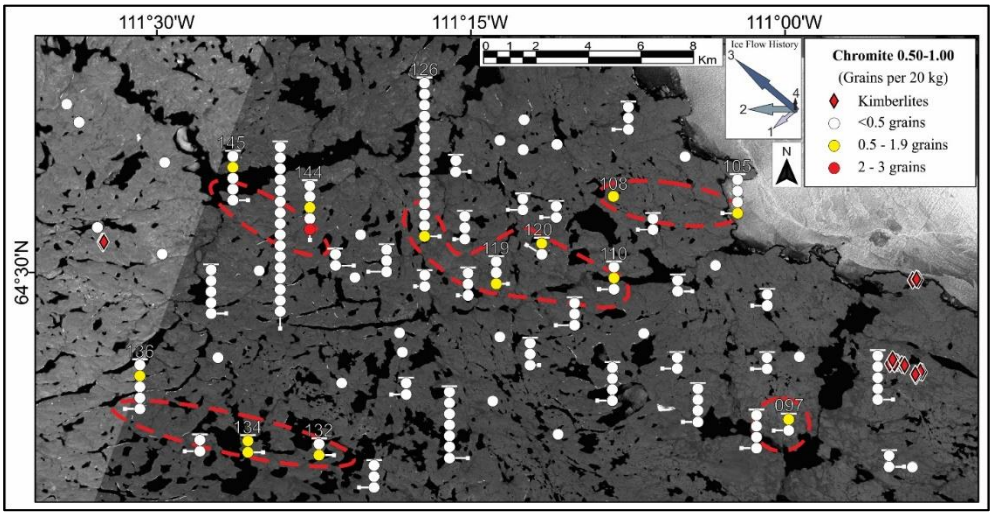

The coarse size fraction (0.50 – 1.00 mm) of chromite plotted according to the background (<0.5), low score (0.5 – 1.9), and high score (2 – 3) in number of grains per 20 kg of till. The red lines are the expression of the chromite grain dispersal. Each stack of dots is a single borehole and each dot represents 1.5 m of downhole till.

Appendix I: Geochemical Pathfinder Analysis

Cobalt - Results

The geochemical pathfinder element Cobalt contains 8 high anomalies and 59 low anomalies.

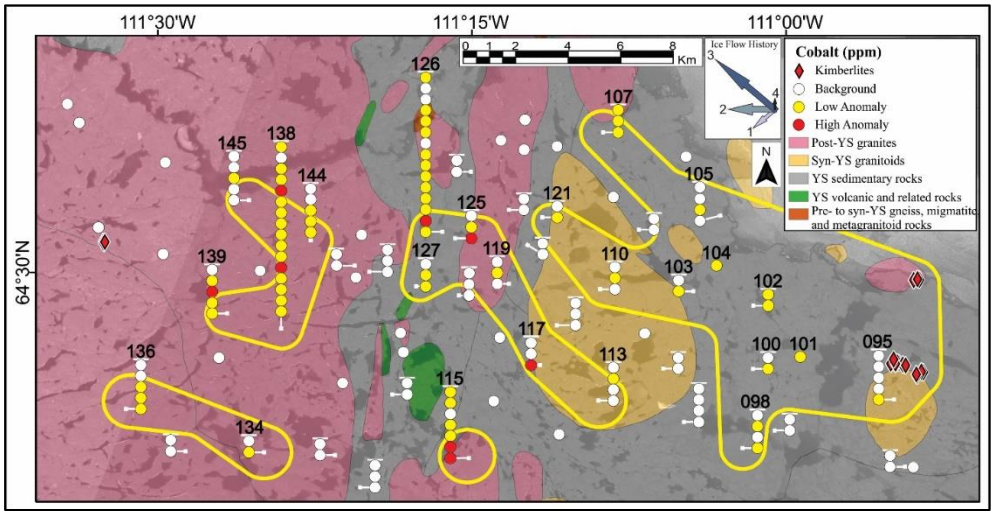

Geochemical pathfinder element Cobalt is plotted according to the background (<8 ppm), low anomalous (8 – 14 ppm), and highly anomalous (>14 ppm) concentrations. The CIT and MIT of the public KIM data are shown for comparison. Each stack of dots is a single borehole and each dot represents 1.5 m of downhole till.

Chromium - Results

The geochemical pathfinder element Chromium contains 7 high anomalies and 51 low anomalies.

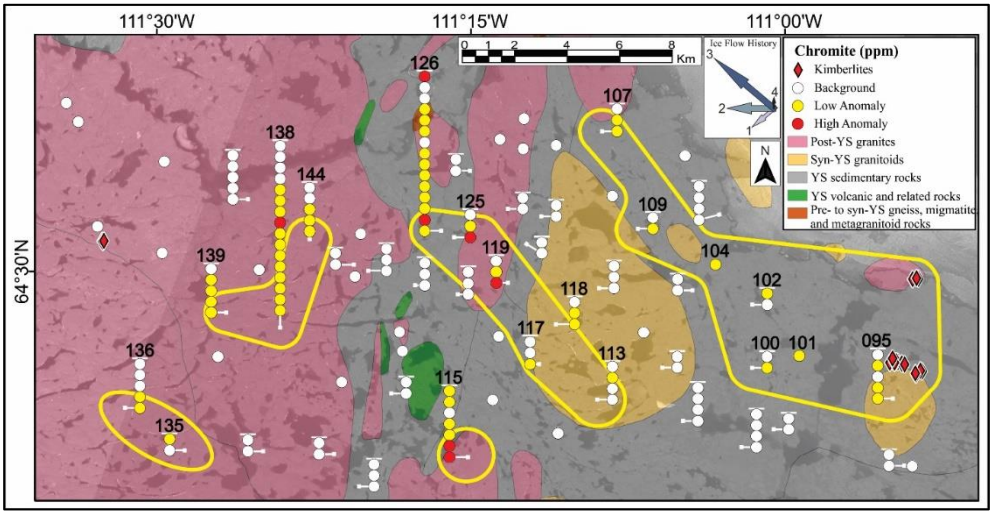

Geochemical pathfinder element Chromium is plotted according to the background (<85 ppm), low anomalous (86-140 ppm), and highly anomalous (>140 ppm) concentrations. The CIT and MIT of the public KIM data are shown for comparison. Each stack of dots is a single borehole and each dot represents 1.5 m of downhole till.

Nickel - Results

The geochemical pathfinder element Nickel contains 7 high anomalies and 44 low anomalies.

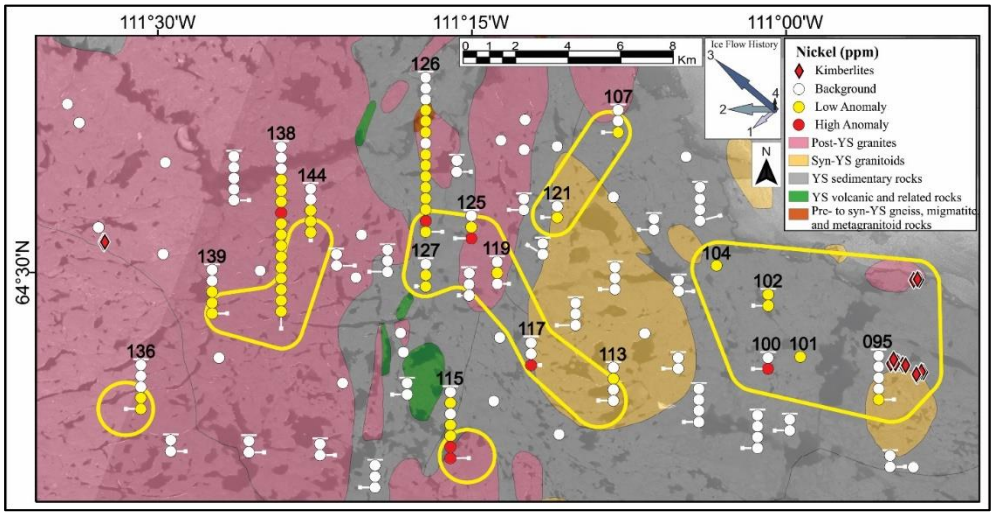

Geochemical pathfinder element Nickel is plotted according to the background (<29 ppm), low anomalous (29 – 50 ppm), and highly anomalous (>50 ppm) concentrations. The CIT and MIT of the public KIM data are shown for comparison. Each stack of dots is a single borehole and each dot represents 1.5 m of downhole till.